8-2006

Accelerated Poisoning of Diesel Oxidation Catalysts by Zinc Dialkyldithiophosphate-Derived Phosphorus

Scott Joseph Eaton
University of Tennessee - Knoxville

To the Graduate Council:

I am submitting herewith a thesis written by Scott Joseph Eaton entitled "Accelerated Poisoning of Diesel Oxidation Catalysts by Zinc Dialkyldithiophosphate-Derived Phosphorus." I have examined the final electronic copy of this thesis for form and content and recommend that it be accepted in partial fulfillment of the requirements for the degree of Master of Science, with a major in Mechanical Engineering.

Ke Nguyen, Major Professor

We have read this thesis and recommend its acceptance:

Bruce G. Bunting, David K. Irick, J. Roger Parsons

Accepted for the Council:
Carolyn R. Hodges

Vice Provost and Dean of the Graduate School

(Original signatures are on file with official student records.)

To the Graduate Council:

I am submitting herewith a thesis written by Scott Joseph Eaton entitled "Accelerated Poisoning of Diesel Oxidation Catalysts by Zinc Dialkyldithiophosphate-Derived Phosphorus." I have examined the final electronic copy of this thesis for form and content and recommend that it be accepted in partial fulfillment of the requirements for the degree of Master of Science, with a major in Mechanical Engineering.

Ke Nguyen
Major Professor

We have read this thesis
and recommend its acceptance:

Bruce G. Bunting

David K. Irick

J. Roger Parsons

Accepted for the Council:

Anne Mayhew
Vice Chancellor and
Dean of Graduate Studies

(Original signatures are on file with official student records.)

ACCELERATED POISONING OF DIESEL OXIDATION CATALYSTS BY ZINC DIALKYLDITHIOPHOSPHATE-DERIVED PHOSPHORUS

A

Thesis

Presented for the

Master of Science

Degree

The University of Tennessee, Knoxville

Scott Joseph Eaton

August 2006

DEDICATION

To my Wife,
Carrie.

ACKNOWLEDGEMENTS

I would like to thank my advisor, Dr. Ke Nguyen, for his encouragement, patience and insight throughout the duration of this project, without which this work would not have been possible. I would also like to express my gratitude to my co-advisor, Dr. Bruce Bunting, for his technical knowledge, wisdom and guidance as well as my graduate committee members Dr. David "Butch" Irick and Dr. J. Roger Parsons for their valued feedback. Within Oak Ridge National Laboratory, I want to thank Dr. Todd Toops, Samuel Lewis, Dr. Karen More, Dr. C. Stewart Daw and Dr. Jim Szibitz for their individual contributions to not only my project, but also my technical growth and confidence. In addition, I want to express my appreciation to Allan Patchen, Xiou (Sherry) Lu, Dr. Robert Compton and Dr. Roberto Benson at the University of Tennessee for each contributing their expertise and knowledge over the course of my graduate career and to my laboratory colleagues, Vitaly Prikhodko, Barath Kumar, Ajit Gopinath, S. Scott Smith, Hakyong Kim and Adam Youngquist for their support and friendship during the project.

Lastly, I want to thank the Office of FreedomCAR within the United States Department of Energy and the Oak Ridge National Laboratory for their financial support of this research with Steve Goguen and Kevin Stork as sponsors.

ABSTRACT

The phosphorus poisoning of diesel oxidation catalysts (DOCs) by the lube-oil additive zinc dialkyldithiophosphate (ZDDP) is investigated in the present study. A 517 cc single-cylinder, naturally aspirated direct-injection diesel engine is used to accelerate the phosphorus poisoning of DOCs by artificially increasing the ZDDP consumption to approximately 700 times of that found during normal engine operation. Three methods of accelerating the ZDDP consumption rate are investigated, which have been shown in previous literature to cause phosphorus poisoning. These include the injection of high concentration ZDDP-doped lube-oil blended with diesel fuel though the fuel injector as well as injecting ZDDP-doped lube-oil directly into the intake manifold and exhaust manifold, respectively. Each method is shown to produce a different phosphorus poisoning behavior on automotive catalysts by creating unique poisoning exhaust environments causing different deactivation mechanisms; ZDDP passing through the combustion chamber results in phosphoric acid, ZDDP injected into the exhaust results in whole ZDDP molecules and their molecular fragments.

The deactivation resulting from each poisoning method is characterized using both total hydrocarbon (THC) and carbon monoxide (CO) light-off degradation as well as phosphorus adsorption and phosphorus chemistry identified within the DOC. Washcoat surfaces evaluated for lube-oil derived contamination using scanning electron microscopy with energy dispersive spectrometers (SEM-EDS) shows that topography depends on the method of ZDDP introduction. Exhaust manifold injection produces a zinc-phosphate glaze, which masks active sites and inhibits gaseous diffusion to the washcoat surface. Fuel and intake manifold injection methods produce chemically absorbed phosphorus, which poison active sites. THC and CO light-off performance degradation is also found to depend on the method of ZDDP introduction, with an increase in light-off temperature between 40 to 100^{o}C. Total phosphorus, zinc, and sulfur accumulation within the DOCs is measured using X-ray fluorescence spectroscopy (XRF) and found to vary with both the ZDDP introduction method and the exhaust temperature during poisoning. Elemental (X-ray) maps and line-scans performed using electron probe microanalysis (EPMA) show

a decreasing phosphorus concentration profile along the DOC length with phosphorus being confined to the uppermost layer of the washcoat.

Three high-mileage, two brick, field-deactivated DOCs were obtained from a bus fleet, which were removed from service due to a catastrophic event, to make comparisons in THC and CO light-off behavior as well as phosphorus poisoning with those undergoing accelerated ZDDP introduction methods. The field-deactivated DOCs are of similar formulation as those used during laboratory tests. It is shown that field-deactivated DOC THC and CO light-off behavior as well as phosphorus accumulation and surface contamination is reproduced using accelerated ZDDP introduction methods. Based on the surface characterization observations and light-off performance, the intake manifold injection method offers the best correlations between accelerated poisoning methods and field-deactivated passenger bus DOCs.

In order to accurately quantify the poisoning of DOCs by phosphorus, a bench-flow reactor system (BFR) is utilized to provide supplementary THC and CO light-off evaluations for more precise control of both DOC temperature and exhaust gases composition. It is found that light-off temperature measurements using the BFR are highly repeatable and show a correlation in the poisoning mechanisms between accelerated ZDDP introduction methods and field-deactivated DOCs. As a byproduct of the BFR evaluations, it is shown that DOC regeneration occurs in both the accelerated ZDDP injection methods and the field-deactivated DOCs by the high temperature oxidation and removal of soot and lube-oil contamination on washcoat surfaces. THC and CO light-off temperatures after regeneration are identical to those obtained for a fresh DOC. Subsequent EPMA and XRF analyses of regenerated DOCs reveal the presence of the phosphorus, sulfur and zinc within the washcoat, indicating that lube-oil derived poisons do not highly influence the THC and CO light-off behavior of DOCs, but rather, DOC performance is more susceptible to the presence of soot and lube-oil contamination on the washcoat surface.

TABLE OF CONTENTS

CHAPTER PAGE

LIST OF TABLES

LIST OF FIGURES

NOMENCLATURE

%.....percentage

Φ……..work function

θ…….angle

λ……...wavelength

μA……microamperes

μm……..micrometers

ν……..frequency

^{o}……..degrees

^{o}C……..…….degrees Celsius

^{o}F…….…….degrees Fahrenheit

A……...amperes

AC…….……alternating current

Al……...aluminum

Al_2O_3…….……alumina

$AlPO_4$…….…...aluminum phosphate

ALVW……adjusted LVW

Ar……..argon

BE……..binding energy

BFR……..…….bench-flow reactor

C……..……carbon atom

C_2H_4…….……ethene

C_3H_6…….…….propene

Ca……..calcium

CAA…….Clean Air Act

cc……cubic centimeters

cc/min……..cubic centimeters per minute

Ce……cerium

CeO_2……..…ceria

Ce_2O_3…….……cerium oxide

$CePO_4$……cerium phosphate

CI……..compression ignition

CH_4……..……methane

CHA……concentric hemispherical analyzer

C_j……....concentration of the j^{th} chemical species

cm……centimeters

CO……..……carbon monoxide

CO_2……...……..carbon dioxide

cpsi……..……..cells per square inch

Cu……copper

d……distance

DAQ…….…….……data acquisition system

DC……..…….……..direct current

DI……...direct injection

dm^3…….……cubic decimeters

DOC……diesel oxidation catalyst

e…….electron

EDS……..energy dispersive spectroscopy

EIA……Energy Information Administration

EPA…….Environmental Protection Agency

EPMA……..electron probe microanalysis

ESCA……electron spectroscopy for chemical analysis

eV…….....electron volts

FID…….flame ionization detector

ft……...feet

FTP……federal testing protocol

g……grams

g/ft^3……grams per cubic foot

GHSV……gas hourly space velocity

GHz…….……..giga-Hertz

h……..…Plank's constant

H_2…….……hydrogen molecule

He……helium

H_2O……..……..…water vapor

H_2S……..hydrogen sulfide

H_3PO_4…….……..phosphoric acid

HC…….…….hydrocarbon

HCHO……..formaldehyde

HLDT…….heavy light-duty truck

hp…….……horsepower

hr……...hours

hr^{-1}…….……per hour

HV…….……high vacuum

Hz……..Hertz

IDI……...indirect injection

in……..inches

in-lbs…….……..inch pounds

k_{abs}…….……global reaction rate constant

KE……...kinetic energy

km……...kilometer

kS……...kilo-samples

kW……...kilowatts

L…….liters

L/min…….……...liters per minute

LaB_6……lanthanum hexaboride

lbs……...pounds

LCD……..liquid crystal display

LLDT……light light-duty truck

LNT…….……..…lean NO_x trap

LPM…….liters per minute

LVW……low vehicle weight

m……..meters

m^2……square meters

M……...mass

mA……...milli-amperes

MDPV……medium-duty passenger vehicle

MFC……mass flow controller

Mg……..magnesium

MgO……..magnesium oxide

mi……..miles

min……minutes

mm……..mm

mph……miles per hour

MVEG……..motor vehicle exhaust gas

n……order of reaction/order of reflection

N_2……nitrogen molecule

Na……..sodium

NA……...naturally-aspirated

NDIR……non-dispersive infrared

nm……..nanometers

NMHC……non-methane hydrocarbon

NMOG……non-methane organic gases

NMR……..nuclear magnetic resonance

NO……..nitric oxide

NO_2……nitrogen dioxide

NO_x……oxides of nitrogen

O……..oxygen

O_2……oxygen molecule

O_3……ozone

P……...phosphorus

P_2O_5……..……...phosphorus pentoxide
PC……..……personal computer
Pd……..…….……palladium
PGE……platinum group elements
PM……..……particulate matter
PMG……precious metal group
ppm……..parts per million
psi……..……pounds per square inch
psig……..……..pounds per square inch gage
Pt……..……platinum
PT……pressure transducer
PtS……platinum sulfide
Rh……rhodium
RPEB……..rapid poisoning engine bench
RPM……..……..revolutions per minute
s……seconds
SEM……scanning electron microscopy
Si……silicon
SI……..……spark ignition
SiO_2……silicon dioxide
SO_2……..……sulfur dioxide
SO_3……..……sulfur trioxide
SOF……..soluble organic fraction
STP……..……standard temperature and pressure
TC……thermocouple
THC……..……..total hydrocarbon
TM……..……..trademark
TPM……..……..total particulate matter
TWC……..……three-way catalyst
UHV……..……ultra-high vacuum

V……volume/volt

wt……weight

XPS……X-ray photoelectron spectroscopy

XRD……X-ray diffraction

XRF……X-ray fluorescence spectroscopy

ZDDP……zinc dialkyldithiophosphate

ZEV……zero emission vehicle

Zn……zinc

$Zn_2P_2O_7$……zinc pyrophosphate

$ZnSO_4$……zinc sulfate

CHAPTER 1

INTRODUCTION

This section is provided to supply the reader with background to motivate the study of diesel oxidation catalysts. An overview of the benefits and problems associated with the use of diesel engines for both transportation and utilities application are presented in Section 1.1. Current and future trends in US emission regulation as well as what techniques industry is using to meet the increasingly stringent requirements is provided in Section 1.2. Finally, a discussion of the deactivation mechanisms of encountered within the oxidation catalyst as well as a detailed discussion of the current investigation is presented in Section 1.3 and 1.4, respectively.

1.1 Overview

Diesel engines encompass a large percentage of power producing devices throughout the world; the majority of which are dedicated solely for transportation purposes. A study performed by Mori [1]* in 1995 estimated that vehicle ownership was approximately 640 million worldwide, of which 67 million are powered by diesel engines. Diesel engines are classified into a number of different categories depending on the duty-cycle and total power requirements. Figure 1.1 shows the total number of diesel powered vehicles in 1995 used worldwide and the percentage of each diesel engine type to the overall number of diesel engines produced. Although diesel powered vehicles are still only a small portion of the total vehicle population, spark ignition (SI) being the vast majority, diesel engines have received much more interest in recent years because of their inherently high fuel efficiency and long-term durability. A typical SI engine is designed for a 100,000-mile lifetime, while the diesel is typically designed to surpass 500,000

* Numbers in [] indicate reference list number

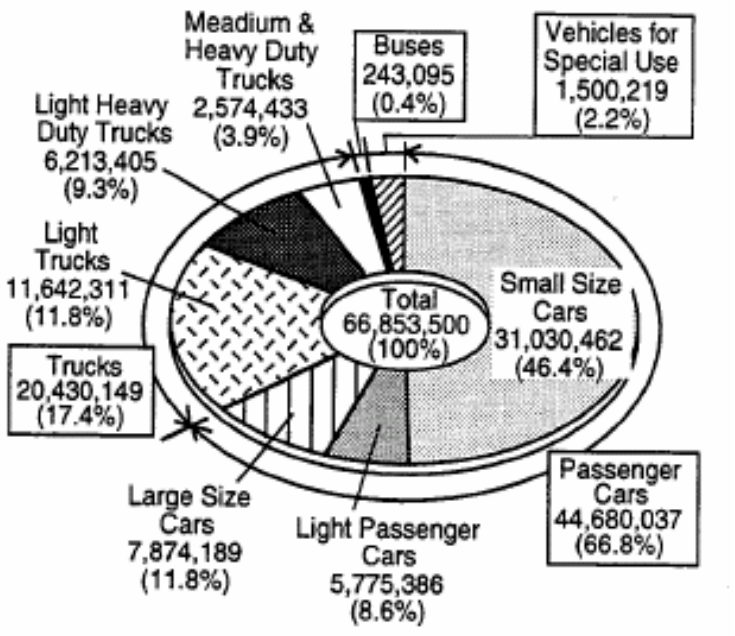

Figure 1.1: Number of diesel engine powered vehicles worldwide in 1995 by type. [1]

miles, and heavy-duty diesel engines are targeted to achieve over 1 million miles [2,3]. The diesel engine is also more fuel-efficient than the SI engine lending it to more heavy-duty applications. The SI engine is designed to operate using a throttle and at a stoichiometric air/fuel ratio that leads to a significant portion of un-reacted hydrocarbons. In contrast, diesel engines are unthrottled and high significantly higher compression ratios with a lean air/fuel ratio resulting in a higher percentage of fuel consumed during each power stroke. Therefore, the diesel engine produces more energy per gallon of fuel. Together, the benefits of the diesel engine have secured its place in the world infrastructure by almost exclusively powering buses, trains, and heavy construction machinery.

Recently diesel engines, along with hybrid technology and other alternative power supplies, have become an important strategy for the easement of the US dependence on foreign oils. Current figures by the EIA indicate that the US imports over 10 million barrels of crude oil daily [4]. As seen in Figure 1.2, approximately one third of that oil is imported from countries which the US deems “hostile”. Reducing the amount of imported oil from these regions is thought to be a necessary step in securing America’s future energy supplies.

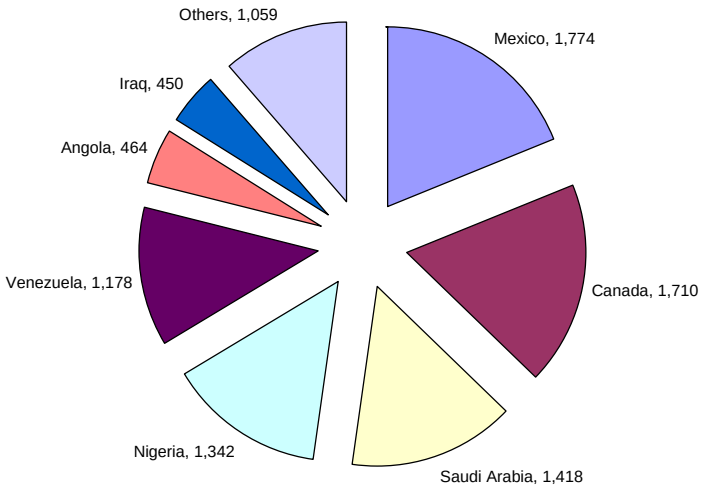

Figure 1.2: US oil imports by country of origin (thousands of barrels per day). Data taken from February 2006 EIA estimates. [4]

Another current issue prompting the use of more diesel engines is global warming from the production of green-house gases. The EIA estimates that in 2003 the world CO_2 production from the consumption of petroleum, natural gas, coal, and the flaring of natural gas from oil wells was approximately 25.2 billion metric tons, an increase of 4.1 billion tons from 1993 [5]. The use of petroleum products such as gasoline, diesel fuel, etc., accounts for a full 42 percent of the total. Other recent studies have found the United States alone is responsible for approximately one quarter of the world CO_2 production [6]. As a result of the increased CO_2 levels in the atmosphere, the EPA estimates an increase of approximately 1^oF in average global temperature over the past 100 years. Figure 1.3 shows a dramatic increase in the departure from the global long-term average temperatures during only the past 25 years in which CO_2 production rates have been the highest [7]. At the current rate of CO_2 production around the world, the EPA estimates that by 2100 the average global temperature will rise by as much as 5^oF and will have a significant, though unknown, effect on the global weather.

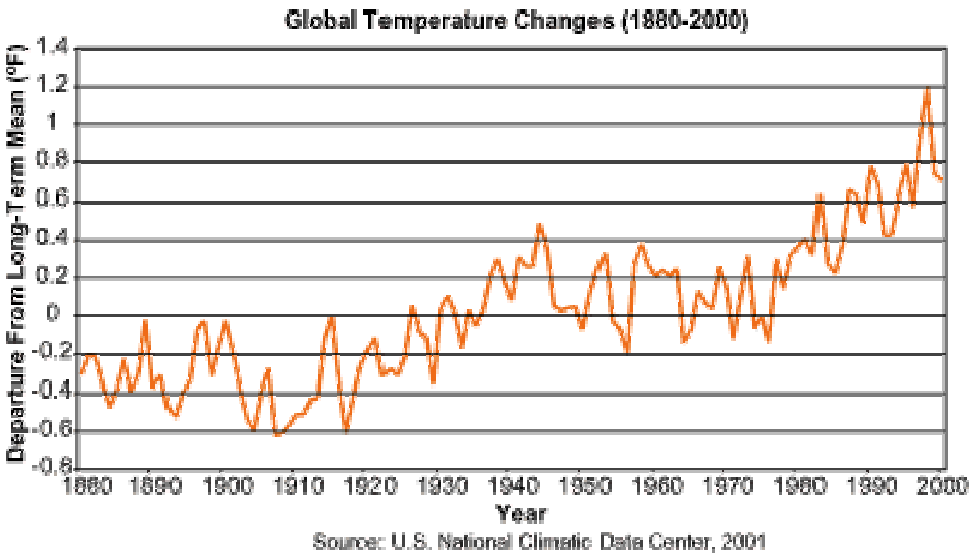

Figure 1.3: Global temperature departure from long-term mean between the years 1880 and 2000. [7]

In an effort to reduce the current rate of CO_2 production in the US and around the world, limits have been placed on the amount of CO_2 that can be released as a result of fossil fuel burning. Since diesel engines are more fuel-efficient than SI engines, they are becoming more common place as passenger transport alternatives throughout the world to help ease the CO_2 burden. The fuel-saving benefits are regrettably counteracted by an increase in particulate matter (PM) and NO_x levels which have been attributed to smog formation, green house effects and acid rain.

1.2 Legislation and Regulation

Beginning in 1970's, the United States began to regulate the production of CO, NO_x, sulfides and other aerosol PM. The ever-increasing world demand for fossil fuels and its subsequent burning have lead to recent and more stringent regulations to limit the production of these harmful emissions. The most current legislation in the US took place in 1990 - the Clean Air Act (CAA) - which places hard compliance deadlines for the easement of air-born pollution from all point sources including passenger cars and heavy-duty equipment. Since the creation of the CAA, numerous amendments have been put

forth to continually decrease the allowable amount of pollutants released by any production vehicle made after the law was passed, with the ultimate goal of reaching a zero emission vehicle (ZEV). In this effort, the EPA created a federal testing protocol (FTP) in which a rolling dynamometer is used to simulate actual driving conditions. Emission samples are taken and analyzed for PM, THC, CO and NO_x.

Legislation passed in 1994 on the allowable limits of THC and CO produced by passenger vehicles and heavy-duty equipment has always been easily achieved with the diesel technology of the time; only PM and NO_x species presented problems and have to be corrected. Often this has been accomplished with the use of flow-though diesel oxidation catalysts (DOCs), and seldom with lean-NO_x traps (LNTs). At the same time, more sophisticated diesel combustion technologies were being developed for low NO_x emissions, thus negating the need for the LNTs in many applications. Figure 1.4 is a plot of the targeted combustion regime which is found to be optimized for the minimal production of both PM and NO_x [1]. As a result, the vast majority of diesel aftertreatment devices at the time were engineered for the sole purpose of reducing SOF and other particulate matter. SOF typically represents an appreciable amount of soot and can be easily oxidized in lean exhaust, typically of diesel engines. Therefore, simply targeting the SOF components of diesel exhaust PM allows car manufactures to be beneath the PM limits of the time.

The recent passing of more stringent regulations has required the development of sophisticated techniques to remain below allowable limits of exhaust gas pollutants. Figure 1.5 shows current diesel technologies being used to meet EPA regulations [8]. An added feature to current regulations is durability requirements of aftertreatment devices in which exhaust systems must be compliant over a lifetime of 100,000 miles or more. A tier system has also been implemented to rate the performance of vehicles made after the year 2000. Tables I and II provide current and future regulations mandated by EPA effective for all vehicles made after model years 2004 and 2009, respectively. In the new regulations, each car manufacturer chooses in which tier to place a vehicle as long as the total fleet is below a set average emission standard. Temporary tiers, 9 and 10, are intermediate steps for the 2009 model year compliance deadline.

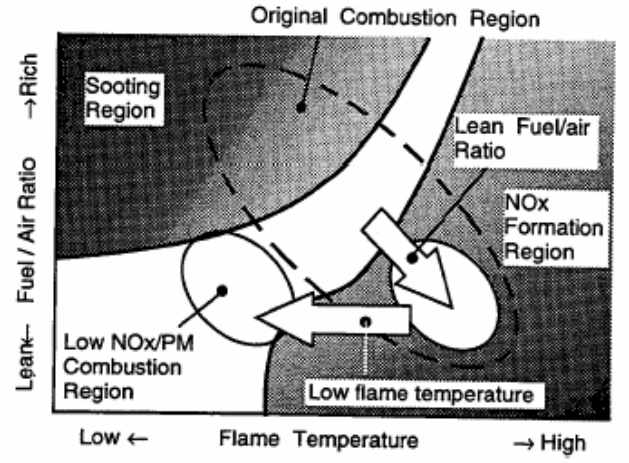

Figure 1.4: Schematic of targeted combustion regimes for clean burn diesel engines. [1]

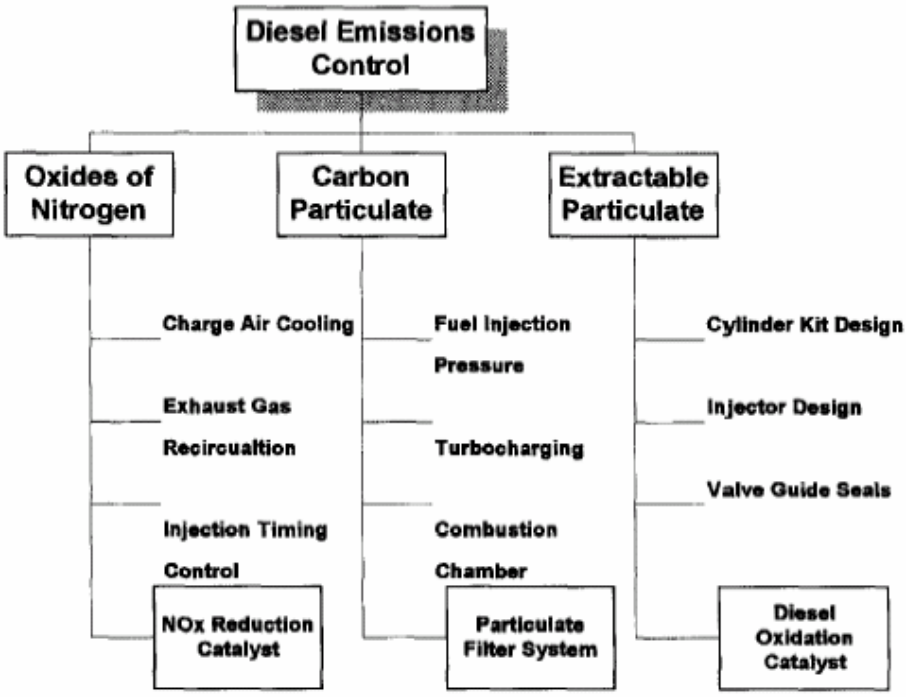

Figure 1.5: List of current techniques available to reduce diesel exhaust emissions. [8]

Table I: EPA standards for US passenger vehicles produced after model year 2004.

Category	50,000 miles/5 years						100,000 miles/10 years[1]					
	THC	NMHC	CO	NOx CI	NOx SI	PM	THC	NMHC	CO	NOx CI	NOx SI	PM
Passenger Cars	0.41	0.25	3.4	1.0	0.4	0.08	-	0.31	4.2	1.25	0.6	0.10
LLDT, LVW <3,750 lbs	-	0.25	3.4	1.0	0.4	0.08	0.80	0.31	4.2	1.25	0.6	0.10
LLDT, LVW >3,750 lbs	-	0.32	4.4	-	0.7	0.08	0.80	0.40	5.5	0.97	0.97	0.10
HLDT, ALVW <5,750 lbs	0.32	-	4.4	-	0.7	-	0.80	0.46	6.4	0.98	0.98	0.10
HLDT, ALVW >5,750 lbs	0.39	-	5.0	-	1.1	-	0.80	0.56	7.3	1.53	1.53	0.12

All units are in g/mile
All standards apply to FTP 75

1 – Useful life 120,000 miles/11 years for all HLDT standards and for THC standards for LDT

Abbreviations:
LVW – loaded vehicle weight (curb weight + 300 lbs)
ALVW – adjusted LVW (the numerical average if the curb weight and the GVWR)
LLDT – light light-duty truck (below 6,000 lbs)
HLDT – heavy light-duty truck (above 6,000 lbs)

Table II: EPA standards for US passenger vehicles produced after model year 2009.

Bin #	50,000 miles					120,000 miles				
	NMOG	**CO**	**NO_x**	**PM**	**HCHO**	**NMOG**	**CO**	**NO_x***	**PM**	**HCHO**
Temporary Bins										
MDPV[c]						0.28	7.3	0.9	0.12	0.032
10[a,b,d,f]	0.125 (0.160)	3.4 (4.4)	0.4	-	0.015 (0.018)	0.156 (0.230)	4.2 (6.4)	0.6	0.08	0.018 (0.027)
9[a,b,e]	0.075 (0.140)	3.4	0.2	-	0.015	0.090 (0.180)	4.2	0.3	0.06	0.018
Permanent Bins										
8[b]	0.100 (0.125)	3.4	0.14	-	0.015	0.125 (0.156)	4.2	0.20	0.02	0.018
7	0.075	3.4	0.11	-	0.015	0.090	4.2	0.15	0.02	0.018
6	0.075	3.4	0.08	-	0.015	0.090	4.2	0.10	0.01	0.018
5	0.075	3.4	0.05	-	0.015	0.090	4.2	0.07	0.01	0.018
4	-	-	-	-	-	0.070	2.1	0.04	0.01	0.011
3	-	-	-	-	-	0.055	2.1	0.03	0.01	0.011
2	-	-	-	-	-	0.010	2.1	0.02	0.01	0.004
1	-	-	-	-	-	0.000	0.0	0.00	0.00	0.000

All units are g/mile
All standards apply to FTP 75

* - average manufacturer fleet NOx standard is 0.07 g/mi

a - Bin deleted at end of 2006 model year (2008 for HLDTs)
b - The higher temporary NMOG, CO and HCHO values apply only to HLDTs and expire after 2008
c - An additional temporary bin restricted to MDPVs, expires after model year 2008
d - Optional temporary NMOG standard of 0.195 g/mi (50,000) and 0.280 g/mi (120,000) applies for qualifying LDT4s and MDPVs only
e - Optional temporary NMOG standard of 0.100 g/mi (50,000) and 0.130 g/mi (120,000) applies for qualifying LDT2s only
f - 50,000 mile standard optional for diesels certified to bin 10

1.3 Long-Term Catalyst Durability

The current EPA standards place a large emphasis on the durability of aftertreatment devices by requiring an operational lifetime of over 120,000 miles. As a result, aftertreatment design engineers have to factor in catalyst deactivation parameters to meet the regulation. Catalyst deactivation can occur as a result of a number of mechanisms, the majority of which occurs at molecular level. Figure 1.6 is an illustration of the most common deactivation mechanisms encountered during normal field-service operation-- *poisoning, fouling* and *sintering* [9].

Poisoning is the process in which unwanted feedstream components become chemically bound to the catalyst active sites. As shown in Figure 1.6, this mechanism has three different methods that affect catalyst durability. Selective poisoning is when the un-wanted compound is bound only to specific catalyst active sites. A typical example is the poisoning of platinum active sites by hydrogen sulfide as described by the following chemical reaction:

$$Pt_{(s)} + H_2S_{(g)} \rightarrow PtS_{(s)} + H_{2(g)}$$

This reaction results in strongly chemically absorbed sulfur to the platinum site, which inhibits further reactions from occurring at that site. On the other hand, non-selective poisoning results when contaminants are not preferentially absorbed on the catalyst sites. Leaching is the process of catalyst material removal by the formation of stable compounds that desorbs from the catalyst surface, usually at high temperatures.

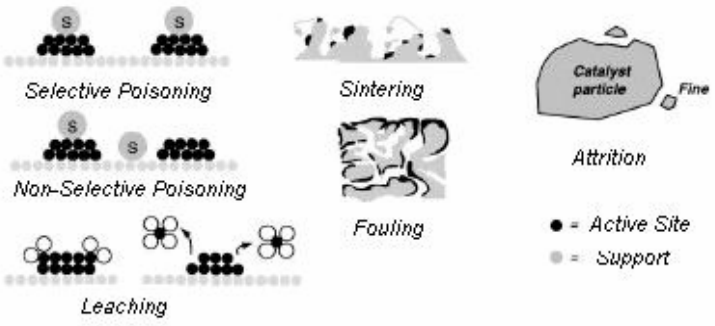

Figure 1.6: Common chemical catalyst deactivation mechanisms encountered during operation. [9]

Fouling, also known as masking or coking, is the large-scale effect of material accumulation on the catalyst surface, which covers active sites. This deactivation mechanism in exhaust aftertreatment is commonly the result of soot and other feedstream insolubles, such as ash, that accumulate on the oxidation catalyst. These contaminants agglomerate on either the catalyst surface or deposit within the porous structure of the washcoat, blocking diffusion of gaseous species to reaction sites. Diesel oxidation catalysts are engineered for such an environment under normal engine operating conditions, but improper combustion control often results in an increase of soot formation that can overwhelm the DOC and cause severe blockage. This event occurs if the rate of soot accumulation is significantly larger than the rate of soot oxidation.

Sintering, the last deactivation mechanism that commonly arises within aftertreatment devices, is the agglomeration of catalyst particles resulting from long durations at high temperatures within the exhaust environment. Platinum group elements (PGEs) such as platinum and palladium, two typical catalyst materials, are thermodynamically stable as metallic agglomerates but have a significantly lower reaction surface area. To maintain a high surface area, catalyst particles are well dispersed throughout a support material such as γ-Al_2O_3. In high temperature environments, however, catalysts particles have a very high migrate rate within the washcoat caused by a number of simultaneous mechanisms and coalesce into larger particles. For example, Ostwald-ripening is the random migration of individual atoms or molecules within or on a solid, which then coalesce to form larger particle agglomerates under the right circumstances [10]. During normal operation, in which exhaust temperatures are within catalyst design criteria, the sintering processes proceed slowly, but have a significant effect over the lifetime of the device.

The deactivation mechanisms have an effect on the overall reaction kinetics and need to be taken into account in the engineering of the aftertreatment devices. Figure 1.7 shows how the many deactivation mechanisms encountered during operation affect the reaction rate constant during oxidation reactions [9]. Reaction rates typically follow the general rate law described by equation 1.1:

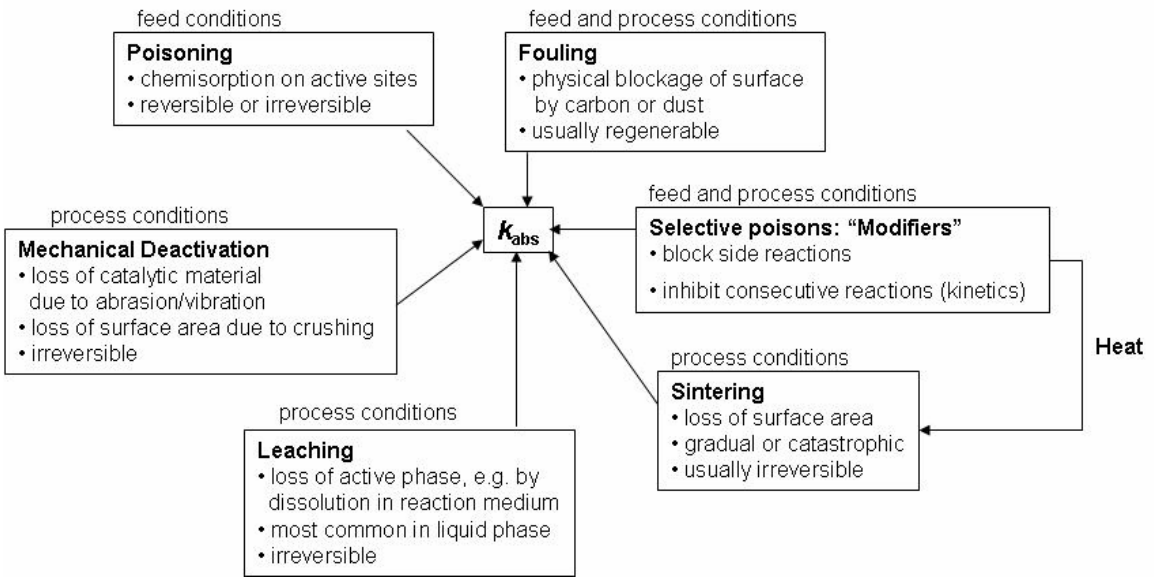

Figure 1.7: Effects of deactivation mechanisms on catalyst performance. [9]

$$-\frac{dC_j}{dt} = k_{abs} C_j^n \qquad \text{(Eq. 1.1)}$$

where C_j is the jth chemical species, n is the global order of reaction for that species and k_{abs} is the global rate constant for the disappearance of the jth chemical species. The order of reaction, n, and the rate constant, k_{abs}, are obtained experimentally for each reacting component as a function of temperature under defined feed stream conditions.

The least understood of the deactivation mechanisms is the poisoning process because of its highly complex nature. In automotive catalysts, exhaust gases can contain as many as 100 species, of which many exhibit poisoning behavior. Phosphorus and sulfur are the two most well known catalyst poisons and are derived from engine lube-oils and fuels. To minimize the poisoning effects of sulfur and the formation of sulfates, a contributor to PM, low- and ultra-low sulfur diesel fuels can be used. On the other hand, sulfur and phosphorus containing lube-oil additives such as zinc dialkyldithiophosphate (ZDDP) are needed for proper engine performance and durability. Studies performed by Chamberlin and Zalar [11], among others, have been aimed at

reducing the amount of ZDDP present in lube-oils, but there appears to be a minimum amount needed for proper antiwear and antioxidant performance. In an attempt to reduce toxic emissions, the EPA has proposed legislation to limit the presence of ZDDP to 0.01% by weight in lube-oil, with the knowledge that a minimum amount is needed until new, more environmentally friendly alternatives are found. Many studies, some dating back to the 1970's, have been performed as a result to understand the complex mechanisms involved with phosphorus poisoning. Although much is known about the poisoning behavior of phosphorus, many open questions remain on how to limit its impact on catalyst deactivation.

Field-service investigations of three-way catalysts (TWCs) and diesel oxidation catalysts (DOCs) have shown that phosphorus, zinc and sulfur-derived from ZDDP can become incorporated in the catalysts in a variety of forms depending on the deactivation mechanism. Studies of field-deactivated TWCs following lube-oil slip into the exhaust system at low exhaust temperatures have shown the formation of a zinc pyrophosphate, $Zn_2P_2O_7$, directly on the washcoat surface. The compound forms an amorphous glaze that acts as a diffusion barrier to catalyst active sites and micro pores; culminating in a reduction of light-off performance [12,13].

Other investigations of TWC poisoning resulting from high-mileage field-service with ZDDP present in the lube-oil have identified the formation of cerium orthophosphate, $CePO_4$, within the catalyst washcoat [14-18]. The formation of cerium orthophosphate has been linked to the high temperature decomposition of $AlPO_4$, which is a poisoning precursor resulting from the adsorption of phosphoric acid in the feed stream exhaust gases. This poisoning mechanism is shown to be detrimental to the oxygen storage component, CeO_2, during lean/rich conditions in SI operation and is thought to limit oxidation reactions within DOCs by reducing available redox sites [15-17].

Scanning electron microscopy and electron probe microanalysis studies of deactivated field-service catalysts have shown a preferential adsorption of phosphorus at the inlet portion of catalysts with a decreasing concentration profile along its length [14,18]. In addition, phosphorus is restricted to the top layers of the washcoat with

washcoat diffusion limited to a depth of typically 40 μm. Phosphorus, therefore, is shown to have a high affinity for washcoat materials and becomes strongly chemically absorbed.

To reproduce field-poisoning behavior, Ball et al. [19] used a combination of rapid ZDDP-doped lube-oil introduction and high-temperature aging with supplemental CO injection. They found that phosphorus profiles and FTP emissions in high-mileage TWCs could be accurately reproduced. Bunting et al. [20] performed DOC poisoning by accelerating the consumption rate of ZDDP lube-oils via three pathways that simulate field-service conditions: exhaust manifold, intake manifold and lube-oil-doped fuel injections.

As a precursor to catalyst poisoning, they performed exhaust phosphorus chemical studies using electrospray mass spectrometry each method of ZDDP introduction. They found that ZDDP-derived phosphorus in the exhaust gases is present in the form of H_3PO_4 for ZDDP passing through the combustion chamber and molecular fragments of ZDDP when injected directly into the exhaust manifold. The resulting phosphorus compounds on the DOC varied depending on the exhaust phosphorus chemistry present with phosphoric acid producing phosphates and fragmented ZDDP molecules yielding a zinc-phosphate glaze. THC and CO light-off performance degradation caused by the presence of phosphorus in the washcoat is consistent with previous studies of DOCs with similar deactivation mechanisms [8,12,14,18,19,21].

1.4 Scope of Investigation

The objective of the current investigation is to extend knowledge obtained from past investigations of phosphorus poisoning by analyzing new DOC formulations under accelerated poisoning conditions using a single-cylinder bench-mounted diesel engine. Deactivated field-service and rapid engine-poisoned DOCs of similar formulation will be compared on the basis of phosphorus content, phosphorus compounds formed and THC and CO light-off behavior. Correlations between engine bench-poisoned deactivation and in-service passenger bus DOCs will be obtained in order to replicate field-

deactivation mechanisms using a laboratory-scaled engine for the rapid development of new catalyst formulations and evaluate new lube-oil and fuel additives for catalyst poisoning behavior.

The engine utilized in this study is a 517 cc, naturally aspirated direct-injection (NA/DI) single-cylinder diesel engine and is used to accelerate DOC phosphorus poisoning by artificially increasing the consumption rate of ZDDP using three different methods: ZDDP-doped fuel injection, and exhaust and intake manifold injection. In each method, ZDDP is mixed with lube-oil to a concentration of approximately 10 times that of commercial lube-oil blends and injected at a rate of approximately 70 times that of normal engine consumption, resulting in a net increase of 700 times the rate of ZDDP consumed in normal operation. The rate of phosphorus consumption is therefore 0.5 g/hr, which corresponds to a doped-oil consumption rate of 50 cc/hr. A total of approximately 6.0 g of phosphorus is introduced into the exhaust system in each method.

Two fresh THC and CO light-off evaluations will be conducted at the beginning of each accelerated poisoning experiment after the DOC is de-greened for 4 hours at variable load cycles to ensure repeatability. THC and CO light-off performance is evaluated incrementally throughout the poisoning process to quantify the rate of poisoning experienced in each method. Finally, two evaluations are performed at the end of the poisoning tests to check the repeatability of the resulting light-off degradation. Three field-deactivated DOCs, each experiencing different deactivation modes and mileage history are evaluated for comparison to accelerated poisoning DOCs.

In order to identify the presence of phosphorus compounds in the exhaust gases during poisoning, electrospray mass spectrometry will be used. It has been shown by Bunting et al. [20] that phosphorus species in the exhaust gases vary depending on the method of ZDDP introduction; however, it is not known how engine load conditions may alter the resulting phosphorus compounds. Therefore, three accelerated poisoning DOC poisoning tests will be performed, each at a different engine load, form 0 to 100 % load, to determine if combustion temperatures have an effect on phosphorus chemistry within the exhaust gases.

Materials characterization of both field-service and accelerated poisoning DOCs will be performed using a multitude of analytic techniques. Scanning electron microscopy will be utilized to examine DOC surface topography, which has been shown in previous studies to vary depending upon the oil-derived contaminant present. Electron probe microanalysis will measure oil-derived contaminant concentration profiles along the length of the DOC as well as their penetration depth into the washcoat. X-ray Fluorescence spectroscopy will provide an overall bulk elemental concentration measurement of oil-derived contaminants within the DOC. Finally, wide-angle X-ray diffraction and X-ray photoelectron spectroscopy will be used to identify oil-derived compounds formed within the DOC as a result of poisoning.

Since engine-bench light-off evaluations are inherently noisy due to variability in both exhaust gas temperature and composition, a bench-flow reactor system will be utilized to increase the accuracy of light-off degradation measurements. The bench-flow reactor, however, cannot reproduce diesel emissions and requires the use of simulated diesel exhaust gases. In BFR testing, exhaust gas concentrations similar to the emissions measured from the laboratory diesel engine will be used. The exception is the hydrocarbon species, which will be replaced with 300 ppm ethylene, a fast hydrocarbon that is often used in literature as a diesel hydrocarbon surrogate.

It is expected that this work will provide a valuable engineering tool for the rapid development of new catalyst formulation and provide additional insight into the deactivation mechanisms associated with phosphorus poisoning. The additional knowledge of phosphorus poisoning behavior gained should contribute to the improvement of current technology by increasing the useful lifetime of diesel oxidation catalysts.

CHAPTER 2

LITERATURE REVIEW

This chapter presents an overview of the necessary technical background for the study of diesel oxidation catalysts. The DOC has been in service as a vehicle exhaust aftertreatment device for over 30 years. In that time, much work has been done to optimize the catalyst formulation for both performance and long-term durability. The complex nature of the chemical reactions occurring within the DOC during operation makes engineering based on fundamental physics difficult and forces the engineer to rely heavily on observation. Therefore, the majority of work cited in this section is the result of experimental investigations designed to measure the impact of different factors on DOC performance. Section 2.1 describes the diesel oxidation catalyst operation including its structure and catalyst materials. In Section 2.2, DOC deactivation by poisoning is presented in which factors and mechanisms leading to performance degradation in field-service catalysts are described. Finally, Section 2.3 provides information on rapid poisoning techniques in which high-mileage field-service DOC deactivation is simulated within a laboratory.

2.1 Diesel Oxidation Catalyst Operation

There are many intrinsic and extrinsic factors influencing the performance of oxidation catalysts. Figure 2.1 is a diagram showing the many different factors that must be taken into account for proper DOC performance [22]. Many of these factors are uncontrollable, such as lube-oil additives and fuel used by the owner. On the other hand, there are other factors that can be controlled such as precious metal loading, washcoat formulation, substrate material, cell density and design. The other parameters such as

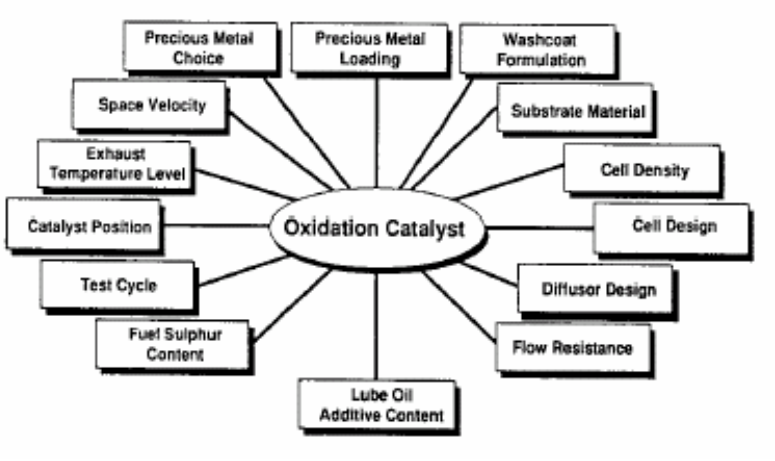

Figure 2.1: List of parameters affecting the performance of diesel oxidation catalysts. [22]

catalyst position, exhaust temperature, space velocity, flow resistance and diffuser design usually follow a design-loop engineering process in which a compromise is made between catalyst functionality and manufacturability. In the following sections, literature will be presented to show the effects of the control parameters on oxidation catalyst performance and what must be done in order to optimize performance.

2.1.1 The Platinum Group Elements

Catalyst material choice and loading are the most significant parameters affecting diesel oxidation performance. Since the principle objective of the oxidation catalyst is to remove the SOF components of soot, studies have been conducted to determine the best catalyst material choice for that application. Tashiro et al. [23] investigated three of the best-known catalyst materials – Pt, Pd and Rh – which are part of the platinum group elements (PGEs), for their ability to oxidize both the SOF components of soot and the gaseous THC using an engine-bench with traditional, high-sulfur diesel fuels. The loading of PGE within each catalyst was equivalent with similar washcoat and substrate formulations. Figure 2.2 shows the oxidation behavior of Pt/Al_2O_3, Pd/Al_2O_3, Rh-Pt/Al_2O_3 and catalysts as a function of temperature [23]. Pt has significantly more activity at low operating temperatures for both PM removal THC oxidation; however

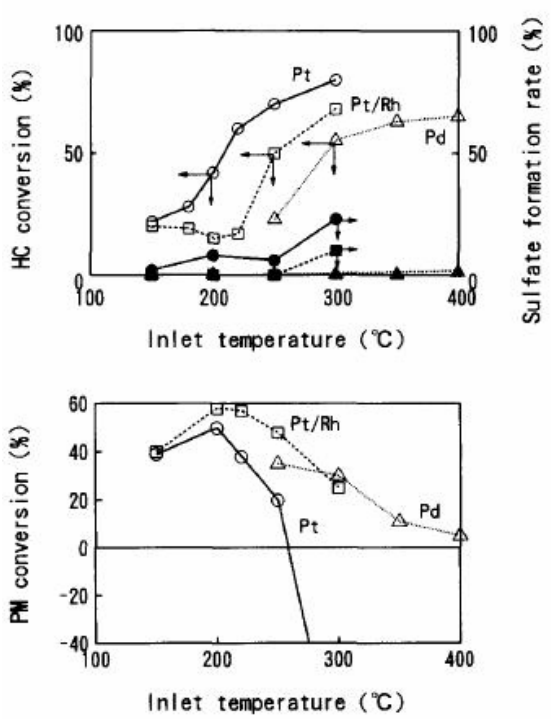

Figure 2.2: Comparison of Pt, Pd and Pt/Rh-loaded DOCs on the oxidation of THC and removal of PM as a function of temperature. Sulfate formation is plotted as dark lines. [23]

high temperatures culminate in higher rates of sulfate production that contributes to a net increase in PM emissions. The Pt/Rh catalyst performs slightly better than Pt in PM reduction but does not exhibit low-temperature THC oxidation activity. On the other hand, Pd does not participate in the formation of sulfates making it ideal for PM conversion. The THC conversion of Pd, however, requires high operating temperatures which can reduce the lifetime of the device.

Investigations by Daniels et al. [24] and Hosoya et al. [25] show that the use of low and ultra-low sulfur diesel fuels result in negligible sulfate production. Figure 2.3 shows the effect of Pt and Pd on the oxidation of PM, THC and CO using the Japan's diesel 13-mode cycle. Pt-loaded catalysts perform much better than Pd-loaded catalysts for both CO and THC conversions as well as smaller PM reduction. Figure 2.4 shows the PM distribution by type resulting from the test conditions in Figure 2.3. No sulfate production is observed from any of the tests using the ultra-low sulfur fuel.

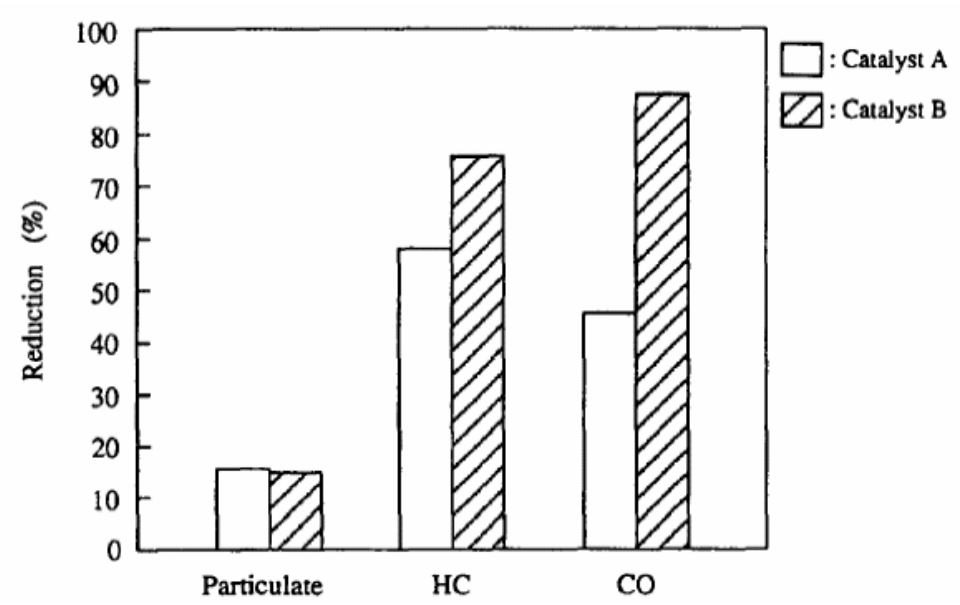

Figure 2.3: Pollutant reduction comparison of (A) Pd (2.0 g/l) and (B) Pt (2 g/l) loaded catalysts undergoing Japan diesel 13-mode cycle using ultra-low sulfur diesel fuel. [25]

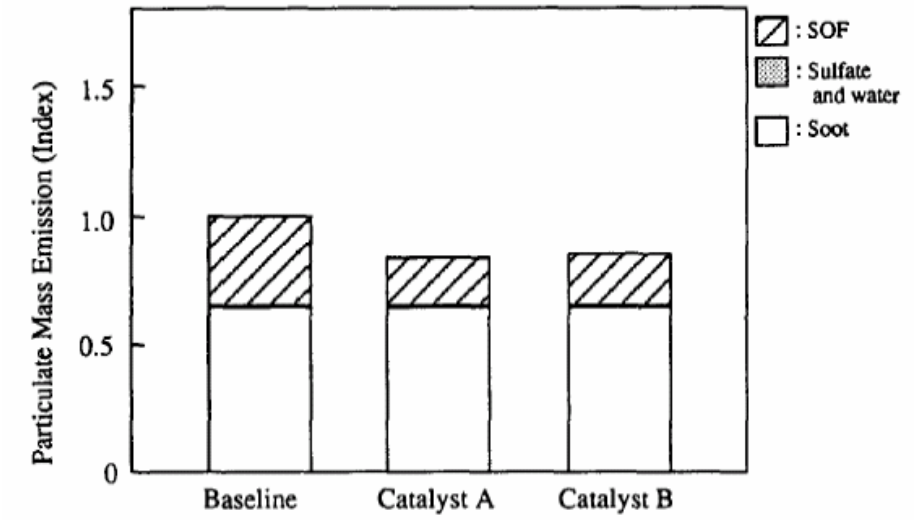

Figure 2.4: Particulate matter emission comparison of baseline, Pd (2.0 g/l) and Pt (2.0 g/l) loaded catalysts undergoing Japan diesel 13-mode cycle with ultra-low sulfur diesel fuel. [25]

Fredholm et al. [26] and Stein [27] investigated the optimal Pt-loading required to reduce THC and CO emissions below EPA standards of the time. Fredholm et al. used a 6.0 L diesel engine to age diesel oxidation catalysts with different Pt-loading for 1,000-hrs at normal operating conditions. A bench-flow reactor system using simulated diesel exhaust gases was used to evaluate the resulting THC and CO oxidation performance. Figures 2.5 and 2.6 are the results obtained by Fredholm et al. for THC and CO performance, respectively. It was found that higher Pt-loading results in both higher maximum THC and CO conversion and an increase in cold-start performance. Stein obtained similar results by comparing catalysts loaded with 0.35 and 0.07 g Pt/l. Measurements using a bench-mounted diesel engine demonstrate a significantly higher light-off temperature for both CO and THC and maximum conversions than those measured on the bench-flow reactor by Fredholm et al. Light-off temperatures between the 0.35 and 0.07 g Pt/l loaded catalysts differed by less than 40^{o}C. Stein, therefore, concluded that a high Pt-loading does not significantly improve light-off performance, but rather there is a minimum amount of Pt-loading needed to initiate oxidation.

Farrauto et al. [3] confirms the finding of Stein using three different DOCs loaded with 0.0, 0.02 and 0.07 g Pt/l, respectively. They used a 5.9 L diesel engine rated at a maximum power 230 hp to measure the light-off performance of each DOC and found that the DOC loaded with 0.02 g Pt/l had much better THC and CO light-off performance than the DOC with no Pt-loading and is within 50^{o}C of the DOC with 0.07 g Pt/l.

2.1.2 Rare Earth Metals – Cerium Oxide

Another important class of materials used in diesel oxidation catalysts is the rare earth metals. Investigations by Aneggi et al. [28] and Oran et al. [29] reveals that the addition of ceria (CeO_2) promotes catalyst activity by supplying additional reaction pathways for the oxidation of THC, CO and soot. The additional reaction pathways are a direct result of the redox behavior of CeO_2. In oxygen rich environments, cerium readily oxidizes to form CeO_2. This oxygenated state of cerium is passive because CeO_2 is

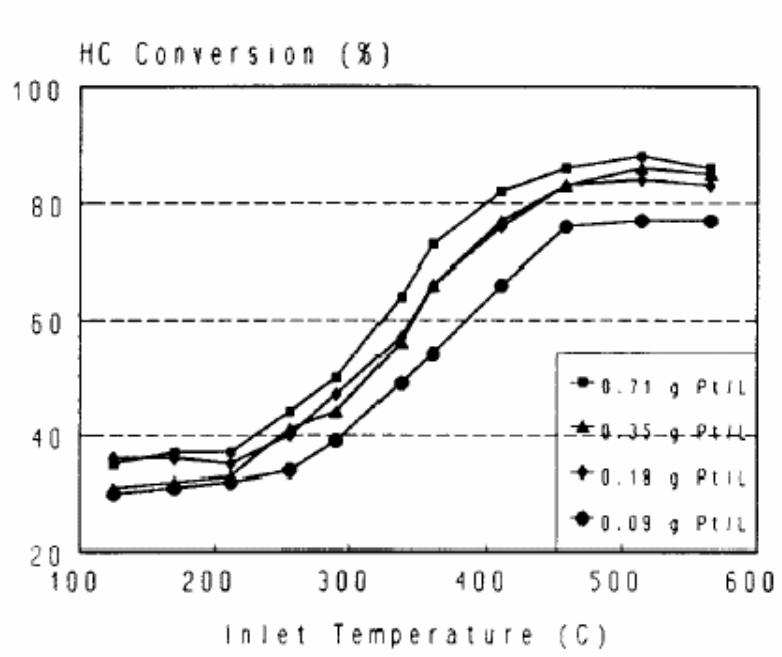

Figure 2.5: Bench-flow reactor THC light-off evaluations of four catalysts of different Pt-loadings. [26]

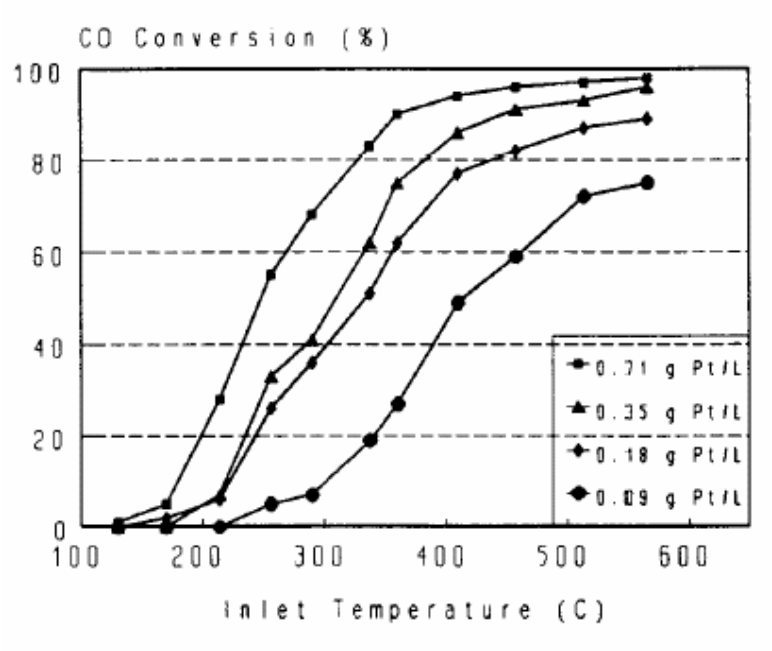

Figure 2.6: Bench-flow reactor CO light-off evaluations of four catalysts of different Pt-loadings. [26]

easily reduced to form cerium oxide (Ce_2O_3). This redox property of CeO_2 is used in to promote the oxidation of THC and CO in three-way catalysts by storing oxygen during fuel-lean phases and releasing the stored oxygen during the fuel-rich phases of operation. The oxidation of diesel emissions, which are always in the lean phase, benefit from the addition of CeO2 by increasing the rate of oxidation through additional heterogeneous reaction pathways. Figure 2.7 shows how the redox property of cerium provides two additional pathways for the oxidation of soot [28]. Similar reaction pathways exist for the oxidation of THC and CO in oxygen rich environments.

Oran et al. studied the effects of three different CeO_2-loaded three-way catalysts on the light-off performance of CO, each containing 1% Pt by weight dispersed in an Al_2O_3 support, using a bench-flow reactor with simulated exhaust gases. They found the addition of CeO_2, regardless of the loading, dramatically improved the light-off performance of CO, as seen in Figure 2.8 [29].

Investigations by other researchers support the findings of Oran and Aneggi using both laboratory engine and bench-flow reactor experiments [3,8,22]. CeO_2 is also observed to have a beneficial effect on the oxidation performance of CH_4 and THC.

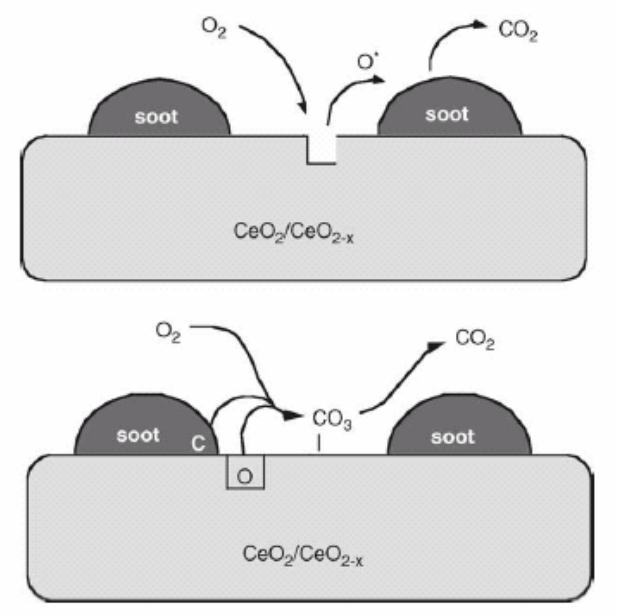

Figure 2.7: Redox route (top) and carbonate route (bottom) mechanism in the CeO_2-catalyzed combustion of soot. [28]

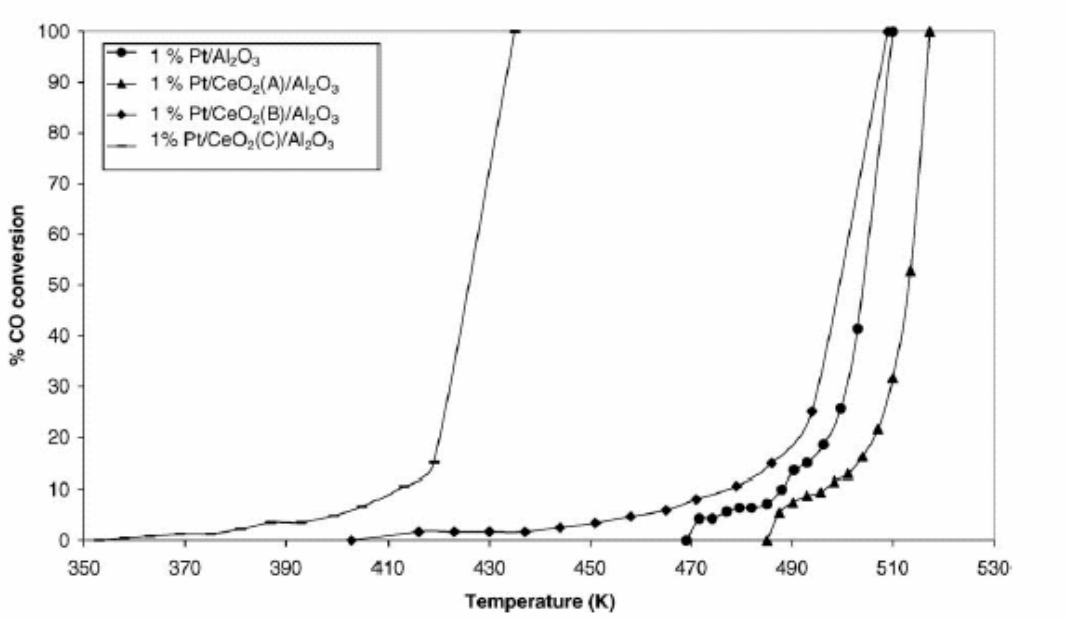

Figure 2.8: Bench-flow reactor CO light-off curves for three Pt/Al_2O_3 catalysts with different CeO_2 loadings. [29]

In these investigations, the incorporation of CeO_2 in the washcoat results in a significant increase of light-off performance compared to non-CeO_2 containing catalysts indicating that the redox property of CeO_2 also contributes to the oxidation of absorbed hydrocarbon species on the catalyst.

2.1.3 Structural Considerations

In addition to catalyst materials, structural considerations are also important in the design of diesel oxidation catalysts. Zelenka et al. [22] studied several different catalyst properties including substrate material, cell density and the catalyst-to-engine volume ratio on federal testing protocol (FTP) 75 emissions. In their investigation of substrate materials, they found that metal substrates provide lower pressure drops across the catalyst, but slower thermal response than ceramic substrates because metal substrates can be made into very thin sheets increasing the cross-sectional flow area. Ceramic substrates, on the other hand, have a highly porous structure, which is a poor conductor of heat and maintains the heat produced during reactions within the washcoat during low-

temperature operation. They concluded that turbocharged engines should employ metal substrates because of the high cross-sectional flow area, while ceramic substrates should be used in all other cases to provide both good thermal response and lightweight.

It is known from previous literature [30] that high cell density ceramic-substrate DOCs have a tendency to become clogged during cold starts. In order to determine the optimal cell density, Zelenka et al. used two different cell density ceramic substrates of 200 and 400 cpsi, respectively, with identical washcoat formulations. Figure 2.9 shows the resulting CO, HC and SO_2 conversion data obtained at a DOC temperature of 250^{o}C and an engine speed of 2500 RPM [22]. They found that more SO_2 is converted to form unwanted SO_3 products in the 200 cpsi catalyst. Therefore, a high cell density is desired provided that soot clogging during cold-starts can be avoided with advanced engine control techniques.

The effect of increasing the catalyst-to-engine volume ratio is equivalent to decreasing the space velocity of the exhaust gases in the DOC, since space velocity related to the volumetric flow rate of exhaust gases from the engine. The volumetric flow rate of exhaust gases, however, depends on the engine load and RPM; therefore, increasing the catalyst-to-engine volume ratio has the net effect of increasing the residence time of the exhaust gases over the entire engine output spectrum. FTP emission data gathered by Zelenka et al. shows that there is an optimum catalyst-to-engine volume ratio of approximately 1.5-2.0 for THC and CO conversion as shown in Figure 2.10. Due to cost restrictions, typical commercial vehicles have a catalyst-to-engine volume ration of 1.5.

2.1.4 Optimal Operating Conditions

The final class of variables affecting catalyst performance is the operating conditions experienced during operation. These factors include space velocity, temperature and pressure. During DOC operation, however, a low backpressure is required by most diesel engines for proper combustion control. Therefore, pressure experienced by the DOC is typically assumed to be atmospheric and constant. Space

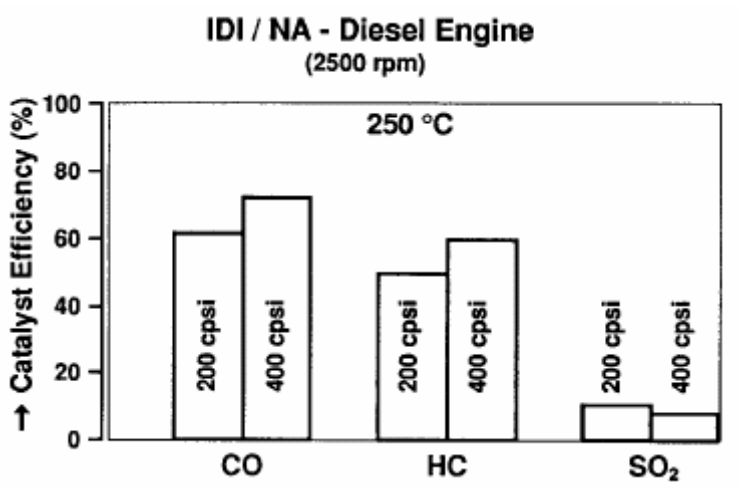

Figure 2.9: Effect of cell density on catalytic oxidation of CO, HC and SO_2. [22]

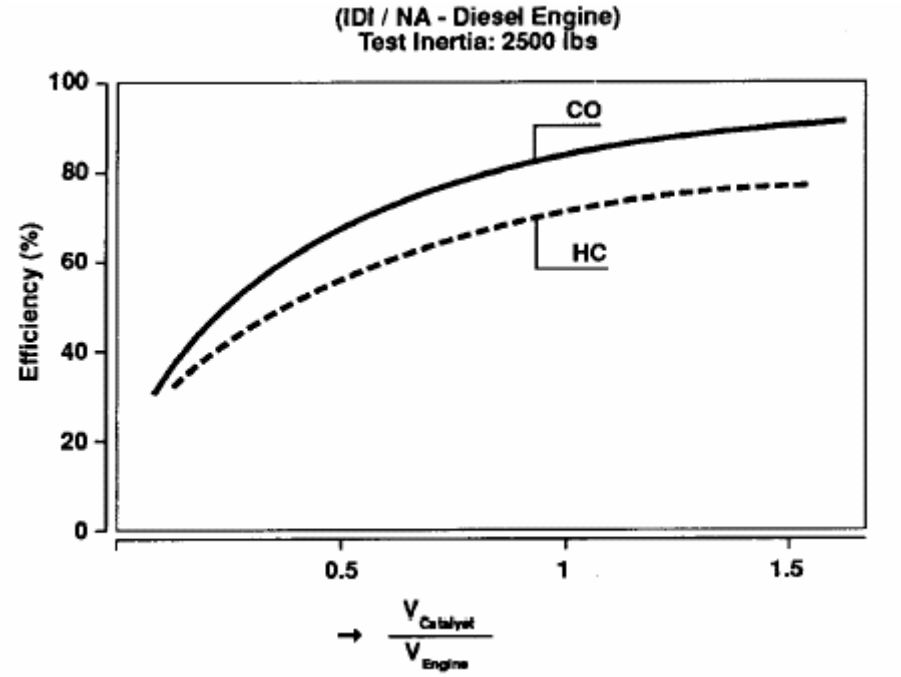

Figure 2.10: Effect of catalyst-to-engine volume ratio on CO and THC conversion. [22]

velocity is determined by the catalyst-to-engine volume ratio, engine capacity, engine load and RPM, as discussed in the previous section, and is therefore a fixed design parameter.

The only controllable parameter that can be optimized is the temperature of the exhaust gases encountered by the DOC during operation, which are determined by varying the location of the DOC in the exhaust system; the closer the catalyst to the engine exhaust manifold, the higher the exhaust gases temperature. The optimal operating temperature range, and hence location is determined by two factors: the light-off temperatures of unwanted exhaust species and the temperature at which SO_2 conversion is minimal. Figure 2.11 are the results obtained from Zelenka et al. [22] who investigated different engine load cycles to determine the optimal temperature range for the removal of particulate matter. SOF components during low-temperature operation are found to not completely reduced, while sulfate production became dominant during high temperature operation. Therefore, the optimal operating temperature range in their study, specific to their proprietary catalyst formulation and engine used, is between 170^o and 350^{o}C. This temperature range is similar to other diesel oxidation catalyst studies found in literature for other DOC formulations [1,23,26,27].

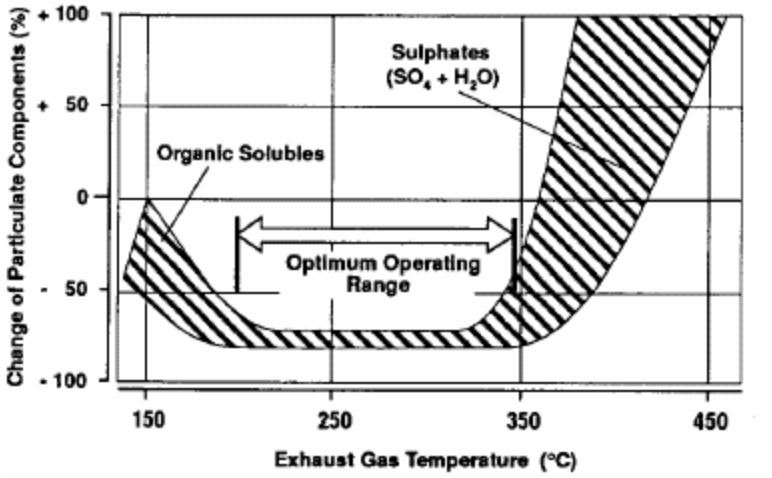

Figure 2.11: Effect of exhaust temperature on particulate matter reduction and formation within a commercial oxidation catalyst. [22]

2.2 Poisoning of Oxidation Catalysts – Field Observations

The deactivation of oxidation catalysts, as stated in Chapter 1, is a serious problem given that the EPA guideline for catalyst durability is 120,000 miles. Of all of the deactivation mechanisms that affect the oxidation catalyst's THC and CO light-off performance, poisoning is the most detrimental and the least understood. In automotive catalysts, sulfur and phosphorus are well-known poisons derived from diesel fuel and lube-oil additives. Since sulfur poisoning is, to a large extent, more controllable than phosphorus poisoning, much work has been performed over the past 30 years to understand the complex chemical mechanisms associated with phosphorus poisoning.

Post mortem catalyst analysis of field-deactivated automotive catalysts has revealed the presence oil-derived contaminants, including phosphorus, within the washcoat. Analytic techniques, such as X-ray Fluorescence Spectroscopy (XRF), Scanning Electron Microscopy (SEM), Electron Probe Microanalysis (EPMA), X-ray Diffraction (XRD), among others, have been used to characterize the chemical compounds, materials changes and phosphorus distribution within the washcoat as a result of the chemical adsorption of phosphorus. Researchers have also measured the loss in oxidation performance for field-poisoned catalysts by using either direct engine data or with the use of a bench-flow reactor using simulated diesel exhaust gases. Although, bench-flow reactor evaluations do differ from actual engine data in THC species, soot content and other feedstream impurities unique to diesel exhaust, it does provide the comparison and approximate performance measurements of automotive catalysts.

Much of the work of phosphorus poisoning on field-service deactivation is done on three-way catalysts, which typically contain a Pt or Pd/Rh/CeO_2/Al_2O_3 washcoat. This is because past EPA legislation on pollutant emissions required SI engines to use more controlled aftertreatment techniques, unlike the diesel engine that easily passed THC and CO emission standards with minimal aftertreatment. Although the formulations of three-way catalysts are different from those of diesel engines, the poisoning effects and resulting phosphorus chemistries are similar.

The amount of phosphorus present within the catalyst washcoat is directly related to the amount of lube-oil phosphorus used and the length of time in service.

Johnson et al. [33] investigated the effects of different lube-oil blends on the accumulation of contaminants on three-way catalysts and light-off degradation of THC and CO. A total of 20 identical vehicles, each using 1 of 5 different lube-oil blends was run in a taxi service until 100,000 miles were accumulated. The vehicles underwent FTP 75 emission testing and their catalysts were disassembled and analyzed for oil-derived contamination. The oil blends used during testing and concentrations of known oil-derived catalyst poisoning are listed in Table III.

Figure 2.12 shows the resulting FTP emission data for the median vehicle of each oil-blend group after 100,000 miles of service [33]. Vehicles with high phosphorus concentration lube-oils yield much higher THC emissions than those with low phosphorus concentrations. The use of oil 33, which has a phosphorus-containing additive, resulted in the worse THC emissions due mostly to the absence of any oil detergents. Oil blends 34 and 35, which contain no phosphorus, yield the best THC emissions. On the other hand, other contaminants such as Zn and Ca show no trend on THC emissions.

Elemental analysis of the disassembled catalysts shown in Table IV reveals that FTP emissions are highly dependent on the amount of phosphorus present within the washcoat as well as the presence of any oil detergents [33]. Oil 33, which produced the largest THC emission, also has the highest concentration of phosphorus. Other phosphorus containing oil blends result in phosphorus accumulation within the catalysts, but to a lesser degree. They attribute the phosphorus accumulation differences to the

Table III: Composition of test oils used by Johnson et al. in three-way catalyst deactivation testing. [33]

Oil Code	**32**	**33**	**34**	**35**	**36**
Detergent	Ca/Mg	None	Ca/Mg	Ca/Mg	All Ca
Analytical Data					
P, ppm	931	911	0	0	928
Ca, ppm	978	2	996	976	2144
Mg, ppm	657	3	649	693	12
Na, ppm	183	189	195	202	207
Zn, ppm	1054	1061	2	1088*	1056

* - Antiwear additive containing Zn but not P

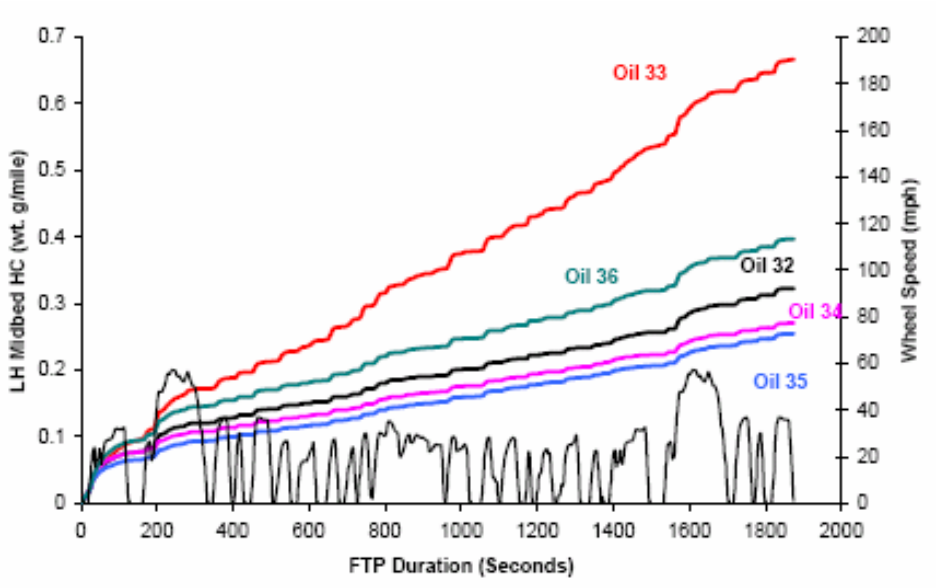

Figure 2.12: THC emissions for four vehicles aged 100,000 miles with different lube-oil additives. Phosphorus in the form of ZDDP is present in the three vehicles that yield the highest THC emissions. [33]

Table IV: Phosphorus, zinc, and calcium concentrations within 100,000 mile aged three-way catalysts and resulting THC and CO FTP emissions. [33]

Oil Used	Catalyst Contaminant Level wt.%			FTP Emission g/mi	
	Phosphorus	Zinc	Calcium	THC	CO
32	1.59	0.23	0.11	~0.3	~4.0
33	2.60	0.38	0.06	~0.6	~6.0
34	0.06	0.05	0.15	~0.15	~1.0
35	0.03	0.24	0.12	~0.15	~1.0
36	1.56	0.16	0.18	~0.3	~3.5

presence of oil detergents, which restricts the release of phosphorus from the engine and increase catalyst's lifetime.

Granados et al. [34] confirmed the presence of phosphorus in high-mileage three-way catalysts. In their study, a fresh and two field-deactivated three-way catalysts with 44,000 and 66,000 km, respectively, were analyzed for phosphorus, zinc and lead content using XRF. Their results, shown in Figure 2.13, reveal that phosphorus accumulation in three-way catalysts is higher with increasing operational history. A difference of approximately 1.2 P to Si mass atomic ratio (M/Si) is measured in catalysts with an increase of 22,000 km.

As in the study by Johnson et al., Granados et al. measured the decrease in THC and CO conversions resulting from the presence of phosphorus. A bench-flow reactor system flowing simulated diesel exhaust gases containing 900 ppm C_3H_6, 10 % CO_2, 10 % H_2O, 900 ppm NO, and Ar balance along with cycled CO, H_2 and O_2 concentrations is used. The concentrations of CO are varied between 0.4-1.6 %, while H_2 and O_2 concentrations are varied between 0.13-0.53 % and 0.77-1.37 %, respectively. In the high mileage catalyst, they measured a THC light–off temperature increase of approximately 50^{o}C and a CO light-off temperature increase of approximately 40^{o}C over the fresh catalyst.

XRD spectra obtained from these catalysts show the formation of cerium phosphate ($CePO_4$) and possibly zinc pyrophosphate ($Zn_2P_2O_7$), which have been identified in other studies. The authors concluded that the formations of these compounds are the major contributing factors increasing THC and CO light-off temperatures. The presence of $CePO_4$ reduces the overall redox behavior of CeO_2 [13,14,15], while $Zn_2P_2O_7$ is shown to act as a diffusion barrier on the catalyst surface [12].

Investigation by Williamson et al. [12], Angove et al. [35] and Angelidis et al. [18] showed that phosphorus preferentially absorbs within the first few centimeters of the catalyst inlet and deposited on the top layers of the washcoat. Phosphorus was observed to migrate into the washcoat to a depth dependent upon the average temperature of the exhaust gases, the time in operation and the surface phosphorus concentration on the

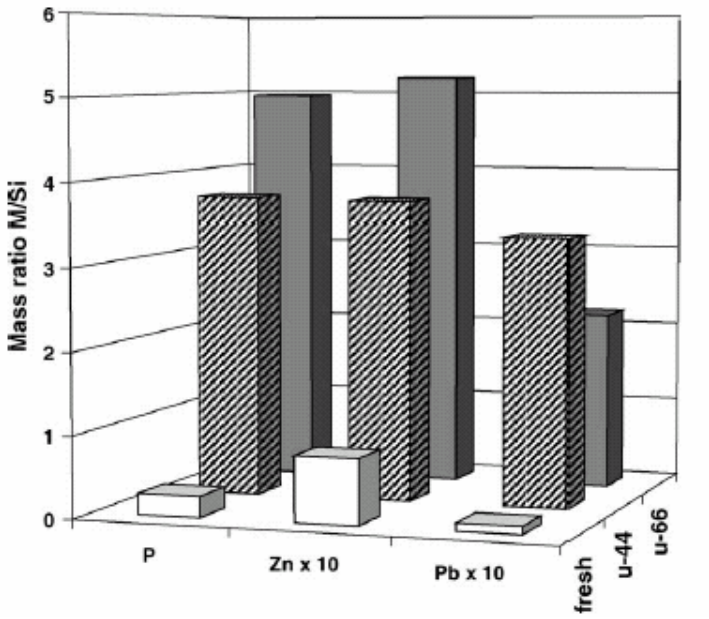

Figure 2.13: Comparison of phosphorus, zinc and lead to silicon atomic-mass ratio for 0, 44,000 and 66,000 km field-aged catalysts. [34]

washcoat. In the work of Rokosz et al. [14], two catalysts labeled T1 and T2 were obtained from the field that have accumulated 120,000 and 102,000 miles and were subsequently analyzed for phosphorus chemistry and phosphorus distribution with the washcoat. Table V shows XRF and BET results obtained at the front, middle and rear portions of the catalysts, which clearly demonstrates that phosphorus, zinc and calcium are all preferentially absorbed at the inlet portion of catalysts and act to reduce the available surface area within the washcoat. Figure 2.14 are SEM images of the front 3 cm of a field-deactivated catalyst, revealing a high surface concentration and a decreasing axial distribution of contaminants on the washcoat [14]. Materials covering the washcoat are determined to be oil-derived contaminants with a maximum thickness of 20 μm.

XRD spectra obtained from washcoat scrapped from the inlet portion of T1 and T2 indicates the formation of $(Mg, Ca)Zn_2(PO_4)_2$ and $(Mg, Ca, Zn)_3(PO_4)_2$ compounds resulting from the deposition of oil-derived contaminants. These complex molecules do not appear to diffuse into the washcoat but rather act as pore blocking agents.

Table V: Surface area and phosphorus, zinc and calcium concentrations for two field-deactivated catalysts at inlet, middle and rear locations. [34]

Catalyst	Location	Contaminant Levels (wt. %)			BET SA ($m^2/g_{catalyst}$)
		Phosphorus	Zinc	Calcium	
T1	Inlet	5.3	3.1	0.5	2.9
	Middle	2.5	0.5	0.0	7.6
	Outlet	1.2	0.3	0.0	7.7
T2	Inlet	3.3	1.6	0.4	5.0
	Middle	1.4	0.3	0.0	10.7
	Outlet	0.5	0.1	0.0	8.7

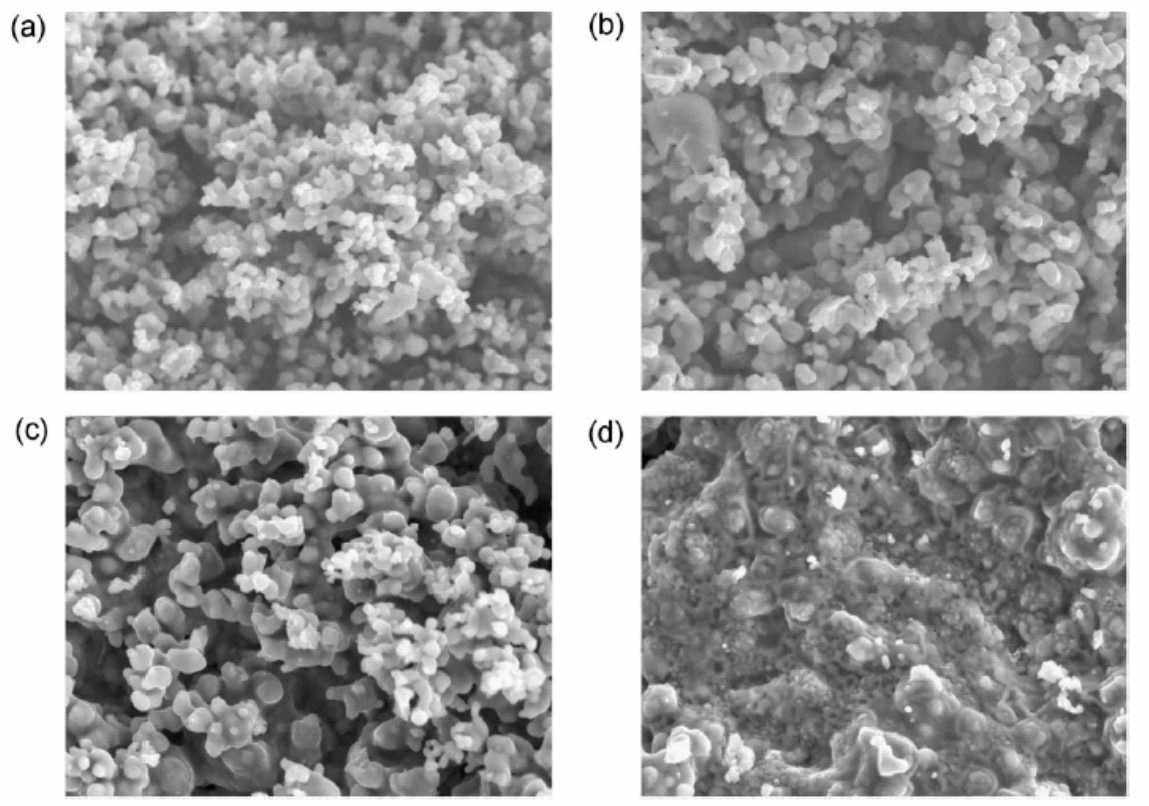

Figure 2.14: SEM images taken at (a) 0 cm, (b) 1 cm, (c) 2 cm and (d) 3 cm from the inlet of catalyst labeled T1. Each frame has a width of 23 microns. [14]

Phosphorus, on the other hand, is observed deep within the washcoat as seen in the EPMA images shown in Figure 2.15. Rokosz et al. identified the phosphorus compounds formed within the washcoat as $AlPO_4$, $Ce(PO_3)_3$ and $CePO_4$ with the use of XRD and ^{31}P and ^{27}Al nuclear magnetic resonance (NMR). Since only Ce and Al are found solely within the washcoat, they concluded that the diffusion of phosphorus into the washcoat is due to high temperatures that decomposed the meta-phosphates into ortho-phosphates. Larese et al. [16] also confirmed the presence of $CePO_4$ and $AlPO_4$ within the catalyst washcoat as a result of field-poisoning, but found that their presence is not dependent upon abnormally high temperature excursions.

To quantify the effect of phosphorus on THC light-off performance, Rokosz et al. used a bench-flow reactor system with simulated diesel exhaust gases consisting of 1500 ppm C_3H_6, 1 % CO, 2.29 % O_2, 10 % H_2O, 12 % CO_2 and N_2 balance. C_3H_6 light-off curves are plotted in Figure 2.16 for fresh, dyno-aged, and front, middle and rear sections of a field-deactivated catalyst [14]. C_3H_6 conversion is dependent on the amount of phosphorus accumulated in each sample. The fresh sample produces the best light-off performance while the inlet section of the field-poisoned catalyst, which has the greatest amount of phosphorus, produces the worst. The dyno-aged catalyst sample was plotted to show the effect of thermal degradation of catalyst performance. The dyno-aged sample experienced high temperature exhaust conditions for 120-hrs, which the authors claim simulates approximately 100,000 miles.

This catalyst was ensured to be devoid of any oil-derived contamination to isolate thermal effects only. Degradation due to poisoning alone is, therefore, distinguishable by the differences in the light-off curves. The most striking result of these plots is the distribution of light-off temperatures that directly correlate to the amount of phosphorus present in each catalyst sample.

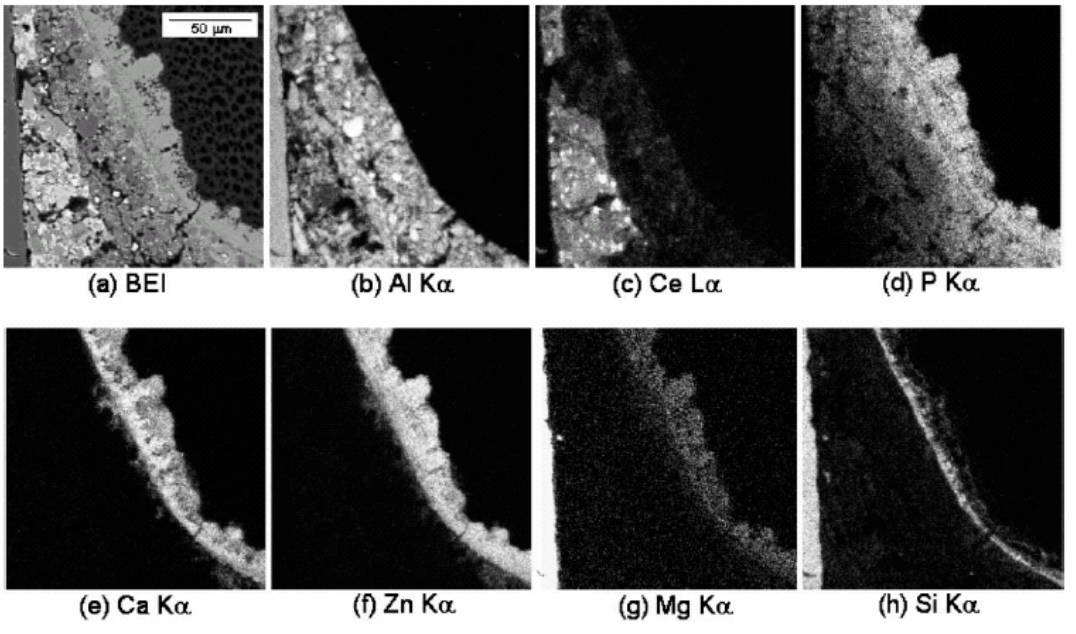

Figure 2.15: EPMA micrographs displaying elemental concentration profiles at a cross-section of the inlet of catalyst labeled T2. [14]

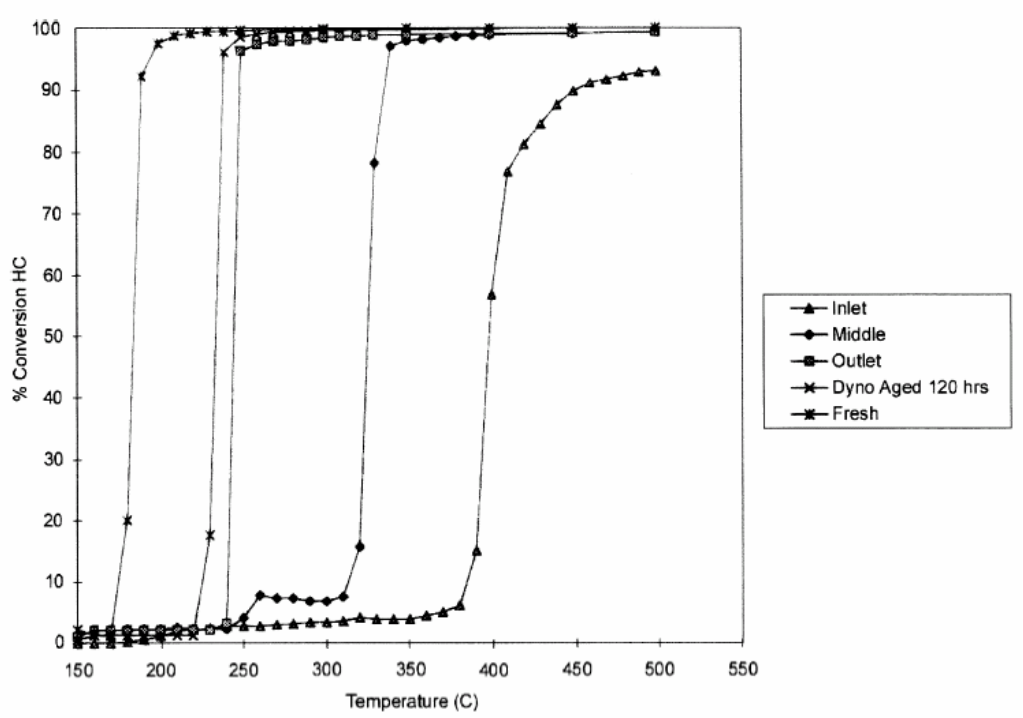

Figure 2.16: Bench-flow reactor light-off curves for propylene of a fresh, dyno-aged and field-poisoned three-way catalyst at three axial locations. [14]

2.3 Poisoning of Oxidation Catalysts - Rapid Aging

Since the poisoning of automotive catalysts occurs slowly over many years, many attempts have been made to artificially increase the poisoning rate of ZDDP-derived phosphorus using accelerated field trials, small and large-scale engine-benches and bench-flow reactors.

Large-scale engine catalyst poisoning experiments performed by Voss et al. [36] and Farrauto et al. [3] artificially aged diesel oxidation catalysts using a 400 hp, 14 L DI/TC diesel engine at elevated exhaust temperatures while using diesel fuel containing 0.3 wt. % sulfur. The catalysts were first de-greened for 24-hours using a 190 hp DI/TC engine using ultra-low sulfur diesel fuel. FTP measurements were performed to ensure catalysts were of comparable performance. The samples were then loaded three at a time into the exhaust system of the 400 hp diesel engine via a fixture allowing the parallel examination of each catalyst by providing the same volumetric flow rate of exhaust gases through each catalyst. Aging was performed using a 15-minute aging cycles consisting of the following time percentages.

- 14 % 330-400^{o}C
- 22 % 400-500^{o}C
- 50 % 500-550^{o}C
- 14 % 550-565^{o}C

The aging cycles were continued until a total of 1000 hours have been accumulated. Phosphorus was used in the crankcase lube-oil in the form of ZDDP and consumed via normal engine consumption. After aging for 100, 500 and 1000 hours, European transient tests (MVEG or Cycle A) were used to determine the degree of catalyst deactivation during accelerated poisoning.

Farrauto et al. used the aging cycle to evaluate a number of different catalyst formulations for long-term durability. Figure 2.17 is a plot of the resulting TPM, THC and CO conversions obtained for a $CeO_2/\gamma\text{-}Al_2O_3$ catalyst with 0.5 g Pt/ft^3 as a function

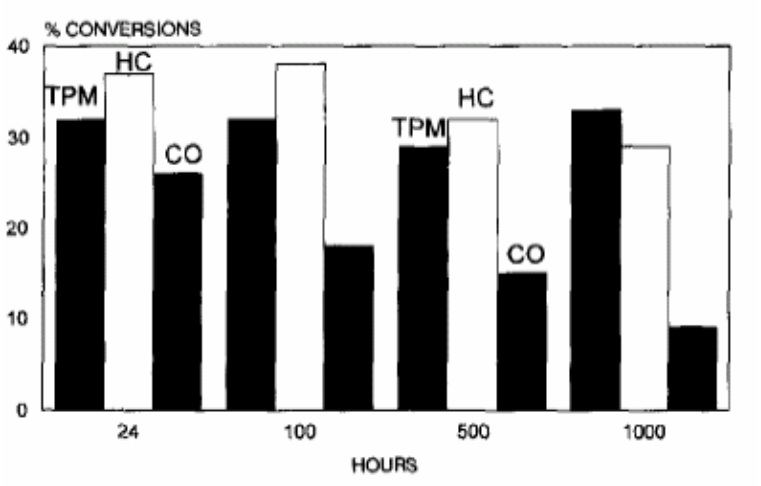

Figure 2.17: THC, CO and TPM conversions as a function of aging time for a $Pt/CeO_2/\gamma\text{-}Al_2O_3$ diesel oxidation catalyst. [3]

of aging time [3]. The particulate matter conversions are stable over time but CO and THC conversions steadily decrease with CO being the most affected.

Line-scans obtained using EPMA for the above-mentioned catalyst confirmed the accumulation of P, Zn, S and Ca within the washcoat. Figure 2.18 shows the concentration profiles of P, S, Ca and Zn in the washcoat at a cross-section at the inlet portion of a 1000-hour aged diesel oxidation catalyst [3]. Phosphorus, zinc and calcium all remain on the catalyst surface with little bulk washcoat diffusion. Sulfur, on the other hand, diffuses deeply into the washcoat and is uniformly dispersed throughout. This result closely resembles that of field-poisoned catalyst undergoing normal operating conditions. The exception is the presence of a high zinc surface concentration on the washcoat. Field studies by Angrove et al. [37] confirmed the presence of zinc on the washcoat, but concentrations did not exceed 2.0 wt. %, which is four times less than that measured by Farrauto et al. in the rapid-poisoning experiments. Angrove et al. also measured phosphorus concentrations of approximately 8 wt. % in contrast to the 12 wt. % measured by Farrauto et al.

Identical aging tests to those of Farrauto et al. conducted by Voss et al. [36] confirmed the presence of oil-derived contaminants on the diesel oxidation catalyst as well as high surface concentrations of P, Zn, S, and Ca on the washcoat after 1000 hour

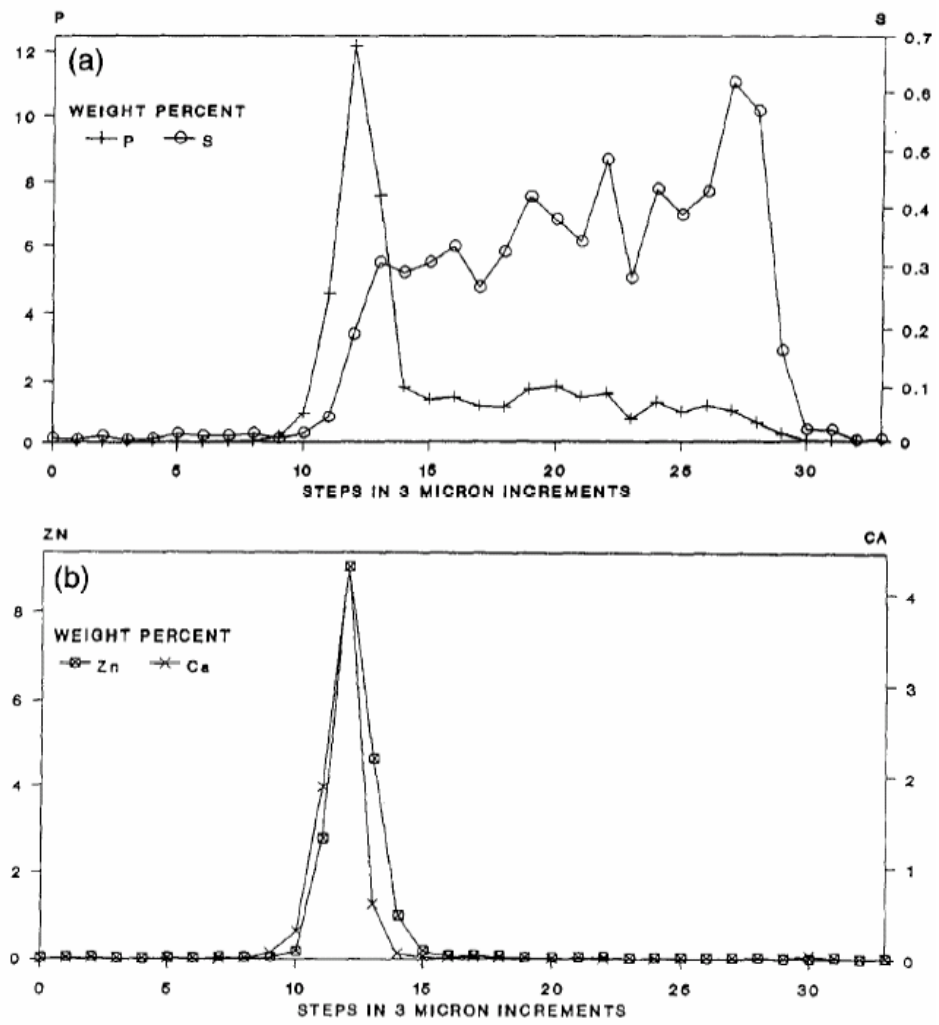

Figure 2.18: Phosphorus, sulfur, zinc and calcium concentration profiles at a cross-section of the inlet of a 1000-hour engine-aged diesel oxidation catalyst. [3]

of aging cycles. They also performed XRF analysis at the front, center and rear portions of the catalysts at aging times of 50 and 500 hours to determine the rate of phosphorus accumulation and the catalyst location at which phosphorus absorption takes place. Table VI shows the accumulation of P and Zn for each section of the DOC as a function of time. They observed that after 50 hours no appreciable phosphorus or zinc accumulation is observed. At 500 hours, however, a significant amount is observed on the front portion of the diesel oxidation catalyst. These observations were also seen in accelerated engine tests conducted by Ball et al. [19] who measured a strong axial phosphorus profile along the catalyst length.

In an attempt to reduce the amount of time necessary to produce catalyst poisoning by phosphorus, Fredholm et al. [26] performed accelerated phosphorus poisoning using two different bench-mounted diesel engines, to produce different GHSV, which consume phosphorus in the form of a ZDDP/diesel fuel blend by direct injection into the combustion chamber. Each engine consumed the same sulfur and ZDDP concentrations of 0.05 % and 0.1 %, respectively to determine which GHSV will produce the fastest phosphorus poisoning catalyst deactivation. Aging cycles similar to those of Farrauto et al. were used but with a one-hour cycle aging time. Once the catalysts were age for a fixed number of hours, a bench-flow reactor system with simulated exhaust gases consisting of 200 ppm CO, 90 ppm C_3H_6, 80 ppm SO_2, 1200 ppm NO, 10 % O_2, 7.5 % CO_2, 6.4 % H_2O and N_2 balance at a gas hourly space velocity of 65,000 hr^{-1} was used to plot CO and THC light-off evaluations.

Table VI: Phosphorus and zinc accumulated on a diesel oxidation catalyst undergoing 50 and 500 hours of engine-aging. [36]

Aging hrs.	Position	% P_2O_5	ppm Zn
0	-	0.04	16
50	Front	0.06	21
	Center	0.04	18
	Back	0.04	17
500	Front	0.51	83
	Center	0.19	54
	Back	0.10	45

Since catalyst deactivation by phosphorus poisoning did not produce significant CO and THC light-off degradation after a 200-hour aging cycle, the accumulated cycle aging time was increased to 500 and 1000 hours. Figure 2.19 shows the THC and CO light-off curves at 0, 200, 500, and 1000-hour aging times. CO is shown to be largely unaffected by the aging cycles with a light-off temperature increase of approximately 20^{o}C and a maximum conversion of CO of nearly 100 % except for the 1000-hour aging cycle test. THC conversion is affected to a larger extent with an increase in light-off temperature of approximately 90^{o}C. The THC conversion measured by Fredholm et al. is, like CO, better than that observed in field-service catalysts. This result is not explained by post mortem analysis of the catalyst after the 1000-hour aging cycles. Table VII shows the phosphorus accumulated at the front and rear of the phosphorus-poisoned catalyst as well as available surface area. Although significant phosphorus accumulated on the catalysts, four times more than measured by Voss et al., however, loss of performance was not as severe. This is attributed to the difference in catalyst formulations; Fredholm et al. used catalysts with significantly more platinum.

The use of small engines for the rapid poisoning and evaluation of diesel oxidation catalysts have proven to be a valuable tool for the study of phosphorus poisoning behavior due to their ease of use and low cost of operation compared to full-scale engine methods. In addition, the use of small engines can produce phosphorus poisoning behavior more rapidly due to the decrease in catalyst volume, accelerating the testing time from hundreds of hours to a few days.

Bunting et al. [20] used a bench-mounted single-cylinder diesel engine to accelerate phosphorus poisoning of DOCs using three different methods that simulate

Table VII: Phosphorus accumulation and available surface area of a fresh and 1000-hour engine-aged diesel oxidation catalysts. [26]

Sample	P_2O_5 (%)	BET Area ($m^2/g_{catalyst}$)
Reference	<0.01	30
Inlet	2.0	20
Outlet	0.4	27

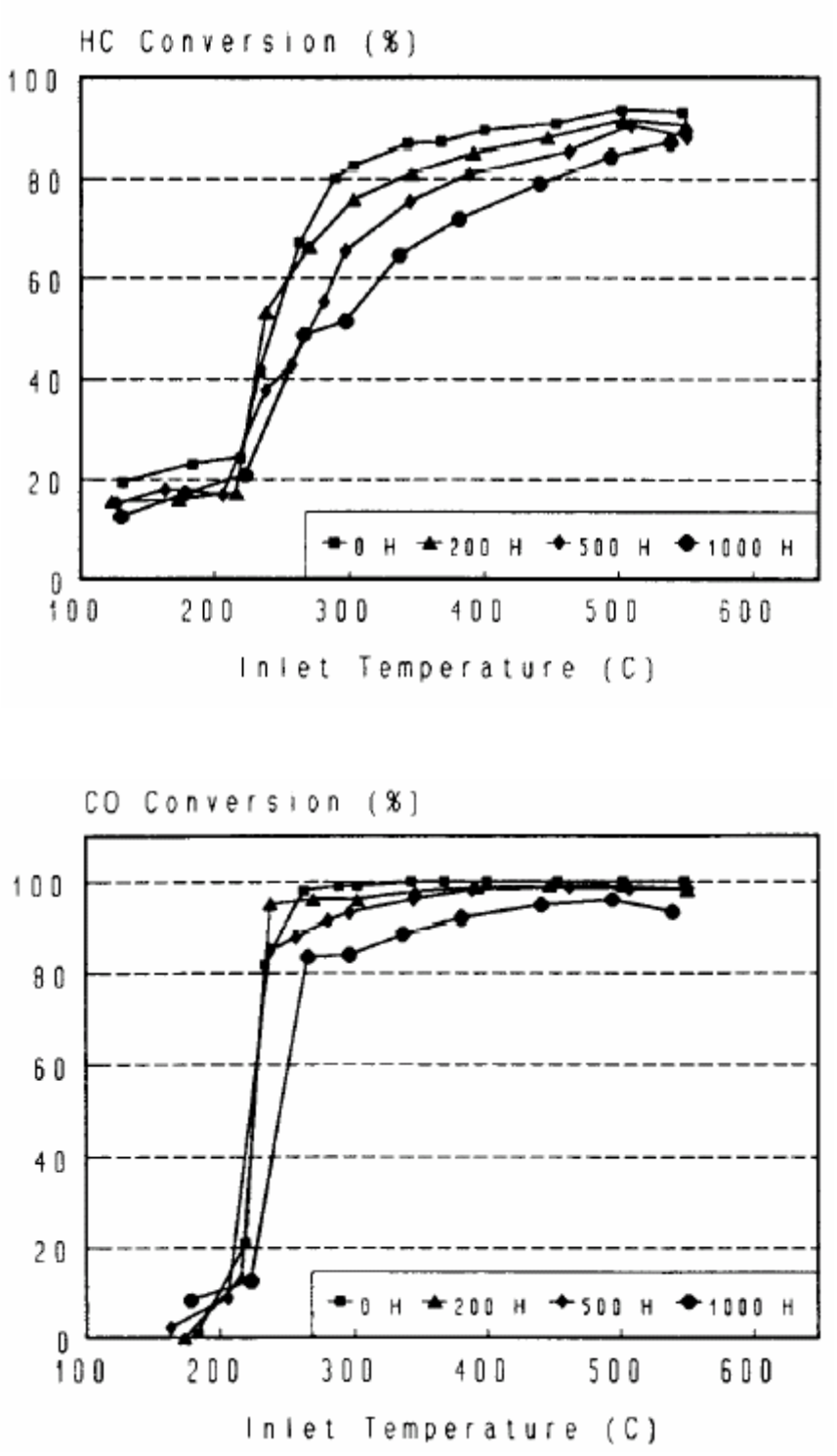

Figure 2.19: THC and CO light-off curves at various engine-aging cycle intervals. [26]

field-service poisoning pathways. Phosphorus in the form of ZDDP is injected at a rate of 700 times that of normal engine oil consumption into either the intake or exhaust manifolds or mixed with fuel and injected directly into the combustion chamber. A total of 3 g of phosphorus is injected for each poisoning method with THC and CO light-off evaluations performed every 0.5 g of phosphorus to measure the progression of DOC deactivation. As a precursor to DOC poisoning, they used electrospray mass spectrometry to analyzed exhaust phosphorus chemistry, from which correlations could be made between phosphorus exhaust chemistry and DOC deactivation.

They found that ZDDP passing through the combustion chamber, i.e., by intake manifold injection or fuel injection poisoning, decomposed to form phosphoric acid (H_3PO_4), while ZDDP injected directly into the exhaust manifold was present in the exhaust as intact ZDDP molecules and their molecular fragments. The resulting phosphorus poisoning behavior is highly dependent on the method of phosphorus introduction. As seen in Figure 2.20, exhaust manifold injection produced an amorphous zinc-phosphate glaze on the catalyst surface. The zinc-phosphate glaze is similar to the zinc pyrophosphate glaze found by Williams et al. [12] using a pulsed-flame combustor system in which isooctane doped with ZDDP was injected directly into the reactor. Phosphorus accumulated within the DOC was found to be restricted to the top few microns of the DOC with a strong axial gradient along the length of the DOC with more phosphorus accumulation at the inlet.

On the other hand, when Bunting et al. passed ZDDP through the combustion chamber, phosphorus is found to diffuse much deeper in the washcoat and no zinc accumulation was measured. They speculate that ZDDP decomposed in the combustion chamber during injections, converting zinc into zinc oxides or zinc phosphates. These compounds are very stable and transit through the DOC without reaction. Phosphorus accumulation resulting from ZDDP passing through the combustion chamber is significantly greater than that found during exhaust manifold injections showing higher surface concentrations and deeper washcoat penetration depths. As observed in exhaust manifold injection poisoning, a strong negative axial concentration profile is present indicating that phosphorus has a high affinity for the washcoat regardless of its chemical

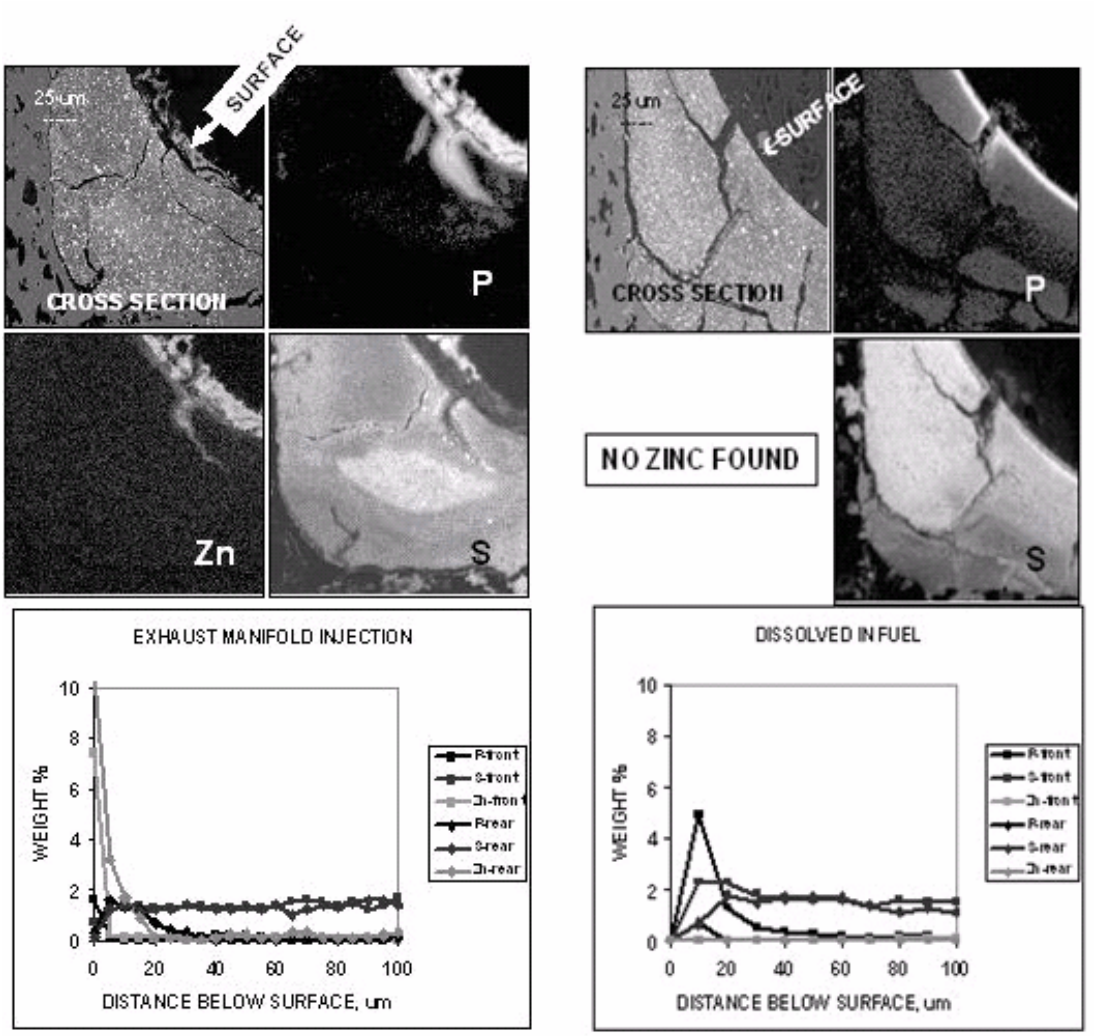

Figure 2.20: EPMA micrographs and line-scans of phosphorus, zinc and sulfur of diesel oxidation catalysts poisoned by exhaust manifold and ZDDP-doped fuel injection methods. [20]

make-up. Field-service contaminant adsorption behavior is more consistent with intake manifold and ZDDP-doped fuel injection poisoning mechanisms indicating that phosphorus poisoning during normal engine operating is due to the presence of phosphoric acid.

XRF analysis of the poisoned catalysts reveals that the amount of phosphorus and zinc collected on the catalysts is within range of that measured in field-service catalysts by Johnson et al. Collection efficiencies, however, depended greatly on the method of poisoning used. Table VIII shows the amount of phosphorus, zinc and sulfur in the catalysts undergoing the three different poisoning methods and the collection efficiency observed for each oil-derived contaminant. Exhaust manifold injection has the highest collection efficiencies for both zinc and phosphorus, while fuel injection poisoning collects the most sulfur.

THC and CO light-off performance degradation resulting from the three poisoning methods are plotted as a function of phosphorus injected in Figure 2.21. Light-off performance degradation in the case of ZDDP that passes through the combustion chamber is less severe. On the other hand, exhaust manifold injection poisoning exhibits more sever deactivation, which is in agreement with the XRF results – phosphorus is collected more efficiently in exhaust manifold injection poisoning.

Table VIII: Phosphorus, sulfur and zinc accumulation and collection efficiencies for three accelerated DOC poisoning protocols. [20]

Catalyst/ Lube-oil	S, wt.%	Efficiency S, %	P wt.%	Efficiency P, %	Zn wt.%	Efficiency Zn, %
ZDDP Doped Oil	2.40	-	1.12	-	1.15	-
New	0.00	-	0.01	-	0.00	-
Intake Manifold Injection	0.79	11.26	0.34	10.40	0.00	0.08
Exhaust Manifold Injection	0.78	16.47	0.64	28.93	0.22	9.76
Dissolved in Fuel	1.22	20.41	0.33	12.04	0.00	0.16

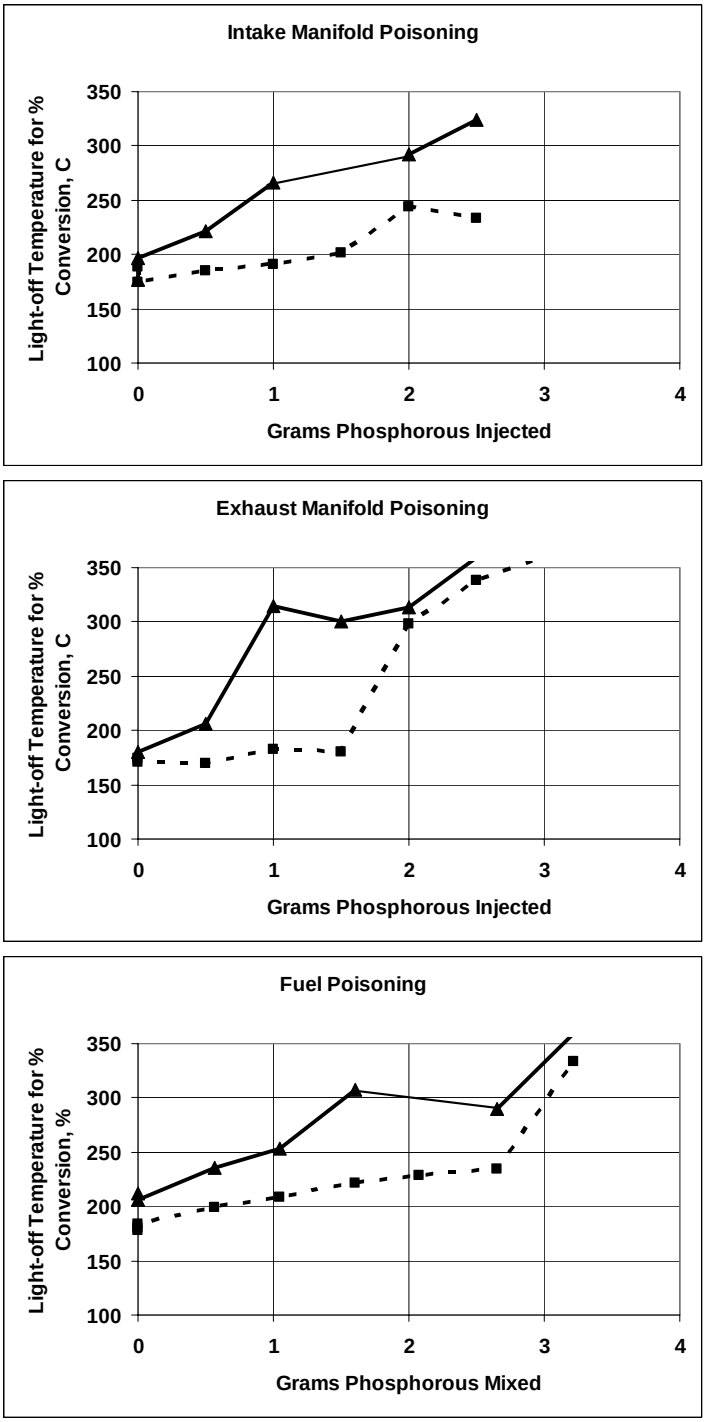

Figure 2.21: THC and CO light-off degradation as a function of phosphorus introduction for three accelerated DOC poisoning protocols. [20]

In the current study the phosphorus poisoning behavior of diesel oxidation catalysts will be performed using a small bench-mounted diesel engine, since they have been shown to considerably decrease the time needed to produce DOC deactivation. Rapid ZDDP introduction methods, similar to those used by Bunting et al., will be examined for both THC and CO light-off deactivation behavior as well as materials changes due to the adsorption of oil-derived contaminants. In order to determine the applicability of accelerated phosphorus poisoning to actual poisoning found in the field, three field-deactivated DOCs will be evaluated using the small bench-mounted engine. Comparisons of the deactivation behavior of DOCs from rapid ZDDP introduction methods and those found in the field will result in the creation of rapid poisoning protocols for the rapid development of new catalyst formulations as well as screen oil and fuel additives for DOC poisoning behavior.

CHAPTER 3

EXPERIMENTAL APPARATUS AND PROCEDURES

This chapter describes the experimental apparatus used, the catalyst formulation and geometry specifications, and the testing procedures employed for the evaluation of catalyst performance. A description of surface characterization techniques is also provided. Section 3.1 offers an overview of the engine bench for rapid poisoning. Section 3.2 describes the bench-flow rector system and its associated components. Section 3.3 discusses the catalysts used during the study. Finally, Section 3.4 provides a detailed overview of the variety of surface characterization techniques used throughout this study.

3.1 Engine Bench for Rapid Poisoning

3.1.1 Overall Description of Rapid Poisoning Engine Bench System

The engine bench rapid poisoning system (RPEB) system utilized for this investigation is located at the Oak Ridge National Laboratory within the Fuels, Engine and Emissions Research Center. The experimental apparatus is nearly identical to that described by Bunting et al. [20] and was developed by at the Center prior to the investigation. A schematic of the RPEB is shown in Figure 3.1. The RPEB comprises of four major components; a bench-mounted single-cylinder diesel engine, an electric drive motor, a DOC-mounted assembly and an emissions analyzer bench. The Hatz diesel engine is connected to a Baldor electric drive motor via a flexible shaft couple and they are both bolted to a metal bench. The bench is enclosed in an acoustically-isolated test chamber outfitted with a vented exhaust duct and forced circulating fresh air. The engine is a 517 cc diesel and was chosen in order to minimize the expenses and mechanical problems associated with full-scale testing. In addition it is capable of providing diesel

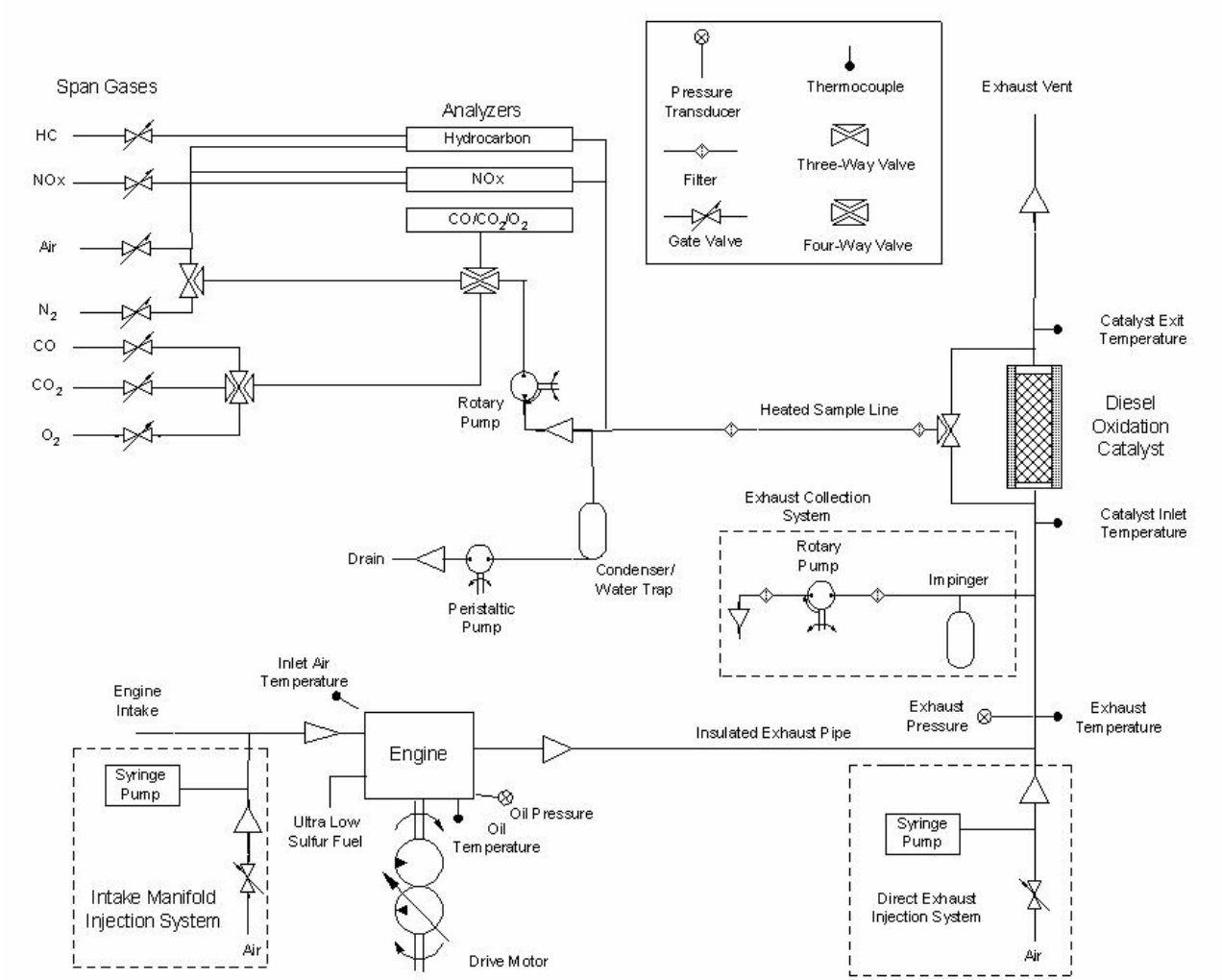

Figure 3.1: Schematic of the RPEB system

exhaust that is similar to full-scale heavy-duty diesel engines. The DOCs used in this study are also smaller than the traditional heavy-duty DOCs. A typical heavy-duty engine DOC consists of two inline catalysts, each 20.32 cm in diameter and 20.32 cm in length. The experimental catalysts consist of a single catalyst 5.08 cm in diameter and 7.62 and 15.24 cm in length. The reasoning behind this approach is to rapidly screen the catalysts for poisoning effects; any tests that are deemed to be interesting can be reproduced at a later time in full-scale. Throughout the present investigation, #2 ultra-low sulfur fuels ranging from 3 and 15 ppm sulfur are used in order to reduce sulfur contamination of the test catalysts. Sulfur has been widely documented as a catalyst poison; therefore reducing its effects on catalyst performance will enhance the ability to measure poisoning effects due solely to ZDDP-derived contaminants. The engine load controller consists of a servo-motor that is linked to the engines' fuel regulator and controlled by an analog feedback control system; a potentiometer located in the control room adjusts the position of the servo-motor. This allows the engine to operate at desired exhaust gas temperatures during poisoning or light-off evaluations. A photograph of the RPEB and ancillary equipment is shown in Figure 3.2.

Exhaust temperatures are measured at three different locations along the exhaust pipe using type K thermocouples. The first thermocouple is positioned approximately 0.3 m from the engine exhaust manifold and measures the engine exhaust temperature. The second and third thermocouples are located approximately 15 cm from the inlet and exit of the DOC, respectively, and are used to determine the average catalyst temperature. Two pressure transducers located near the exhaust manifold are used to measure the engine backpressure and the pressure drop across the DOC – one measures gauge pressure and another for absolute pressure. It is assumed that the pressure at the exit of the DOC is atmospheric; therefore, the pressure drop in the DOC can be approximated by measuring pressure at one location. The diesel oxidation catalyst is positioned approximately 2.0 m from the engine exhaust manifold and mounted into a 5.08 cm-diameter pipe. Vermiculite-coated ceramic fiber matt is placed between the DOC and the pipe walls to act as insulation and protection during thermal expansion while preventing

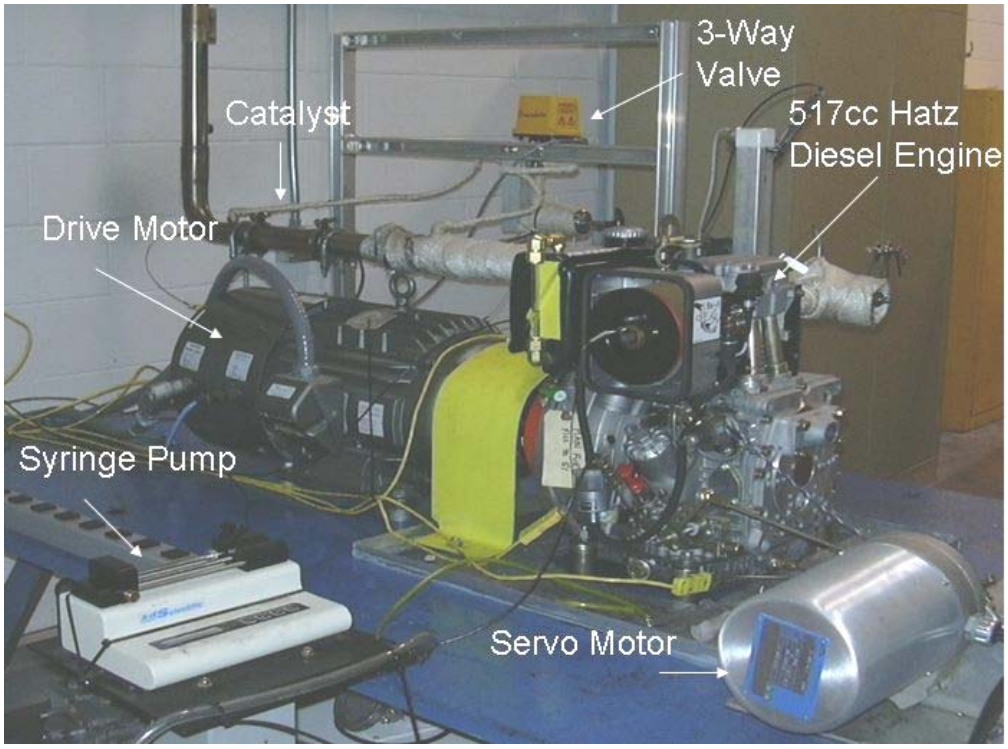

Figure 3.2: Photograph of the RPEB system bench components.

gas slip. The exhaust pipe is wrapped in insulation to maintain an exhaust gas temperature at the catalyst inlet representative to that of normal driving conditions.

A manually activated high-temperature three-way switching valve is used to sample the exhaust gases at the inlet and outlet locations of the DOC. The step motor driven three-way valve allows the selection of exhaust gases entering or leaving the catalyst to be sent to the analyzer bench. Heated cartridge filters located directly downstream of the three-way valve and directly in front of the analyzer bench remove any carbonaceous material present in the exhaust gases that cause analyzer fouling. The exhaust gases are carried, via a temperature controlled heated sample line, to the analyzer bench, shown in Figure 3.3, for the volumetric concentration measurement of O_2, CO, CO_2, NO_x and THC. The flame ionization detector (FID) and the chemiluminescence analyzer each have an internal heated sample pump while the infrared analyzer utilizes an external vacuum pump located within the analyzer bench. Water is removed from the system before the infrared analyzer, but after the FID and chemiluminescence analyzer, because condensation may occur within the infrared analyzer. The condensed water

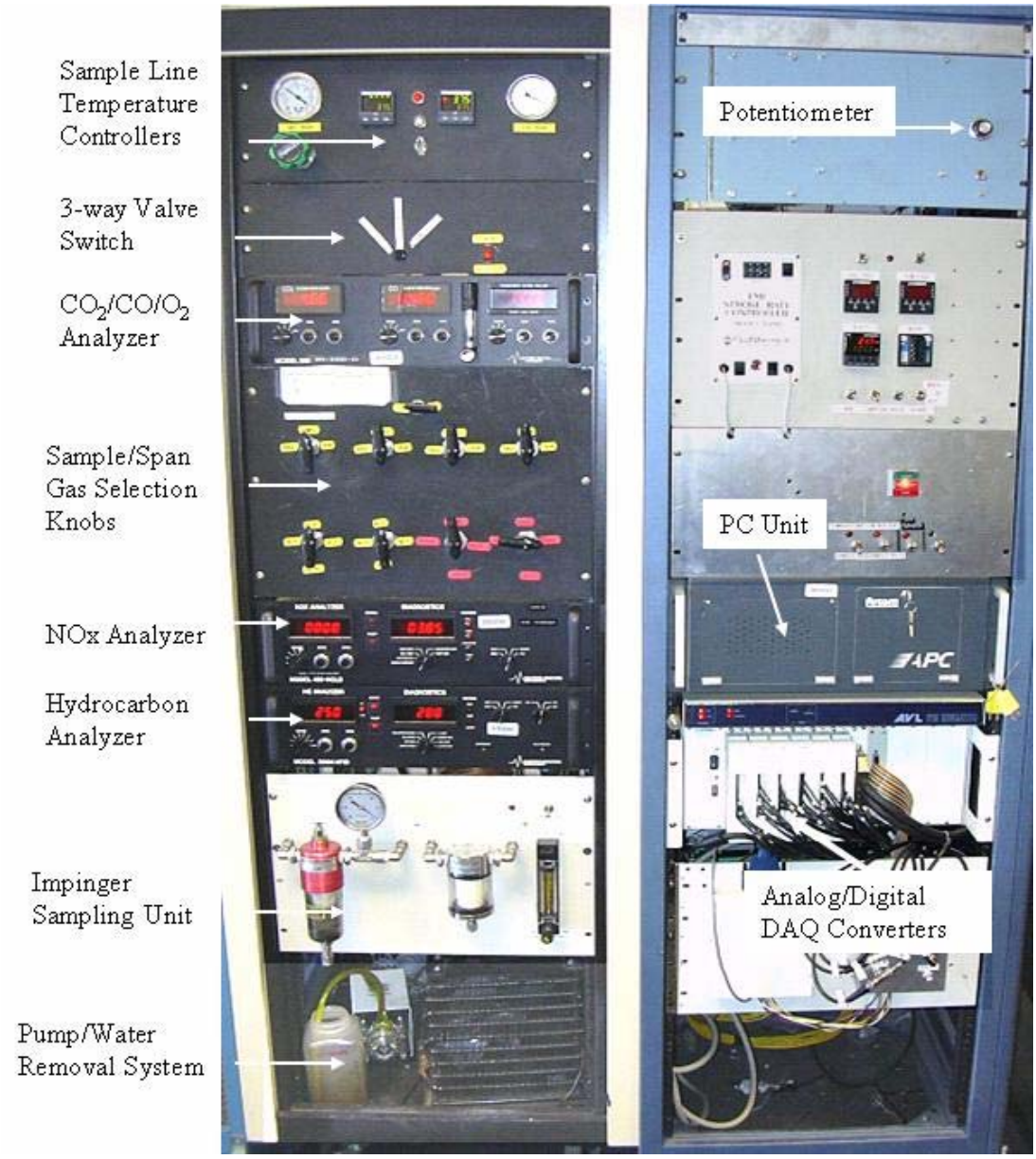

Figure 3.3: Photograph of the analyzer bench.

is collected in a water trap and pumped from the system using a peristaltic pump. A second vacuum pump located on the analyzer bench is connected to an impinger that collects exhaust gas samples to be analyzed with electrospray mass spectrometry. Particulate matter present in the exhaust gases is trapped in the impinger water reservoir while exhaust gases are siphoned away using the vacuum pump after passing through a series of cartridge filters to remove any bypass particulate matter. Exhaust gases are collected prior to entering the DOC at a flow rate regulated using a flow-metering valve.

Catalyst poisoning is achieved by introducing ZDDP into the system via three different methods. In the first method, ZDDP is mixed with lube-oil and dissolved into the fuel in known quantities and injected into the combustion chamber via the engine fuel injector, consumed and the by-products are carried with the diesel exhaust gases through the DOC. This method of introduction simulates rapid burning of lube-oil due to piston ring leaks. The consumption rate of ZDDP-doped lube-oil is maintained at 50 cc/hr using the engine load controller.

Lube-oil containing a high ZDDP concentration is also mixed with engine lube-oil and injected into either the intake of exhaust manifolds to simulate a blown turbo seal or compressor and valve seal leaks, respectively. In this method, the ZDDP-doped lube-oil is injected using a syringe pump at a rate of 50 cc/hr. The oil is entrained using compressed air to atomize the oil and sweep it through the injection nozzle. If the atomized oil is introduced through the exhaust pipe, lube-oil will be swept to the DOC directly with the exhaust gases. On the other hand, if the atomized lube-oil is introduced into the engine intake manifold, lube-oil is carried through the air intake and into the combustion chamber. After combustion, the consumed oil follows the path of the exhaust gases and encounters the DOC.

3.1.2 Mechanical Components

3.1.2.1 Diesel Engine

A naturally aspirated, direct-injection (NA/DI) Hatz diesel engine, Type 1D50Z, is used in this study. The engine, shown in Figure 3.4, is a 517 cc single-cylinder engine that produces 7.0 kW at 2700 RPM. An electric induction drive motor, discussed in Section 3.3.2, is used to start and maintain the engine at a constant speed of 1500 RPM during operation such that a nearly constant gas hourly space velocity (GHSV) through the DOC is achieved. The diesel fuel is of #2 ultra-low sulfur type to reduce the contribution of fuel-derived sulfur DOC poisoning.

3.1.2.2 Drive Motor

A three-phase electric induction Baldor drive motor is used to motor and start the Hatz diesel engine. The motor is capable of delivering/absorbing 15 hp at 1765 RPM with a maximum RPM of 4000. The Baldor electric motor is controlled by a Baldor Vector drive variable frequency conversion unit that is programmable to maintain either constant RPM or constant torque when motoring the engine. During testing, the drive motor is set to maintain the engine at a constant 1500 RPM while enabling the engine to operate at various loads to alter exhaust gas temperatures for catalyst poisoning and light-off evaluations. A photograph of the drive motor is shown in Figure 3.5.

3.1.2.3 Engine Load Controller

To regulate the amount of fuel injected into the combustion chamber an external controller is used. The controller consists of a Jordan Controls Inc., model TA-1200-6-N DO40 servo-motor rated at 17 VDC and 2.5 A, connected to an analog feedback control system located in the control room. A potentiometer mounted on the front panel of the

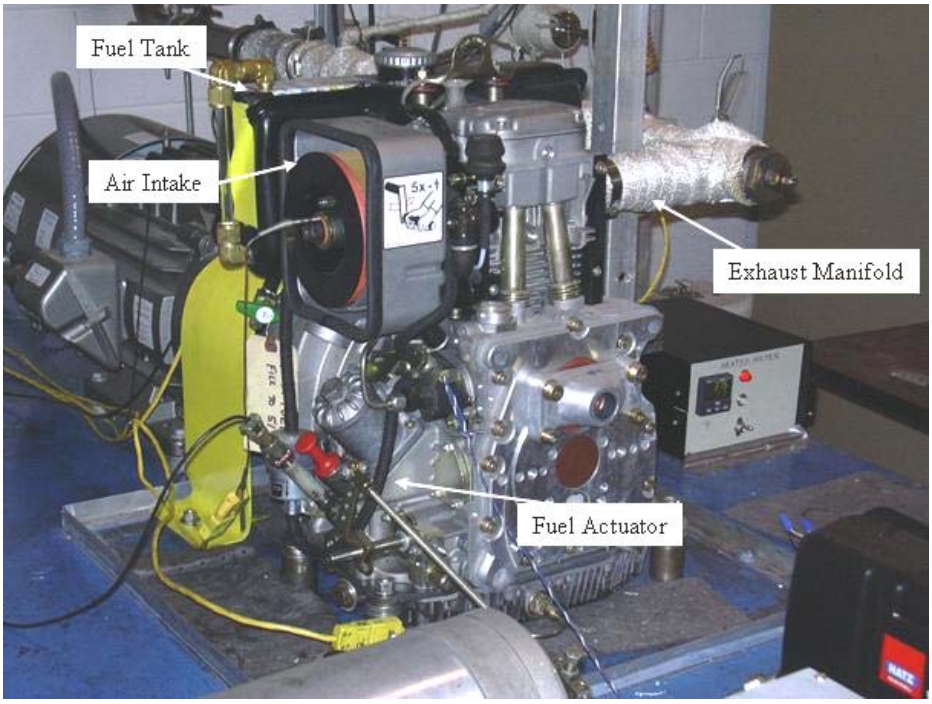

Figure 3.4: Photograph of the Hatz diesel engine used for DOC poisoning.

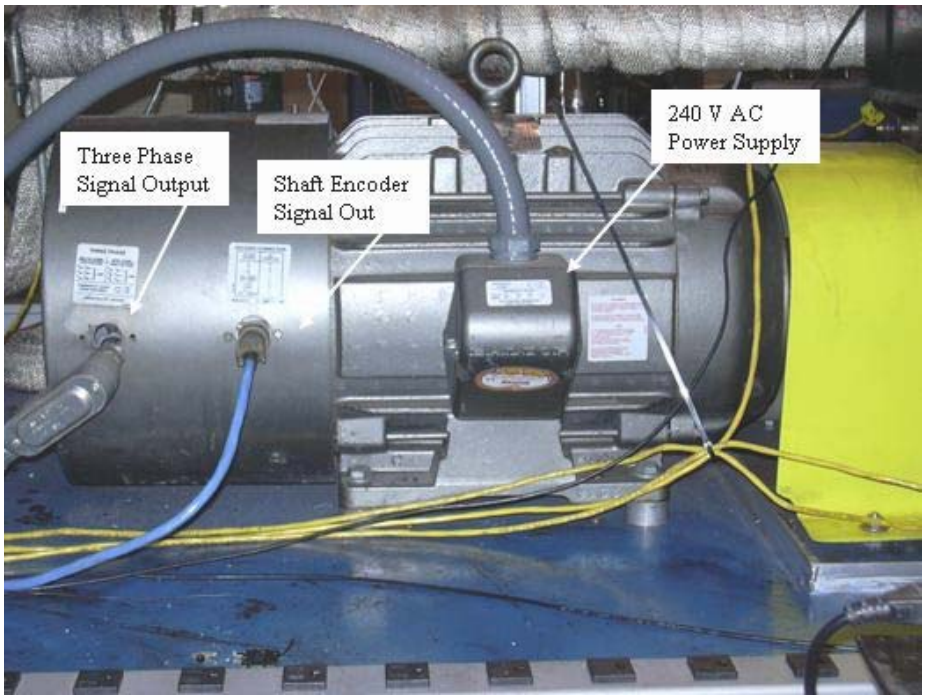

Figure 3.5: Photograph of the Baldor drive motor used to control the Hatz engine.

analyzer bench adjusts the position of the motor, which is linked to the fuel regulator. The servo-motor is mounted onto the engine bench with mechanical fasteners. A picture of the motor and linkage is shown in Figure 3.6.

3.1.2.4 Impinger

A 500 cc Greenburg-Smith impinger is used to collect PM present in the exhaust gases to be analyzed using electrospray mass spectroscopy. The impinger consists of a glass expansion nozzle immersed in 200 cc of de-ionized water with an impinger plate at the end. Exhaust gases pass through the expansion nozzle and strike the impinger plate located at a small distance from the nozzle. PM in the exhaust gases is collected in the de-ionized water. A vacuum pump is used to circulate exhaust gases from the engine through the impinger. The PM is then extracted from the distilled water chemically or mechanically for analysis.

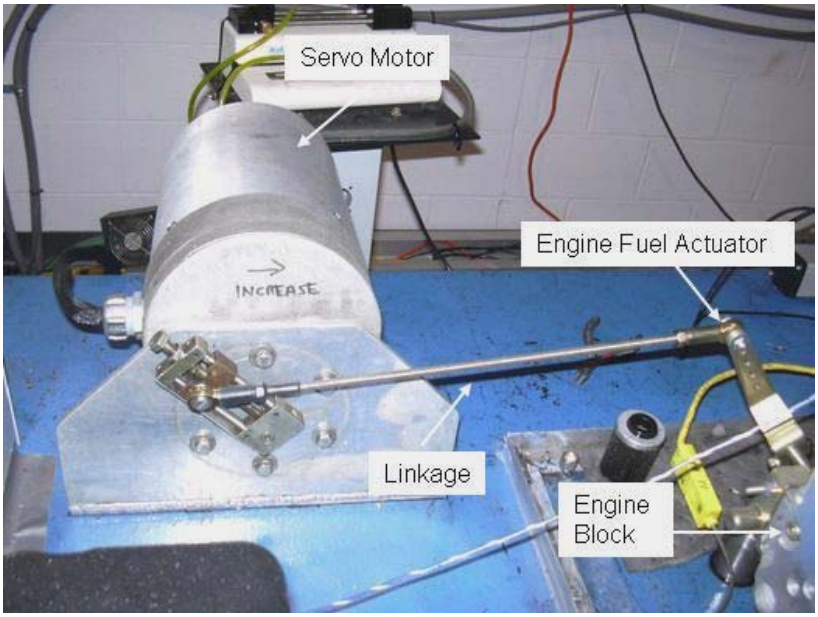

Figure 3.6: Photograph of the engine load controller assembly.

3.1.2.5 High Temperature Three-Way Valve

Exhaust gases are sampled at the DOC inlet and exit locations using a Whitey model MS-141ACX high-temperature three-way valve. The valve has an electronic actuator that produces 25 in-lbs torque with a switching time of 2.5 s for every 90^{o}. The actuator is powered by 60 Hz at 120 VAC with a maximum of 1.1 A. A three-way positioning switch located on the front panel of the analyzer bench allows for the selection of sample exhaust gases at the DOC inlet and exit as well as system leak check. A photograph of the three-way valve with actuator is shown in Figure 3.7.

3.1.2.6 Syringe Pump

In order to inject ZDDP-doped lube oil into the RPEB system, a Kd Scientific Model 100 syringe pump is utilized. The syringe pump, rated at 115 VAC at 60 Hz and a maximum current of 10 A, is a power-screw type design that produces a programmable constant volumetric injection rate using syringes of specified inside diameter. A photograph of the syringe pump is shown in Figure 3.8.

Oil displaced by the syringe is atomized and entrained by fast moving air to be carried to either the intake or exhaust manifolds to cause accelerated DOC poisoning.

3.1.3 Instrumentation and Displays

Three pressure transducers are used in the RPEB system. An Omega Model PX61 pressure transducer mounted on the engine block, measures engine lube-oil pressure. The remaining two pressure transducers, Omega models PX61 and PX177, located approximately 0.3 m from the exhaust manifold, are used to measure absolute and gage exhaust pressures, respectively. The pressure transducers are used to detect potential problems such as soot build up within the DOC by monitoring backpressure and pressure drop across the DOC.

Five Watlow type-K thermocouples are used to measure temperatures of atmospheric air, oil sump, exhaust gases and catalyst. Three thermocouples are used to

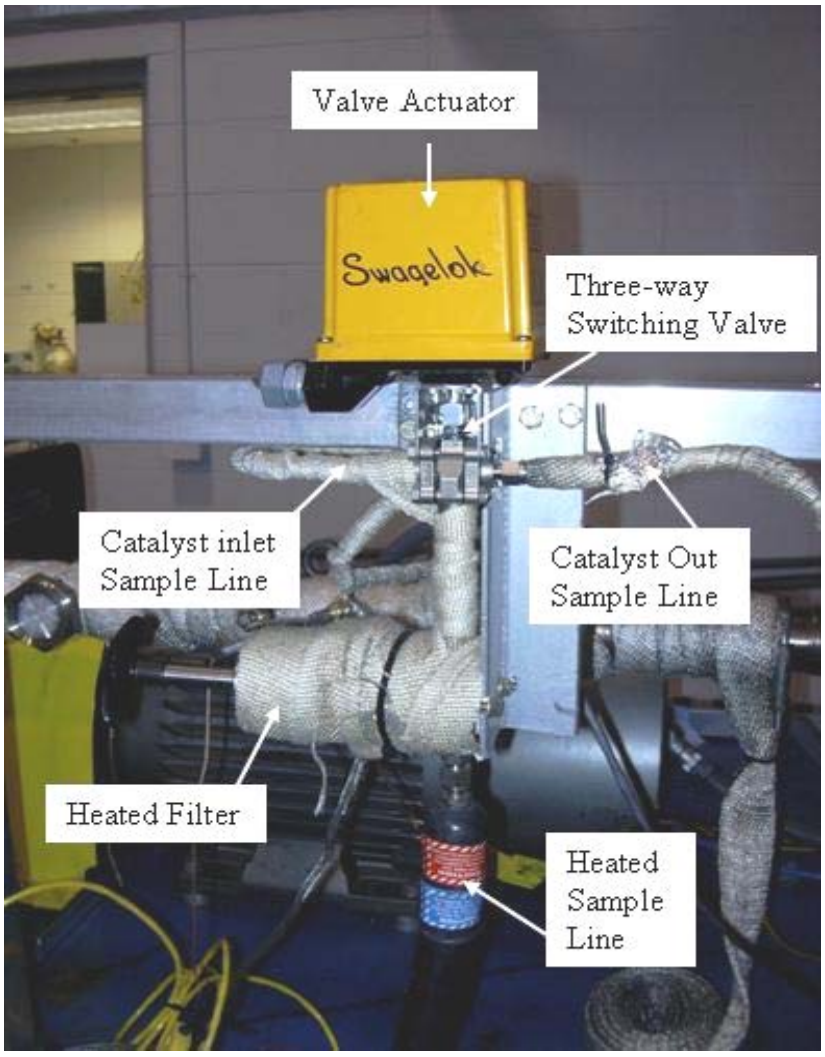

Figure 3.7: Photograph of the high-temperature three-way valve and associated exhaust sampling equipment.

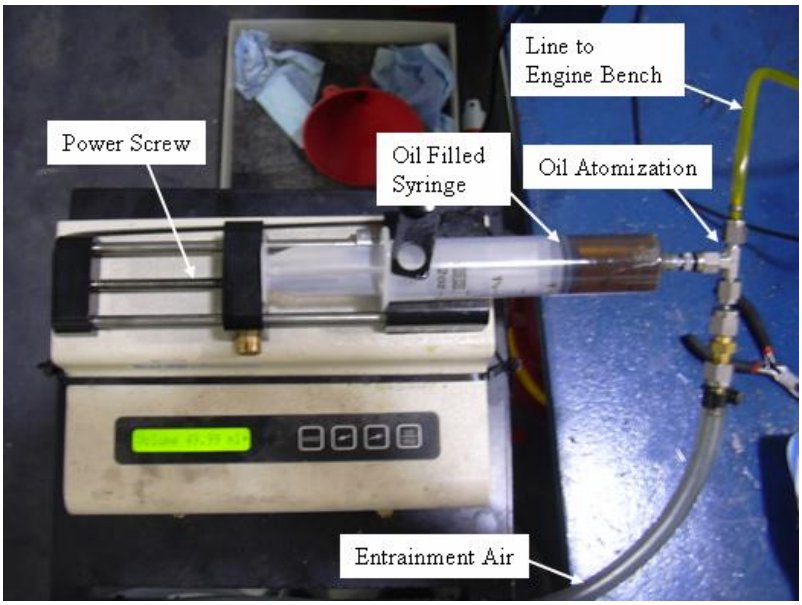

Figure 3.8: Photograph specifying the operation of the lube-oil injection apparatus.

measure exhaust gas temperatures; one at approximately 0.3 m from the engine exhaust manifold to measures the exhaust gases temperatures at the exhaust manifold and the other two are placed at the DOC inlet and exit to measure the average DOC temperature.

Three Athena Model M400 temperature controllers are used to control the temperature of the heated sampling line and the heat tapes covering the cartridge filters. The temperature controllers have an accuracy of ±0.25 % full-scale and have a maximum operational range of 300^{o}C. Each temperature controller used in the RPEB system is maintained at 190^{o}C.

3.1.4 Gas Analyzers

A California Analytical Instruments Model 300 IR-300-D analyzer is used to measure CO, CO_2 and O_2 concentrations in the exhaust gases. Non-Dispersive Infrared (NDIR) is the method of detection used to determine the concentration of CO_2, CO, while the paramagnetic principle is used to measure O_2. The analyzer used has an accuracy of ±1.0 % full-scale and a low operational threshold of 200 ppm.

To determine the concentration of THC in the exhaust gas, a California Analytical Instruments Model 300M-HFID analyzer is used. The analyzer is capable of continuous sampling with an internal heated gas pump and variable burner temperature of 60 to 200^{o}C. To measure the hydrocarbon concentration the analyzer uses flame ionization detection (FID). The analyzer has a sensitivity of 0.1 ppm and is accurate to 1.0 % full-scale.

A California Analytical Instruments Model 400-HCLDCE gas analyzer is used to measure NO_x concentrations in the exhaust gases. The analyzer utilizes the principle of chemiluminescence for analyzing the NO_x concentration and has a sensitivity of 5 ppm NO/NO_2 and an accuracy better than 1.0 % at full-scale.

3.1.5 Data Acquisition System

The purpose of the data acquisition system (DAQ) is to monitor and store information during RPEB system operation. The DAQ is capable of acquiring voltage and current signals from the equipment listed in Table IX. The main components of the DAQ include a PC, data acquisition boards, LabVIEW software, terminal blocks, patch panels and adaptor. A patch panel located in the test cell supplies electrical power to the pressure transducers and receives voltage signals from the thermocouples and pressure

Table IX: List of available signals and components handled by the DAQ.

Component	Source Type	Component	Source Type
Hydrocarbon Analyzer	Voltage	Catalyst Out Temp. TC	Voltage
NOx Analyzer	Voltage	Oil Sump Temp. TC	Voltage
$CO_2/CO/O_2$ Analyzer	Voltage	Ambient Air Temp. TC	Voltage
Exhaust Temp. TC	Voltage	Oil Sump Pressure PT	Voltage
Catalyst In Temp. TC	Voltage	Exhaust Pressure PT (gage)	Voltage
Exhaust Pressure PT (abs.)	Voltage	Shaft Encoder	Voltage
Drive Motor Torque	Current		

transducers, which are sent to the analyzer bench in the control room. A National Instruments Model TC-2095 terminal block gathers thermocouple leads, while the voltage signals are transferred to National Instruments terminal block SCXI-1102 where the signals are amplified and filtered by a 2 Hz low-pass filter at a sampling rate of 333 kS/s. The pressure transducer signals are gathered using a National Instruments Model SCXI-1328 terminal block along with signals from the gas analyzers and routed along with the filtered thermocouple signals to through a National Instruments Model SCXI-1349 adapter board which carries the signals to the National Instruments Model PCI-3036E PCI card in the PC. LabVIEW version 7.0 software produces data displays and stores data onto the hard drive. The drive motor data signals are read directly into the National Instruments SCXI-1328 terminal block and stored by LabVIEW. A wiring diagram of the DAQ is shown in Figure 3.9.

The computer used to run the DAQ is an industrial type manufactured by Arcom with 12 PCI slots and a dual output video card. The main LabVIEW program containing the RPEB system data acquisition is called "3 engine daq HR2" and is divided into three user interfaces. The "Hatz Diesel Engine" tab located at the top of the program screen must be pressed to display the main engine bench data acquisition program as shown in Figure 3.10. Channels allocated for monitoring equipment, such as thermocouples and pressure transducers, are displayed on this screen in real-time. To change the channels that are present or to add additional channels, the "DAQ and File Saving Configuration" tab is selected. This program allows the user to specify which channels will be allocated to the "Hatz Diesel Engine" program.

Once the desired channels are selected, the user is also able to calibrate each channel through the "Calibrate Channels" subprogram shown in Figure 3.11. This subprogram is used to calibrate the gas analyzer outputs before every poisoning and light-off evaluation test. Once the program is opened, the channel to be calibrated is chosen from the pull-down menu and high and low linear calibrating points are set by the user by placing the corresponding calibration values in the "Set High Value" and "Set Low Value" dialog boxes. When calibrating the gas analyzers, the calibration values are determined by sending span gases, which produces low or high valued signals from the

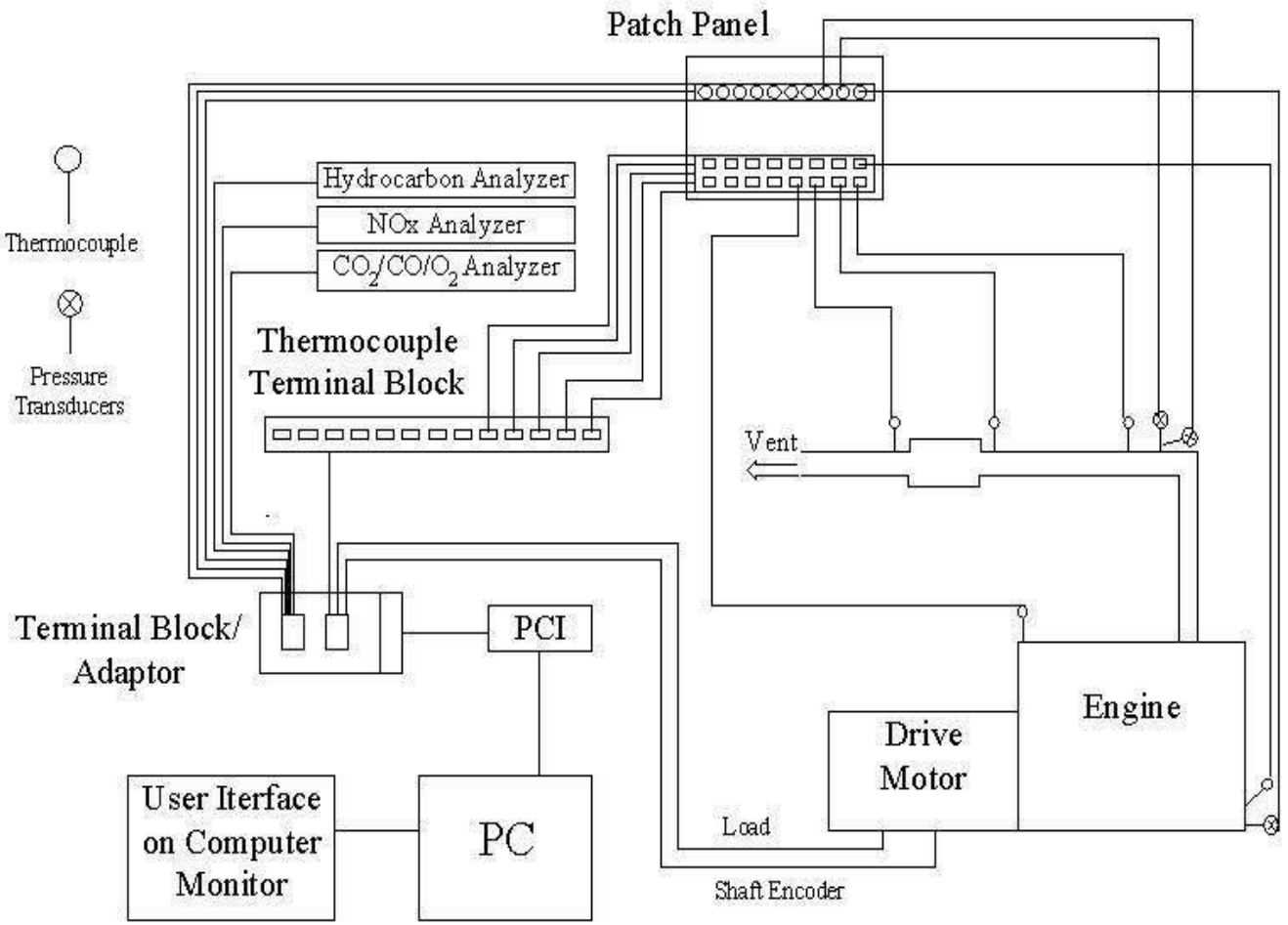

Figure 3.9: Wiring diagram of the DAQ and ancillary equipment

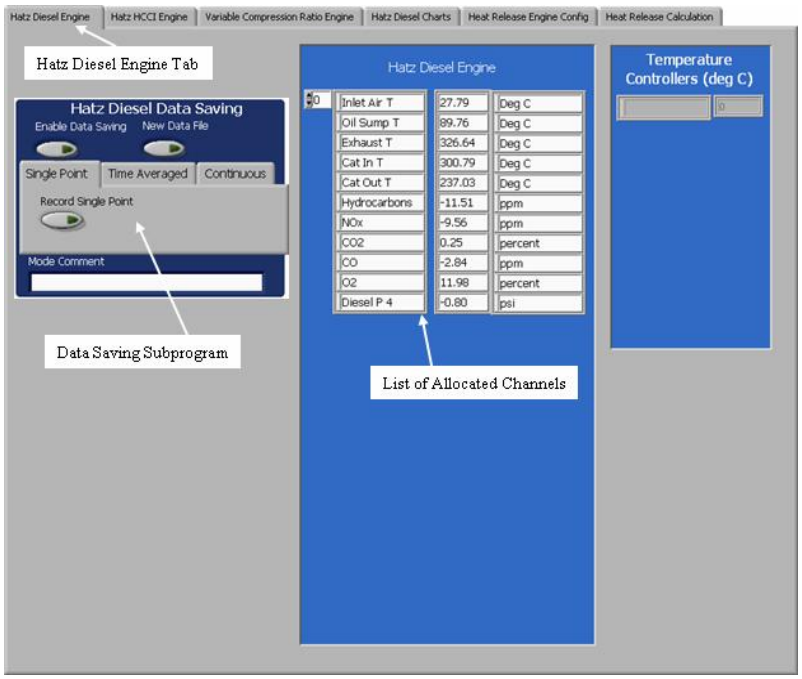

Figure 3.10: Screen capture of the "Hatz Diesel Engine" DAQ program user interface.

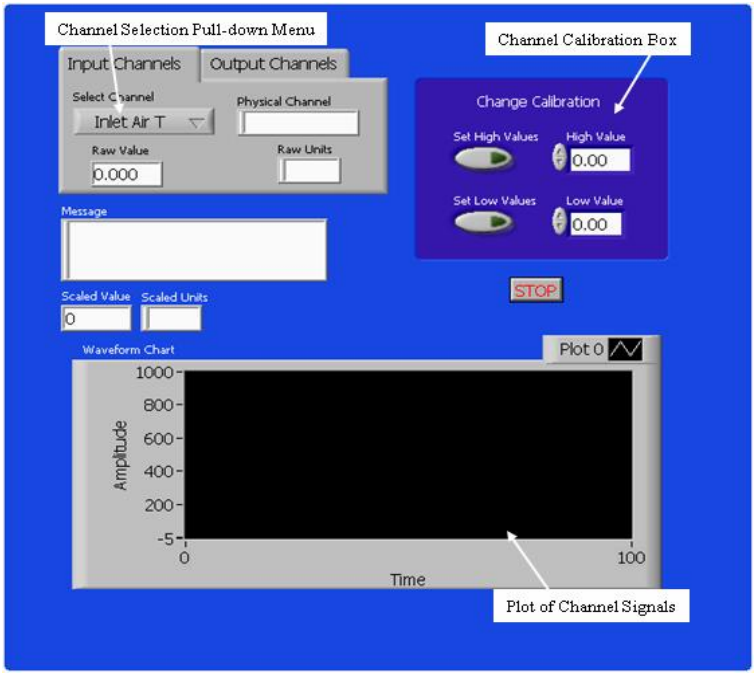

Figure 3.11: Screen Capture of the "DAQ and File Saving Configuration" DAQ program user interface.

analyzer to the DAQ. Values sampled from the gas analyzer are time averaged for 10 s to reduce signal noise. After calibrating all analyzer channels the "Hatz Diesel Engine" program is again opened and the DAS is ready to save data. On the "Hatz Diesel Engine" program display is the option to save data in three different ways: single point, time averaged or continuous. For all data saved during RPEB testing, the time-averaged option is chosen which averages all signals that were allocated to the program for 10 s and saved to a file of choice. This function only occurs if the "Enable Data Saving" button has been pressed prior to data saving.

3.1.6 Bench Engine Rapid Poisoning System Operation

3.1.6.1 Engine Start-up Procedure

To begin the RPEB system start-up procedure, a visual safety inspection is preformed to ensure all electrical and mechanical equipment is properly connected. Once the safety inspection is complete, the analyzer bench is turned on to provide power to the PC, gas analyzers, temperature controllers and mechanical hardware. The cartridge filters and sample line temperature controllers are set to 190^{o}C and approximately 15 minutes are required for the heaters to reach operating temperatures. During this time the engine oil level is checked and diesel fuel is added to the fuel tank. The engine bench is visually checked to ensure thermocouples and pressure transducers are connected properly and the old cartridge filters are replaced with fresh filters. Once the engine is inspected, the overhead exhaust fan that ventilates the test cell is turned on as well as the circulator fan that pumps in fresh air. In the control room, the data acquisition program LabView file "3 engine daq HR2" is opened on the PC and begins monitoring all measurement devices. A visual inspection of the operating program interface confirms that instrumentation in the test cell is working properly by displaying correct sensor information.

Pressing the power relay switch, the green button on the power supply console shown in Figure 3.12, initializes the drive motor controller. Once power is turned on, the drive motor's control computer boots up and requires approximately 5 s to perform a self-check and indicates "READY" when it is safe to turn on the drive motor. On the drive motor control console, the controller switch is turned to "VELOCITY"; thereby the computer controls the drive motor at constant velocity mode instead of constant torque. The velocity control knob below the control switch is then set to 542, which corresponds to 1500 RPM. The drive motor is started by setting the control ON/OFF switch at the top of the console to "ON".

3.1.6.2 Catalyst Light-off Measurement Procedure

Light-off behavior of THC and CO is used to quantify deactivation during rapid engine poisoning tests as well as be a basis for the comparison of field-service DOCs. The light-off evaluation consists of measuring the oxidation performance of the DOC at 8 engine load steps from idle to full load at a constant speed of 1500 RPM that corresponds to a gas hourly space velocity of 80,000 hr^{-1} at STP. Table X lists typical CO and THC concentrations and exhaust gas temperatures at the DOC inlet for each load step. To begin a light-off test, it is necessary to first warm up both the catalyst and the engine. This is achieved by running the engine at 33, 67 and 100 % load for twenty-minute durations at each load. During engine warm-up the gas analyzers are calibrated and all temperature controllers are checked for proper temperatures.

Once the engine and catalyst are thermally stable, the engine load is reduced to full electric motoring by turning the engine fuel regulator actuator to fully-closed. This is done to ensure that no hysteresis is present in the measurements and thus a higher factor of repeatability in the test. The engine fuel consumption is then slowly increased so the engine is back to idle conditions and the light-off evaluation is initiated. At each step, the engine is allowed to equilibrate for approximately 10-minutes before engine emissions are measured. An additional 5-minutes is allowed for the DOC to reach thermal equilibrium before sampling exit gas concentrations.

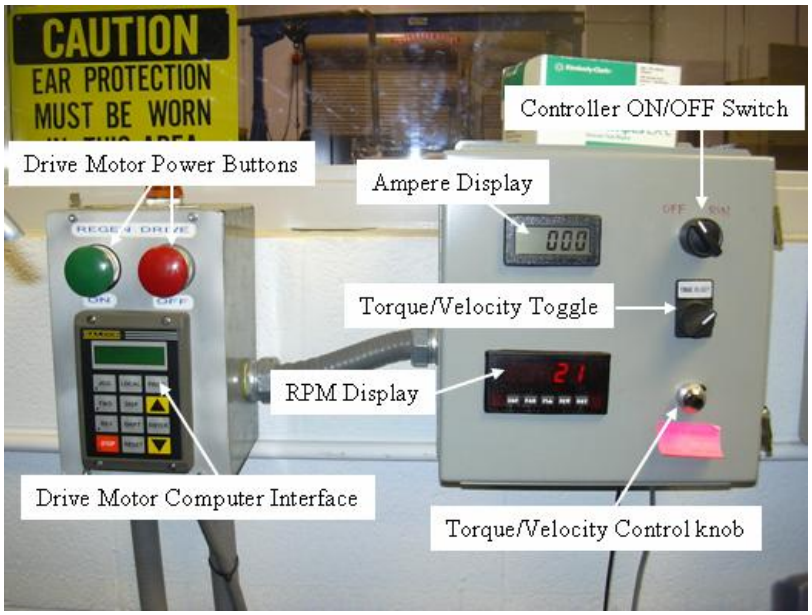

Figure 3.12: Photograph of the drive motor power and control units.

Table X: Typical CO and THC concentrations and exhaust temperatures obtained by the Hatz engine at various loads and 1500 RPM.

Engine Load (%)	DOC Inlet Temperature (C)	Average THC (ppm)	Average CO (ppm)
Idle	165	95	160
15	200	95	150
30	240	105	100
50	290	115	100
60	320	120	95
75	365	135	230
90	400	115	650
100	420	100	650

Since this particular DOC formulation was first introduced approximately 10 years ago to optimize only soluble particulate reduction with minimum sulfate production from conventional sulfur fuels, THC and CO conversion are relatively low. Therefore, light-off temperatures for THC and CO are defined as the DOC inlet temperature corresponding to 20 % and 25 % conversion, respectively. These light-off temperatures are about half of maximum conversion measured under fresh DOC conditions.

3.1.7 Experimental Tests

3.1.7.1 Accelerated DOC Poisoning

Three methods of artificially increasing the consumption rate of ZDDP, as seen in Table XI, are used to simulate field- service pathways causing DOC poisoning. In each method, ZDDP is mixed with lube-oil to a concentration of approximately 10 times that of commercial blends and introduced at a rate of approximately 70 times that of normal engine consumption. This results in a net increase of 700 times more than normal consumption. During each accelerated poisoning method, the engine is maintained at a constant RPM of 1500, which corresponds to a nearly constant gas hourly space velocity of 80,000 hr^{-1} at STP. The rate of phosphorus through the engine is 0.5 g/hr, which corresponds to a doped-oil consumption rate of 50 cc/hr. A total of approximately 6.0 g of phosphorus is introduced into the exhaust system during each poisoning method. The resulting total DOC time under poisoning conditions is approximately 12 hours.

Prior to engine-bench poisoning, a fresh commercial DOC is de-greened by cycling between 5, 50 and 100 % load in twenty-minute increments for four hours. This is done to "break-in" the catalyst surface by allowing the catalyst and support material to reach thermodynamic equilibrium. Two light-off evaluations are then performed to ensure repeatability of results; if the DOC exhibits significant variability then the DOC is de-greened for an additional 2 hours.

Table XI: List of accelerated ZDDP introduction methods with corresponding field-service pathways.[20]

Form of Phosphorus	Location of Introduction	Field Pathway
None	None	Fresh DOC
ZDDP + Lube-Oil	Intake Manifold Injection	Compressor or Valve Seal Leaks, Closed Crankcase Ventilation
ZDDP + Lube-Oil	Exhaust Manifold Injection	Blown Turbo Seal
ZDDP + Lube-Oil	ZDDP-Doped Fuel Injection	Burning of Used Lube-Oil, Ring Leaks

In fuel injection poisoning, once the fresh DOC has shown repeatable light-off performance, the fuel is drained and replaced with a blend of 600 cc of ZDDP-doped lube-oil and BP-15 diesel fuel totaling 8,400 cc. The engine is allowed to consume the entire fuel blend at 75 % load corresponding to a DOC inlet temperature of 365^{o}C. At this engine condition, the fuel consumption rate is approximately 700 cc/hr resulting in a phosphorus consumption rate of 0.5 g/hr. Finally, BP-15 diesel fuel free of ZDDP is added to the engine fuel tank and two final light-off evaluations are performed to measure the resulting catalyst deactivation. The DOC is then dismounted from the exhaust system, weighed and sectioned into equal volume wedges for chemical analysis.

In intake and exhaust manifold injection methods, a syringe pump is used to inject ZDDP-doped lube-oil, blended to a phosphorus loading of 10 g/L, at the desired rate of 50 cc/hr in increments of 50 cc per injection. For intake manifold injection poisoning, lube-oil is injected directly above the intake valve. Air atomization is used to entrain the lube-oil and carry it through the injection nozzle to either the intake or exhaust manifolds. The engine is run at a fixed load cycle at 5.0, 50, and 100 % load in 20-minute intervals during the injection process to vary the engine and catalyst operating. After each 50 cc injection increment, a light-off evaluation is performed to measure DOC deactivation. Once twelve 50 cc syringe pump lube-oil injections are completed, a total of 6.0 g of

phosphorus, two final light-off evaluations are performed. The DOC is then disassembled, weighed and sectioned for chemical analysis.

For exhaust manifold injection poisoning, a nozzle located directly behind the exhaust manifold allows the injected lube-oil to spray directly in the exhaust pipe. Air atomization entrains lube-oil and carries it to the exhaust manifold where it is evaporated and carried with the diesel exhaust gases to the DOC. The engine is run at a 50 % fixed load during each injection to ensure that the lube-oil is evaporated, yet the exhaust gases are not so severe as to decompose the ZDDP. After two 50 cc injections, a light-off evaluation is performed to measure DOC deactivation. Once a total of 6.0 g of phosphorus is injected, two final light-off evaluations are performed. The DOC is then disassembled, weighed and sectioned for chemical analysis. The intake and exhaust manifold injection poisoning procedure is summarized as follows:

- De-green catalyst 4-6 hours with variable load cycle
- Two light-off evaluations
- Inject phosphorus at 0.5 g/hr
- Light-off evaluation
- Repeat poisoning and light-off evaluations until 6.0 g phosphorus is consumed

The final experimental investigation performed using the RPEB is a ZDDP decomposition study in which a ZDDP and lube-oil blend, identical to that used in DOC poisoning, is passed through the engine via intake manifold injection poisoning at 0, 50 and 100 % engine load. The engine is maintained at a constant RPM of 1500 corresponding to a nearly constant gas hourly space velocity of 80,000 hr^{-1} at STP. A total of 6.0 g of phosphorus is injected into the engine intake at a rate of 50 cc/hr, identical to that of earlier experiments. An impinger sample is obtained during DOC poisoning from the exhaust gases and analyzed using electrospray mass spectrometry described in Section 3.4.4.

For the purposes of the ZDDP decomposition study, no intermediate light-off evaluations are obtained during poisoning. However, once the injection of 6.0 g of phosphorus is complete, two light-off evaluations are performed to compare fresh DOC performance to that of poisoned for each method. Once poisoning is complete the DOCs are disassembled, weighed and sectioned for chemical analysis. Table XII provides a summary of the engine loadings and their associated DOC inlet temperatures used for both accelerated DOC poisoning and ZDDP combustion tests.

3.2 Bench-Flow Reactor

3.2.1 Overall Description of the Bench-Flow Reactor System

A photograph and schematic of the bench-flow reactor (BFR) system are shown in Figures 3.13 and 3.14, respectively. The BFR, which is located at the University of Tennessee, is comprised of 5 main components: a steam generator, a DOC reactor, a simulated diesel exhaust gas introduction system, an analyzer bench and a DAQ. Simulated diesel exhaust gases used during BFR testing consist of 5 % CO_2, 500 ppm CO, 300 ppm C_2H_4, 10 % O_2, 1000 ppm NO_x, 10 % H_2O and balance N_2 at a gas hourly space velocity of 80,000 hr^{-1}. The volumetric flow rate of each gas component is controlled with the use of mass flow controllers (MFCs). Steam is introduced into the system via a steam generator fed by a peristaltic pump with de-ionized water.

The main bank supplies CO_2 and N_2 as carrier gases for sweeping water vapor from the steam generator into the BFR system. The remaining main bank gases consisting of CO, C_2H_4, NO_x, air and O_2 are introduced into the BFR at the steam generator exit. Once mixed, the gases pass through either the oxidation reactor or the reactor bypass line. The bypass line allows the measurement of the simulated diesel exhaust gases at the DOC inlet conditions. A three-way solenoid valve is used to switch between inlet and outlet gases of the oxidation reactor. Backpressure and pressure-drop across the oxidation reactor are monitored with two pressure transducers located at the DOC inlet and outlet.

Table XII: Engine load and associated exhaust gas temperatures used during each accelerated DOC poisoning methods.

Poisoning Method	Engine Load (%)	Catalyst Inlet Temperature (C)
Intake Manifold Injection	100	420
Intake Manifold Injection	50	290
Intake Manifold Injection	0	165
Intake Manifold Injection	15-100	200-420
Exhaust Manifold Injection	50	290
Fuel Injection	75	365

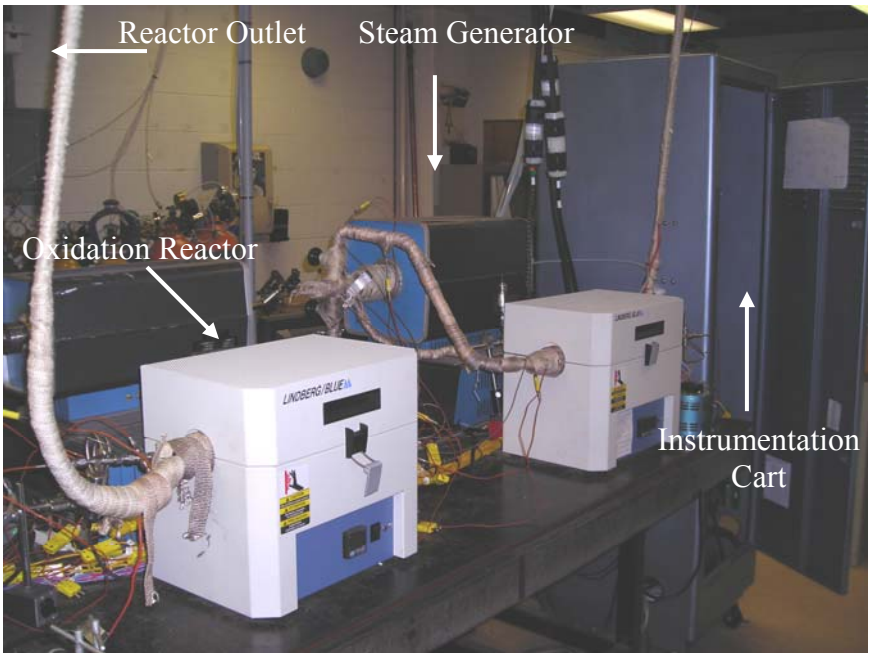

Figure 3.13: Photograph of the bench-flow reactor system.

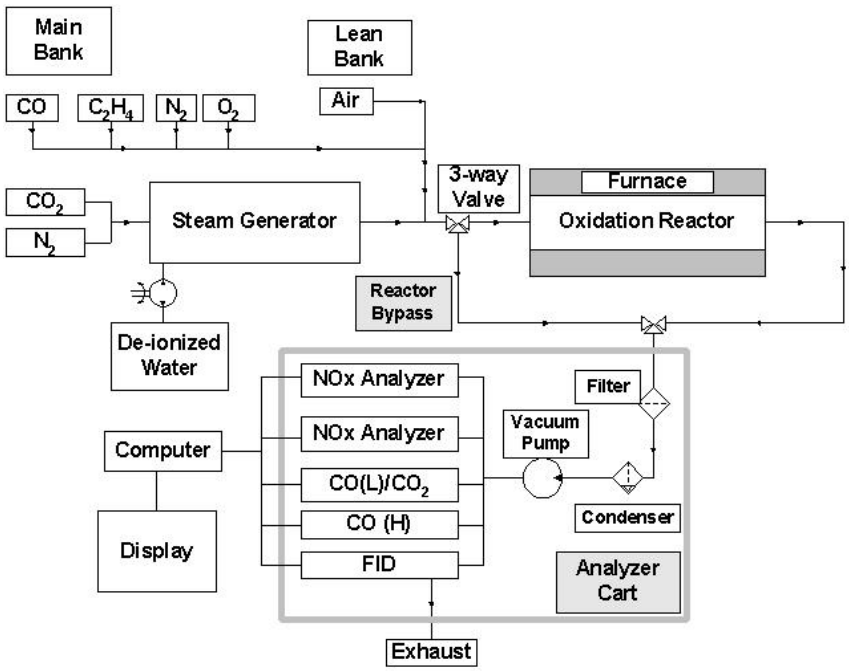

Figure 3.14: Schematic of the bench-flow reactor system.

The DOC monolith samples, which are 7.60 cm long by 2.0 cm diameter, are core drilled from either field-service or rapid engine-poisoned DOCs using the RPEB system as described in Section 3.3.4. The samples are mounted in a quartz reactor and placed inside an electric furnace to control temperature. Heated sample lines are used throughout the system to both preheat the simulated diesel exhaust gases and ensure no water condensation occurs within the flow passages. The inlet portion of the reactor is filled with 5 mm diameter Pyrex^{TM} beads for effective preheating of simulated diesel exhaust gases before entering the DOC.

Six Omega type-K thermocouples are used to measure the gas inlet and exit temperatures as well as the internal DOC temperatures as shown in Figure 3.15. Two thermocouples located approximately 5 mm from the inlet and exit of the DOC are used to measure the inlet and exit simulated diesel exhaust gases temperature. The remaining four thermocouples positioned at 5, 19, 38 and 57 mm from the DOC inlet are used to measure the DOCs' axial temperature distribution.

A Horiba analyzer bench is used to measure the concentrations of CO, C_2H_4, NO_x, and CO_2 in the simulated diesel exhaust gases. The gases are drawn through the bench

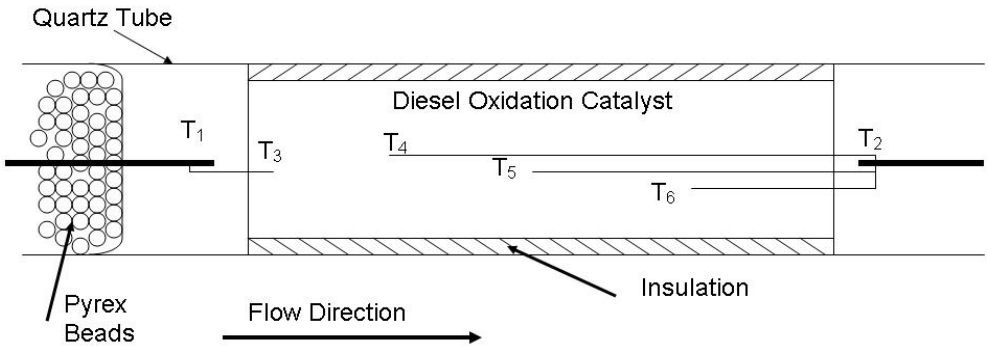

Figure 3.15: Schematic of the six thermocouple locations with respect to the DOC during bench-flow reactor evaluations.

flow system with the use of a vacuum pump and enter the Horiba analyzer bench, described in Section 3.2.2.6, from either the reactor by-pass or reactor sample lines. A condenser unit is used to remove water vapor from the system prior to entering the gas analyzers. A series of cartridge filters are also used to remove particulate matter present in the simulated diesel exhaust gases and prevent fouling of the gas analyzers.

Pressure, temperature and analyzer signals from the BFR are acquired, displayed and stored using a LabVIEW based DAQ system. A virtual control panel is used as a user interface to both monitor and control the BFR during operation. The control panel allows for the control of the MFCs and displays real-time data. The user can save data at any point during BFR operation and write to files created by LabVIEW on the hard drive.

3.2.2 Mechanical Components

3.2.2.1 Mass Flow Controllers

Mass flow controllers (MFCs) are used to regulate the volumetric flow rate of simulated diesel exhaust gases entering the BFR. MFCs are located within the instrumentation panel described in Section 3.2.3.1, and are controlled using the LabVIEW control panel discussed in Section 3.2.6.2. The volumetric flow rate of each

individual gas component is controlled using a MFC dedicated solely to that particular gas species. All of the Omega manufactured MFCs, Model FMA 5400/5500, are calibrated for the flow of N_2 gas. Gases other than N_2 are controlled with the use of correction factors, called K factors, which correct for the difference in atomic weight between the gases. LabVIEW software controls each MFC by varying the input voltage within the range of 0-5 V to correspond to the desired user input volumetric flow rate. Each MFC has a different linear response to the supplied voltage. Therefore, an internal feedback system is utilized by the manufacturer to ensure correct volumetric flow rates. The operational ranges and K factors of each mass flow controller are listed in Table XIII. Concentrations of both CO and C_2H_4 are small and balanced with N_2 so that K factors for these species are very close to that of pure N_2.

3.2.2.2 Peristaltic Pump

A Masterflex^{TM} peristaltic pump is used to inject de-ionized water into the steam generator described in Section 3.2.2.3. The peristaltic pump allows for continuous water injection which produces a uniform water vapor concentration exiting the steam generator. The peristaltic pump, shown in Figure 3.16, can achieve steam flow rates

Table XIII: List of mass flow controller volumetric flow rate ranges and associated correction factors.

Species	Volumetric Flow Rate (LPM)	K Factor
N_2	0 – 10	1.000
CO_2	0 – 10	0.737
CO	0 – 1	~ 1.000
Air	0 – 20	1.006
C_2H_4	0 – 5	~ 1.000
NO_x	0 – 5	0.976

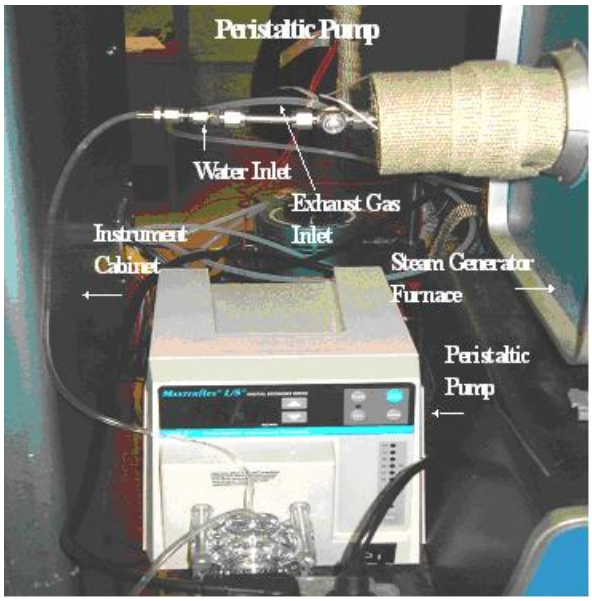

Figure 3.16: Photograph of the peristaltic pump used to inject de-ionized water into the steam generator.

between 0.1 and 580 cc/min. The peristaltic pump siphons de-ionized water from a reservoir and injects it through a water injection nozzle in the steam generator where it mixes with carrier gases. The water then passes into the steam generator where it is vaporized and passed into the BFR system.

3.2.2.3 Steam Generator

The steam generator consists of a Lindberg heavy-duty tube furnace, shown in Figure 3.17, with a 2.54 cm diameter stainless steel tube through which water is converted into steam. The steam generator is maintained at 200^{o}C to ensure water is completely vaporized before exiting. The stainless steel evaporator tube is 70 cm long with stainless steel flanges that house copper gaskets that are pressure tested to 1.70 bar (20 psig) before each use to ensure no leaks are present. Inside the evaporator tube is a water injection nozzle located approximately 35 cm from the steam generator inlet. The nozzle allows for preheating of the water and carrier gases before being directed onto a

Figure 3.17: Photograph of the steam generator used in the bench-flow reactor system.

Siltemp™ fabric strip that absorbs any remaining liquid present. The fabric acts to absorb and disperse the water and aid in the production of steam. The vaporized water finally exits the steam generator with the aid of the carrier gases consisting of CO_2 and N_2.

3.2.2.4 DOC Reactor

The DOC reactor consists of a 44.45 cm long quartz tube with 2.22 cm ID and 2.54 cm OD, reactor end fittings, Pyrex™ beads and the DOC. The Pyrex™ beads are 5 mm diameter and occupy the front half of the reactor to enhance mixing and preheat the simulated diesel exhaust gases. The reactor end fittings, shown in Figure 3.18, consist of a 2.54 cm Swagelock end cap and tube fitting. The cap nut is modified to accommodate three Swagelock weld fittings that allow for the insertion of thermocouples and pressure transducers. Graphite ferrules are used to form a compression seal between the quartz tube and the end fitting because graphite can withstand the high temperatures encountered during operation. Before the DOC is placed within the quartz tube it is first

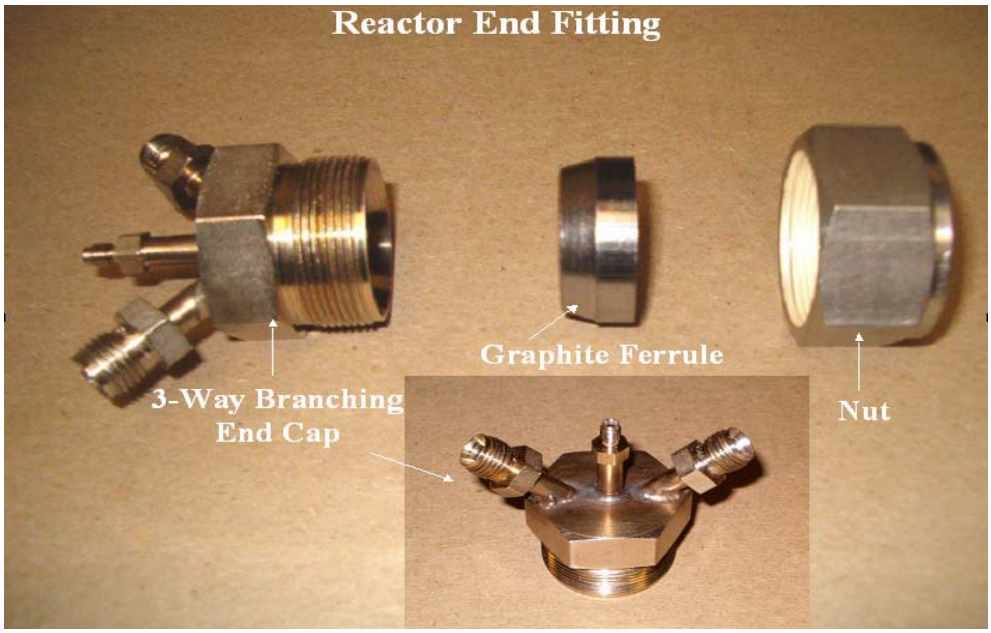

Figure 3.18: Photograph of the reactor end-fitting used to pass simulated diesel exhaust gases through the diesel oxidation catalyst and allow temperature and pressure measurements.

wrapped in FiberFrax^{TM} glass wool to prevent gas slip. Thermocouples are positioned within the DOC in accordance with Figure 3.15 shown in Section 3.2.1. A Lindberg Model TF55035A-1 electric furnace is used to maintain the DOC reactor at isothermal condition and has a maximum operating temperature of 1100^{o}C. The furnace is equipped with a feedback system to ensure that mid-furnace temperatures are maintained to within +/- 1^{o}C of the target temperature. Figures 3.19 and 3.20 are photographs of the DOC reactor positioning within the Lindberg/Blue M furnace and temperature controller, respectively.

3.2.2.6 Horiba Analyzer Bench

The Horiba analyzer bench consists of four gas analyzers, water condenser, vacuum pump and cartridge filters. Simulated diesel exhaust gases enter the analyzer bench through a water condenser to remove all water vapor. The dry exhaust gases then

Figure 3.19: Photograph of the DOC reactor placement inside the Lindberg furnace.

Figure 3.20: Photograph of the Lindberg electric furnace used to maintain the diesel oxidation catalyst operating temperatures.

enter a series of two cartridge filters that remove any particulate matter (PM). Once the simulated diesel exhaust gases are properly treated for the removal of water vapor and PM, they enter the gas analyzers. The analyzer matrix switches located on the control panel of the analyzer bench, shown in Figure 3.21, is used to select each gas analyzers to be used. The matrix switch is wired to solenoid-activated three-way valves that regulate the flow pathways to each analyzer. The FID, chemiluminescence and infrared analyzers are selected by placing each respective switch to "sample" allowing the simulated diesel exhaust gases to enter the analyzers for measurement.

A throttling valve and a pressure regulator located on the control panel determine the flow rate and pressure of the simulated diesel exhaust gases in the analyzer bench. The throttling valve and the pressure regulator are connected in parallel with a gas manifold containing the solenoid-activated three-way valves. A flow rate of approximately 22 LPM at a pressure of 1.29 bar (4 psig) is used throughout the study to maintain a pressure of approximately 1.36 bar (5 psig) at the inlet of the DOC reactor. Gases that are not extracted for gas composition analysis are evacuated though the exhaust vent.

Figure 3.21: Photograph of the Horiba analyzer bench control panel.

3.2.3 Instrumentation and Displays

An instrumentation cabinet houses all of the control and monitoring equipment used in BFR operation. Temperature and pressure indicators as well as temperature controllers, power switches, simulated diesel exhaust gas inlet connectors and DAQ terminal blocks are located on the front panels as shown in Figure 3.22. The front panel is designed to provide the user with an easily accessible interface to monitor and control BFR operations by housing pressure and temperature indicators as well as control switches. The DAQ system is positioned at the bottom of the cabinet to be easily wired to both the monitoring equipment and the PC. MFCs, switching valves, sensor patch panels and power supplies are located within the instrumentation cabinet and are accessed through the rear panel as shown in Figure 3.23. Measurement device signals are routed through the instrumentation cabinet to be connected to both the DAQ and the indicators located on the front panel. A simulated diesel exhaust gas manifold, located directly after the MFCs within the instrument cabinet, is used to mix the lean and main bank gases before being introduced into the BFR.

Cole-Parmer pressure transducers Model 68072 – 06 installed at the inlet and exit of the DOC reactor are used to monitor the pressure drop across the DOC and the backpressure at the gas manifold. The pressure transducers have a linear operating range of 0 to 3.45 bar (50 psi) and a maximum operating temperature of 126^{o}C. Since pressure transducers are susceptible to thermal damage when exposed to the high temperatures of the exhaust gases, stainless steel tubing in the form of helix is used to enhance the heat losses and thus prevent overheating.

Two Cole-Parmer Model 94785–00 pressure indicators are used to display pressure during BFR operation. The indicators are programmable with 11 calibration set points for use in non-linear applications. The indicators have a LCD display and are manufactured for compatibility with the process signal range specific to the pressure transducers described in Section 3.2.3.2.

Seven Omega type-K thermocouples are used to monitor temperatures in the BFR system. One thermocouple located immediately downstream of the steam generator is used as a feedback signal for the heat tape temperature controller that regulates the heated

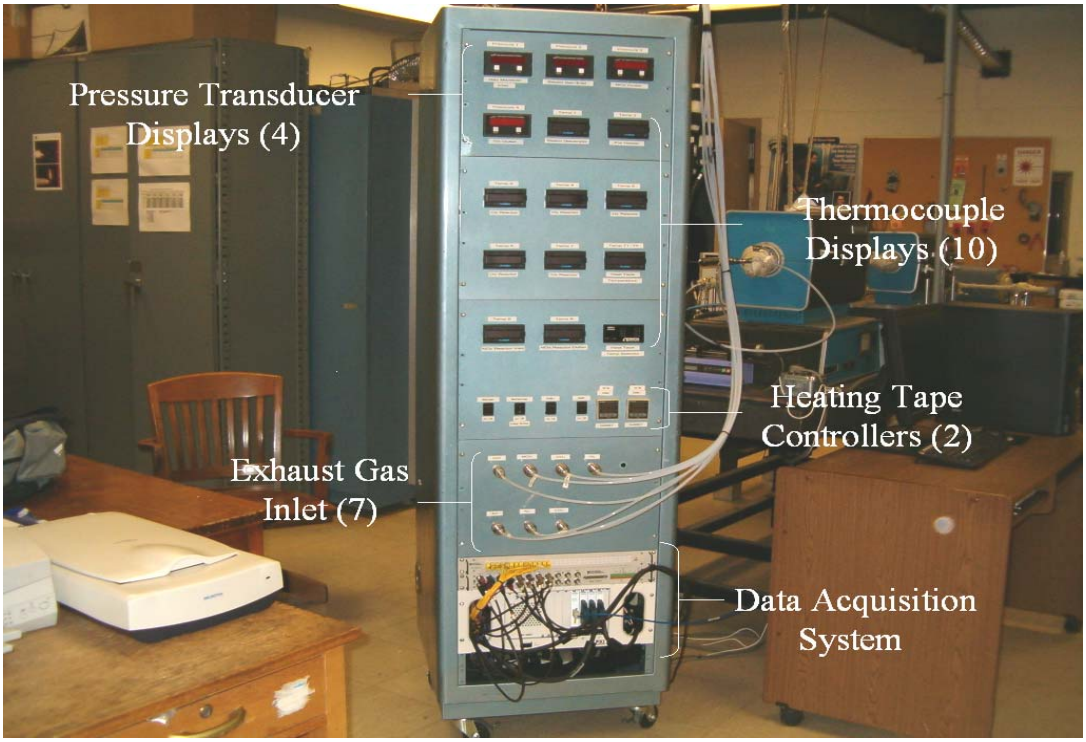

Figure 3.22: Photograph of the front panel of the instrumentation cabinet.

Figure 3.23: Photograph of the back panel of the instrumentation cabinet.

sample line leading to the DOC reactor. The other six thermocouples are allocated for temperature measurement within the reactor as discussed in section 3.2.1. Two thermocouples of 61.0 cm long and 0.3 cm in diameter positioned at the front and rear of the DOC sample measure the inlet and exit gas temperature. The four thermocouples located within the DOC are each 61.0 cm in length and 0.16 cm in diameter. The small diameter of the thermocouple serves two functions: to fit within the channels of the DOC as well as offer fast response times to accurately measure temperature excursions within the DOC during reaction.

Seven Omega Model DP 18-KC1 temperature indicators are used to display the simulated diesel exhaust gas temperatures to the user on the instrumentation panel. The temperature indicator is equipped with programmable analog input/out and has 8 calibration points for non-linear signals. The indicator is made specifically for use with type-K thermocouples and has a resolution of ± 1^{o}C with a maximum temperature reading of 1250^{o}C.

Two Athena Model – XT16 temperature controllers are used to adjust the preheat temperature of the simulated diesel exhaust gases entering the DOC reactor by adjusting two Omega heavily-insulated Samox heating tapes. The heating tape has a maximum operating temperature of 760^{o}C. The temperature controllers can be programmed to provide a constant heating rate and accept a 120 VAC power supply.

3.2.4 Gas Analyzers

A dual Horiba CO and CO_2 analyzer Model AIA-220 is used to measure CO concentrations up to 1500 ppm and CO_2 up to 20% concentration. The analyzer employs non-dispersive infrared (NDIR) absorptiometry to measure both CO and CO_2 concentrations. The analyzers have a maximum voltage output of 5 VDC at full scale.

To measure total hydrocarbon (THC) species in the simulated diesel exhaust gas, a Horiba THC analyzer Model FIA-220 is used. This particular analyzer does not have a heated sample chamber as the California Analytic THC analyzer does; therefore, water vapor must be removed prior to sampling. The analyzer uses flame ionization detection

(FID) to measure the THC concentration. The analyzer is capable of measuring THC a maximum concentration of 3000 ppm.

A Horiba chemiluminescence analyzer Model CLA-220 is used to measure NO_x concentrations in the simulated diesel exhaust gases. The analyzer is equipped with an ozone generator to convert any NO present into NO_2 and an internal NO_2 to NO converter.

3.2.5 Data Acquisition System

The purpose of the data acquisition system (DAQ) is to monitor, process, display and save all data obtained during the BFR operation as well as control the MFCs. The DAQ consists of a Dell personal computer (PC), data acquisition boards, shielded BNC adapter chassis, terminal blocks and LabVIEW software. All thermocouple signals are gathered using a National Instruments Model TC-2095 shielded terminal block and routed through a National Instruments Model SCXI-1102 thermocouple signal amplifier. A National Instruments Model PXI-6040E multifunction DAQ card converts the signals from analog to digital and sends them to the PC through a National Instruments Model PXI-8330 PCI card. Pressure transducer and gas analyzer signals are acquired and conditioned using a National Instruments Model TBX-68 terminal block and sent directly to the PC for LabVIEW display. MFC signals are gathered using a National Instruments Model BNC-2090 connector block and routed through an additional National Instruments Model PXI-6040E PCI card for data sampling and display. Finally, the signals are routed along with the thermocouple signals to the PXI-8330 PCI card.

3.2.6 Data Acquisition System Components

A Dell Model PWS 350 PC is used for both LabVIEW software operation and data storage. The computer utilizes a 2.8 GHz Intel Pentium 4 processor and houses the National Instruments data acquisition boards discussed in Section 3.2.5. LabVIEW

version 6.1, graphics-based software developed by National Instruments, is used to monitor, display and store data as well as provide control of BFR components. The LabVIEW program consists of a control panel that serves as a user interface, shown in Figure 3.24. The control panel contains real-time data displays and control functions that can be either initiated by the user or programmed for autonomous control. Temperatures and pressure as well as MFC flow rates within the BFR during operation are displayed in both display boxes and in real-time XYZ plots that shows the BFR history. MFC flow rates are prescribed using input value boxes located at the top left of the screen. Finally, data storage can be performed at any point during testing with the save data button prompting the computer to write all collected data to a storage file created on the PC hard drive.

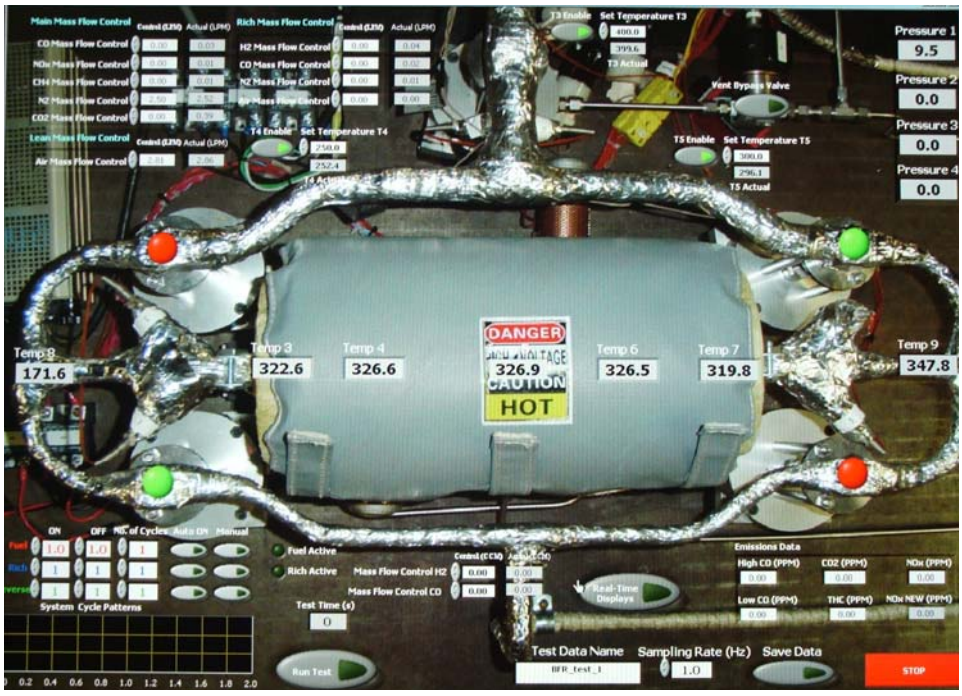

Figure 3.24: Screen capture of the LabVIEW control panel used to control and monitor the bench-flow reactor.

3.2.7 Bench-Flow Reactor Operation

3.2.7.1 Start-up Procedures

Prior to BFR start-up, a safety inspection is made to verify that the exhaust fan and CO detector in the laboratory are working properly. After the initial safety inspection, the gas analyzers and water chiller are turned on and allowed to reach steady state operating conditions by turning on the master power switch on the Horiba analyzer bench. The water chiller must be brought to a temperature below 6^{o}C - the saturation temperature of 10 % water at atmospheric pressure.

The FID and NO_x analyzers are supplied with feed gases consisting of 40 % H_2 in He and 100 % air, and 100 % O_2, respectively to reach operating conditions. Pure nitrogen flowing at 2 L/min is passed through each analyzer for 2 hours to reach steady-state operation. Once the analyzers have reached steady-state they are calibrated using span and zero gases. The instrumentation cabinet is turned on to provide power to the MFCs, pressure and temperature indicators and the DAQ system. A check of the LabVIEW control panel ensures proper control of the MFCs before the gas cylinders are opened. For proper MFC operation, gas cylinders are regulated to an exit pressure of 1.72 bar (25 psig).

Once all ancillary equipment is operational, the BFR is brought to an initial operating temperature of 200^{o}C by turning on the heat tape controllers and as well as the reactor and steam generator furnaces while passing pure nitrogen through the system at a GHSV that is to be used during the BFR evaluation. At the same time, the Horiba analyzer bench is readied to receive flow gases by selecting the analyzers to be used with the matrix switches. Once selected, the exhaust fan and the vacuum pump are turned on to provide sample pressure to the analyzers. De-ionized water is then injected into the steam generator and allowed to reach steady-state for approximately ten minutes. The final step is to adjust the BFR pressure to approximately 1.36 bar (5 psig) by manually adjusting the throttling valve and pressure regulator located on the front of the Horiba analyzer bench.

3.2.7.2 Light-off Measurement Procedures

Before light-off measurements begin each catalyst must be de-greened to allow the DOC to reach thermal equilibrium. This process is only necessary for fresh DOC samples because aged catalysts are stable. DOC de-greening is achieved by exposing the sample to simulated exhaust gases at 400°C and a gas hourly space velocity of 40,000 hr^{-1} with 10 % H_2O, 10 % O_2 and balance N_2 for approximately 4 hours. Two light-off evaluations are performed to ensure light-off repeatability by introducing simulated diesel exhaust gases comprised of 10 % H_20, 10 % O_2, 5 % CO_2, 500 ppm CO, 300 ppm C_2H_4, 1000 ppm NO_x and balance N_2 at a gas hourly space velocity of 80,000 hr^{-1} over a temperature range of 200 to 500°C in increments of 50°C. The cost to flow these gases continuously through the BFR for testing is high; therefore a substitute mixture of 10 % H_2O, 10 % O_2 and N_2 balance is used to reach steady-state operation within the DOC before flowing simulated diesel exhaust gases at each 50°C increment.

Temperature within the DOC reactor is adjusted by varying both heat tape and reactor furnace settings. Since isothermal conditions are unattainable within the DOC at elevated temperatures, the temperature at the DOC mid-bed location is assigned as the steady-state temperature to be reached before simulated diesel exhaust gases are passed through the DOC. LabVIEW stores all BFR data at the initiation of simulated diesel exhaust gases into the BFR until approximately three minutes, the time that the DOC reaches thermal equilibrium. The simulated diesel exhaust gases are then switched from the DOC to the reactor bypass line where the analyzers measure DOC inlet gas composition. A summary of heat tape and furnace settings are provided with the corresponding DOC mid-bed steady-state temperatures used during light-off evaluations in Table XIV.

3.3 Experimental Catalysts

The DOCs used in the present investigation are both commercially available and found on many heavy-duty, commercial diesel vehicles. The DOCs used come from two

Table XIV: Bench-flow reactor temperature settings required to maintain target DOC mid-bed temperatures.

Heat Tape Setting (C)	Reactor Furnace Setting (C)	DOC Mid-bed temperature (C)
315	200	200
375	250	250
425	300	300
475	352	350
525	410	400
575	470	450
575	525	500

sources; fresh DOCs obtained are manufactured for heavy-duty turbo diesel pickup trucks and deactivated DOCs from a bus fleet are obtained that were removed because of catastrophic deactivation occurring during field-service. The DOCs serve two functions in this study. The first is to understand how laboratory rapid poisoning tests affect DOC light-off performance and material properties. The second is to make a comparison between laboratory poisoning DOCs and field-service deactivated DOCs in both THC and CO light-off performance and material properties. The fresh commercial DOCs obtained are discussed in Section 3.2.1. The field-service deactivated commercial DOCs will be described in Section 3.3.2. Finally, Section 3.3.4 provides information pertaining to BFR DOC samples.

3.3.1 Rapid Poisoning DOCs

A fresh commercially-available DOC for heavy-duty turbo diesel pickup trucks was obtained for rapid poisoning tests. The DOC is manufactured by Engelhard Corporation and was obtained in its original housing. The DOC is 20.3 cm in diameter and 20.3 cm in length with a cell density of 300 cells/in^2 (cpsi). A total of eight 5.08 cm diameter cores are drilled from the catalyst and cut to a length of 15.2 cm. The resulting catalyst volume to engine capacity ratio is approximately 0.8 times that of a production device. Therefore, poisoning effects and light-off performance degradation will deviate

from those experienced during normal field service, but is sufficient for the comparison nature of this study. The monolithic structure is made of cordierite ($2MgO\text{-}2Al_2O_3\text{-}5SiO_2$ + trace elements) and has a washcoat consisting of alumina (Al_2O_3), ceria (CeO_2) and platinum with a loading of 0.5 gm/ft^3. The washcoat is double layered with the bottom layer approximately 20 μm thick and made entirely of alumina that is attached to the cordierite substrate. An overlay of alumina impregnated with ceria and platinum comprises the second layer and has a thickness of approximately 25 μm. The bottom layer acts as a bonding agent for the catalyzed top layer and acts as a filler to round the sharp corners of the monolith.

3.3.2 Field Deactivated DOCs

Three sets of field-service, two brick, diesel oxidation catalysts were obtained through Fleetguard Emissions Solutions that experienced high-mileage service and were removed due to a catastrophic event occurring while in operation in a bus fleet. Two catalyst pairs, each consisting of a front and rear brick, were contaminated with engine lube-oil, most likely a result of a blown turbo seal. The remaining pair has a thick soot deposit only at the inlets of the front and rear bricks, most likely a result of a light load duty cycle. Each brick of the catalyst system is used in this study to obtain an axial gradient of oil contaminants along the length of the catalyst as well as light-off performance. Each catalyst of two brick pair is of similar size and formulation as those of the pick-up truck DOC used in engine-bench poisoning tests. A summary of the field-service DOCs used during testing is provided in Table XV.

The DOCs were unassembled from their housing and two cores were removed from their centers. The cores measure 5.08 cm in diameter by 15.2 cm in length and are used in engine-bench light-off evaluations. A photograph of one DOC brick and a core sample is shown in Figure 3.25.

Table XV: List of mileage, age and reason for removal of the field-service diesel oxidation catalysts used in this study.

Catalyst Designation	Age (Years)	Mileage	Reason For Removal
4363-180	1.5	82,562	Soot Clog at Inlet
29921N	Unknown	Unknown	Oil Contaminated
28656N	2.0	115,625	Oil Contaminated

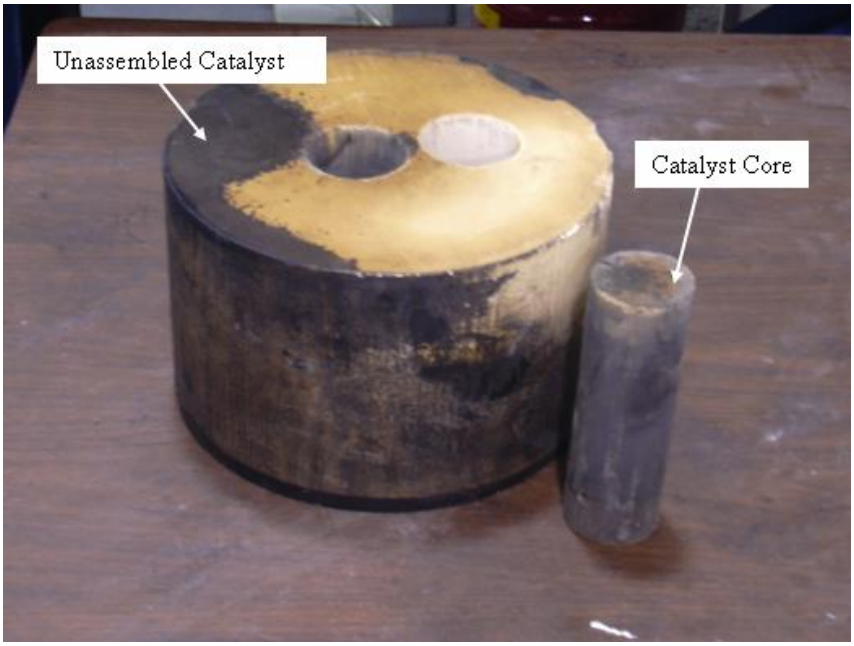

Figure 3.25: Photograph of an unassembled field-deactivated DOC with drilled core sample.

3.3.3 Bench-Flow Reactor DOCs

Bench-flow reactor DOC samples consist of core samples drilled from either a fresh, field-deactivated, or engine-poisoned DOC. Each core is approximately 2.22 cm in diameter and 7.62 cm in length. A total of 7 catalyst samples are used during the BFR testing with each catalyst history shown in Table XVI. Each catalyst used is of exact formulation as previously described in Sections 3.3.1 and 3.3.2. Since phosphorus is known to absorb preferentially at the front portion of the first brick, only the front brick of each two brick pair is used to measure light-off performance with the BFR. The two engine-poisoned DOCs selected for light-off performance evaluations on the BFR were selected because they exhibited severe light-off degradation as a result of poisoning. Phosphorus poisoning effects are therefore reasoned to be the most distinguishable in these DOCs.

3.4 Characterization Techniques

Analytical chemical and surface characterization techniques are utilized in this study in order to understand phosphorus poisoning mechanisms and for the comparison accelerated and field poisoned DOCs. Each surface characterization technique used in this study is outlined in its theory of operation, equipment and instrumentation and sample preparation. Also, a brief discussion of qualitative and quantitative information that can be obtained in each technique is provided. Section 3.4.1 will discuss X-ray photoelectron spectroscopy. Electron probe microanalysis and X-ray fluorescence spectroscopy information is presented in Sections 3.4.2 and 3.4.3, respectively. Section 3.4.4 contains information on secondary ion electrospray mass spectrometry and Section 3.4.5 describes the powder X-ray diffraction. Finally, Section 3.4.6 provides an overview of scanning electron microscopy and energy dispersive X-ray spectroscopy.

Table XVI: List of DOC history and deactivation-method evaluated using the bench-flow reactor system.

Catalyst	Type	History
Fresh	Commercial Catalyst	____
4363-180	Field-Aged	Soot Clogged
29921N	Field-Aged	Oil Contamination
28656N	Field-Aged	Oil Contamination
Exhaust Injection	Engine-Poisoned	6 grams phosphorus
Fuel Injection	Engine-Poisoned	6 grams phosphorus

3.4.1 X-ray Photoelectron Spectroscopy

X-ray photoelectron spectroscopy (XPS), also known as electron spectroscopy for chemical analysis (ESCA), is used to analyze the upper surfaces of materials. The principle behind XPS is the photoelectric effect in which the kinetic energy of an ejected electron is dependent on the energy of the impinging photon. The relationship is expressed in equation 3.1:

$$KE = h\nu - BE - \Phi \qquad \text{(Eq. 3.1)}$$

where KE is the kinetic energy of the ejected photon, h is Plank's constant, ν is the frequency of the impinging photon, BE is the binding energy of the parent atom relative to the ejected electron and Φ is the work function which is normally neglected because it is negligibly small.

XPS utilizes the photoelectric effect by ionizing atoms in a sample by bombarding the surface with high energy X-rays from either a Mg Kα (1253.6 eV) or Al Kα (1486.6 eV) source in an ultra-high vacuum (UHV). The electrons on the surface of the sample absorb the X-rays energy providing enough energy to escape from the parent atoms. An electrostatic field forces the ejected photons through a sweep lens that focuses the photons through the aperture concentric hemispherical analyzer (CHA). In the CHA, the photons encounter another electrostatic potential between two concentric hemispheres

bends the photon beam path an amount proportional to the applied potential. Photons with energy equal to the median equipotential surface contact the photon detector. Varying the voltage potential between the concentric hemispheres changes the median equipotential surface and thus a range of photon energies can be swept. A schematic of XPS operation is shown in Figure 3.26. Photons contacting the detector are counted and the binding energies are calculated from Eq. (3.1) and knowing the incident X- ray energy, $h\nu$, and the kinetic energy of the photons, which are specified by the median equipotential surface. The resulting data is presented as a plot of counts versus binding energy. Since every chemical compound has a unique binding energy spectrum, identification is made by inspection of the resulting plots [68,73,77,81,88,95].

The XPS machine utilized in the study is manufactured by Elmore and is located at the University of Tennessee. The machine uses a monochromated Al Kα source which produces slightly higher energy X-rays and sensitivity which translates into better spectrum resolution. The DOC samples, which are required only to be flat and approximately 2.54 centimeters diameter with a thickness of 2.54 centimeters, are loaded into the UHV chamber where they are positioned under the X-ray source and left for 24 hours under high vacuum. An Argon sputtering gun is used to clean contaminants from the surface of the sample prior to X-ray bombardment. The argon gun uses ionized argon gas to raster the sample surface. When the ionized argon hits the surface, enough energy is imparted to eject entire atoms from the surface, exposing an area approximately 3.0 μm in diameter to a desired depth. The argon gun penetrates the surface at a rate of 1.0 nm depth per minute. Once the surface is exposed, the XPS technique can be utilized effectively. A photograph of the XPS machine used in this study is shown in Figure 3.27.

3.4.2 Electron Probe Microanalysis

Electron Probe Microanalysis (EPMA) is used for DOC materials characterization and provides both elemental and spatial information. EPMA information is acquired by analyzing X-rays emitted from a sample when probed by a high-energy electron beam.

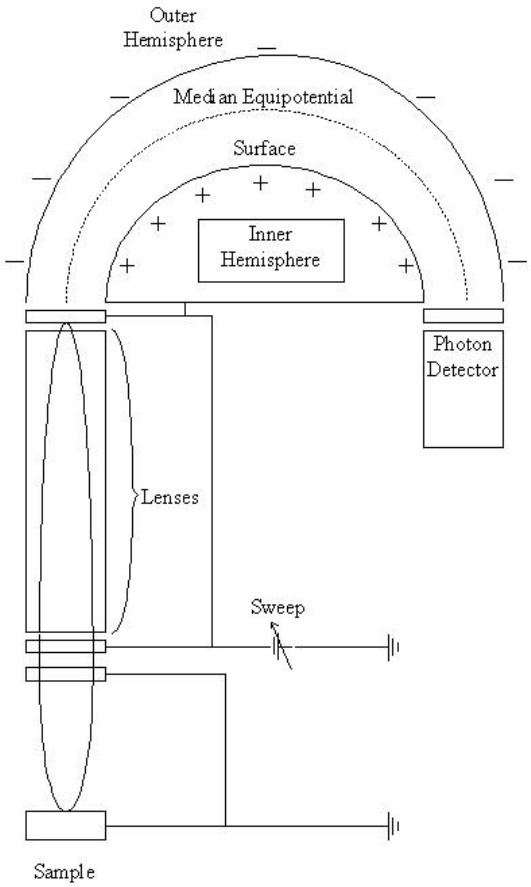

Figure 3.26: Schematic of X-ray photoelectron spectroscopy operation.

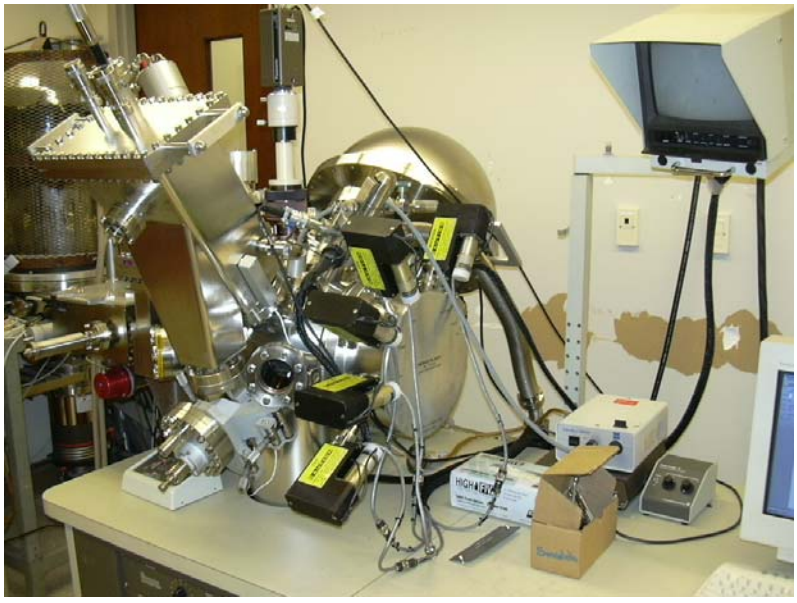

Figure 3.27: Photograph of X-ray photoelectron spectrometer hardware.

The X-ray detectors along with sophisticated software packages determine which elements the photoelectrons originated from and where on the sample surface.

EPMA is performed in much the same way as XPS discussed in the previous section. A finely focused beam of electrons from an electron gun impinges on the surface of the sample in an UHV. The electron collisions impart energy to the electrons samples atoms inducing an energized state. Energy is released in the form of an X-ray radiation, a high-energy photon, during the electron relaxation process when the electrons "jump" back to a lower energy state. The X-ray energy released in the relaxation process is precisely the same energy required to excite the electron to the energized state. Since each element has unique energy states, element identification can be made by measuring the produced X-rays.

A schematic of X-ray production process used in EPMA is shown in Figure 3.28. The schematic demonstrates the four mechanisms that are accessible for the production of X-rays. The first mechanism involves the impingement of an incident X-ray from a radioactive or electron gun, which collides with an electron. Energy from the X-ray is transferred to the electron providing the enough energy to overcome the atoms binding energy. The energy of the emitted electron is equal to the energy of the incident X-ray minus the potential energy barrier binding the electron. The second mechanism is the release of energy from electrons that occupy vacancies in the K-orbital. Once an electron is emitted from an atom it leaves a vacancy. Thermodynamics demands that electrons from either the L-orbital of the M-orbital occupy these vacancies. When this occurs, the electrons release energy in the form of X-rays. The X-rays emitted from this process are referred to as the K-line and are unique for each element. The third mechanism is similar to the second in that electrons giving up energy to vacancies in the L-orbital emit X-rays. In this case the permitted electron jumps are from the M-orbital and the N-orbital. The X-rays emitted by this mechanism is referred to the L-line and are most utilized for the analysis high atomic number.

The final process is the release of "auger" electrons. These electrons are emitted when X-rays that are produced in either the L-line or the K-line collide with the electrons in the outer most shell of the atom. Since the ionization energy is small for these

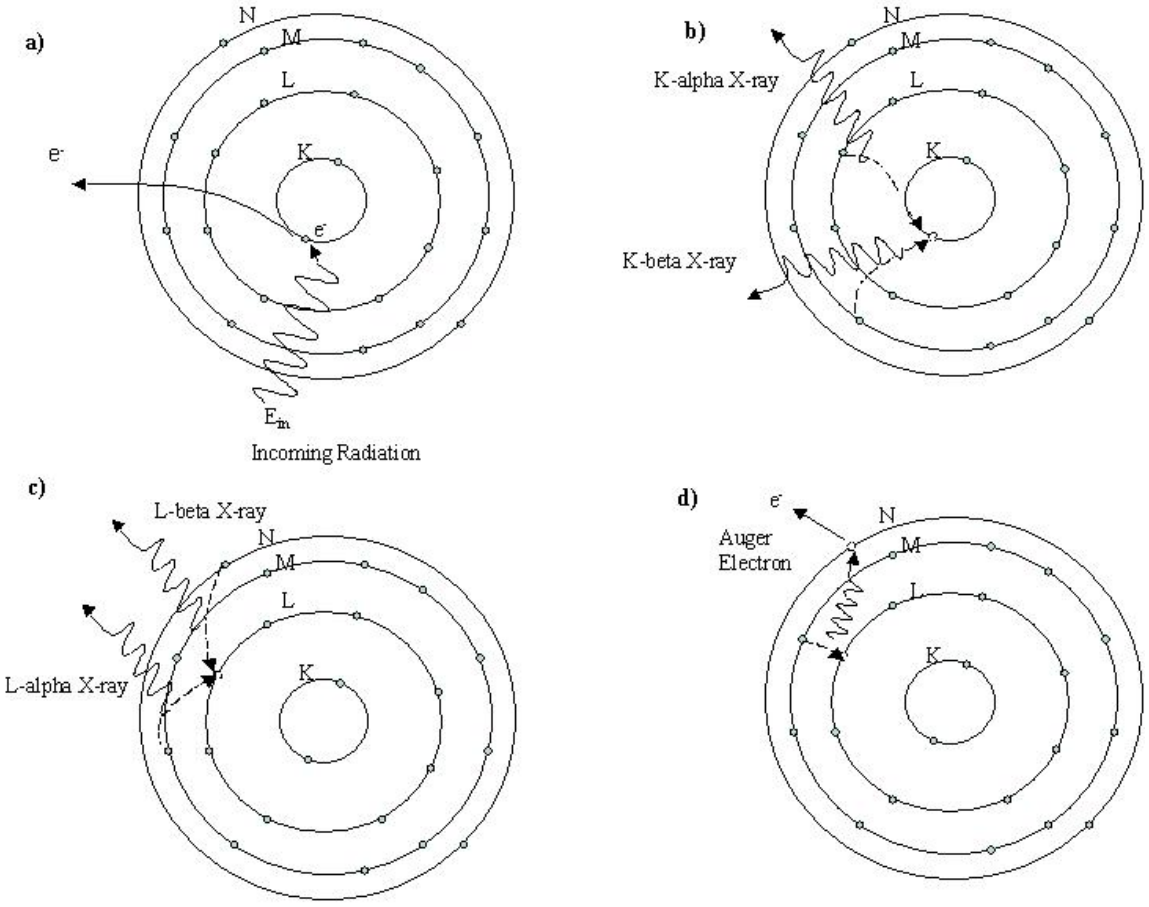

Figure 3.28: Schematic of available electron emission pathways.

electrons, they are readily ejected from the atom. The energy with which they leave the atom is equal to the potential energy of the parent-orbital binding energy minus the potential energy difference between the two orbitals of the shifted electrons [72,73,81,88].

The Cameca Model SX-52 EPMA device used in the current investigation is shown in Figure 3.29 and is located at the University of Tennessee. The device contains 5 vertical wavelength-dispersive spectrometers, a high-resolution energy dispersive solid-state detector and an electron optical column to produce a high electron beam. The electron beam is produced by a self-biasing LaB_6 cathode with double aperture beam regulation with a 0.5 to 300 nA beam current capable of fully automated alignment, focus and astigmatism correction. The X-ray spectrometers have a range of 0.22 to 0.83 sin-theta with a 40 degree X-ray take-off angle and 1E-5 sin-theta resolution. The solid-state energy dispersive detector is an Xflash 2000 detector with a resolution of less than 159 eV at 1000 counts/sec and less than 170 eV at 30,000 counts/sec. This detector has the ability to analyze elements in the atomic range of Sodium to Uranium.

Line-scans and elemental maps are obtained for each catalyst at the front and rear cross-sections. Line-scans are a trace of elemental concentrations of Ce, S, P, Al, Si, Zn, and Ca which are measured from the emitted X-ray radiation at a cross-section of the washcoat. The scans are used to determine the absorption of oil-derived contaminants

Figure 3.29: Photograph of the Cameca electron probe microanalysis hardware.

within the DOC. Elemental maps are rastered areas of the DOC in which X-ray data is collected and discretized to produce an image showing the locations of each element.

Sample preparation in EPMA is very important to ensure accuracy of results. The manner in which X-rays are analyzed require that the sample be perfectly flat and smooth. In reality this can never be obtained, however, much care is taken to come as close to the limit as possible. DOC samples are sectioned at cross-sections approximately 0.6 cm from he inlet and exit. The samples are placed in a mold and embedded with a low-viscosity resin, which is specially blended to fill pore sizes smaller that 1 μm. Vacuum assisted infusion is used to ensure all gases are extracted from the epoxy before curing. The molded sample is then further cross-sectioned to expose the surface of interest and polished to a 1 μm finish. The resulting area of analysis is approximately 2.54 cm in diameter and contains cross-sections of approximately 30 to 75 channels.

3.4.3 X-ray Fluorescence Spectroscopy

X-ray Fluorescence Spectroscopy (XRF) is used to measure elemental concentrations. Samples can be either in a liquid or a solid phase, but not the gas phase. XRF measures the energy X-rays emitted from the surface of a sample in the same manner as XPS and EPMA. The difference is in the way XRF analyzes the X-ray data. XRF analysis characterizes elements solely on the information received from the X-ray K- and L-lines rather than photoelectrons or auger-electrons as described in the previous section. The X-rays produced from the K- and L-lines are called secondary electrons. Fluorescence is defined as the release of secondary X-rays from a surface occurring when an incident X-ray from an electron tube interacts with surface atoms. The wavelengths of the secondary X-rays are dependent upon the elements in the sample and the intensity is dependent on the concentration. Since X-ray energy is directly related to the wavelength with which it moves, measuring both the energy and the number of the X-rays emitted from a sample will determine both the elements present and their respective concentration.

In this study, all XRF analysis was performed at Southwest Research Institute. The analyzer has three detectors, a flow and a sealed proportional detector with a parallel scintillation detector. This combination reduces background noise and increases signal resolution. In powder sampling, the method used for DOC analysis, the sample chamber is filled with helium or, if the sample allows, a high vacuum is used for high-resolution analysis of solid mineral samples. For DOC analysis high accuracy is required due to the relatively low concentrations of oil-derived contaminants and PMG elements. Therefore, the HV technique is used for the analysis.

XRF, like EPMA and XPS, requires a flat surface and a high vacuum for accurate the X-ray analysis. This is achieved by creating a "pellet" by pulverizing the DOC to a fine powder using a mortar and pestle. Approximately 5 g of the fine powder containing both DOC substrate and washcoat is placed in a mold and compressed to 15,000 psi to form a flat surface approximately 2.54 cm in diameter. Boric acid is included to the mixture to act as a binder during high vacuum conditions and is invisible to the XRF detectors.

The samples are scanned and a computer interprets the gathered data by comparing the spectra to a standards library of known elements and concentrations. A matrixing program calculates the elemental composition and concentration of the unknown sample by statistical data fitting techniques using the standards library. This process is limited, however, to elemental information present in both the standard; all other information is dropped along with information relating to light elements of which the detectors could not analyze.

3.4.4 Electrospray Mass Spectrometry

Electrospray mass spectrometry is used to determine compounds present in a solution. Since almost every other mass spectrometry method requires compounds to be in the gas phase, they are limited in their ability to measure high molecular weight molecules, which are difficult to "fly" without decomposing. Typical mass spectrometers use either thermal de-sorption or electron impact to liberate molecules under high

vacuums. However, high molecular weight molecules are often easily decomposed using these methods and are, therefore, unable to be identified. Electrospray mass spectrometry enables the identification of these compounds by suspending them in solution and passing them through a capillary held at a high electric potential to generate charged molecular ions. The capillary produces a droplet, which is induced across the high potential toward the mass spectrometer through a series of orifices within differential pumping zones. During the transition, either Coulomb explosion or evaporation is utilized to fragment the droplets and produce fully desolvated ions. Quadrapole mass spectrometers are used to isolate molecules by mass by varying an electric field. A collection plate detector is then commonly used to measure the number of incident molecules passing through the quadrapole and produce a mass spectrum. Compound identification is done by mass number calculation and by comparison to known standards. A schematic of the electrospray mass spectroscopy technique is shown in Figure 3.30.

Electrospray mass spectrometry, performed at the Fuels, Engines and Emissions Research Center at the Oak Ridge National Laboratory, was used to identify chemical species present in the exhaust gases during poisoning using the RPEB. During DOC poisoning an exhaust impinger sample is taken as described in Section 3.3.6 with a sample flow rate of approximately 28 liters per minute at room temperature and pressure. The samples are collected for at least one hour minimum, and in one extreme case 24 hours to ensure enough particulate matter was collected. The samples are diluted to a

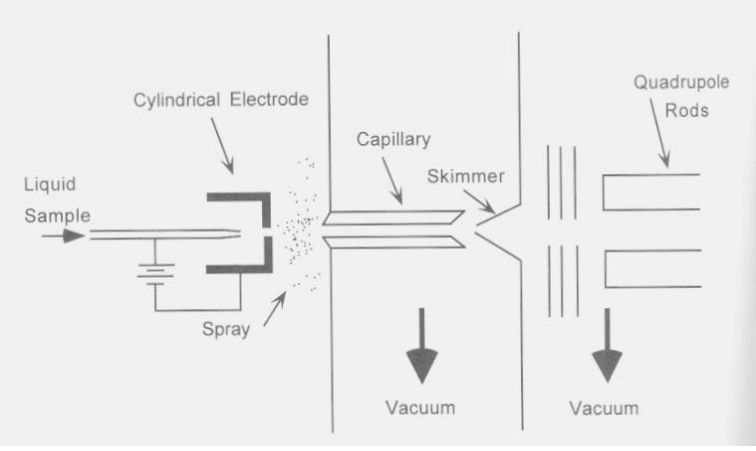

Figure 3.30: Schematic of electrospray mass spectrometer operation.[97]

50/50 mixture with acetonitrile and buffered to a pH of 10 with ammonium acetate. A settling time of 24 hours separates any particulate matter or oily residue present in the samples. The resulting clear phase material is used for the electrospray analysis [52,97].

3.4.5 Powder X-ray Diffraction

X-ray diffraction utilizes the phenomenon known as Bragg reflections to determine chemical compounds present within a sample. When a crystalline structure is bombarded with monochromatic X-ray radiation of wavelength λ, Bragg reflections result due to atomic lattice spacing that acts as a three-dimensional grating that diffracts the incident X-rays at specific angles. Reflections occur only when Bragg's law (Eq. 3.2) is satisfied:

$$n\lambda = 2d\sin(\theta) \qquad \text{(Eq. 3.2)}$$

where n is the order of the reflection, λ is the wavelength of incident X-rays, d is the atomic spacing between atoms and θ is the incident angle between the surface and the X-ray beam. If Bragg's law is not satisfied, then no predictable X-ray reflections will be produced.

In typical XRD devices, an incident X-ray beam made up of monochromatic X-rays of a prescribed wavelength is directed towards a sample. A spectrum is produced by measuring the angle and intensity of X-rays reflected off the surface with the use of a rotating arm X-ray detector. The spectrum consists of a series of peaks located at angles in which X-rays are reflected and has an intensity corresponding to the total number of reflected X-rays with the wavelength. Since the spacing between atomic layers in each compounds crystalline structure is unique, the angle of diffraction determines the compound present in the sample. In addition, it is known that the total amount of X-ray reflected at a certain wavelength is dependant on the available concentration of the compound in the sample and is observable in the XRD spectra by being proportional to the area under the obtained peaks [73,83,85,88].

In this study, approximately 1 g of washcoat material is scrapped from the monolith and ground to a fine powder. The material is placed in a sample holder to a thickness of approximately 1.5 mm and held in place with the use of ethyl acetate and polyester resin. Scans are taken using a Philips wide-angle XRD, located at the University of Tennessee, with a Cu Kα radiation source over a 2θ angle of 5-70^{o} in a scan mode of 0.02^{o} in 2 sec. The XRD spectra obtained are used to determine the chemical composition of oil-derived compounds formed within the DOC during poisoning. A photograph of the wide-angle XRD instrument used is shown in Figure 3.31.

3.4.6 Scanning Electron Microscopy

Scanning electron microscopy and energy dispersive X-ray spectroscopy are essentially identical in operation to electron probe microanalysis and X-ray fluorescence spectroscopy. A high-energy electron beam is focused onto a sample, which is situated within a UHV. The surface area of the sample is discretized by a computer and rastered by the electron beam. The incident beam induces the release of high-energy electrons

Figure 3.31: Photograph of wide-angle X-ray diffraction hardware.

and X-ray radiation. An electron and/or X-ray detector count the number of incident particles on the detector for each discretized area of the sample. The computer interprets the total number of electrons or X-rays counted and allocates the numerical value to an image generating routine, which produces and displays an image based on the relative electron and/or X-ray intensities.

Two forms of electron information are produced by this method, secondary electrons and backscattered electrons. Secondary electrons are emitted from the top surface atoms in the sample being analyzed. They are the primary source of information yielding surface topography and morphology. Backscattered electrons are produced when the incident beam electrons are reflected back to the detectors. The intensity of the reflected electrons is directly proportional to the atomic number of the elements preset in the sample. Backscattered electrons, however, are reflected relatively deep within a sample and therefore does not yield accurate surface topography.

Electron dispersive X-ray spectroscopy is used to determine the concentration of elements within the top few atomic layers of a sample. X-rays emitted form the surface are characteristic to the parent element from which they came. Detecting the energy of the emitted X-rays produces energy spectra from which elements can be identified [73,81,88].

In the present investigation, DOC surface topography is obtained using a Leo 1525 field emission SEM outfitted with a Link Oxford EDS detector located at the University of Tennessee and shown in Figure 3.32. DOC samples are taken at a location of 0.64 cm from the inlet of the DOC and are approximately 1 mm^2 in observable surface area. Washcoat is exposed by splitting the DOC along the length of a channel and removing all vertical obstructions. The samples are then coated with a 3 nm over-layer of gold, coving the observable washcoat and cordierite substrate, and placed in the UHV. The gold coating allows for increased image resolution while retaining all available elemental information for EDS analysis.

Figure 3.32: Photograph of the scanning electron microscopy hardware with energy dispersive spectrometry detector.

CHAPTER 4

RESULTS AND DISCUSSION

This chapter is divided into three main sections devoted to a discussion of the accelerated phosphorus poisoning degradation on DOC light-off behavior and material changes using the RPEB system. In addition, BFR light-off measurements and subsequent DOC regeneration are presented revealing that catalyst surface contamination by soot and lube-oil, rather than phosphorus, is the major contributor to DOC deactivation. Section 4.1 presents THC and CO light-off performance degradation resulting from accelerated ZDDP introduction methods. Section 4.2 describes the adsorption behavior of oil-derived contaminants within the DOC washcoat as well as compounds formed. Finally, Section 4.3 discusses BFR light-off performance measurements and subsequent regeneration behavior of DOCs including material changes.

4.1 THC and CO Light-off Performance

The light-off temperature is typically defined as the temperature at which 50 % conversion of a particular species is achieved. Engine-bench evaluations of phosphorus poisoned DOCs in this study, however, produce low THC and CO conversions: on the order of 50 % conversion or less. Consequently, THC and CO light-off temperatures of fresh, engine-poisoned and field-deactivated DOCs are defined as the temperature corresponding to 50 % of the maximum conversion observed in this study. Using this definition, the corresponding light-off temperatures for both CO and THC are 25 % and 20 %, respectively, and are used in the comparison of the deactivated DOCs. The reason for the poor conversion is low platinum content used in this particular DOC washcoat

formulation, which was designed 10 years ago to optimize only soluble particulate reductions with minimal sulfate production using traditional sulfur containing diesel fuels.

Fresh DOCs undergoing accelerated RPEB poisoning have two initial light-off evaluations performed after de-greening to check repeatability and ensure the DOC is in proper condition before testing. In each case, the fresh DOC produced THC and CO light-off behavior with maximum conversions between 39-45 % and 51-66 %, with corresponding light-off temperatures between 282-287^{o}C and 258-264^{o}C, respectively. This suggests a slight difference in either the DOC formulations, as a result of the manufacturing process, or error in the RPEB measurements and need to be considered when comparing the behavior of accelerated and field poisoned DOCs.

4.1.1 Rapid Engine-Poisoned

4.1.1.1 Intake Manifold Injection Poisoning

Four DOCs underwent intake manifold injection poisoning, each under different engine load conditions. The purpose of this approach is twofold: to determine the effect of engine load on exhaust phosphorus chemistry during ZDDP injection, and to obtain a correlation between engine load and DOC light-off performance degradation and phosphorus poisoning behavior. Bunting et al. [20] used electrospray mass spectrometry to identify phosphorus compounds. They found that ZDDP injected into the intake manifold was present in the form of phosphoric acid and adversely affected DOC light-off performance by reacting with the washcoat. Samples collected for analysis in their investigation were collected over a range of engine loads from 15 – 100 % producing no phosphorus chemistry dependence on engine load. In order to determine if phosphorus exhaust chemistry is altered by the combustion temperature, exhaust samples are collected at 0, 50 and 100 % engine loads.

For each of the engine load conditions investigated using intake manifold injection poisoning, phosphoric acid is the only phosphorus containing species measured by electrospray mass spectrometry in the exhaust gases. Figures 4.1 and 4.2 are mass

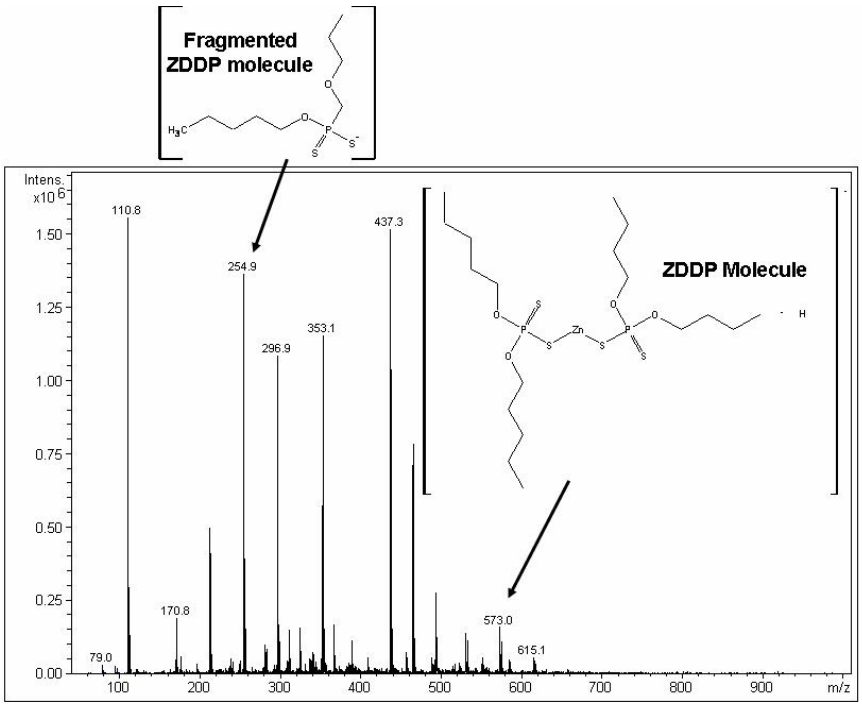

Figure 4.1: Mass spectra of the exhaust manifold injection poisoning sample at 50 % engine load obtained by electrospray mass spectrometry.

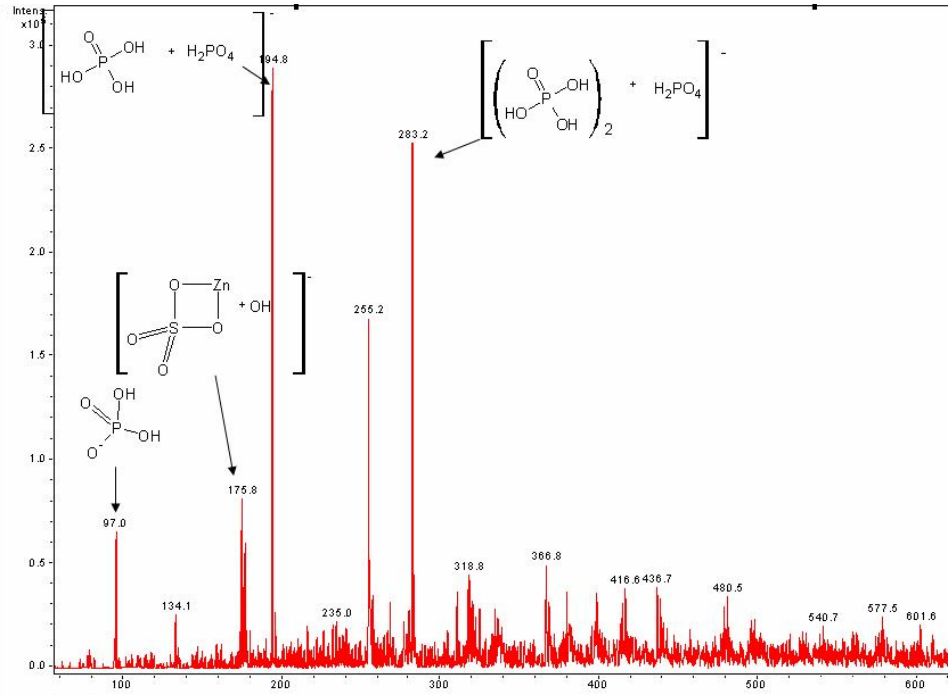

Figure 4.2: Mass spectra of exhaust gases obtained during intake manifold injection poisoning at 0 % load.

spectra for the exhaust manifold injection poisoning sample and the intake manifold exhaust sample at 0 % engine load, respectively. Raw ZDDP molecules are present at a mass-to-charge ratio (m/Z) of 573.0 as indicated in Figure 4.1. The 0 % engine load exhaust sample, which is representative of all three engine load tests, has no distinguishable peak at 573.0 m/Z, indicating no ZDDP survives the combustion process. The sample, however, does have observable peaks located at 97, 175, 195 and 283 m/Z, which correspond to zinc sulfate and phosphoric acid as well as their hydrolyzed multiples.

In none of the exhaust samples was phosphorus pentoxide (P_2O_5) identified, which has been presumed in past studies as a possible exhaust species contributing to phosphorus poisoning [15-17]. Organic phosphorus compounds were not measured in this investigation due to difficulties in sample preparation technique. It is, however, likely that the compounds are present within the soot in the form of carbon chain terminating radicals as described by Zhang et al. [40]. In addition, the only sulfur compound found in the exhaust is zinc sulfate, which Bunting et al. has identified as a stable particulate that passes through the DOC without contributing to poisoning.

In order to identify compounds within the exhaust gases in the solid phase, SEM-EDS are used to analyze soot samples collected during poisoning. Figure 4.3 is a backscatter and SEM image of a region of soot analyzed using EDS. The majority of soot collected is grouped into agglomerates of 6 μm or less in diameter. Backscatter images confirm the presence of heavy atomic weight elements incorporated within the soot and are seen as light discolorations due to their ability to reflect incident electrons. EDS analysis performed on the region shows that phosphorus, sulfur, zinc and calcium are present in the solid phase. It is not known, however, if these contaminants can become chemically adsorbed within the washcoat or simply passed through the DOC along with ash.

THC and CO light-off degradation resulting from intake manifold injection poisoning exhibits dependence on both the rate of ZDDP injection and the engine load

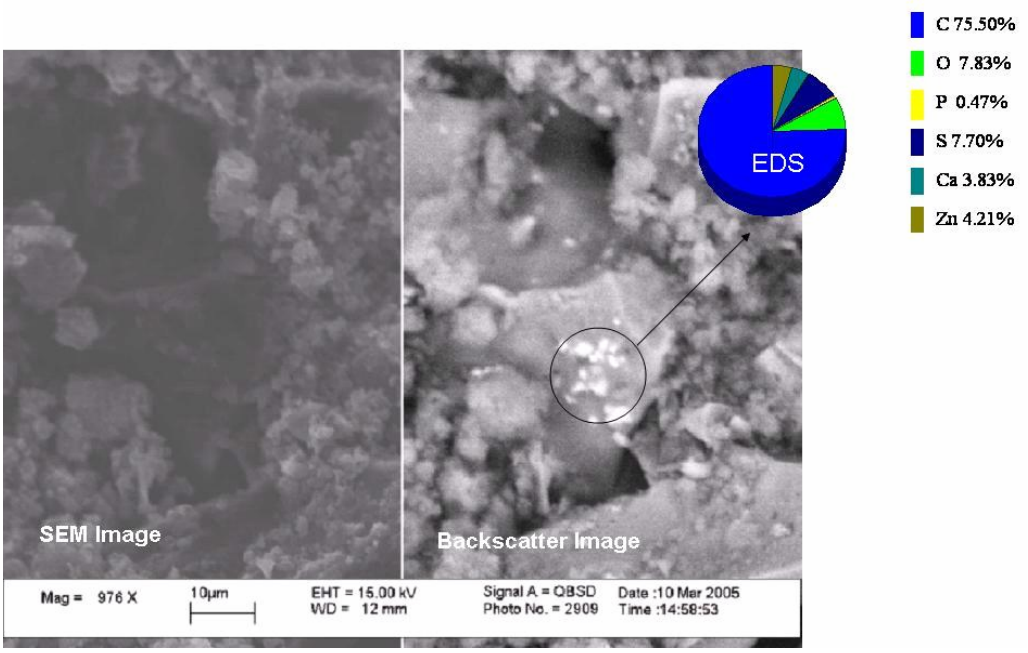

Figure 4.3: SEM and backscatter image of soot and elemental concentrations obtained from intake manifold injection poisoning.

during accelerated poisoning. Figure 4.4 is a plot of THC and CO light-off performance degradation for both the fresh and poisoned DOC with 6.0 g of phosphorus undergoing intake manifold injection poisoning at variable engine loads. The decrease in THC and CO light-off performance is approximately mid-range of that observed in all of the intake manifold injection poisoning methods with corresponding increase of approximately 100^{o}C and 30^{o}C, respectively.

Figure 4.5 is a plot of THC and CO light-off temperatures as a function of phosphorus introduced. The scattering of the light-off temperatures seen in Figure 4.5 is attributed to engine variability between evaluations. Although there are large light-off temperature differences between consecutive measurements, a clear THC deactivation trend is observed with the amount of phosphorus accumulated in the DOCs. CO oxidation is largely unaffected by phosphorus poisoning with temperatures remaining within ± 25^{o}C of the initial light-off temperature.

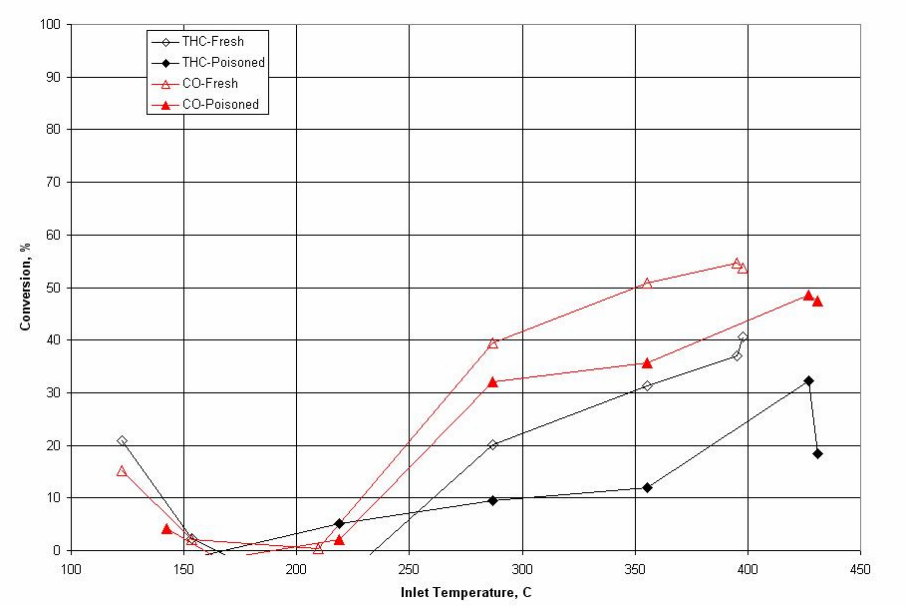

Figure 4.4: THC and CO light-off performance comparison of fresh and intake manifold injection poisoning at variable engine loads DOCs.

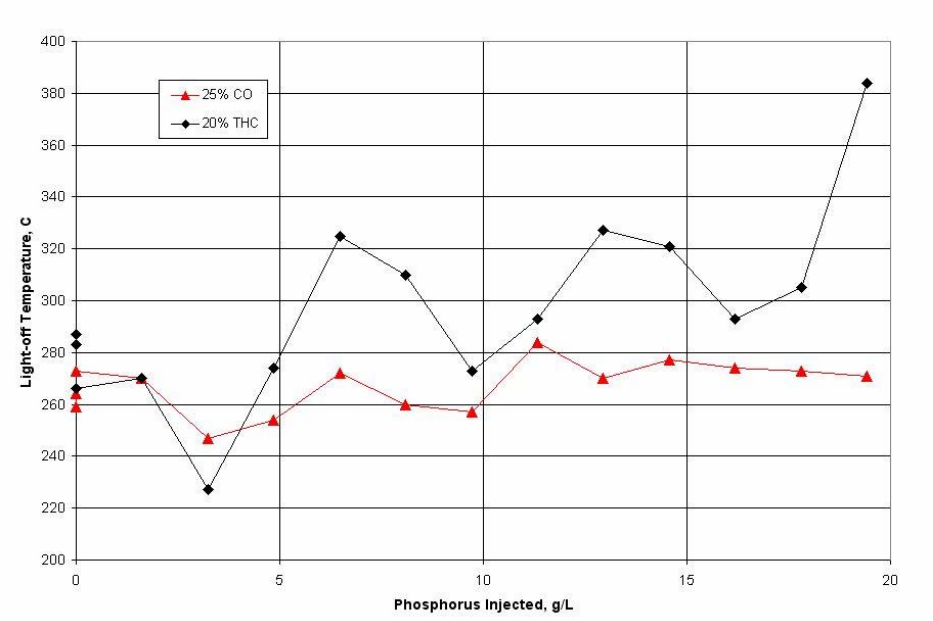

Figure 4.5: Plot of THC and CO light-off temperatures as a function of phosphorus injected during intake manifold injection poisoning at variable engine loads.

THC and CO light-off performance degradation of 0, 50 and 100 % engine load intake manifold injection poisoning tests are shown in Figures 4.6, 4.7 and 4.8, respectively. In each test, CO conversion is largely unaffected by the presence of phosphorus in the exhaust gases, but does show a dependence on the engine load used during poisoning with high engine loads producing greater degradation. The largest CO light-off temperature increase measured is 54^{o}C and is observed in the 100 % engine load test, which is more than double that measured at 50 % load and triple that of 0 % load. Maximum CO conversions, on the other hand, are not affected by phosphorus accumulation within the DOC with maximum conversions equivalent to fresh DOCs, irrespective of the engine load during poisoning.

THC light-off performance and maximum conversions are greatly affected by the presence of phosphorus with severe degradation observed in each engine load test. 100 % engine load yields the worst degradation with a maximum THC conversion of 21 % and a light-off temperature of 430^{o}C - an increase of 160^{o}C. The 0 % and 50 % engine load tests produce similar increases in THC light-off temperatures of approximately 140^{o}C each.

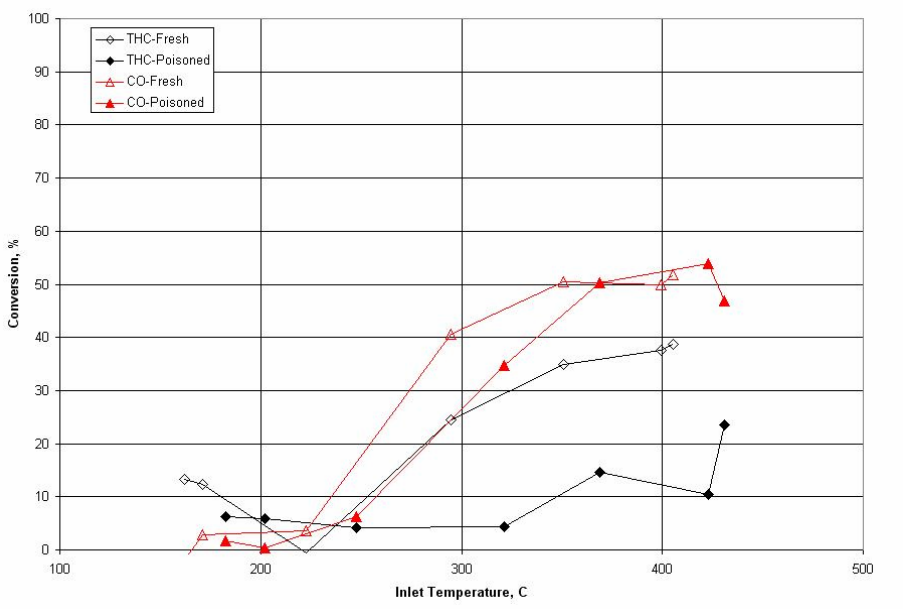

Figure 4.6: THC and CO light-off comparison of fresh and intake manifold injection poisoning at 0 % engine load DOCs.

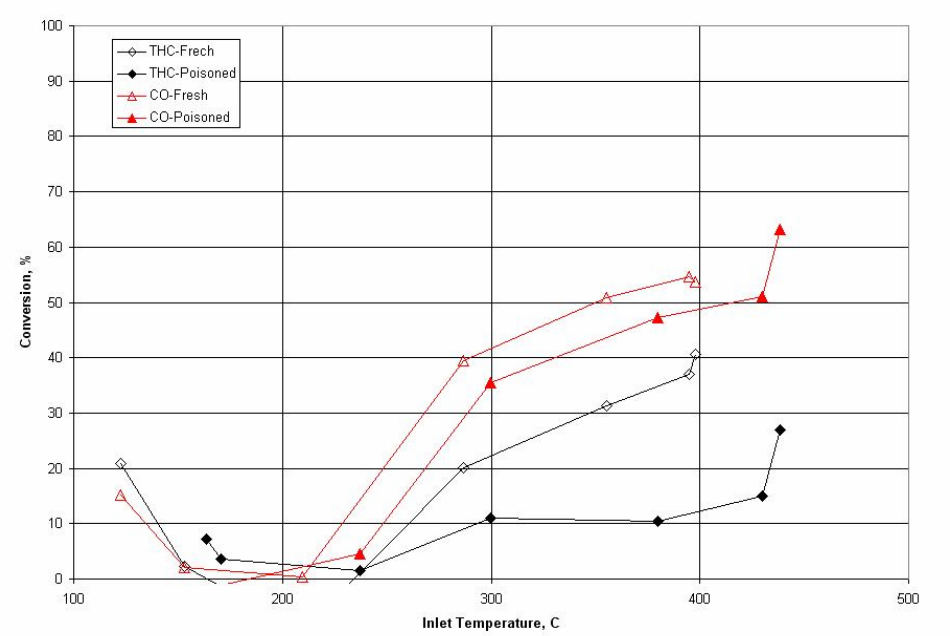

Figure 4.7: THC and CO light-off comparison of fresh and intake manifold injection poisoning at 50 % engine load DOCs.

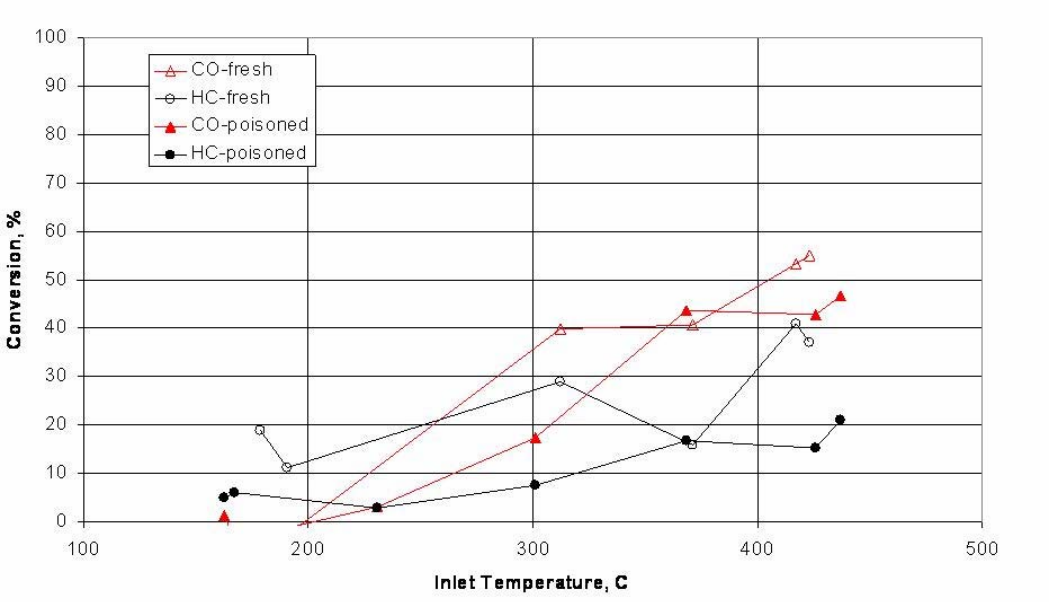

Figure 4.8: THC and CO light-off comparison of fresh and intake injection poisoning at 100 % engine load DOCs.

The shapes of the THC and CO light-off curves convey information on the degradation process and how phosphorus affects DOCs conversion. THC light-off curves are gradual which indicates a decrease in cold-start light-off performance in field-service DOCs. Past investigations [3,12,14,18,20,35-39] show this result occurs by accumulating oil-derived contamination at the front portion of the DOC, which reduces the low-temperature storage of gaseous hydrocarbons for oxidization at high exhaust temperatures. In addition, a steep increase in both CO and THC conversions between 250^{o}C and 350^{o}C is observed which signifies the beginning of the light-off region where the rate of reaction is dramatically increased due to an increase of available thermal energy to bypass the reaction activation energy threshold. For CO and THC species, the light-off temperature region is shifted after poisoning indicating much higher energies are required to induce reactions by the loss of available surface area on the DOC washcoat.

4.1.1.2 Exhaust Manifold Injection Poisoning

Exhaust manifold injection poisoning results in significant THC and CO light-off performance degradation as seen in Figure 4.9 for the fresh and poisoned DOC with 6.0 g phosphorus. CO oxidation performance is severely degraded, more than in intake manifold injection poisoning tests, and is attributed to the formation of a zinc-phosphate washcoat glaze. The glaze is a result of the introduction of raw ZDDP-doped lube-oil into the exhaust gases. Bunting et al. [20] confirmed the formation of a zinc-phosphate glaze on the washcoat using similar methods and is found to act as a diffusion barrier limiting catalytic reactions. Subsequently, the maximum CO conversion after poisoning is approximately 30 % less than that of the fresh DOC and is accompanied by a light-off temperature increase of approximately 80^{o}C. SEM and EPMA analyses confirm the formation of the zinc-phosphate glaze on the DOC washcoat surface with elemental concentrations that are consistent with zinc pyrophosphate ($Zn_2P_2O_7$) as will be discussed in detail in Section 4.2.

THC conversion is also affected by the zinc-phosphate glaze causing a loss in maximum THC conversion of 10 % compared to the fresh DOC. The degradation is not

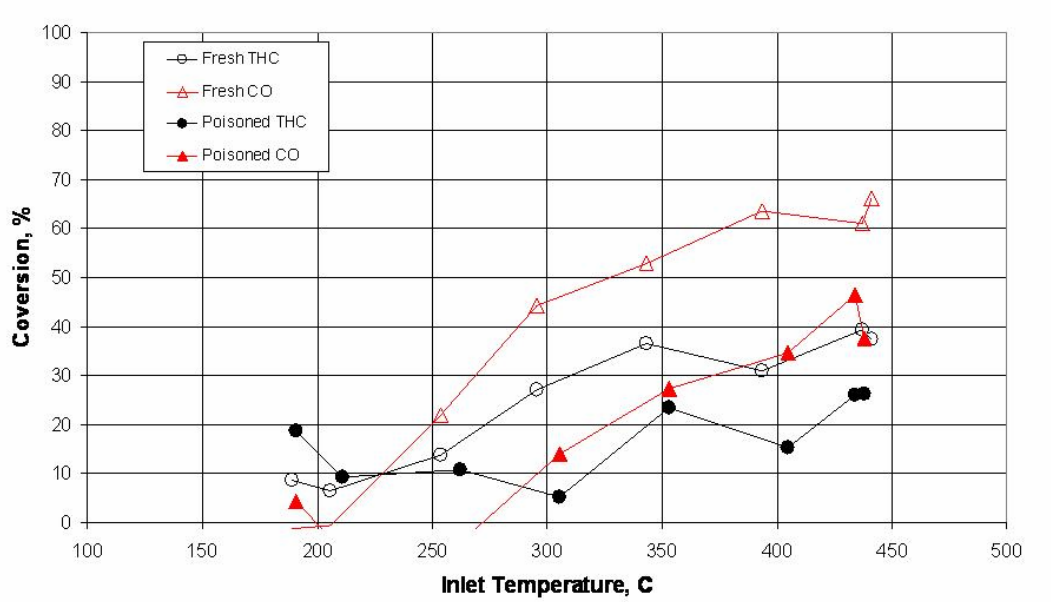

Figure 4.9: THC and CO light-off comparison of fresh and exhaust manifold injection poisoning DOCs.

as severe as observed during the intake manifold injection method, however. Though not confirmed, THC conversion in exhaust manifold injection appears to be higher by the redox behavior of CeO_2, which is not altered by the presence of the zinc-phosphate glaze. The maximum conversion is higher, over 25 %, and is accompanied by a light-off temperature increase of approximately 65^{o}C.

Figure 4.10 is a plot of THC and CO light-off temperature degradation as a function of phosphorus injected during the exhaust manifold injection poisoning method. Again, THC and CO performance is increased after an initial ZDDP injection, as occurred during intake manifold injection poisoning. In addition, a sharp CO light-off performance decrease is observed at high phosphorus loadings. As in the case of intake manifold injection poisoning, light-off temperature measurements tend to have much variability and is attributed to the behavior of the engine. A trend is observable, however, for high phosphorus accumulation.

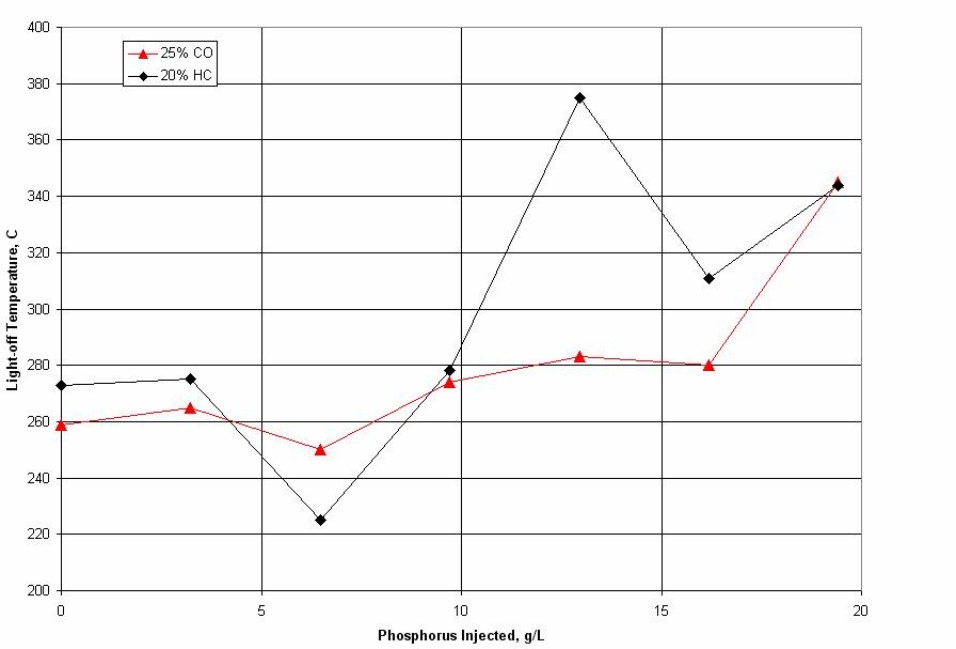

Figure 4.10: Plot of THC and CO light-off temperatures as a function of phosphorus injected during exhaust manifold injection poisoning.

4.1.1.3 Fuel Injection Poisoning

ZDDP-doped fuel injection poisoning produces the greatest amount of light-off degradation compared to any other accelerated poisoning method. Figure 4.11 is a plot of CO and THC light-off performance for the fresh and ZDDP-doped fuel injection poisoned DOC after 6.0 g of phosphorus is introduced. Both THC and CO performance is degraded with THC conversion remaining below the 20 % light-off threshold. Negligible CO oxidation is observed at low exhaust temperatures with a sharp conversion increase as temperatures approach 350^{o}C. As a result, the increases in THC and CO light-off temperatures are 85^{o}C and 95^{o}C after poisoning, respectively.

The extreme reduction in light-off performance is the result of a thick soot over-layer developed on the DOC during poisoning as described in Section 4.2. The high soot content is the result of fuel injector fouling by lube-oil-derived ash deposits. During poisoning, the viscous lube-oil was not properly atomized with the fuel during injection. The lube-oil left on the injector nozzle was consumed during combustion leaving an ash

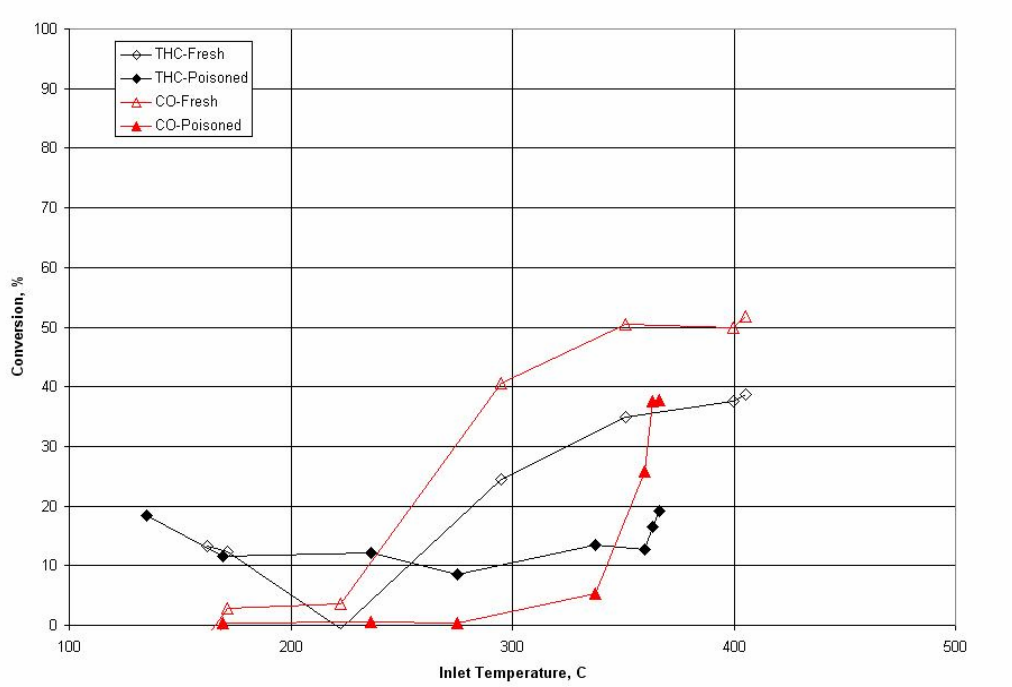

Figure 4.11: THC and CO light-off comparison of fresh and ZDDP-doped fuel injection poisoning DOCs.

residue which fouls the injector nozzle tip, leading to an increase in soot formation. Since fuel is no longer properly atomized, incomplete combustion occurs resulting in low exhaust gas temperatures during the light-off evaluation. A maximum exhaust gas temperature of 365^{o}C is experienced by the DOC, 50^{o}C less than maximum temperatures obtainable in normal operation. Once exhaust gas temperatures were raised above 325^{o}C, however, the DOC began to regenerate by burning more soot than is being accumulated on the surface and increasing the conversion of THC and CO.

4.1.2 Field-Deactivated DOCs

Each of the three, two brick, DOC pairs received from field-service exhibits severe light-off degradation. DOC 4363-180 - soot-clogged front and rear brick inlets - yields the worst light-off performance of all the field-deactivated DOCs. Figure 4.12 compares the THC and CO light-off performance of the front and rear bricks of DOC 4363-180 and shows more activity within the front brick over the rear. This observation is in contrast to observations made in the literature, which found the front brick to

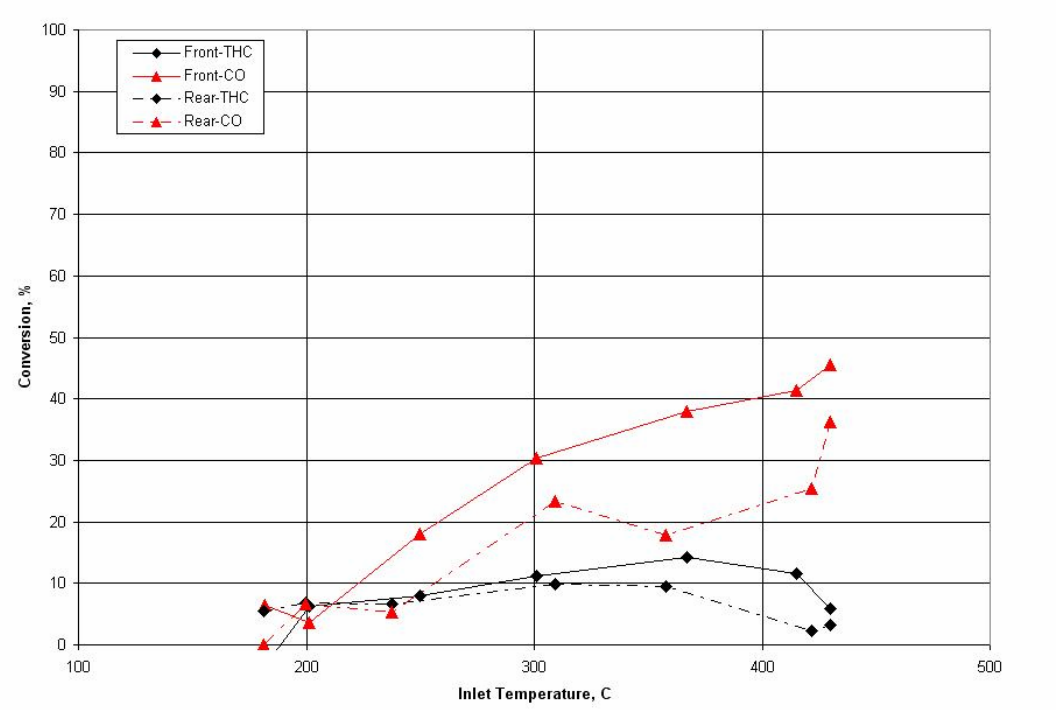

Figure 4.12: THC and CO light-off comparison of the front and rear bricks of DOC 4363-180.

perform the worse [13,39]; however, the rear brick of DOC 4363-180 had a noticeably thicker soot-clog at the inlet causing greater flow obstruction and channel blockage. The blockage of channels produces a decrease in the DOC flow cross-sectional area, resulting in higher GHSV; and hence a reduction in DOC performance. As a result, a CO light-off temperature difference between the front and rear catalysts of approximately 140^{o}C with a maximum CO conversion difference of 10 % is measured. On the other hand, THC conversion is highly affected by the presence of soot and failed to reach the 20 % light-off threshold in either brick.

The other DOC pairs experienced raw lube-oil deposition during field-service operation and are better than DOC 4363-180 in both light-off performance and maximum THC and CO conversions. Figures 4.13 and 4.14 are plots of the front and rear catalyst light-off performance of 28656N and 29921N, respectively. Each DOC shows a higher maximum conversion and lower THC and CO light-off temperatures in the rear brick than in the front. This is expected based upon the observation that raw lube-

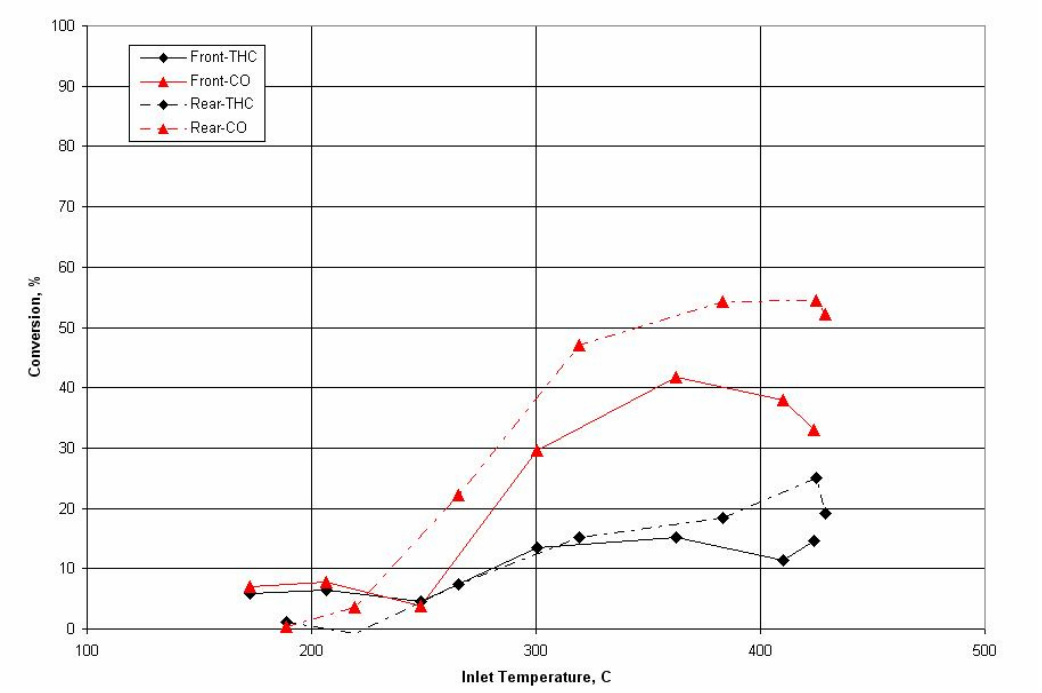

Figure 4.13: THC and CO light-off comparison of the front and rear bricks of DOC 28656N.

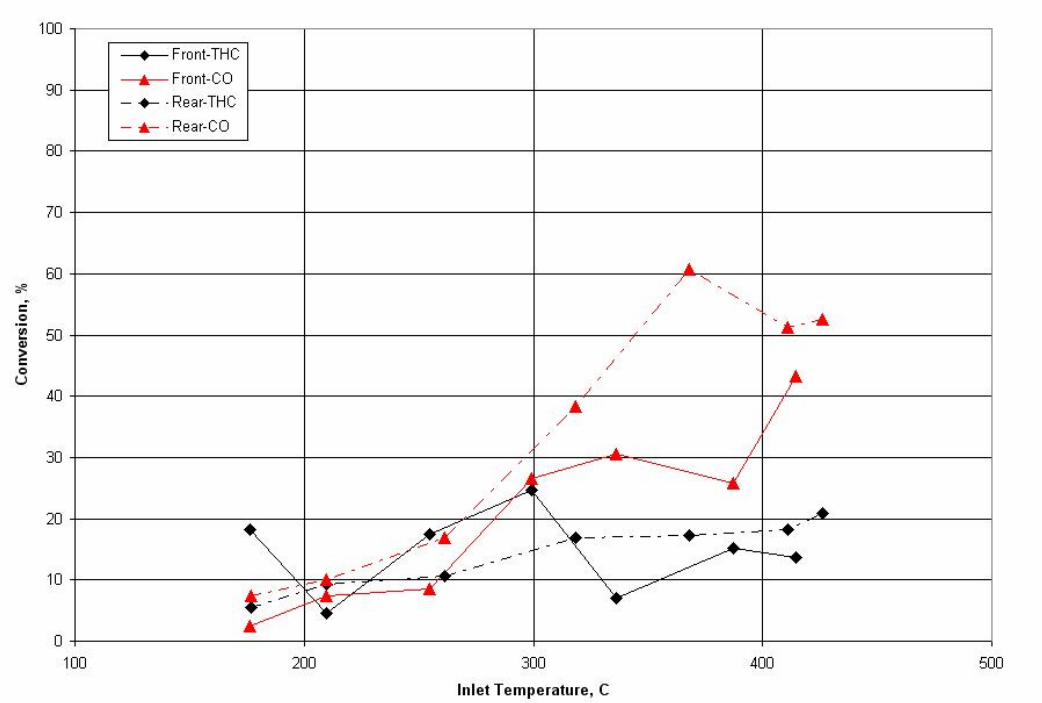

Figure 4.14: THC and CO light-off comparison of the front and rear bricks of DOC 29921N.

oil introduced into the DOC assembly during field-service did not penetrate to the rear brick. In addition, oil-derived poisons in the gas phase, such as phosphorus, have been shown to deposit preferentially in the front portion of the DOC [3,12,14,18,20,35-39]]. Therefore, poisoning on the rear brick is due solely to normal driving conditions, which are not as severe. The light-off curves of each DOC pair are similar in shape, but DOC 28656N performs better overall. This is attributed to a noticeably smaller lube-oil deposit within that close-coupled pair.

4.1.3 Comparison and Summary

Figures 4.15 and 4.16 are a comparison of CO and THC light-off behavior for fresh, engine-poisoned and field-deactivated DOCs in which the conversions are plotted at three different temperatures: 200, 300 and 375^{o}C. These temperatures are chosen because they are representative of the overall light-off behavior. THC conversion is highly affected by poisoning in both the engine-poisoned and the field-deactivated DOCs, irrespective of the deactivation mechanisms. CO light-off behavior appears to be mildly affected by the presence of oil-derived poisons. The exception being the DOCs undergoing exhaust manifold and fuel injection poisoning methods as well as the soot clogged field-deactivated DOC, which contain a high level of washcoat surface contamination. It is concluded that CO oxidation is not significantly affected by the presence of phosphorus, but rather is inhibited by soot and lube-oil derived contamination acting as a diffusion barrier. On the other hand, DOCs without significant washcoat contamination exhibit CO light-off behavior close to that measured in the fresh DOCs.

Based on the CO and THC light-off behavior comparisons, intake manifold injection poisoning provides the best correlation to field-service deactivated DOCs. Each engine load test using intake manifold injection poisoning results in THC and CO light-off behavior comparable to the average performance measured in both the front and rear bricks of DOCs 29921N and 28656N – lube-oil contaminated DOCs. ZDDP-doped fuel and exhaust manifold injection poisonings show behavior more consistent with DOC 4363-180 – soot clogged. Fuel injection poisoning results in THC light-off performance

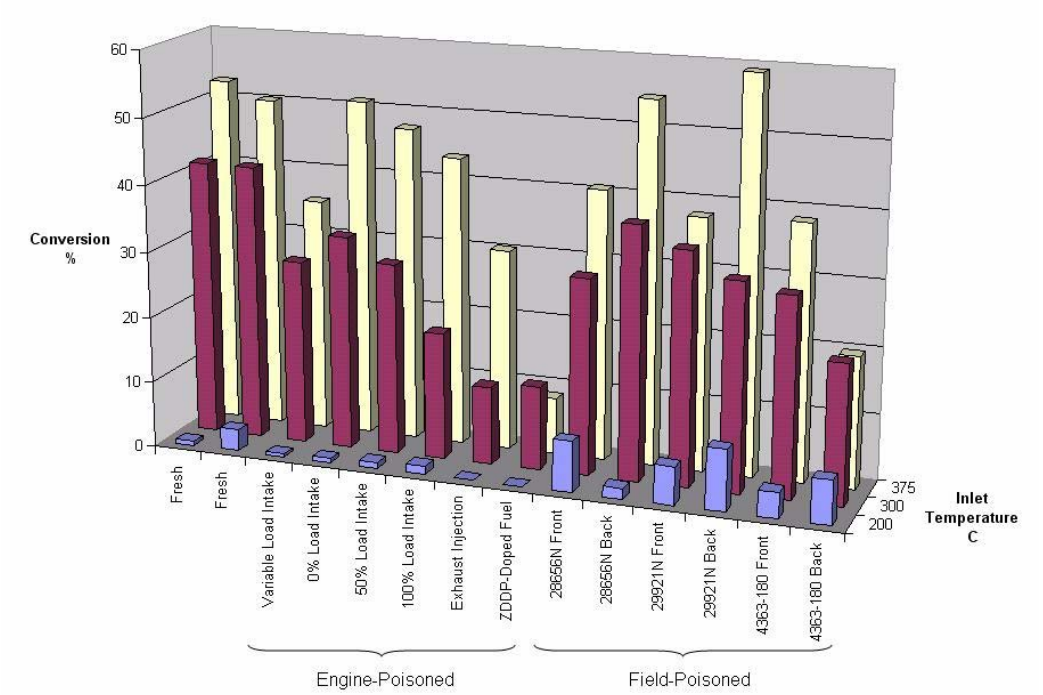

Figure 4.15: Comparison of CO light-off behavior of fresh, accelerated poisoning and field-deactivated DOCs using the engine-bench.

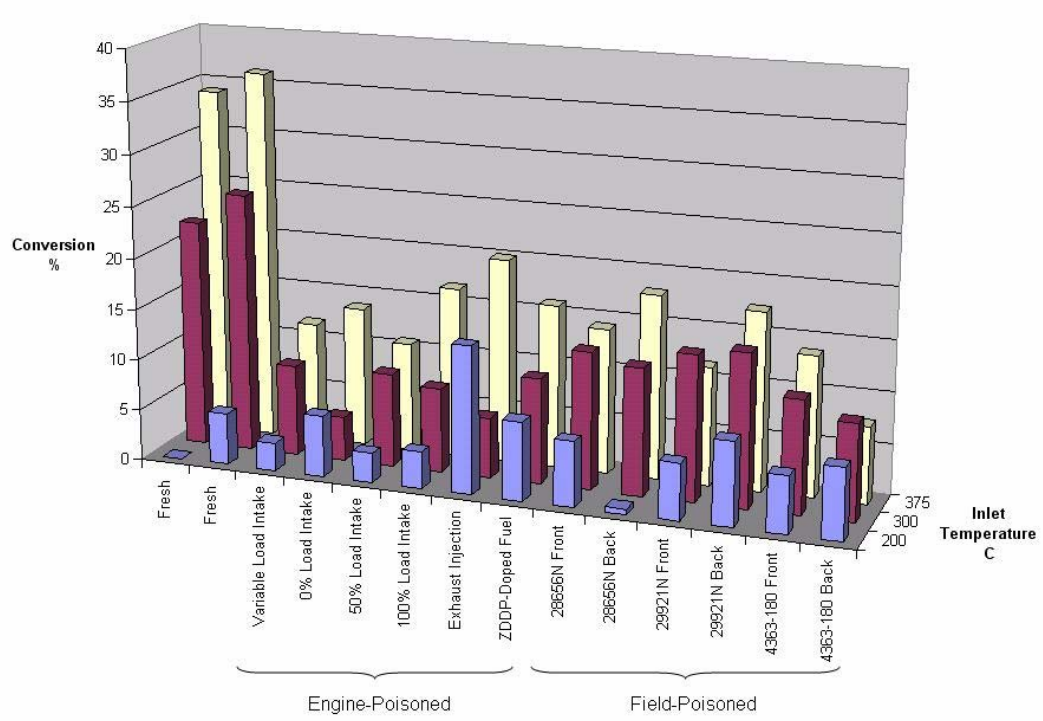

Figure 4.16: Comparison of THC light-off behavior of fresh, accelerated poisoning and field-deactivated DOCs using the engine-bench.

that closely matches the conversion obtained in DOC 4363-180, but yields poor CO oxidation – far below that of any other DOC. Exhaust manifold injection poisoning also matches the CO oxidation performance of DOC 4363-180, but the THC conversion is significantly higher. It is concluded that phosphorus poisoning is best simulated using the intake manifold injection method, which produces a similar poisoning process to that experienced during normal engine operation.

4.2 Materials Characterization

XRF analysis confirms the presence of oil-derived contaminants in all DOCs examined in this study. Contamination levels of phosphorus, sulfur and zinc in each DOC exhibits dependence on the ZDDP introduction method as well as the engine load during poisoning, as shown in Tables XVII and XVIII. As expected, DOCs that experienced high sustained engine loads during accelerated poisoning yield an increased level of oil-derived contamination within the DOC; since the rate of diffusion is proportional to the square root of the average temperature. In addition, the rate of poison adsorption on catalysts is known to be temperature dependent, with higher rates typically occurring at high temperatures [12,14,15,17,20]. As an example, the difference in phosphorus and sulfur adsorption during intake manifold injection poisoning at 0 % and 100 % loads are 0.83 g $P/g_{catalyst}$ and 1.77 g $S/g_{catalyst}$, respectively, with an increase in DOC inlet temperature of 250^{o}C.

Table XVII: Bulk phosphorus, sulfur and zinc composition within the front and rear bricks of the field-deactivated DOCs.

DOC	Brick	Phosphorus (Mass %)	Sulfur (Mass %)	Zinc (Mass %)
4363-180	Front	1.96	4.56	0.15
	Rear	1.96	3.34	0.19
28656N	Front	1.72	4.43	0.22
	Rear	0.71	0.42	<0.01
29921N	Front	0.18	0.35	0.15
	Rear	0.12	0.61	0.09

Table XVIII: Bulk phosphorus, sulfur and zinc composition of DOCs undergoing accelerated ZDDP introduction poisoning.

Element	Fresh	Variable Load Intake	100 % Load Intake Injection	50 % Load Intake Injection	0 % Load Intake Injection	ZDDP-Doped Fuel Injection	Exhaust Manifold Injection
	Concentration (Mass %)						
Phosphorus	<0.01	0.53	1.72	1.49	0.89	0.64	1.19
Sulfur	0.02	0.49	2.44	1.25	0.67	1.04	0.58
Zinc	<0.01	<0.01	0.08	0.26	0.06	0.03	0.17

Intake manifold injection poisoning at 100 % engine load produces the greatest amount of absorbed phosphorus and sulfur on the DOC, whereas variable load intake manifold injection produces the least. The small accumulation during variable load intake poisoning is partly attributed to cylinder wall wetting that occurs during intake manifold lube-oil injections. It was observed at the conclusion of the tests that a fraction of the ZDDP-doped lube-oil deposits within the crankcase after bypassing the piston rings. It is believed that the injection rate of lube-oil during the tests is faster than the rate of evaporation and decomposition within the combustion chamber. The accumulation of phosphorus and sulfur is, therefore, higher since the intake manifold injection poisoning at 100 % engine load test remained at higher cylinder wall temperatures.

Cylinder wall wetting did not occur during ZDDP-doped fuel injection poisoning, even though ZDDP is introduced at the same rate of 50 cc/hr. It is thought the fuel injector nozzle is more efficient in atomizing the ZDDP-doped lube-oil during injections than the syringe pump apparatus, increasing the burning rate of the lube-oil. The effect of increased burning rate is an increase in the total amount of phosphorus incorporated into the exhaust system and subsequently depositing on the DOC. Table XIX lists total phosphorus accumulation within DOCs undergoing accelerated phosphorus poisoning as well as the percentage of phosphorus accumulated for each method and demonstrates the dependence of both temperature and method on phosphorus adsorption behavior.

Table XIX: List of phosphorus accumulation and uptake percentage on DOCs after accelerated ZDDP introduction poisoning.

Method	Phosphorus Injected (g)	Phosphorus Accumulated (g)	Percent Collected (%)
Variable Load Intake	6.0	0.95	16
100 % Load Intake	6.0	3.22	54
50 % Load Intake	6.0	2.78	46
0 % Load Intake	6.0	1.6	27
Exhaust Injection	6.0	2.25	38
ZDDP-doped Fuel Injection	6.0	1.23	21

Zinc is observed in two DOCs undergoing accelerated poisoning: exhaust manifold injection and intake manifold injection at 50 % engine load. On the other hand, no zinc is found during the intake and fuel injection methods and is consistent with the formation of zinc sulfate in the exhaust as measured by electrospray mass spectrometry. Since zinc sulfate is a stable particulate it does not contribute to poisoning. It is suspected that the zinc measured as a result of intake manifold injection poisoning at 50 % engine load is not accurate.

Overall phosphorus accumulation during accelerated poisoning methods does correlate with that found in the front brick of the field-service DOCs. The intake manifold injection poisoning method at 100 % engine load produces identical concentrations to those of DOC 4363-180. The oil-contaminated DOC 29921N shows insignificant phosphorus accumulation. This particular DOC has an unknown mileage history with oil-contamination that is noticeably less than other oil-contaminated DOCs, which explains the small amount of phosphorus accumulation. On the other hand, sulfur accumulation, as expected, is typically lower in accelerated poisoning DOCs than field-service due to the use of ultra-low sulfur diesel fuel and the short durations of the poisoning methods. In addition, zinc measured in each of the field-deactivated DOCs

shows consistency with high-mileage histories as well as lube-oil contamination within the DOCs.

Elemental maps and line-scans obtained in EPMA corroborate XRF analyses by confirming the presence of phosphorus, sulfur and zinc within the washcoat of each DOC analyzed. Contaminant concentrations measured, however, vary from XRF significantly. Sulfur is found to be well dispersed throughout each layer of the double-layer washcoat in all accelerated phosphorus-poisoning methods, with the highest concentrations measured in the ZDDP-doped fuel injection method. This measurement is in contrast to that obtained from XRF, which indicates the largest amount of sulfur in the intake-poisoning test at 100 % engine load. The differences in XRF and EPMA analyses are attributed to poison adsorption channel-to-channel variability, which is found to be as high as 15 % in the case of phosphorus. Phosphorus deposits are generally found in a thin surface layer on the washcoat with diffusion typically limited to the top 10-40 μm. The phosphorus layer exhibits a sharply decreasing concentration gradient into the washcoat with the highest concentration occurring on the surface. Phosphorus also exhibits a preferential adsorption at the front portion of the DOC with a decreasing axial concentration profile towards the rear. These results are consistent with phosphorus profiles measured in literature [3,12,14,18,20,35-39]].

Figures 4.17, 4.18 and 4.19 show elemental maps at a cross-section of 0.64 cm from the inlet portion of exhaust manifold, intake manifold and ZDDP-doped fuel injection DOCs, as well as of concentration profiles within the washcoat at the front and the rear locations, respectively. Exhaust manifold injection produces a thin zinc-phosphate glaze on the surface at both the front and rear locations as seen in Figure 4.17. Though not yet confirmed, the atomic weight ratio of phosphorus to zinc appears to be consistent with zinc pyrophosphate ($Zn_2P_2O_7$) and is similar to that found by Williamson et al. [12] using a pulsed-flame reactor. It is suspected that the glaze is formed from fragmented ZDDP molecules in the exhaust gases during injection. The fragmented molecules are large and unstable and readily react within the top few microns of the DOC washcoat, where the organic constituents of ZDDP are oxidized leaving

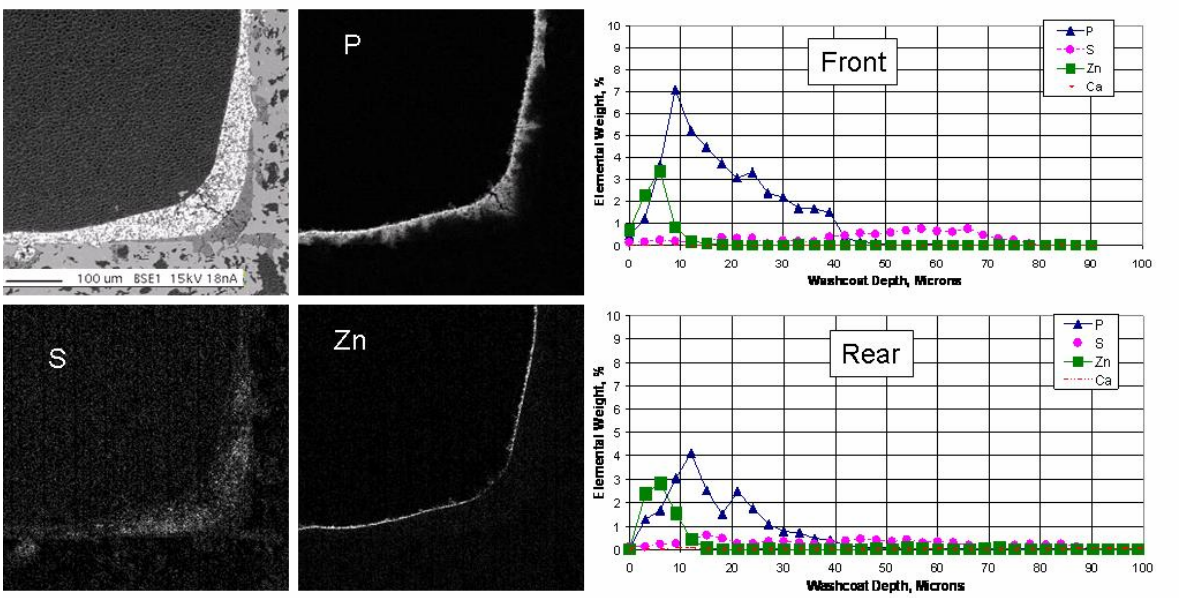

Figure 4.17: Elemental maps of phosphorus, sulfur and zinc at the inlet and concentration profiles at the front and rear locations of the exhaust manifold injection DOC.

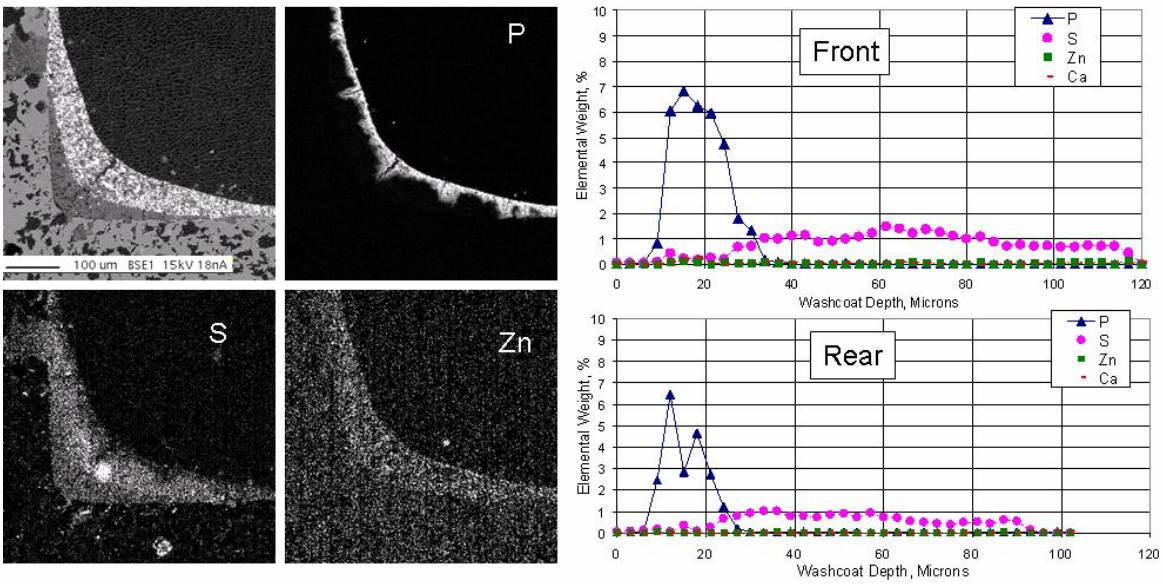

Figure 4.18: Elemental maps of phosphorus, sulfur and zinc at the inlet and concentration profiles at the front and rear locations of the intake manifold injection DOC at 50 % engine load.

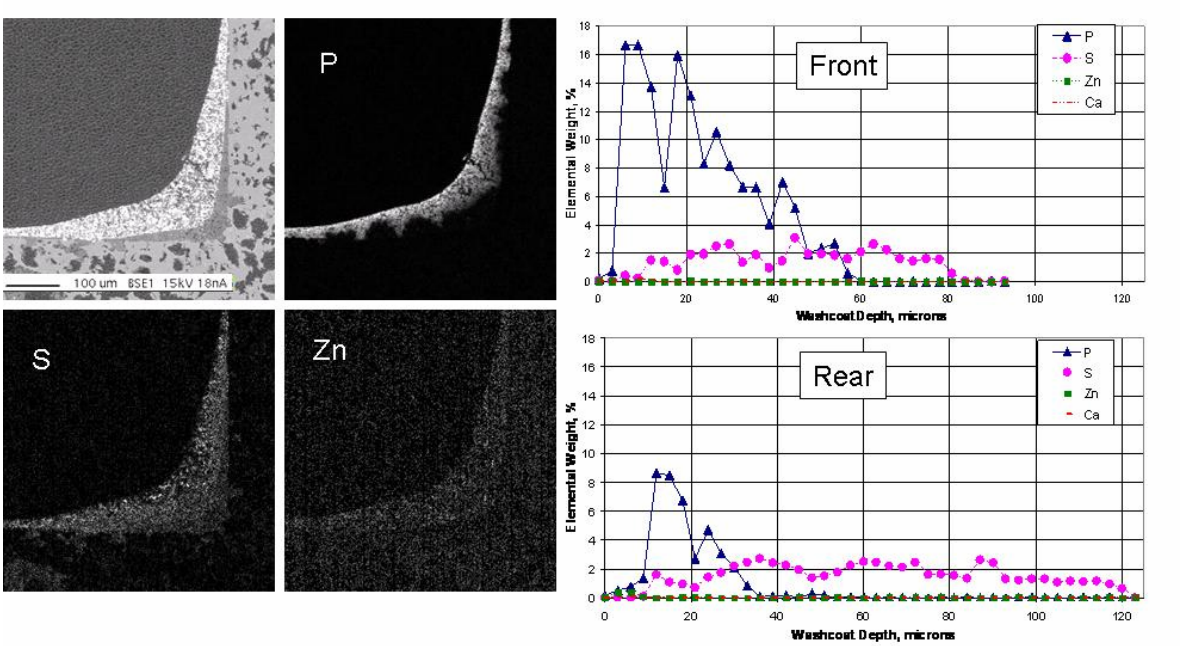

Figure 4.19: Elemental maps of phosphorus, sulfur and zinc at the inlet and concentration profiles at the front and rear locations of the ZDDP-doped fuel injection DOC.

behind zinc-phosphates and sulfates on the DOC surface. The amount of phosphorus on the washcoat surface at the front portion of the DOC is approximately twice that of the rear. The surface concentration of zinc, however, remains constant along the DOC length, indicating additional zinc compounds are formed on the DOC besides zinc-phosphates.

As seen in Figure 4.18, intake manifold injection at 50 % engine load shows phosphorus at the front location of the DOC deposits within the top 20 μm of washcoat with a surface concentration of approximately 7 % by weight. This result is representative of the intake manifold injection poisoning tests performed at 0 and 100 % as well as variable engine loads which are shown in the appendix. In addition, no zinc is found within the washcoat at any engine load during intake manifold injection poisoning and agrees with the formation of zinc sulfate ($ZnSO_4$) as the sole zinc compound in the exhaust for ZDDP passing through the combustion process.

As seen in Figure 4.19, the ZDDP-doped fuel injection poisoning produces the highest surface phosphorus concentration and washcoat penetration depth with a

phosphorus surface concentration of over 16 % by weight; more than double that in any other accelerated phosphorus poisoning method. In addition, phosphorus is found to diffuse into the washcoat to a depth of approximately 60 μm. Again, this result is in contrast to the measurements of XRF in which the ZDDP-doped fuel injection poisoning produces only average phosphorus accumulation compared to the other accelerated poisoning methods. The results obtained from EPMA are consistent with THC and CO light-off performance evaluations in which ZDDP-doped fuel injection poisoning exhibits the greatest DOC degradation.

EPMA analyses of field-deactivated DOCs show similar phosphorus profiles to those obtained in accelerated poisoning methods. Each of the field deactivated DOCs has higher phosphorus concentrations at the inlet portion than at the rear. In addition, the inlet portion of the rear brick shows higher phosphorus concentration than the rear portion of the front brick. This is explained by an increase in the diffusion of phosphorus at the inlet portion of the DOC due to channel entrance effects. Similarly, sulfur is well dispersed throughout the washcoat with higher concentrations found generally in the front brick. The exception is DOC 4363-180, which shows higher sulfur content in the rear brick. This difference is attributed to a noticeably thicker soot-layer in the rear. Phosphorus and zinc concentration differences between the front and rear brick inlet conditions of DOC 4363-180 are shown in Figure 4.20.

Table XX compares EMPA quantitative information obtained for fresh, field-service and engine-poisoned DOCs. The table lists only phosphorus concentration at the front portion of the first bricks, which is known to cause the largest light-off performance degradation [3,18,20,35-39]. Zinc is found at isolated locations on field-service DOC contaminated with lube-oil, which is most likely due to the formation of ash during lube-oil burning.

Surface phosphorus concentrations and phosphorus penetration into the washcoat in field-deactivated DOCs also exhibit dependence on the deactivation mechanisms: either soot or lube-oil contamination. The least amount of phosphorus is found in the rear brick of DOC 29921N, indicating that the lube-oil did not penetrate past the front brick. EPMA analysis on the front brick of DOC 29921N is unable to be performed due

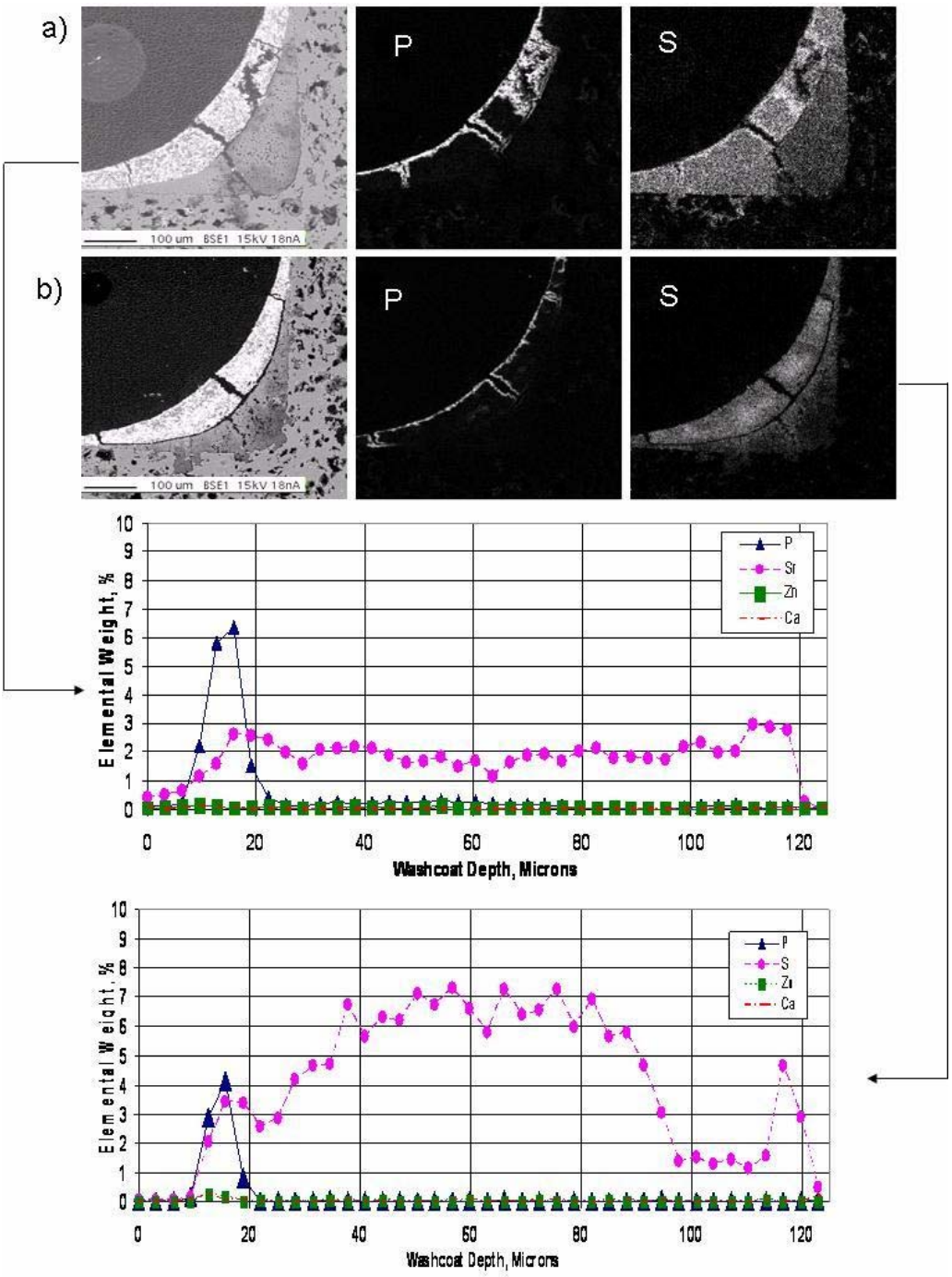

Figure 4.20: Elemental maps and concentration profiles of oil-derived contaminants at the front and rear locations of DOC 4363-180 a) Front b) Rear.

Table XX: Summary of phosphorus, sulfur and zinc concentrations and washcoat penetration depth at the inlet portion of fresh, field-service and accelerated ZDDP injection poisoned DOCs.

DOC	Brick	Phosphorus Surface (Mass %)	Phosphorus Depth (Microns)	Sulfur Surface (Mass %)	Sulfur Depth (Microns)	Zinc Surface (Mass %)	Zinc Depth (Microns)
Fresh	-	-	-	-	-	-	-
4363-180	Front	6.5	16	2.7	Full	0.12	10
	Rear	4.13	12.6	7.27	Full	0.24	10
28656N	Front	5.92	15	2.9	Full	0.6	6
	Rear	3.0	12	0.8	Full	0.16	18
29921N	Front	No Data					
	Rear	0.4	9	0.68	Full	-	-
100 % Intake		7.83	42	2.44	Full	-	-
50 % Intake		6.82	33	1.48	Full	0.14	12
0 % Intake		3.3	27	1.0	Full	-	-
Variable Intake		6.75	24	1.3	Full	0.1	9
Exhaust Manifold		5.08	18	1.08	Full	5.59	9
Oil/Fuel		16.65	54	2.69	Full	-	-

to a large amount of lube-oil present within the washcoat, which diffuses from the washcoat during analysis under the low-pressure environment, creating a film over the sample that X-rays cannot penetrate.

Correlations between phosphorus surface concentration and phosphorus penetration depth into the washcoat on THC and CO light-off performance are shown in Figures 4.21 to 4.24 for all accelerated poisoning and field-deactivation DOCs. Phosphorus accumulation is found to cause significant THC light-off performance degradation, regardless of the surface concentration, as seen in Figure 4.22. Similarly, the depth of phosphorus penetration into the washcoat produces no THC light-off degradation trend as seen in Figure 4.22. The THC light-off performance of DOC 4363-180 is not shown in Figure 4.21 because THC conversion never exceeds 10 %. Together, these observations indicate that THC oxidation is confined within the top 10 μm of the washcoat and is highly affected by the presence of surface contamination such as soot and lube-oil as seen in SEM images presented later in this Section.

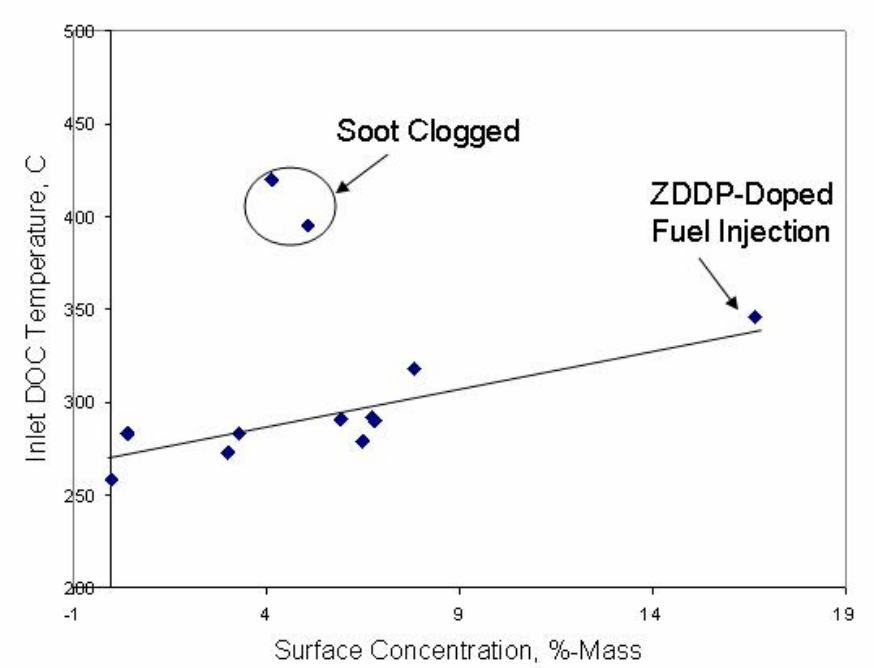

Figure 4.21: Plot of DOC inlet temperatures at 25 % CO conversion as a function of washcoat surface phosphorus concentration for each DOC evaluated.

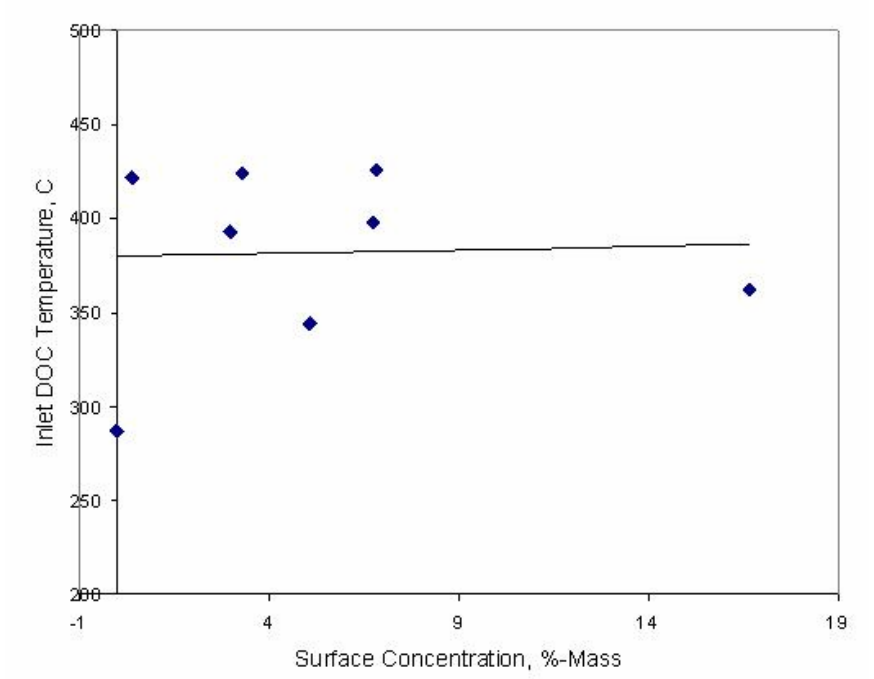

Figure 4.22: Plot of DOC inlet temperatures at 20 % THC conversion as a function of surface phosphorus concentration for each DOC evaluated.

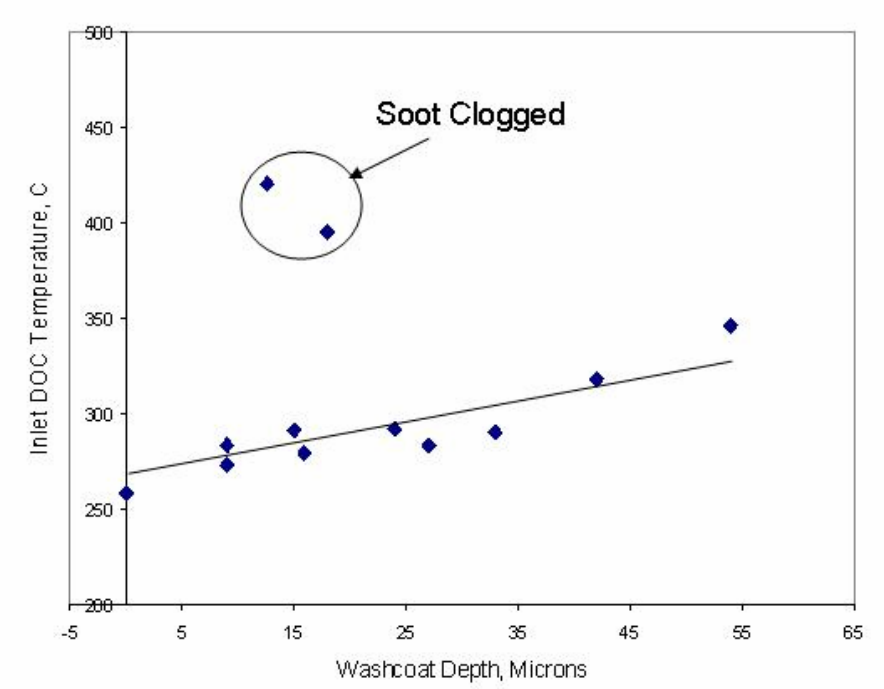

Figure 4.23: Plot of DOC inlet temperatures at 25 % CO conversion as a function of washcoat phosphorus penetration for each DOC evaluated.

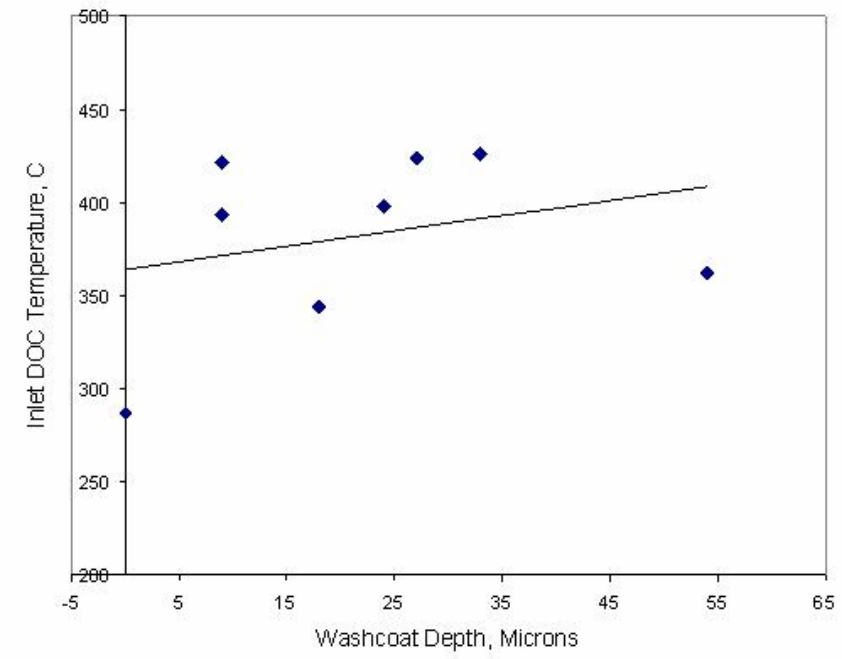

Figure 4.24: Plot of DOC inlet temperatures at 20 % THC conversion as a function of washcoat phosphorus penetration for each DOC evaluated.

On the other hand, CO light-off performance is strongly dependent on phosphorus surface concentration and phosphorus penetration into the washcoat as seen in Figures 4.21 and 4.23, respectively. The outlying data points are from front and rear bricks of the soot-clogged field-service DOC 4363-180, which exhibit extremely poor light-off performance due to the loss in flow cross-sectional area. Also observed is the large amount of phosphorus present on the ZDDP-doped fuel injection DOC, which lies far outside the domain of the other DOCs examined, but continues the CO light-off degradation trend. This strongly suggests that phosphorus poisoning, rather than the presence of soot, is the governing factor in the degradation CO light-off performance. SEM-EDS analyses of DOC washcoat surfaces show the presence of surface contamination as seen in Figure 4.25 for DOCs obtained from a field-service and poisoning methods.

The presence of soot is observed on the surface of each of the DOCs analyzed. In addition, the exhaust manifold injection poisoning DOC contains a zinc-phosphate glaze, which is clearly visible in Figure 4.25c. The glaze has an amorphous structure and completely masks the DOC surface. The soot particles on each of the DOCs appear as agglomerates with diameters on the order of 10 μm or less. As seen in Figure 4.25d, ZDDP-doped fuel injection poisoning produces the greatest amount of soot, completely covering the washcoat surface and is thought to cause the severe light-off degradation. The large soot content is a result of high levels of soot produced by the engine caused by the injector deposits formed from fuel containing lube-oil. Intake manifold injection poisoning produces the least amount soot deposit and phosphorus accumulation on the DOC surface as seen in Figure 4.25b. Consequently, degradation of light-off performance of is not as severe as that measured from either ZDDP-doped fuel or exhaust manifold injection poisoning methods. As seen in Figure 4.25a, the intake manifold injection poisoning method also produces surface contamination similar to those of DOC 28656N, and correlates with the similar light-off performance measured for these DOCs. DOC 28656N has surface contamination representative of those found in DOC 4363-180, however, DOC 29921N was unable to be analyzed due to the release of lube-oil absorbed within the washcoat under the ultra-high vacuum (UHV) environment during imaging.

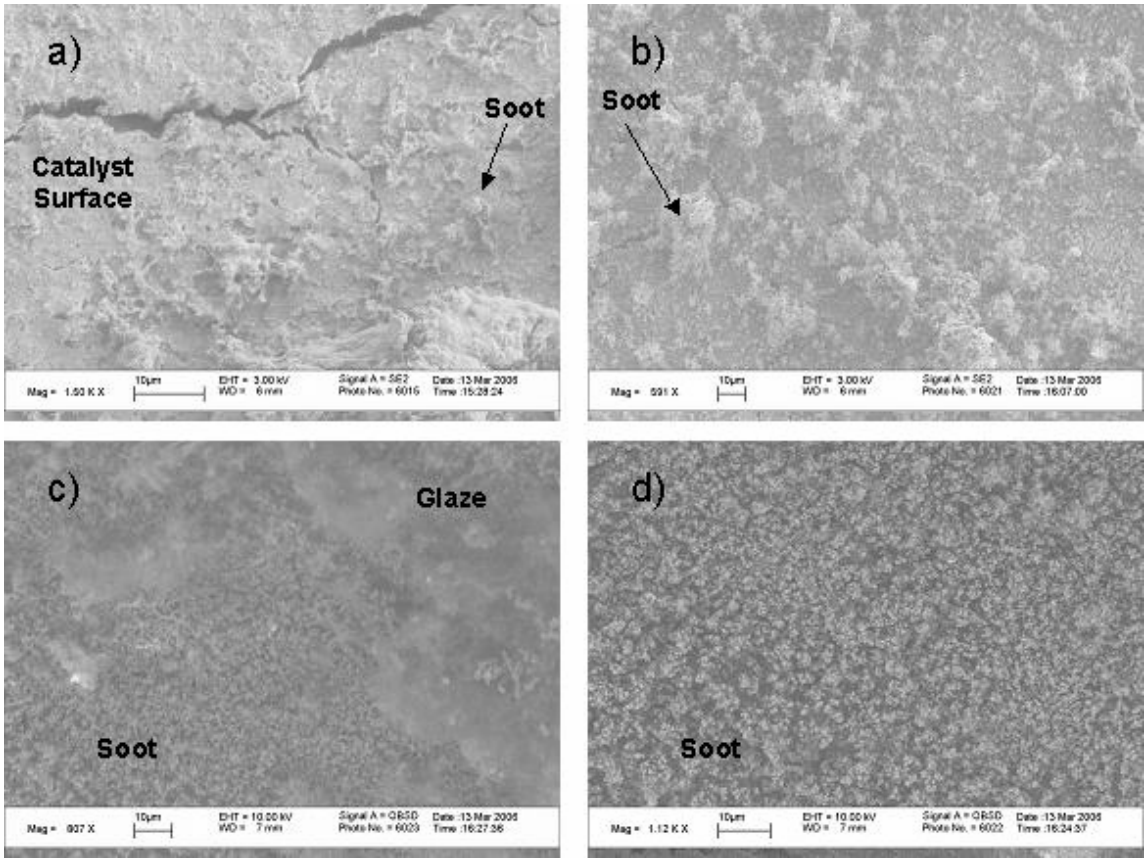

Figure 4.25: SEM images comparing field-deactivated and accelerated ZDDP injection poisoned DOCs surface contamination characteristics. a) Field-poisoned b) Intake manifold injection c) Exhaust manifold injection d) ZDDP-doped fuel injection.

X-ray photoelectron spectroscopy (XPS) measurements of electron binding energies within the compounds on the DOC surface confirms the presence of zinc, phosphorus and sulfur as well as catalyst materials such as cerium, platinum and aluminum. Figure 4.26 is a plot of electron binding energy spectra of surface compounds in a fresh DOC and DOC 4363-180 showing growth in oil-derived poison associated peaks. The scans are taken at a washcoat depth of 30 nm after being ablated using an argon sputtering gun to clear the surface of carbon to produce higher resolution measurements.

From the spectra, broadening of the cerium $3d_5$-orbital peak is observed, indicating that additional cerium compounds may have formed as a result of poisoning. In addition, the location of the phosphorus 2s-orbital peak is consistent with meta- and ortho- phosphorus group compounds, with a maximum peak intensity located at 189.3 eV. The actual phosphorus compounds are not distinguishable, however, because of unknown phosphorus compounds present as well as the presence of an unknown spectra shift caused by DOC surface charging during analysis. The cordierite substrate of the DOC is a very good electronic insulator and creates a surface electrostatic charge that alters the binding energies measured.

Charging also inhibits the identification of the sulfur associated peaks as shown in the sulfur $2p_{3/2}$-orbital peak plotted using XPSPEAKS software in Figure 4.27. This particular peak is shown because it clearly demonstrates the problems encountered in identifying DOC surface compounds. XPSPEAKS is a statistical software package designed specifically for the interpretation of XPS data. The software approximates the area under the peak data provided and optimizes the distribution of a number of user normal distributions to approximate and de-convolute the peak of interest. Convolution occurs when more than one compound of a particular element is present during sampling, producing concurrent peaks very close to one another which cannot be resolved by equipment resolution

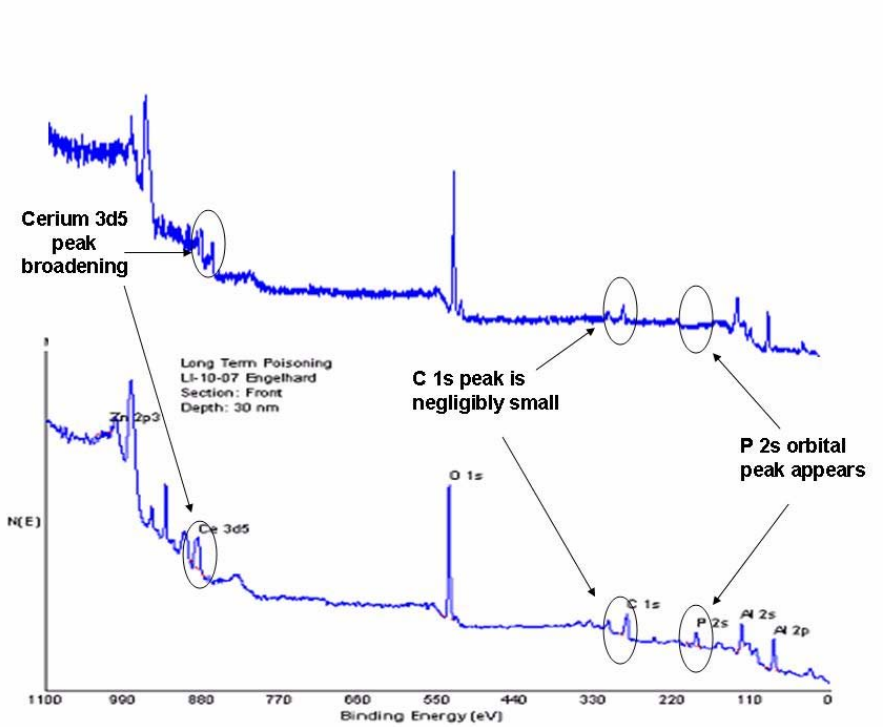

Figure 4.26: X-ray binding energy spectra of fresh and intake manifold injection poisoning at variable engine load DOCs. Top-fresh, Bottom-intake manifold injection poisoning.

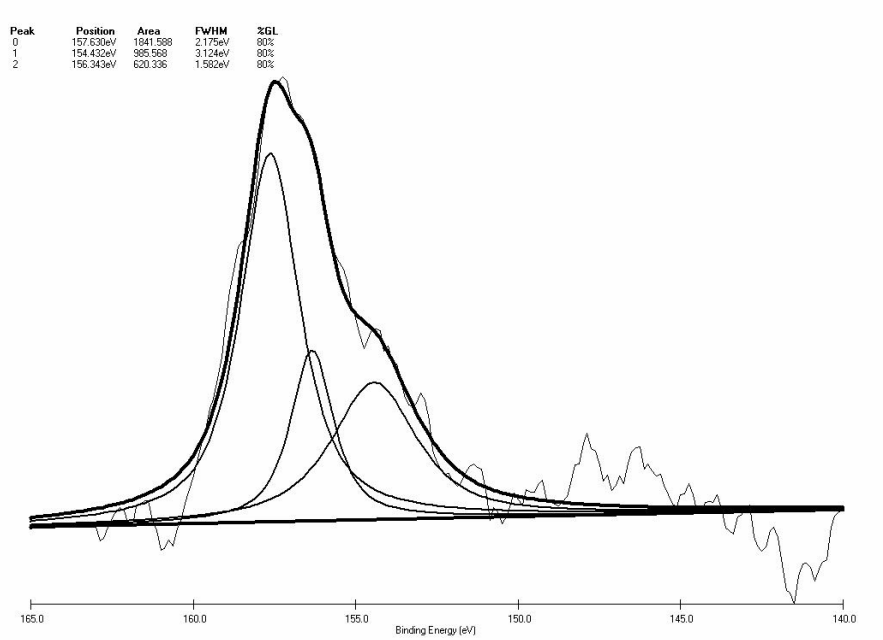

Figure 4.27: Screen capture of XPSPEAK peak analysis of the sulfur $2p_{3/2}$ peak for the intake manifold injection poisoning DOC at variable engine loads.

The sulfur $2p_{3/2}$-orbital peak is best approximated using three curves, however, the location of the fitted peaks are not identified when compared to known standards, indicating that the shift of peak data due to the electrostatic charging was not corrected properly. Therefore, it is suggested that further XPS studies be performed using standards containing compounds of interest for a comparison to the spectra obtained for the poisoned DOCs to identify the oil-derived compounds.

In order to identify compounds formed within the DOC, X-ray diffraction spectra are collected for fresh and accelerated poisoning DOCs of each method. Figure 4.28 is XRD spectra of the fresh and intake manifold injection poisoning at 100 % load DOCs. The XRD spectra for the intake manifold injection are similar to those obtained for the fuel and exhaust manifold and ZDDP-doped fuel injection methods shown in Figures 4.29 and 4.30, respectively. The peak denoted by ▲ at 36.68^{o} is identified as $AlPO_4$ and shows an increase in intensity indicative of DOC phosphorus poisoning. Minor peaks of $AlPO_4$ located at 29.83^{o} and 42.67^{o} are not discernable, since they are masked by alumina and cordierite peaks. The presence of $AlPO_4$ in the washcoat is also confirmed by other investigators and is thought to be the initial step in the incorporation of phosphorus into the washcoat [14,15].

The major peaks of $CePO_4$ and $Zn_2P_2O_7$, located respectively at 29.35^{o} and 29.57^{o}, could not be resolved in the intake or fuel injection methods, since they are superimposed upon larger peaks of CeO_2 and cordierite, but are thought to appear within the DOC undergoing exhaust manifold injection poisoning. Minor peaks associated with these compounds are small and cannot be detected within the spectra. This does not exclude the formation of these compounds within the intake manifold or ZDDP-doped fuel injection methods, since they have been observed in other studies [12,15,16,17].

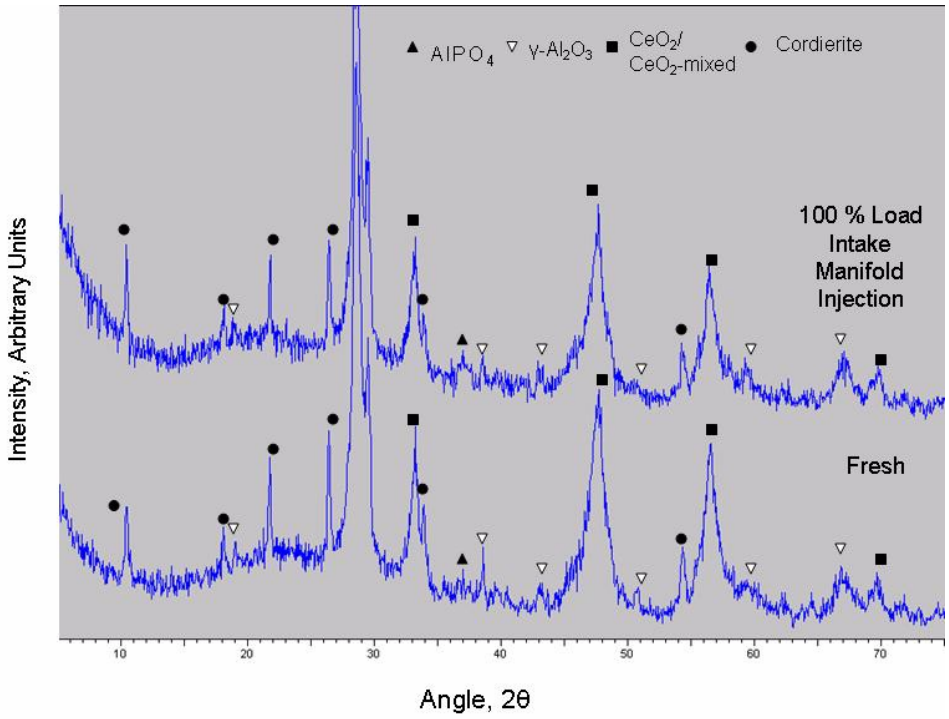

Figure 4.28: XRD spectra of fresh and intake manifold injection poisoning DOC at 100 % engine load.

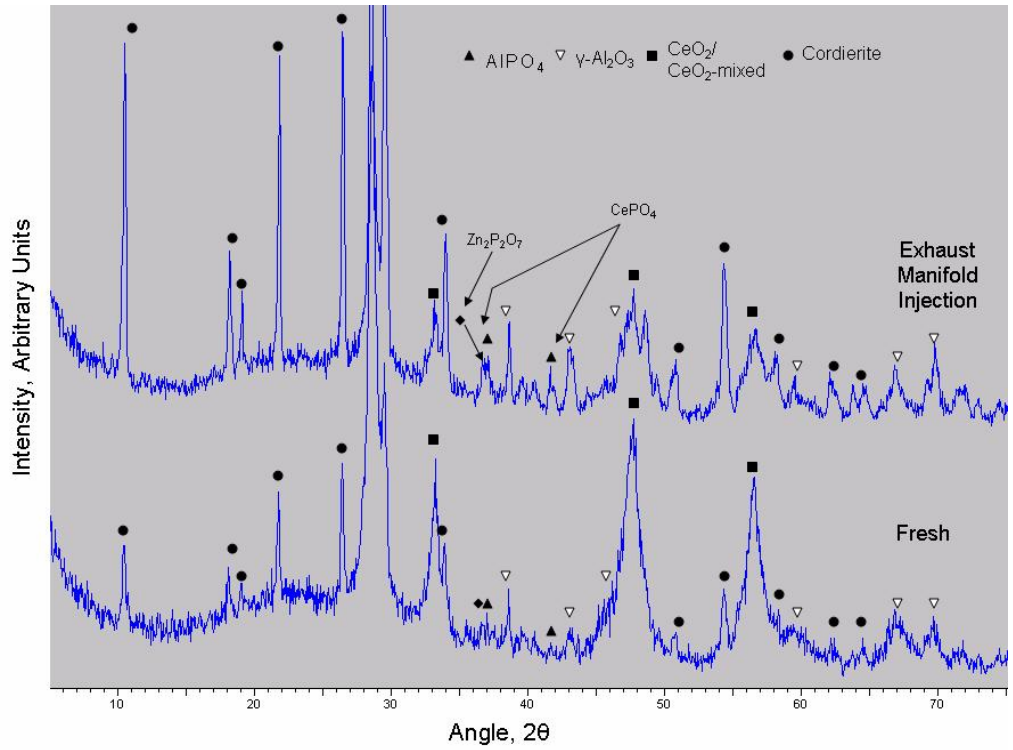

Figure 4.29: XRD spectra of fresh and exhaust manifold injection poisoning DOCs.

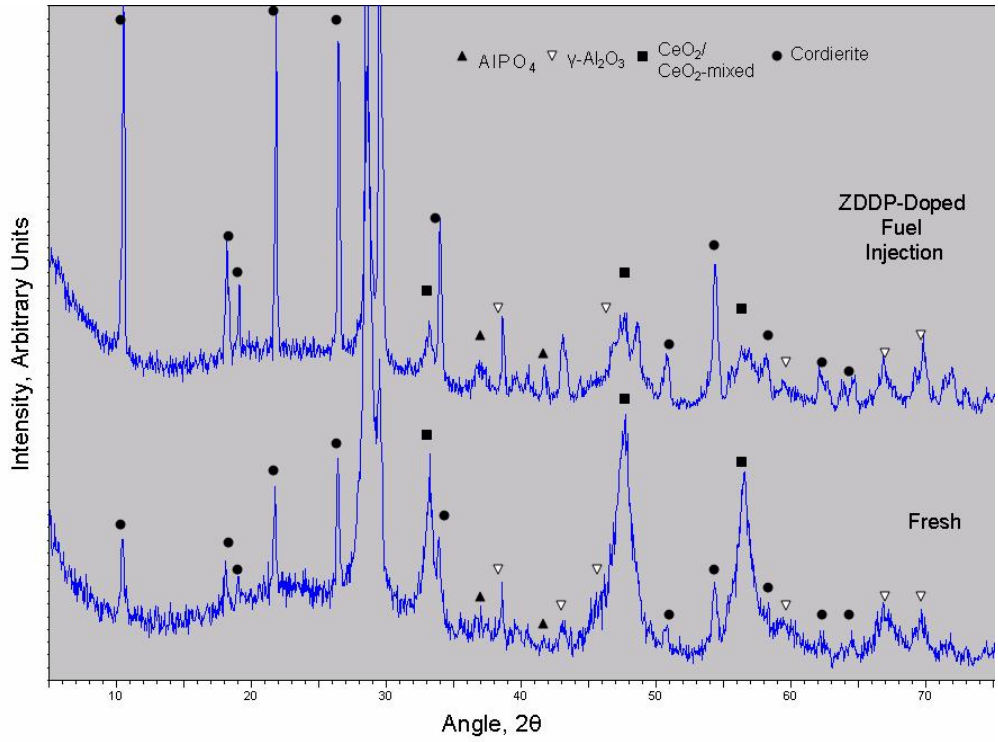

Figure 4.30: XRD spectra of fresh and ZDDP-doped fuel injection poisoning DOCs.

4.3 Bench-Flow Reactor Evaluations

Due to the complex poisoning behavior phosphorus exhibits on DOC performance, a bench-flow reactor (BFR) system with better temperature and composition control is used to evaluate CO and THC light-off performance. The increase in control of the DOC operation offers less light-off performance variability during evaluations, which produces a more accurate comparison between the poisoning methods as well as field-deactivated DOCs. Only fresh, exhaust manifold injection, ZDDP-doped fuel injection and the front bricks of the three field-deactivated DOCs are compared using the BFR for evaluations. Light-off performance measurements of the intake manifold injection poisoning DOCs are not obtained because the samples were completely consumed for chemical analyses before the utilization of the bench-flow reactor system was deemed necessary.

4.3.1 Light-off Performance – Regeneration

All light-off evaluations are carried out using simulated diesel exhaust gases consisting of 300 ppm C_2H_4, 500 ppm CO, 5 % CO_2, 1000 ppm NO_x, 10 % O_2, 10 % H_2O and balance N_2 with a gas hourly space velocity of 80,000 hr^{-1} over a temperature range of 200-500^oC in 50^oC increments. C_2H_4 is used to represent the THC species present in the diesel engine exhaust gases. Measurements are taken by sweeping both the increasing and decreasing temperature directions to check repeatability of data as well as hysteresis. The use of the bench-flow reactor system is primarily designed to control the DOC temperature. Figure 4.31 is a plot of typical axial temperature distribution profiles across the DOC for each evaluation temperature used in light-off measurements. Each temperature sweep appears to provide consistent DOC temperature conditions, however isothermal conditions are not maintained at high operating temperatures. The DOC is at isothermal conditions during low-temperature operation, which is ideal for light-off performance measurements. At high temperature operating conditions, however, the DOC experiences a large axial temperature gradient resulting from the high GHSV and insufficient preheating of the simulated diesel exhaust gases with a maximum difference between the DOC inlet gas temperature and the target temperature of 30^oC. In addition, exothermic oxidation reactions within the DOC contribute to deviations from isothermal conditions as seen in the 500^oC evaluation shown in Figure 4.32. The initial temperature deviation between the DOC front and rear locations is approximately 40^oC before reaction, due solely to improper preheating of the simulated exhaust gases and then the additional 60^oC exotherm during reaction results in a highly non-isothermal reactor.

Also observed in the Figure 4.32 is the reaction location distribution and the DOC wall temperature increase due to the exothermic reaction. A slight temperature increase is measured at the front section of the DOC the instant simulated diesel exhaust gases are introduced into the system. This is because of a significant time lag, approximately 5 s, which occurs during switching from inert gases to the simulated diesel exhaust gases. Within that short time period, the gases are heated well above that obtained during steady-state conditions because of the decrease in flow rate. The initial temperature increase then diminishes due to a lack of chemical reactions. This is important because it

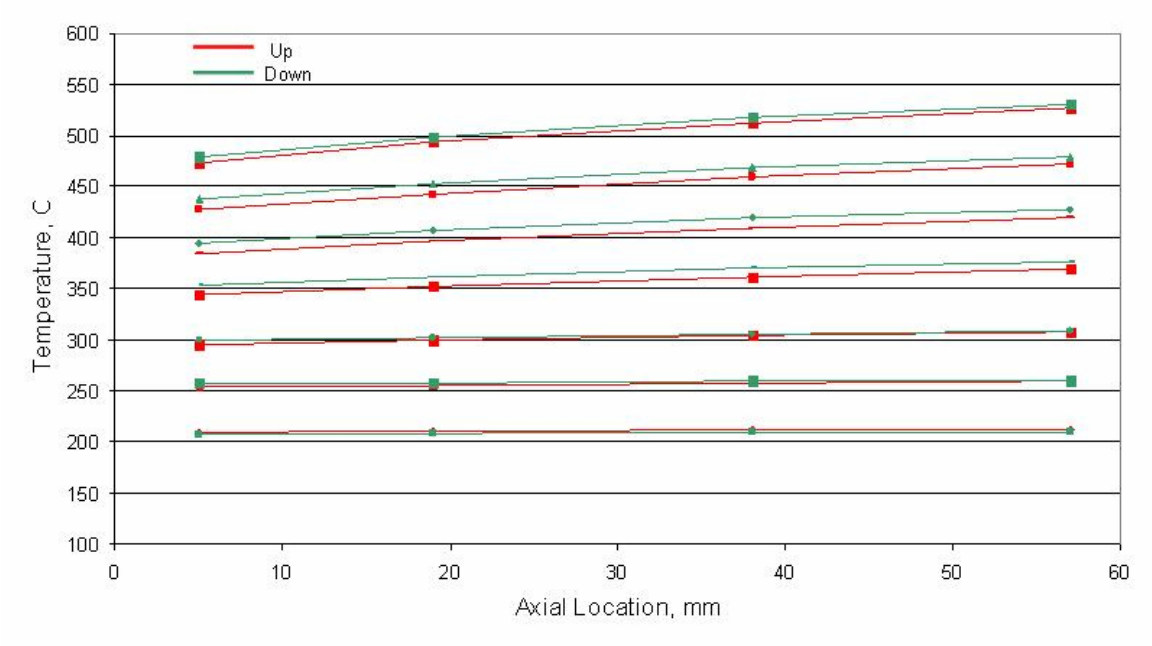

Figure 4.31: Typical DOC axial temperature distributions at steady-state light-off evaluation conditions.

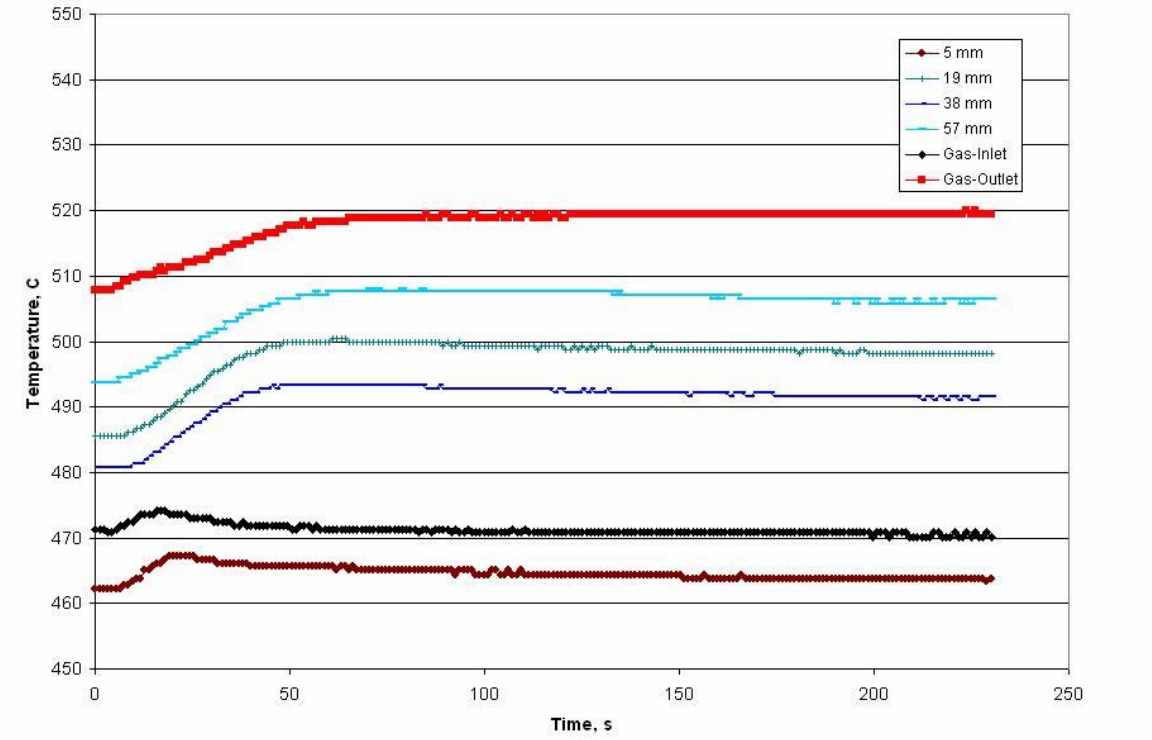

Figure 4.32: Typical exotherms produced at four axial DOC locations during CO and C_2H_4 oxidation at 500°C.

proves that the presence of contamination, which is known to be higher at the front portion of the DOC, adversely affects the catalyst activity and shifts the reaction zone away from the DOC inlet. Large temperature exotherms are observed in the middle portion of the DOC where the majority of oxidation takes place. Since the DOC is not maintained at isothermal conditions, the light-off performance measurements at each temperature step during evaluations are referenced to the DOC inlet temperature, which are constant for each DOC analyzed.

Figures 4.33 and 4.34 are plots of the four CO and C_2H_4 light-off curves for the exhaust manifold injection poisoning DOC, respectively. Each light-off curve represents a temperature sweep either in the increasing or decreasing direction. C_2H_4 and CO conversions are significantly better than those obtained using the engine-bench due to the absence of soot, which competes for catalyst active sites, and the use of C_2H_4 which is a fast hydrocarbon species, faster than the THC produced by the engine. Conversions are nearly 100 % are reached for CO and C_2H_4. The CO light-off temperature at 50 % of maximum conversion is approximately 350^{o}C, which is identical to that measured using the engine-bench. This indicated that the DOC activity is not significantly altered by the use of simulated diesel exhaust gases.

Also evident in the plots is an increase in CO and C_2H_4 light-off performance after the first temperature sweep. In the first temperature sweep, at low-temperatures, soot and lube-oil contamination in the form of a zinc-phosphate glaze are present on the DOC inhibiting oxidation reactions. At elevated temperatures during the evaluation, approximately 400^{o}C and higher, significant soot and lube-oil oxidation is observed as reflected in the increase CO_2 emissions from the DOC. The removal of soot and lube-oil regenerates the DOC by cleansing the surface of contamination. Figure 4.35 is a plot of CO_2 emissions from the DOC as a function of temperature for the first up and down temperature sweep. The CO_2 concentrations entering the DOC are shown as a black line with calculated values of CO_2 production resulting from CO and C_2H_4 oxidation in red. The difference in CO_2 emissions from those calculated from the CO and C_2H_4 are the emissions from soot oxidation.

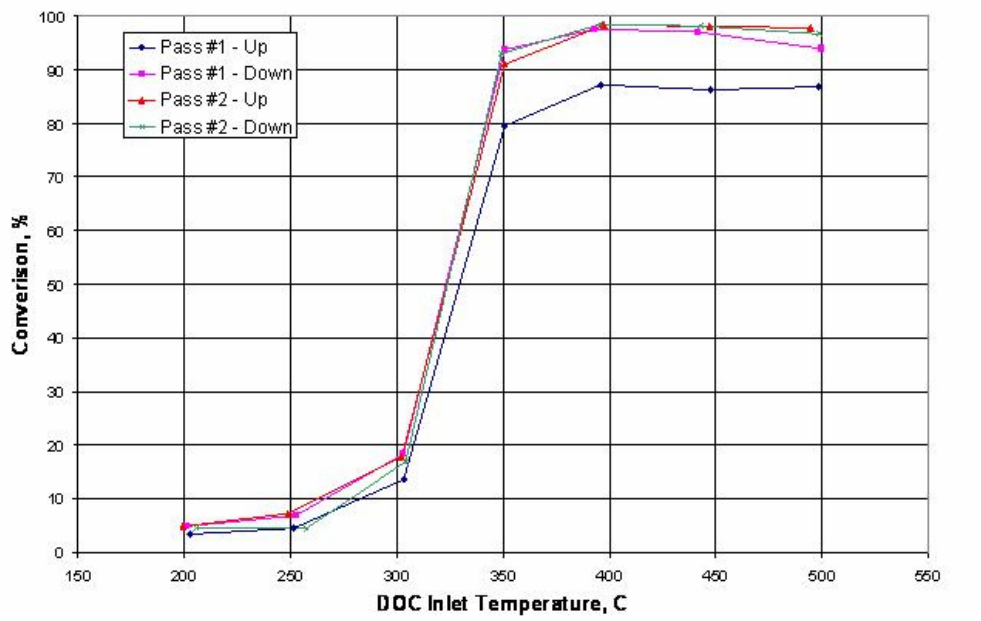

Figure 4.33: CO light-off curves for four temperature sweeps from 200-500°C for the exhaust manifold injection poisoning DOC.

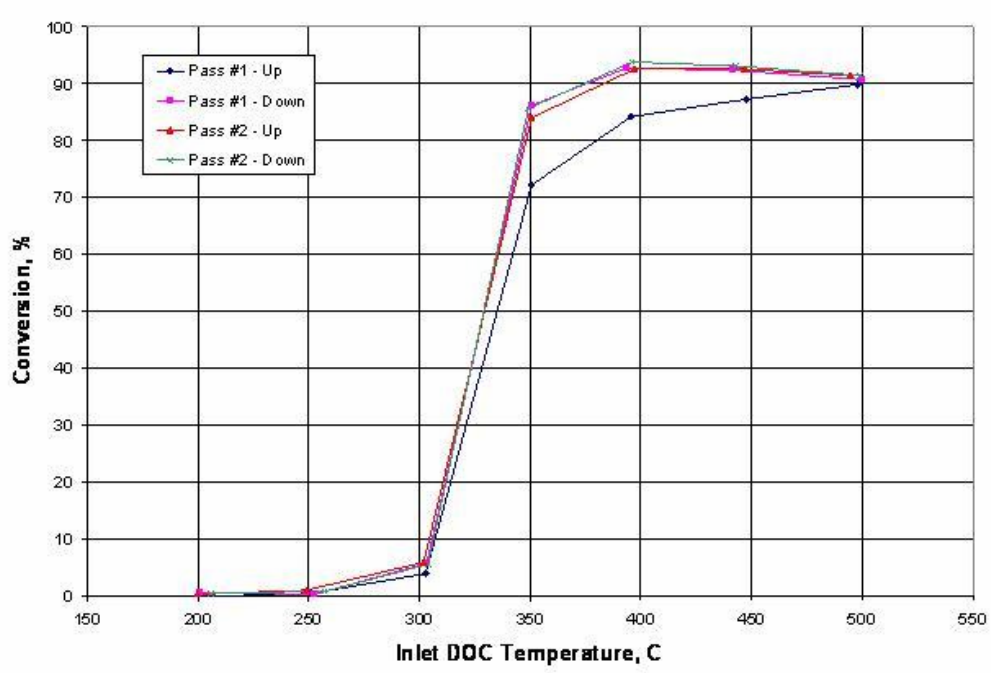

Figure 4.34: C_2H_4 light-off curves for four temperature sweeps from 200-500°C for the exhaust manifold injection poisoning DOC.

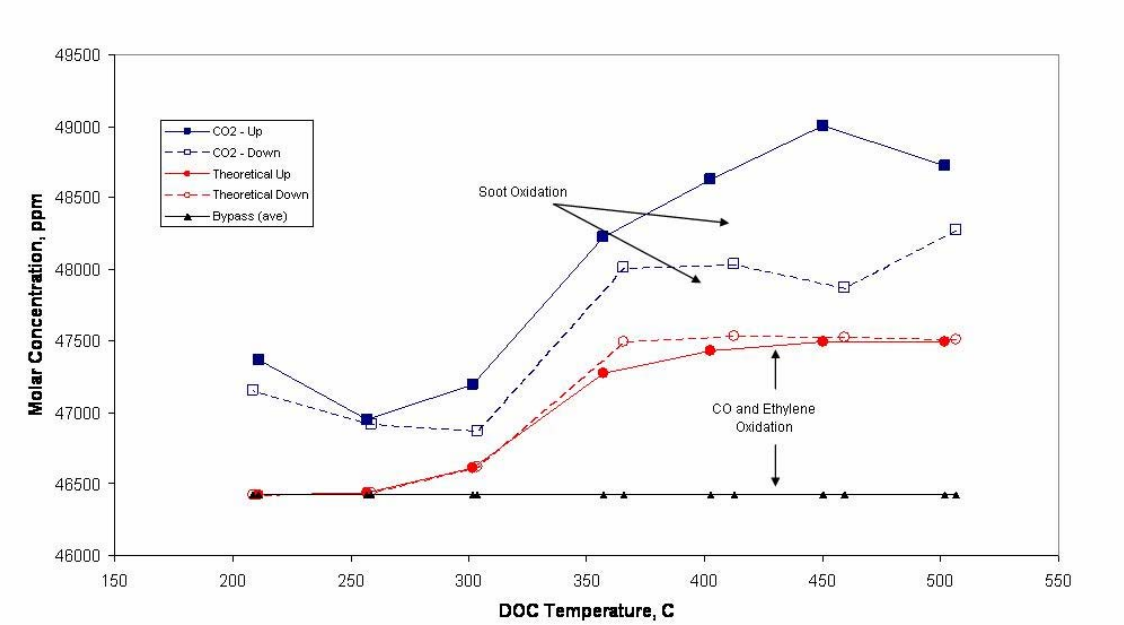

Figure 4.35: Typical CO_2 formation as a function of temperature during the first and second bench-flow reactor light-off evaluations plotted with bypass and CO and C_2H_4 contributions.

CO_2 emissions higher than those of the baseline at low operating temperatures are thought to be the result of the oxidation of SOF components within the soot. As the temperature is increased, CO_2 production decreases because less SOF is present in the soot. At temperatures above 400^{o}C, however, CO_2 production again increases when soot oxidation becomes significant. The total amount of soot removal is not calculated from these plots, however, because of the procedure used during evaluations. 10 % O_2, 10 % H_2O and balance N_2 is used to preheat the DOC to steady-state conditions prior to the introduction of the simulated diesel exhaust gases. Therefore, a large amount of soot and lube-oil is oxidized during the preheating without being recorded. The decrease in CO_2emissions in the second temperature sweep is due to the disappearance of the soot layer on the DOC washcoat. As expected, THC and CO light-off performance is better in subsequent temperature sweeps.

A DOC mass decrease of 0.25 g is measured after BFR evaluations, which is a direct result of the removal of soot and lube-oil contamination. Figure 4.36 is a photograph of a typical DOC before and after BFR evaluations demonstrating the

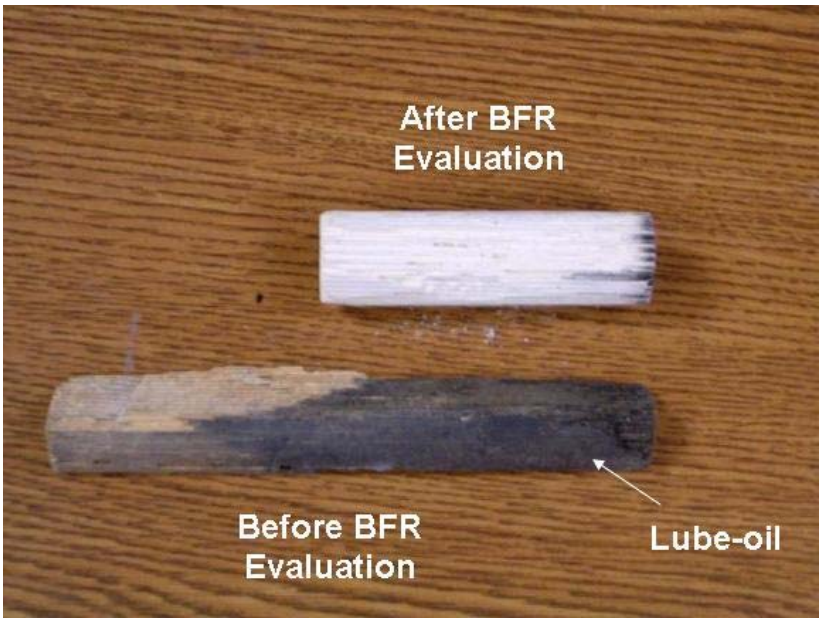

Figure 4.36: Photograph of typical DOC washcoat contamination before and after light-off evaluations using the bench-flow reactor.

noticeable effect of soot and lube-oil removal from the DOC surface. Originally, the DOC obtained after poisoning contains large quantities of soot and lube-oil which appear black. After BFR evaluations, the DOC appears completely white which corresponds to the clean washcoat material. A thin region near the inlet of the DOC remains dark, however, even after BFR evaluations due to the increase contamination level and lower temperatures experienced during evaluations.

BFR evaluations of the ZDDP-doped fuel injection poisoning DOC are similar to those found in exhaust manifold injection poisoning in both C_2H_4 and CO light-off performance and regeneration behavior. As previously mentioned, the ZDDP-doped fuel injection poisoning method produced severe soot coverage on the DOC surface, as a result, the CO and C_2H_4 light-off performance in the first temperature sweep is highly degraded as shown in Figures 4.37 and 4.38, respectively. The light-off temperature in the first temperature sweep is 30^{o}C higher than those obtained in subsequent sweeps. In addition, an increase in DOC light-off performance at temperatures above 450^{o}C is observed. The increase in activity is attributed to the high rate of soot removal at these

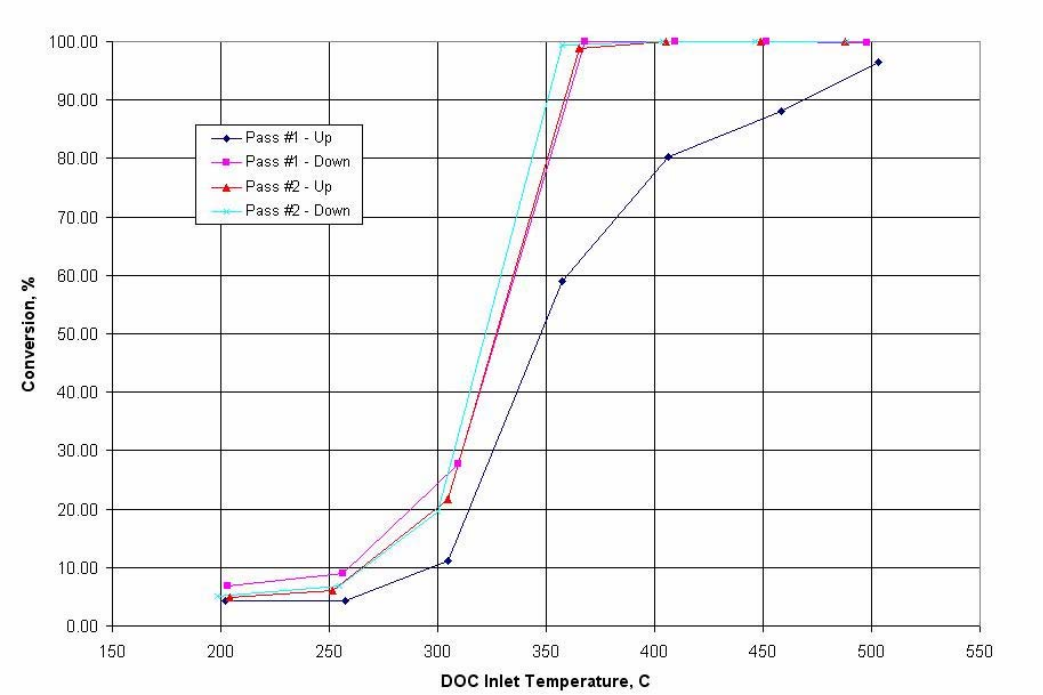

Figure 4.37: CO light-off curves for four temperature sweeps from 200-500°C for the ZDDP-doped fuel injection poisoning DOC.

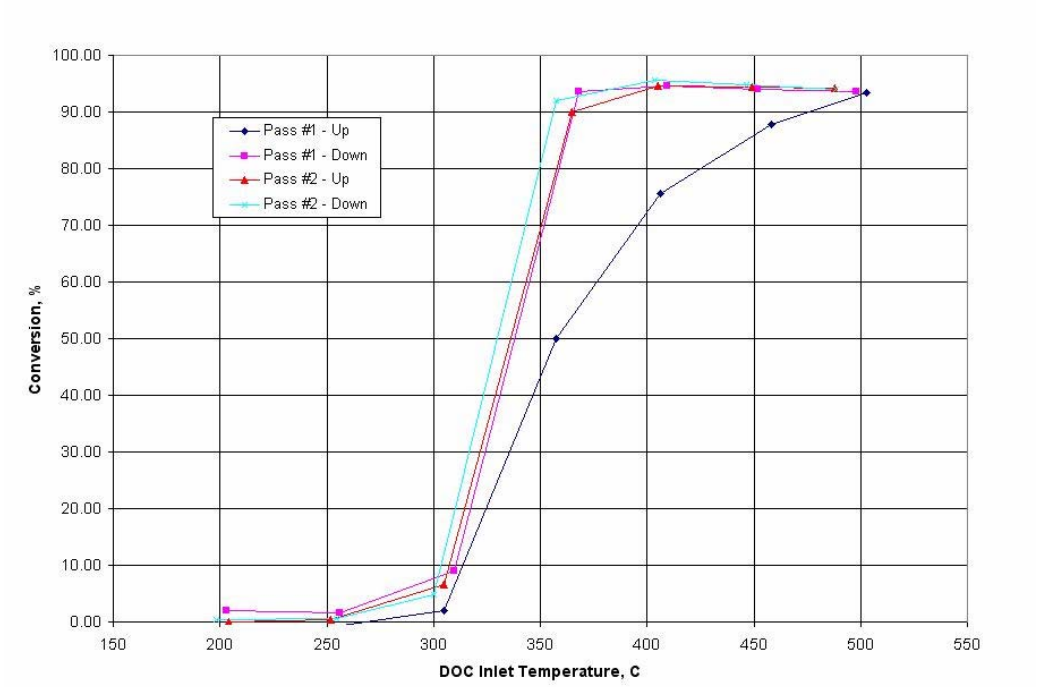

Figure 4.38: C_2H_4 light-off curves for four temperature sweeps from 200-500°C for the ZDDP-doped fuel injection poisoning DOC.

temperatures resulting in higher CO and C_2H_4 conversions. In subsequent temperature sweeps, C_2H_4 and CO conversion reaches 96 % and 100 %, respectively.
The ZDDP-doped fuel injection poisoning DOC produces a mass difference after BFR evaluations of 0.3 g, which is 0.05 g more than that measured in the exhaust manifold injection case and is consistent with the thick soot contamination observed in the SEM images in Figure 4.25. However, it is not known if the mass difference of accumulated contamination is statistically significant. The increase in the amount of soot removal in the ZDDP-doped fuel injection case is also consistent with the poor light-off performance obtained in the first temperature sweep, even though this DOC exhibits better overall conversion than measured for the exhaust manifold injection DOC. The presence of soot on the DOC is, therefore, determined to be the largest contributor to DOC deactivation.

For comparison, BFR light-off evaluations of field-deactivated DOCs are performed on the front portion of the first brick in the close-coupled pairs. Results show significantly higher CO and hydrocarbon conversions than those obtained from engine-bench evaluations. In addition, each field-deactivated DOC is regenerated during light-off evaluations with CO and C_2H_4 light-off temperatures as well as maximum conversions approaching or exceeding those found in regenerated accelerated poisoning and fresh DOCs.

Figures 4.39 and 4.40 are plots of CO and C_2H_4 light-off evaluations of DOC 28656N – catastrophic oil contamination - using the BFR. This field-deactivated DOC is representative of the other field-deactivated DOCs evaluated, which are shown in the appendix. This particular DOC, however, exhibits a slower rate of regeneration than the other field-deactivated DOCs. It is suspected that this DOC contains a higher amount of lube-oil embedded within the washcoat, as was observed in EPMA analysis, which oxidized more slowly than soot. This phenomenon can be seen in the CO and C_2H_4 light-off curves in which 100 % regeneration is not achieved until the third temperature sweep is performed. Once regenerated, CO and C_2H_4 conversions are identical to those measured in the fresh DOC and regenerated accelerated poisoning DOCs.

The resulting increase in light-off performance of DOC 28656N after regeneration, however, is not as high as those obtained for all other DOCs. Though not

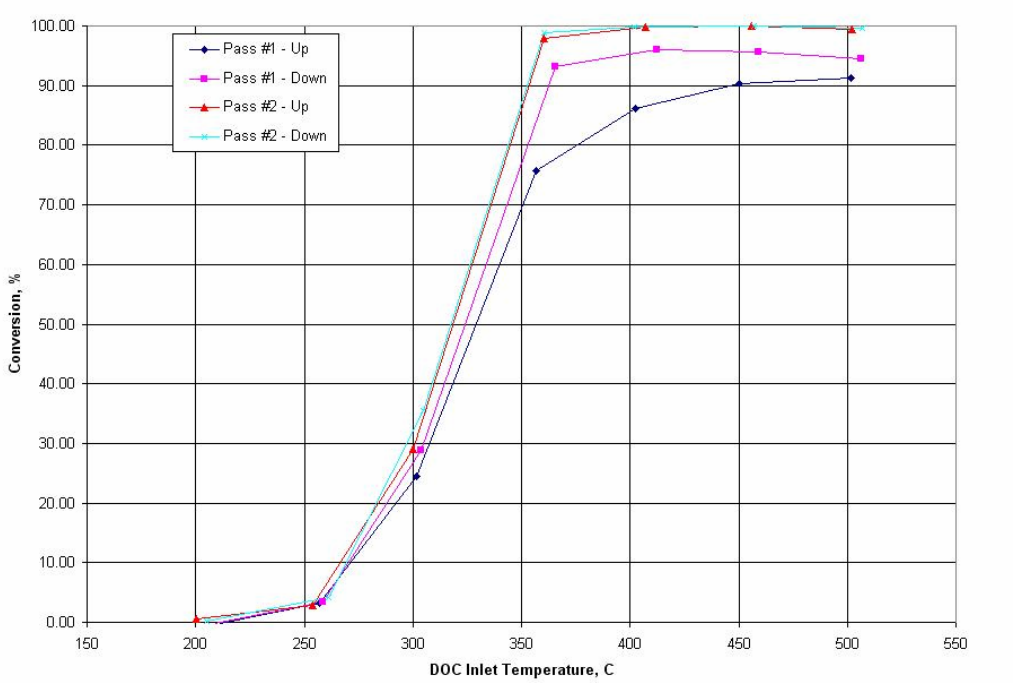

Figure 4.39: CO light-off curves for four temperature sweeps from 200-500°C for field-deactivated DOC 28656N.

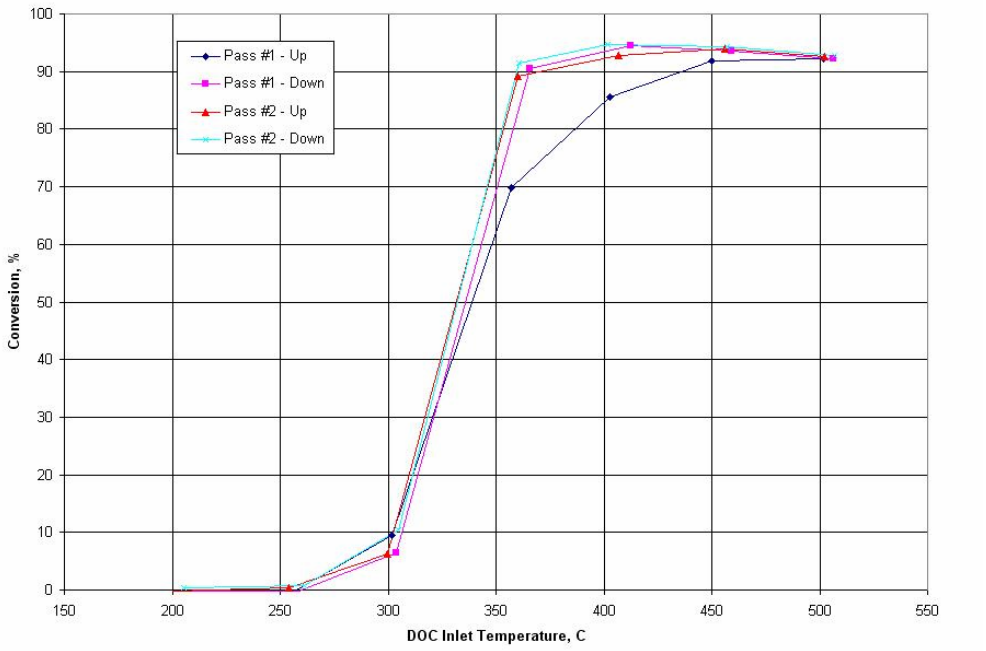

Figure 4.40: C_2H_4 light-off curves for four temperature sweeps from 200-500°C for field-deactivated DOC 28656N.

confirmed, this is most likely the result of inconsistencies in the washcoat formulations, since none of the field-service DOCs are obtained from the same batch. In addition, this DOC has an unknown mileage history which could be a factor contributing to the lower light-off performance.

Figures 4.41 and 4.42 are comparisons of CO and C_2H_4 light-off temperatures before and after regeneration for all DOC light-off evaluations. Since the light-off temperatures in the first temperature sweeps are reached before any significant soot or lube-oil oxidation is observed, the light-off temperatures obtained are considered to be equivalent to what would be measured if no soot oxidation occurs. The CO and C_2H_4 light-off temperatures obtained during the first evaluation are approximately 350^{o}C, whereas appreciable soot oxidation is not observed until 400^{o}C – 500^{o}C.

The ZDDP-doped fuel injection poisoning method is shown to accurately reproduce light-off degradation measured in the soot-clogged DOC 4363-180, and each DOC with high soot accumulation exhibits higher light-off temperatures. Likewise, exhaust manifold injection poisoning is shown to reproduce CO and C_2H_4 light-off performances obtained for catastrophic lube-oil contaminated field-deactivated DOCs. CO and C_2H_4 light-off temperatures obtained in exhaust manifold injection poisoning are approximately mid-range of those obtained from DOCs 29921N and 28656N.

CO and C_2H_4 light-off temperatures obtained after regeneration for each DOC examined, however, approach or exceed those obtained in the fresh DOC. In general, the field-deactivated DOCs produce a greater increase in light-off performance than the accelerated poisoned DOCs after regeneration. The exception is DOC 29921N, which is shown to contain deeply embedded lube-oil within the washcoat, which subsequently regenerated more slowly. The important fact to note is that regardless of the deactivation mechanism occurring during poisoning, the DOC is able to be regenerated and perform as well as a fresh DOC.

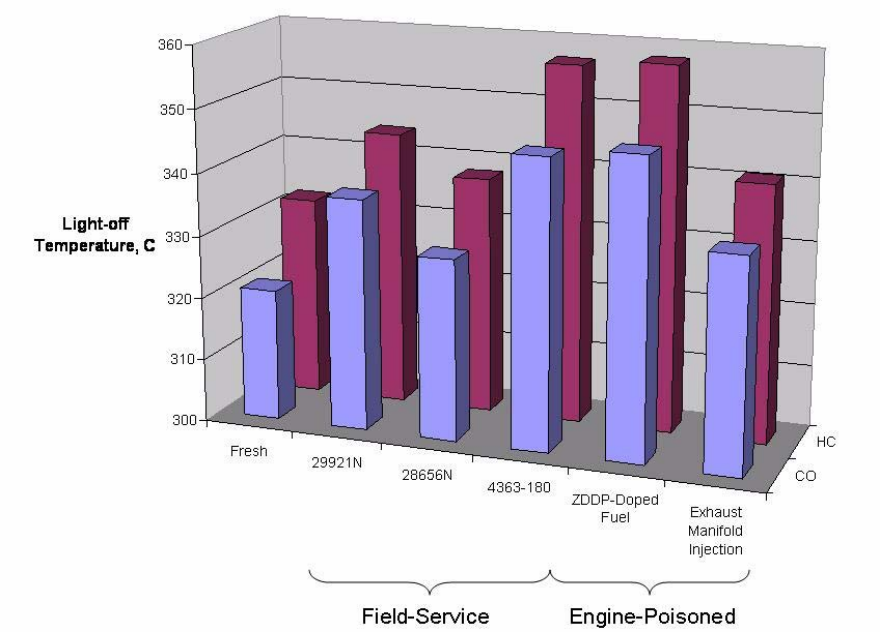

Figure 4.41: Comparison of the first temperature sweep CO and C_2H_4 light-off temperatures obtained for fresh, accelerated ZDDP introduction poisoning and field-deactivated DOCs using the bench-flow reactor.

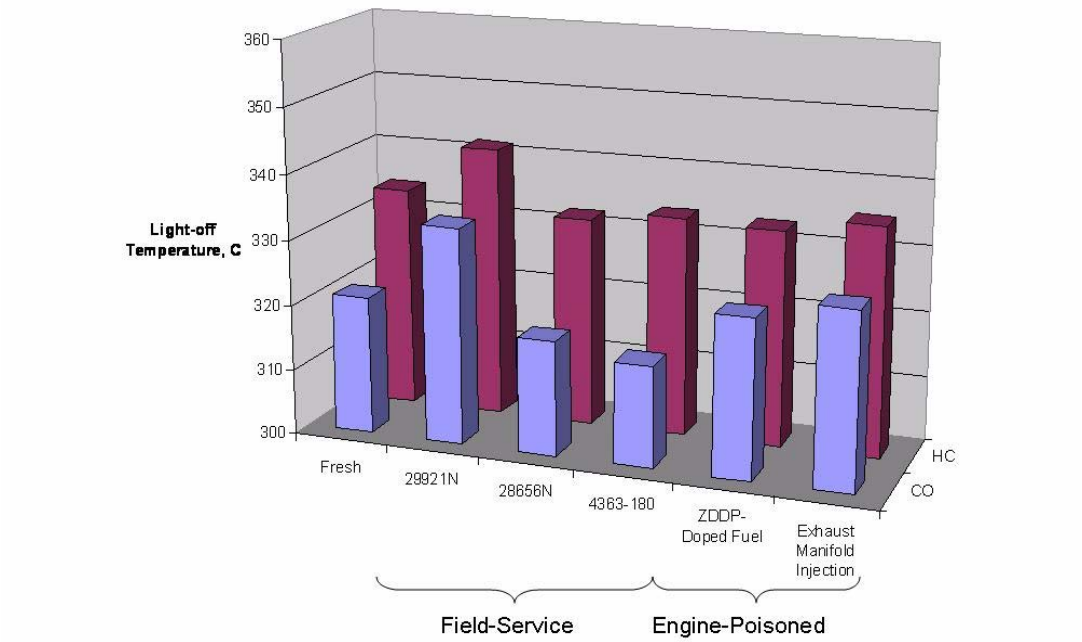

Figure 4.42: Comparison of the final temperature sweep CO and C_2H_4 light-off temperatures obtained for fresh, accelerated ZDDP introduction poisoning and field-deactivated DOCs using the bench-flow reactor.

4.3.2 Materials Characterization

XRF measurements of oil-derived contaminants after regeneration reveals that overall concentrations of phosphorus, sulfur and zinc are maintained within the washcoat. Table XXI shows phosphorus, sulfur and zinc concentrations in the fresh, exhaust manifold and ZDDP-doped fuel injection poisoned DOCs as well as field-deactivated DOCs after regeneration. The presence of poisoning species within the DOC indicates that neither thermal-desorption nor oxidization of the compounds occurs during the high temperature light-off evaluations. This result implies that the presence of oil-derived contaminants within the DOC do not significantly degrade the light-off performance, indicating that soot and lube-oil fouling is the dominant factor contributing to DOC deactivation. It is also noteworthy that DOC 29921N is found to have the least amount of phosphorus, sulfur and zinc within the DOC, yet yielded the worse light-off performance.

EPMA analysis of regenerated DOCs also shows the presence of phosphorus, sulfur and zinc within the washcoat with similar concentrations and profiles as those measured before DOC regeneration. Figure 4.43 provides elemental maps of phosphorus, sulfur and zinc at the front portion of DOC 29921N as well as line-scans at the front and rear sections. A layer of ash is observed on the surface of the washcoat, which is derived from the oxidation of soot and embedded lube-oil on the surface of the DOC. It appears that the presence of ash is the reason DOC 29921N did not completely regenerate. In addition, the DOC is shown to retain a surface layer of phosphorus accompanied by a small amount of calcium and zinc. Since calcium and zinc within this DOC was not observed before regeneration, their appearance is attributed to the oxidation of embedded lube-oil present within the washcoat.

Table XXI: Bulk phosphorus, sulfur and zinc concentrations within DOCs after bench-flow reactor evaluations.

Concentration (Mass %)	Fresh	Exhaust Manifold Injection	ZDDP-Doped Fuel Injection	4363-180	29921N	28656N
Phosphorus	<0.01	1.23	1.05	0.97	0.15	1.16
Sulfur	0.02	0.58	1.04	1.97	0.39	1.79
Zinc	<0.01	0.21	0.01	0.02	0.04	0.05

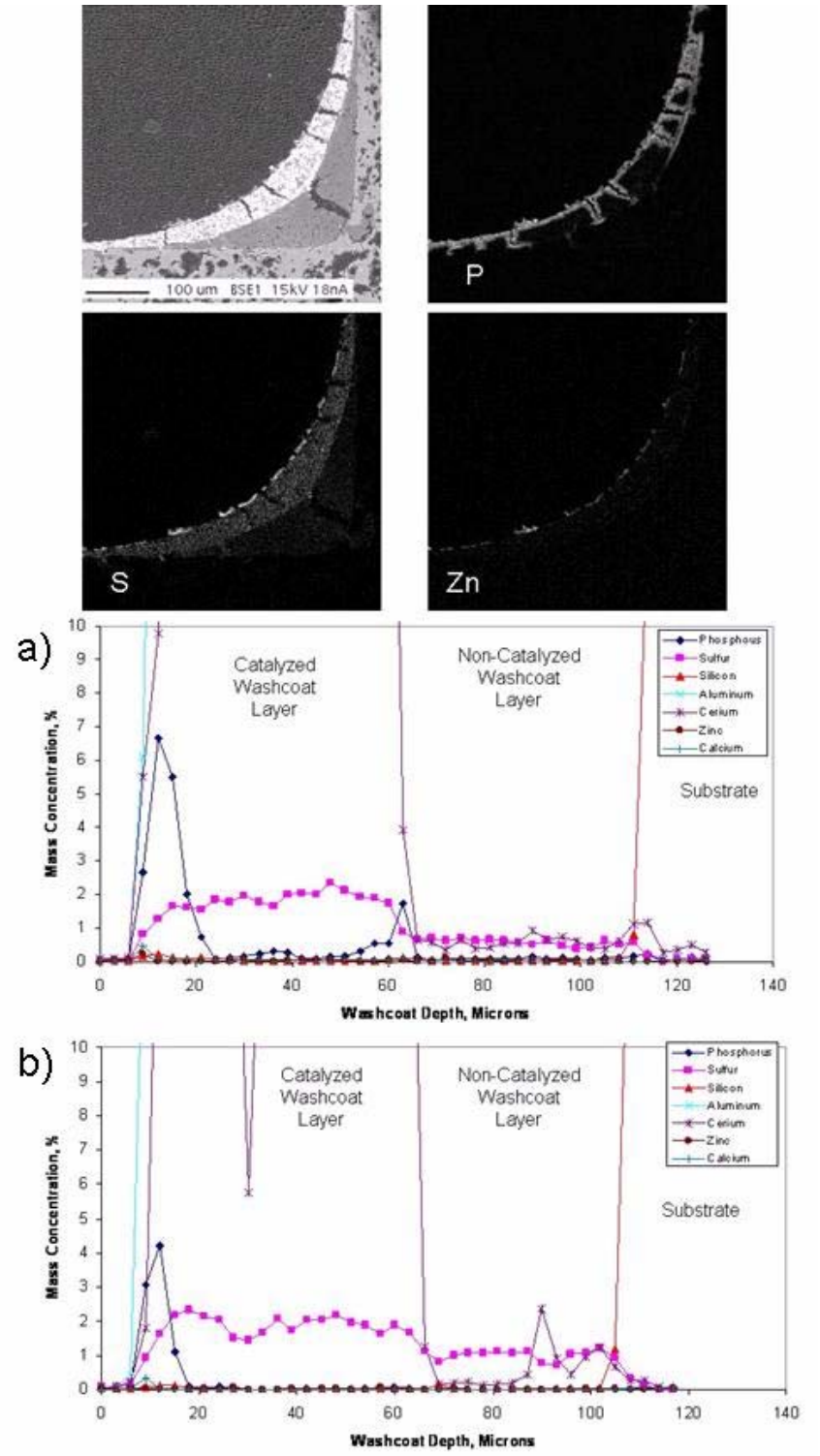

Figure 4.43: Elemental maps of phosphorus, sulfur and zinc at the front location and concentration profiles of oil-derived contaminants at the front and rear locations of DOC 29921N after bench-flow reactor evaluations. a) Front b) Rear.

Figure 4.44 is a backscatter image of an ash particle observed in DOC 29921N and shows the presence of high atomic weight elements, which appear as bright spots. EDS analysis preformed on each of the light and dark spots shows the presence of heavy metals, most likely the result of the disassembly process in which steel fragments can become incorporated within the DOC. The darker ash material, however, is comprised of approximately 50 % calcium, along with measurable amounts of sulfur, phosphorus, and zinc. This result implies that phosphorus is contained within the soot and remains on the DOC surface after soot oxidation. This observation may provide an addition poisoning mechanism though which phosphorus can become chemically adsorbed within the washcoat aside from the adsorption of phosphoric acid.

EPMA analysis of the exhaust manifold injection DOC after regeneration also shows the presence of phosphorus, sulfur and zinc within the washcoat and shows the preservation of the zinc-phosphate layer on the DOC surface as seen in Figure 4.45. The exhaust manifold injection analyses are representative of those obtained in ZDDP-doped fuel injection poisoning which is shown in the appendix. The exhaust manifold

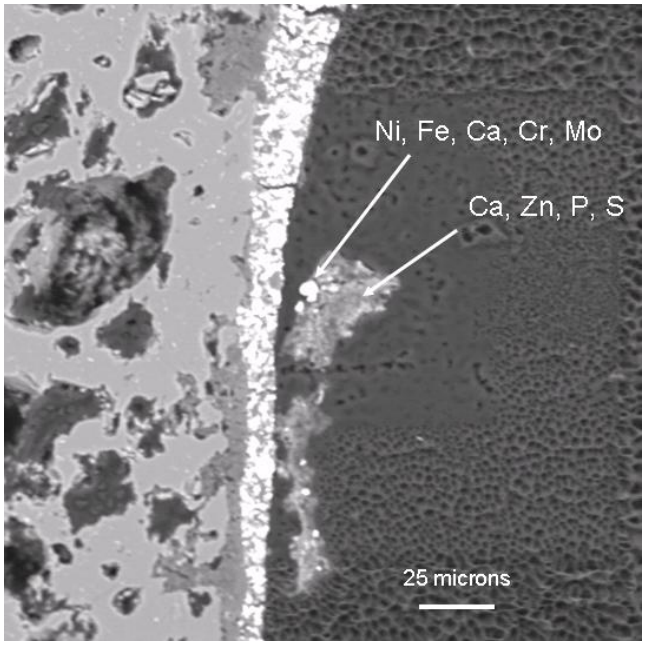

Figure 4.44: Backscatter image and composition of a single ash particle observed in DOC 29921N after bench-flow reactor evaluations.

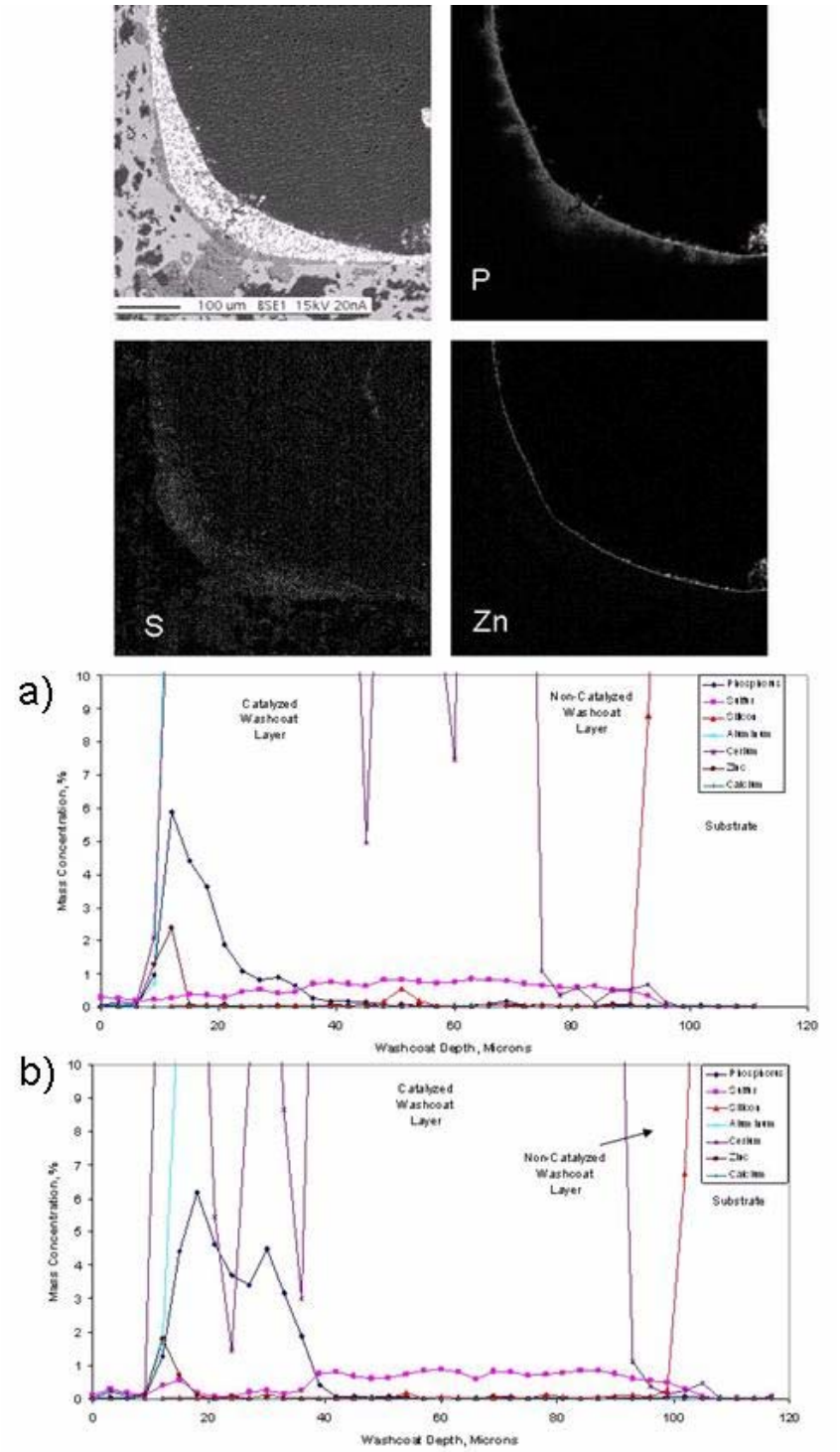

Figure 4.45: Elemental maps of phosphorus, sulfur and zinc at the front location and concentration profiles of oil-derived contaminants at the front and rear locations of the exhaust manifold injection poisoning DOC after bench-flow reactor evaluations. a) Front b) Rear.

injection poisoning DOC is nearly completely regenerated, which implies that the presence of the zinc-phosphate glaze does not significantly alter the light-off performance. This is possibly because not enough glaze is present on the DOC surface or the glaze is not as impervious as thought in previous studies [12,16,20].

An ash layer is also observed on the surface of the accelerated poisoning DOCs and is the result of soot and lube-oil oxidation. The ash layers observed on these DOCs are much less than those observed from DOC 29921N, but more than the layers observed from DOC 28656N and 4363-180. This is attributed to the accelerated poisoning DOCs experiencing a much heavier surface contamination and is consistent with SEM images shown in Figure 4.25.

CHAPTER 5

CONCLUSION

Poisoning of diesel oxidation catalysts by ZDDP-derived phosphorus using a laboratory-scale diesel engine is shown to cause degradation of a DOC's THC and CO light-off performance. Each poisoning method used in this investigation results in a different overall DOC deactivation mechanism which is a direct result of the different poisoning environments produced. Intake manifold and ZDDP-doped fuel injection poisoning protocols, in which ZDDP passes through the combustion chamber, electrospray mass spectrometry identified the only phosphorus compound in the exhaust as phosphoric acid. In addition, zinc was found as zinc sulfate, a stable particulate which does not react with the washcoat. In contrast, exhaust manifold injection poisoning resulted in entire ZDDP molecules and fragments which can incorporate both phosphorus and zinc in the DOC as shown in the resulting materials characterization.

In all poisoning methods, phosphorus is found to deposit preferentially at the inlet portion of the DOC with a decreasing concentration profile along the axial length. Phosphorus deposited within the DOC is observed to be restricted to the surface of the washcoat, penetrating to a maximum depth of approximately 65 microns in the case of fuel injection poisoning. Sulfur, also a constituent in ZDDP is observed to become well-dispersed within the DOC washcoat in low concentrations.

Poisoning via ZDDP-doped fuel injection produces the most severe light-off degradation through the accumulation of a thick soot over-layer on the surface of the washcoat. In addition, this method also results in the greatest phosphorus accumulation within the washcoat, as seen in both the surface concentration as well as phosphorus washcoat penetration depth. Aluminum phosphate ($AlPO_4$) is observed within the DOC

washcoat and is thought to be the initial step leading to the incorporation of phosphorus into the washcoat. The significant soot layer present on the DOC is not indicative of normal engine operation, however, and is therefore not recommended as a rapid poisoning protocol for the acceleration of long-term phosphorus poisoning behavior. The accumulation of soot within the DOC has been observed in long-term idle operation from bus fleets, as seen in the case of DOC 4363-180, which is thought to be simulated using this method at low exhaust temperatures.

Exhaust manifold injection poisoning is observed to form a zinc-phosphate glaze, consistent with the formation of zinc pyrophosphate ($Zn_2P_2O_7$) as measured by Williamson et al. [12]. The glaze is found on the washcoat surface creating a diffusion barrier limiting surface catalytic reactions. In addition to aluminum phosphates, cerium phosphate ($CePO_4$) also appears to be formed within the washcoat, which has been shown to affect the overall redox behavior of ceria reducing light-off performance [13-17,28,34, 35,37]. Although the formation of zinc-phosphates is not characteristic of high-mileage DOCs undergoing normal engine operation, however, although their formation has been observed in the field as a result of improper engine performance.

The intake manifold injection poisoning method produces light-off behavior, surface chemistry and material properties that are most similar to field-deactivated DOCs. Soot accumulation on the DOC during intake manifold poisoning is much less than that of exhaust manifold and ZDDP-doped fuel injection poisoning and is more consistent with deactivation found during normal engine operation. Different engine load conditions effect the accumulation of phosphorus within the DOC with more phosphorus accumulation observed for higher engine loads. In addition, the higher engine loads produce more severe light-off degradation, but remain within range of those found in field-deactivated DOCs. This method is therefore, shown to produce phosphorus poisoning that is most consistent with normal engine operation and is recommended to be used as a rapid phosphorus poisoning protocol.

In contrast to the RPEB evaluations, bench-flow reactor experiments of exhaust manifold and ZDDP-doped fuel injection poisoning as well as field-deactivated DOCs show that surface contamination by soot and lube-oil, rather than phosphorus poisoning,

is the major contributor to DOC deactivation. In each DOC evaluation, THC and CO light-off performance is regenerated to that of a fresh DOC by oxidizing all soot and lube-oil surface contamination. After regeneration, phosphorus concentrations within the DOC remain consistent with those measured before regeneration. This observation indicates that phosphorus adsorption is not a major factor contributing to the deactivation of DOC light-off performance.

Regeneration of DOCs by the removal of soot while preserving the adsorbed phosphorus is in stark contrast to phosphorus poisoning observations in three-way oxidation catalysts in which phosphorus accumulation is found to be a severe deactivation mechanism [13-17]. Though not yet confirmed, it is reasoned that differences in catalyst formulation and operation is the explanation for these observations. Three-way catalysts have a high platinum loading, typically 75 – 100 g Pt/ft^3, while DOCs typically have a low platinum loading, 0.5 g Pt/ft^3. Since platinum sites are the dominant reaction nodes, at which the majority of oxidation reactions take place, the lower loading of the DOCs is more affected by the presence of soot. In addition, three-way catalysts rely heavily on the cerium redox reactions to oxidize THC and CO in lean/rich cycle exhaust environment. It is shown in this study, as well as others in the literature, that cerium phosphate is formed within the oxidation catalyst as a result of phosphorus poisoning. The loss of available cerium reaction sites dramatically reduces the effectiveness of the three-way catalyst during operation. On the other hand, DOCs are less affected by the loss of cerium reaction sites because they are a less crucial component of the overall catalyst formulation.

Despite these findings, accelerated ZDDP introduction methods do recreate DOC THC and CO light-off performance degradation, as found during engine testing, through a variety of mechanisms. Therefore, they are recommended to be utilized as a rapid screening tool for the development of new catalyst formulations and oil additives with the knowledge that soot has a significant role in the oxidation performance of diesel oxidation catalysts.

LIST OF REFERENCES

[1] Mori, K. "Worldwide Trends in Heavy-Duty Diesel Engine Exhaust Emission Legislation and Compliance Technologies," SAE Paper 970753, 1997

[2] Pihl, J. Byproduct Formation During Regeneration of Lean NO_x Traps. Thesis: University of Wisconsin-Madison, 2005

[3] Farrauto, R.J. and Voss, K.E. "Monolithic Diesel Oxidation Catalysts," Appl. Catal. B: Environmental 10 (1996) 29-51

[4] Energy Information Administration. *Crude Oil and Total Petroleum Imports Top 15 Countries:* May 2006. Website: http://www.eia.doe.gov/pub/oil_gas/petroleum/data_publications/company_level_imports/current/import.html

[5] Energy Information Administration. *Emissions of Greenhouse Gases in the United States:* April 2006. Website: http://www.eia.doe.gov/oiaf/1605/87-92rpt/cover.html

[6] Environmental Protection Agency. *Clean Air Markets:* March 2006. Website: http://www.epa.gov/airmarkets/emissions/

[7] Environmental Protection Agency. *Global Warming – Climate:* April 200. Website: http://yosemite.epa.gov/oar/globalwarming.nsf/content/Climate.html

[8] Clerc, J.C. "Catalytic Diesel Exhaust Aftertreatment," Appl. Catal. B: Environmental 10 (1996) 99-115

[9] Moulijn, J.A., van Diepen, A.E. and Kapteijn, F. "Catalyst Deactivation: Is it Predictable? What to do?" Appl. Catal. A: General 212 (2001) 3-16

[10] Harris, P.J.F. "The Sintering of Platinum Particles in an Alumina-Supported Catalyst: Further Transmission Electron Microscopy Studies," J. of Catalysis 97 (1986) 527-542

[11] Chamberlin, W.B. and Zalar, F.V. "Balancing Crankcase Lubricant Performance with Catalyst Life," SAE Paper 841407, 1984

[12] Williamson, W.B., Perry, J., Goss, R.L., Gandhi, H.S. and Beason, R.E. "Catalyst Deactivation Due to Glaze Formation from Oil-Derived Phosphorus and Zinc," SAE Paper 841406, 1984

[13] Gandhi, H.S., Williamson, W.B., Bomback, J.L. “Deactivation of Three-way and Oxidation Catalyst Dual-Bed Emission Control Systems: Catalyst Post-Mortem Analyses from Methanol-Fueled Vehicles,” Appl. Catal. 3 (1982) 79

[14] Rokosz, M.J., Chen, A.E., Lowe-Ma, C.K., Kucherov, A.V., Benson, D., Peck, M.C.P., McCabe, R.W. “Characterization of Phosphorus-Poisoned Automotive Exhaust Catalysts,” Appl. Catal. B: Environmental 33 (2001) 205-215

[15] Xu, L, Guo, G., Uy, D., O’Neill, A.E., Weber, W.H., Rokosz, M.J., McCabe, R.W. “Cerium Phosphate in Automotive Exhaust Catalyst Poisoning,” Appl. Catal. B: Environmental 50 (2004) 113-125

[16] Larese, C., Galisteo, F.C., Granados, M.L., Marical, R., Fierro, J.L.G., Furio, M., Ruiz, R.F. “Deactivation of Real Three Way Catalysts by $CePO_4$ Formation,” Appl. Catal. B: Environmental 40 (2003) 305-317

[17] Uy, D., O’Niell, A.E., Xu, L., Weber, W.H., McCabe, R.W. “Observation of Cerium Phosphate in Aged Automotive Catalysts Using Raman Spectroscopy,” Appl. Catal. B: Environmental 41 (2003) 269-278

[18] Angelidis, T.N. and Sklavounos, S.A. “A SEM-EDS Study of New and Used Automotive Catalysts,” Appl. Catal. A: General 133 (1995) 121-132

[19] Ball, D.J., Mohammed, A.G., Schmidt, W.A. “Application of Accelerated Rapid Aging Test (RAT) Schedules with Poisons: The Effects of Oil Derived Poisons, Thermal Degradation and Catalyst Volume on FTP Emissions,” SAE Paper 972846, 1997

[20] Bunting, B.G., More, K., Lewis, S., Toops, T., “Phosphorus Poisoning and Phosphorus Exhaust Chemistry with Diesel Oxidation Catalysts,” SAE Paper 2005-01-1758, 2005

[21] Spearot, J.A. and Caracciolo, F. “Engine Oil Phosphorus Effects on Catalytic Converter Performance in Federal Durability and High-Speed Vehicle Tests,” SAE Paper 770637, 1977

[22] Zelenka, P., Ostgathe, K., Lox, E. “Reduction of Diesel Exhaust Emissions by Using Oxidation Catalysts,” SAE Paper 902111, 1990

[23] Tashiro, K., Ito, S., Oba, A., Yokomizo, T. "Development of Oxidation Catalyst for Diesel Passenger Car," JSAE Review 16 (1995) 131-136

[24] Daniels, T.L., McCormick, R.L., Graboski, M.S., Carlson, P.N., Rao, V., Rice, G.W. "The Effect of Diesel Sulfur Content and Oxidation Catalysts on Transient Emissions at High Altitude from a 1995 Detroit Diesel Series 50 Urban Bus Engine," SAE Paper 961974, 1996

[25] Hosoya, M., Shimoda, M. "The Application of Diesel Oxidation Catalysts to Heavy Duty Diesel Engines in Japan,"Appl. Catal. B: Environmental 10 (1996) 83-97

[26] Fredholm, S., Andersson, S., Marsh, P., D'Aniello, M.J., Zammit, M.G., Brear, F. "Development of Diesel Oxidation Catalysts for Heavy Duty Engines," SAE Paper 932719, 1993

[27] Stein, H.J. "Diesel Oxidation Catalysts for Commercial Vehicle Engines: Strategies on Their Application for Controlling Particulate Emissions," Appl. Catal. B: environmental 10 (1996) 69-82

[28] Aneggi, E., Boaro, M., de Leitenburg, C., Dolcetti, G., Trovarelli, A. "Insights into the Redox Properties of Ceria-Based Oxides and Their Implications in Catalysis," J. Alloys (in press)

[29] Oran, U., Uner, D. "Mechanisms of CO Oxidation Reaction and Effect of Chlorine Ions on the CO Oxidation Reaction Over Pt/CeO_2 and $Pt/CeO_2/\gamma\text{-}Al_2O_3$ Catalysts," Appl. Catal. B: Environmental 54 (2004) 183-191

[30] Mueller, E. "Der VW-Kat-Diesel mit leichter Aufladung (The Lightly Turbocharged VW Diesel with Catalyst)," 2. Aachener Kolloquium, Fahrzeug- und Motortechnik 1989

[31] Levenspiel, O. Chemical reaction Engineering. 3rd Ed. New Jersey: John Wiley & Sons Inc., 1999

[32] Fogler, H.S. Elements of Chemical Reaction Engineering. 3rd Ed. New Jersey: Prentice Hall, 1999

[33] Johnson, M.D., McCabe, R.W., Hubbard, C.P., Riley, M.J., Kirby, C.W., Ball, D.J., Tripp, G., McDonnell, T.F., Lam, W.Y. "Effects of Engine Formulation

Variables on Exhaust Emissions in Taxi Fleet Service," SAE Paper 2002-01-2680, 2002

[34] Granados, M.L., Larese, C., Galisteo, F.C., Mariscal, R., Fierro, J.L.G., Fernandez-Ruiz, R., Sanguino, R., Luna, M. "Effect of Mileage on the Deactivation of Vehicle-Aged Three-Way Catalysts," Catal. Today 107-108 (2005) 77-85

[35] Angove, D.E., Cant, N.W., Bailey, G.M., Cohen, D.D. "The Application of PIXE to the Mapping of Contaminants Deposited on a monolithic Automotive Catalytic Converter," Nuclear Instruments and Methods in Physics Research B 109-110 (1996) 563-568

[36] Voss, K., Yavuz, B., Hirt, C., Farrauto, R. "Performance Characteristics of a Novel Diesel Oxidation Catalyst," SAE Paper 940239, 1994

[37] Angove, D.E., Cant, N.W. "Position Dependent Phenomena During Deactivation of Three-Way Catalytic Converters on Vehicles," Catal. Today 63 (2000) 371-378

[38] Angelidis, T.N., Papadakis, V.G. "Partial Regeneration of an Aged Commercial Automotive Catalyst," Appl. Catal. B: Environmental 12 (1997) 193-206

[39] Beck, D.D., Sommers, J.W., DiMaggio, C.L. "Axial Characterization of Catalytic Activity in Close-Coupled Lightoff and Underfloor Catalytic Converters," Appl. Catal. B: Environmental 11 (1997) 257-272

[40] Zhang, J., Wu, W., Coa, Z. "Theoretical Study of Low-Lying States in Phosphorus-Containing Carbon Chains $PC_{2n}P$," J. of Molecular Structure: THEOCHEM 756 (2005) 79-85

[41] Ainslie, B., Rideout, G., Cooper, C., McKinnon, D. "The Impact of Retrofit Exhaust Control Technologies in Emissions From Heavy-Duty Diesel Construction Equipment," SAE Paper 1999-01-0110, 1999

[42] Angove, D.E., Cant, N.W., French, H.D., Kinealy, K. "The Effect of Temperature on a Ceria-Alumina-Baria-Cordierite Monolith Combination Under Oxidizing and Reducing Conditions," Appl. Catal. A: General 194 (2000) 27-34

[43] Baba, N., Yokota, K., Matsunaga, S., Kojima, S., Ohsawa, K. "Numerical Simulation of Deactivation Process of Three-Way Catalytic Converters," SAE Paper 2000-01-0214, 2000

[44] Bartholomew, C.H. "Mechanisms of Catalyst Deactivation," Appl. Catal. A: General 212 (2001) 17-60

[45] Botas, J.A., Gutierrez-Ortiz, M.A., Gonzalez-Marcos, M.P., Gonzalez-Marcos, J.A., Gonzalez-Velasco, J.R. "Kinetic Considerations of Three-Way Catalysis in Automotive Exhaust Converters," Appl. Catal. B: Environmental 32 (2001) 243-256

[46] Culley, S.A., McDonnell, T.F. "The Impact of Passenger Car Motor Oil Phosphorus Levels on Engine Durability, Oil Degradation, and Exhaust Emissions in a Field Trail," SAE Paper 952344, 1995

[47] Damyanova, S., Bueno, J.M.C. "Effects of CeO_2 Loading on the Surface and Catalytic Behaviors of CeO_2-Al_2O_3-Supported Pt Catalysts," Appl. Catal. A: General 253 (2003) 135-150

[48] Darr, S.T., Choksi, R.A., Hubbard, C.P., Johnson, M.D., McCabe, R.W. "Effects of Oil-Derived Contaminants on Emissions From TWC-Equipped Vehicles," SAE Paper 2000-01-1881, 2000

[49] Drury, C., Whitehouse, S. "The Effect of Lubricant Phosphorus Level on Exhaust Emissions in a Field Trial of Gasoline Engine Vehicles," SAE Paper 940745, 1994

[50] Duprat, F. "Light-off Curve of Catalytic Reaction and Kinetics," Chemical Engineering Science 57 (2002) 901-911

[51] Froment, G.F. "Modeling of Catalyst Deactivation," Appl. Catal. A: General 212 (2001) 117-128

[52] Gaskell, S.J. “Electrospray: Principles and Practice,” J. of Mass Spectrometry 32 (1997) 677-688

[53] Gasser, R.P.H. An introduction to Chemisorption and Catalysis by Metals. NY: Oxford UP, 1985

[54] Harmsen, J., Jozef, M.A., Hoebink, H.B.J., Schouten, J.C. "Transient Kinetic Modeling of the Ethylene and Carbon Monoxide Oxidation Over a Commercial Automotive Exhaust Gas Catalyst," Ind. Eng. Chem. Res. 39 (2000) 599-609

[55] Hayes, R.E., Kolaczkowski, S.T. Introduction to Catalytic Combustion. Amsterdam: Overseas Association, 1997

[56] Heck, R.M., Farrauto, R.J. "Automobile Exhaust Catalysts," Appl. Catal. A: General 221 (2001) 443-457

[57] Hegedus, L.L., Baron. K. "Phosphorus Accumulation in Automotive Catalysts," J. Catal. 54 (1978) 115-119

[58] Holmgren, A., Andersson, B. "Oxygen Storage Dynamics in $Pt/CeO_2/Al_2O_3$ Catalysts," J. Catal. 178 (1998) 14-25

[59] Holmgren, A., Duprez, D., Andersson, B. "A Model of Oxygen Transport in Pt/Ceria Catalysts from Isotope Exchange," J. Catal. 182 (1999) 441-448

[60] Holmgren, A., Andersson, B., Duprez, D. "Interactions of CO with Pt/Ceria Catalysts," Appl. Catal. B: Environmental 22 (1999) 215-230

[61] Imelik, B., Vedrine, J.C. eds. Catalyst Characterization Physical Techniques for Solid Materials. NY: Plenum P, 1994

[62] Johnson, J.E., Kittelson, D.B. "Deposition, Diffusion and Adsorption in the Diesel Oxidation Catalyst," Appl. Catal. B: Environmental 10 (1996) 117-137

[63] Kakuta, N., Morishima, N., Kotobuki, M., Iwase, T., Mizushima, T., Sato, Y., Matsuura, S. "Oxygen Storage Capacity (OSC) of Aged $Pt/CeO_2/Al_2O_3$ Catalysts: Roles of Pt and CeO_2 Supported on Al_2O_3," Applied Surface Science 121 (1997) 408-412

[64] Kalakkad, D., Daytye, A.K. "Interaction of Platinum and Ceria Probed by Transmission Electron Microscopy and Catalytic Reactivity," Appl. Catal. B: Environmental 1 (1992) 191-219

[65] Kaleli, H. "The Impact of Crankcase Oil Containing Phosphorus on Catalytic Converters and Engine Exhaust Emissions," Industrial Lubrication and Tribology 53.6 (2001) 237-255

[66] Kamijo, M., Kamikubo, M., Akama, H., Matsushita, K. “Study of an Oxidation catalyst System for Diesel Emission Control Utilizing HC Adsorption,” JSAE Review 22 (2001) 277-280

[67] Kumar, S.V., Hochmuth, J.K., Heck, R.M. “A Novel Approach to Studying the Effect of Various Rapid Aging Cycles on the Performance of High Tech Palladium Only Three Way Catalyst,” SAE Paper 941997, 1994

[68] Kvon, R.I., Boronin, A.I., Shaikhutdinov, S.K., Buyanov, R.A. "XPS and STM Study of Carbon Deposits at the Surface of Platinum," Applied Surface Science 120 (1997) 239-242

[69] Lafyatis, D.S., Petrow, R., Bennett, C. "The Effects of Oil-Derived Poisons on Three-Way Catalyst Performance," SAE Paper 2002-01-1093, 2002

[70] Leyrer, J., Lox, E.S., Ostgathe, K., Strehlau, W., Kreuzer, T., Garr, G. “Advanced Studies on Diesel Aftertreatment Catalysts for Passenger Cars,” SAE Paper 960133, 1996

[71] Lie, B., Himmelblau, D.M. "Catalyst Deactivation: Control Relevance of Model Assumptions," Ind. Eng. Chem. Res. 39 (2000) 1242-1248

[72] Liu, D.R., Park, J.S. "Electron Microprobe Characterization of Phosphorus Containing Deposits on Used Automotive Catalyst Surfaces," Appl. Catal. B: Environmental 2 (1993) 49-70

[73] Macdonald, R.J., Taglauer, E.C., Wandelt, K.R.eds. Surface Science Principles and Current Applications. Berlin: Springer-Verlag, 1996

[74] Monzon, A., Romeo, E., Borgna, A. "Relationship Between the Kinetic Parameters of Different Catalyst Deactivation Models," Chemical Engineering Journal 94 (2003) 19-28

[75] Morrison, S.R. The Chemical Physics of Surfaces. 2nd ed. New York: Plenum P, 1990

[76] Mosey, N.J., Muser, M.H., Woo, T.K. “Molecular Mechanisms for the Functionality of Lubricant Additives,” Science 307 issue 5715 (2005) 1612-1615

[77] Nascente, P.A.P. "Materials Characterization by X-ray Photoelectron Spectroscopy," J. of Molecular Catalysis A: Chemical 228 (2005) 145-150

[78] Navarro, R.M., Alvarez-Galvan, M.C., Sanchez-Sanchez, M.C., Rosa, F., Fierro, J.L.G. "Production of Hydrogen by Oxidative Reforming of Ethanol over Pt Catalysts Supported on Al_2O_3 Modified with Ce and La," Appl. Catal. B: Environmental 55 (2005) 229-241

[79] Nibbelke, R.H., Campman, M.A.J., Hoebink, J.H.B.J., Marin, G.B. "Kinetic Study of the CO Oxidation Over Pt/γ-Al_2O_3 and Pt/Rh/CeO_2/γ-Al_2O_3 in the Presence of H_2O and CO_2," J. of Catalysis 171 (1997) 358-373

[80] Nibbelke, R.H., Nievergeld, A., Jozef, J.L., Hoebink, H.B.J., Marin, G.B. "Development of a Transient Kinetic Model for the CO Oxidation by O_2 Over a Pt/Rh/CeO_2/γ-Al_2O_3 Three-Way Catalyst," Appl. Catal. B: Environmental 19 (1998) 245-259

[81] Niemantsverdriet, J.W. Spectroscopy in Catalysis An Introduction. 2nd ed. Weinheim: Wiley-VCH Verlag GmbH, 2000

[82] Obert, E.F. Internal Combustion Engines. 3rd ed. Scranton, PA: International Textbook Company, 1968

[83] Ozawa, M., Loong, C.K. "In Situ X-ray and Neutron Powder Diffraction Studies of Redox Behavior in CeO_2-Containing Oxide Catalysts," Catal. Today 50 (1999) 329-342

[84] Pantu, P., Gavalas, J.R. "Methane Partial Oxidation on Pt/CeO_2 and Pt/Al_2O_3 Catalysts," Appl. Catal. A: General 223 (2002) 253-260

[85] Parola, V.L., Deganello, G., Tewell, C.R., Venezia, A.M. "Structural Characterization of Silica Supported CoMo Catalysts by UV Raman Spectroscopy, XPS and X-ray Diffraction Techniques," Appl. Catal. A: General 235 (2002) 171-180

[86] Pattas, K.N., Stamatelos, A.M., Koltsakis, G.C., Konstantinidis, P.A. "Computer Aided Assessment of Catalyst Aging Cycles," SAE Paper 950934, 1995

[87] Pattas, K.N., Stamatelos, A.M., Pistikopoulos, P.K., Koltsakis, G.C., Konstandinidis. P.A. "Transient Modeling of 3-Way Catalytic Converters" SAE Paper 940934, 1994

[88] Riviere, J.C. Surface Analytical Techniques. NY: Oxford UP, 1990

[89] Santos, A.C.S.F., Damyanova, S., Teixeira, G.N.R., Matos, L.V., Noronha, F.B., Passos, F.B., Bueno, J.M.C. "The Effect of Ceria Content on the Performance of $Pt/CeO_2/Al_2O_3$ Catalysts in the Partial Oxidation of Methane," Appl. Catal. A: General 290 (2005) 123-132

[90] Shinjoh, H. "Rare Earth Metals for Automotive Exhaust Catalysts," J. of Alloys (2005) (in press)

[91] Tabata, T., Baba, K., Kawashima, H. "Deactivation by Poisoning of Three-Way Catalyst for Natural Gas-Fuelled Engines," Appl. Catal. B: Environmental 7 (1995) 19-32

[92] Tamanouchi, M., Morihisa, H., Araki, H., Yamada, S. "Effects of Fuel Properties and Oxidation Catalyst on Exhaust Emissions for Heavy Duty Diesel Engines and Passenger Cars," SAE Paper 980530, 1998

[93] Tiernan, M.J., Finlayson, O.E. "Effects of Ceria on the Combustion Activity and Surface Properties of Pt/Al_2O_3 Catalysts," Appl. Catal. B: Environmental 19 (1998) 23-35

[94] Ueda, F., Sugiyama, S., Arimura, K., Hamaguchi, S., Akiyama, K. "Engine Oil Additive Effects on Deactivation of Monolithic Three-Way Catalysts and Oxygen Sensors," SAE Paper 940746, 1994

[95] Venezia, A. "X-ray Photo,electron Spectroscopy (XPS) for Catalysts Characterization," Catal. Today 77 (2003) 359-370

[96] Williamson, W.B., Perry, J., Gandhi, H.S., Bomback, J.L. "Effects of Oil on Deactivation of Monolithic Three-Way Catalysts," Appl. Catal. 15 (1985) 277-292

[97] Lewis, S., Bunting, B., and Eaton, S. (2005) Determining the Combustion Product of Zinc Dialkyldithiophosphate using Electrospray Mass Spectrometry. The 53rd ASMS Conference on Mass Spectrometry.

APPENDIX

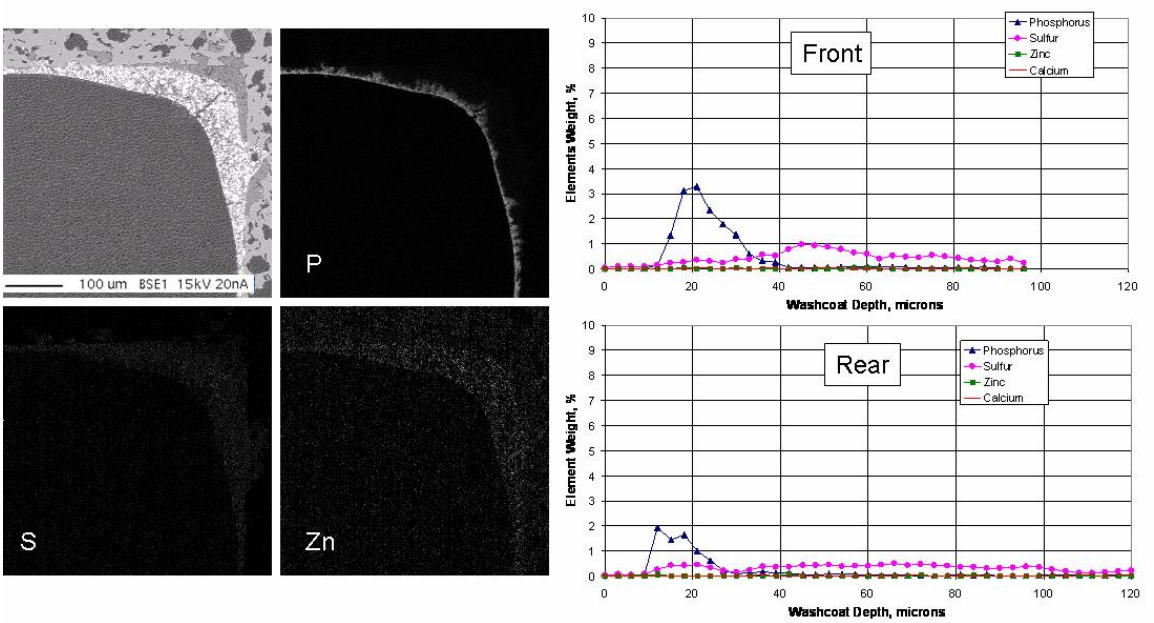

Figure A-1: Elemental maps of phosphorus, sulfur and zinc at the inlet and concentration profiles at the front and rear locations of the intake manifold injection DOC at 0 % engine load.

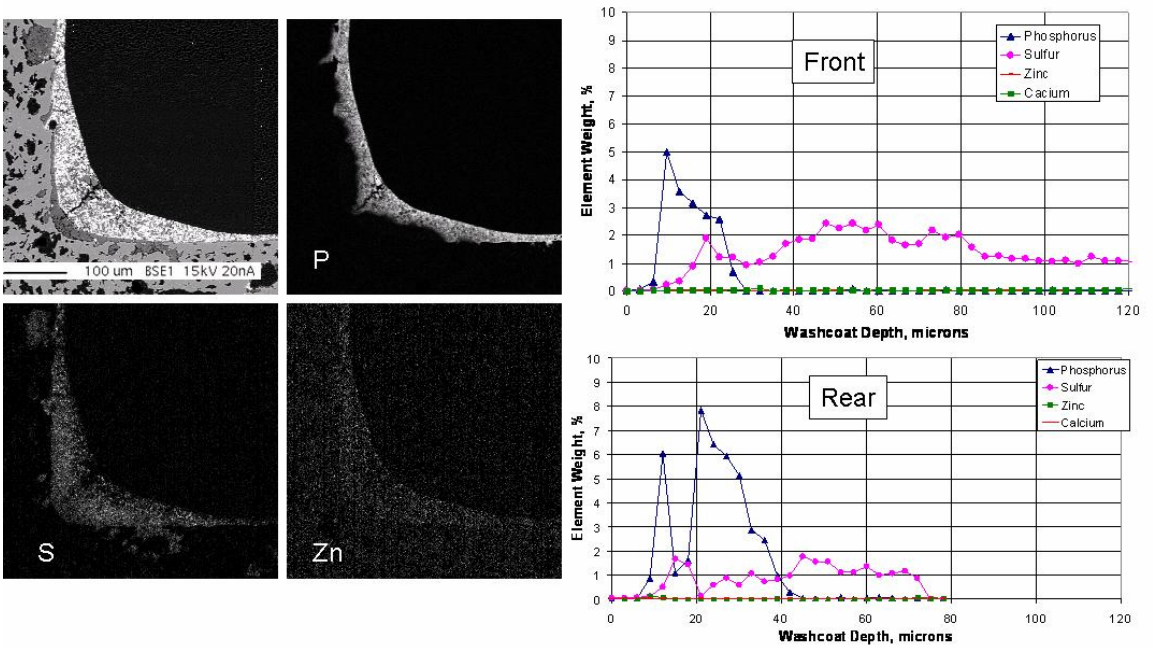

Figure A-2: Elemental maps of phosphorus, sulfur and zinc at the inlet and concentration profiles at the front and rear locations of the intake manifold injection DOC at 100 % engine load.

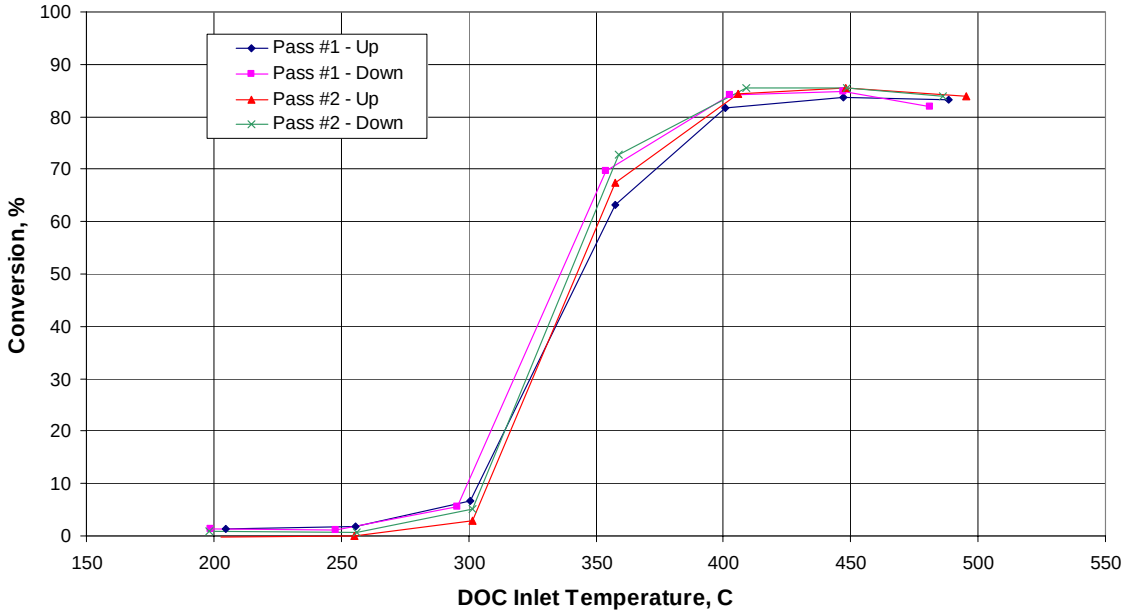

Figure A-3: C_2H_4 light-off curves for four temperature sweeps from 200-500°C for field-deactivated DOC 29921N.

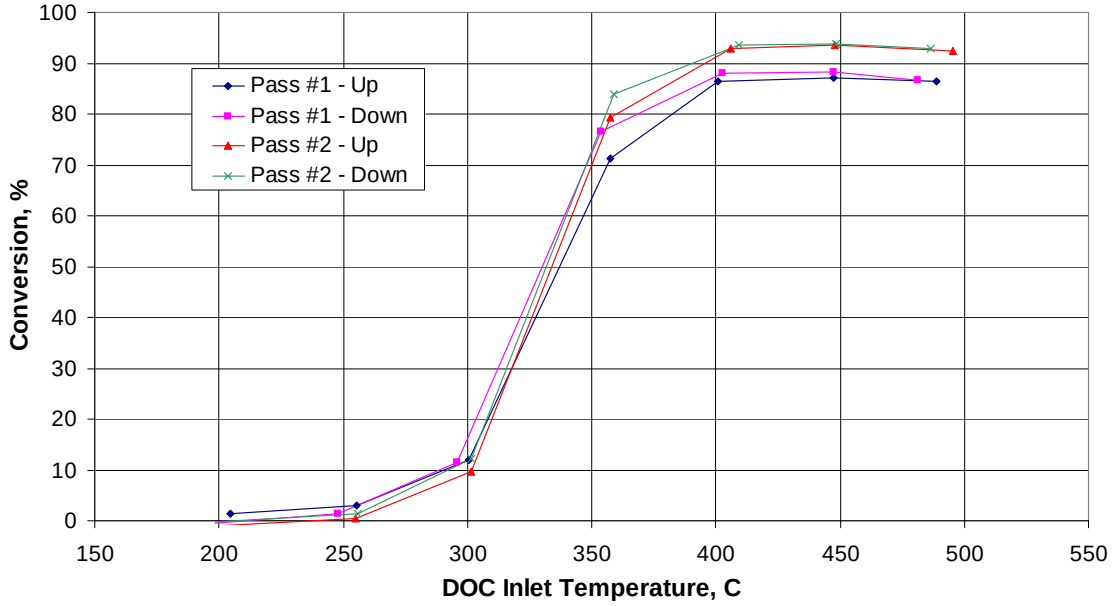

Figure A-4: CO light-off curves for four temperature sweeps from 200-500°C for field-deactivated DOC 29921N.

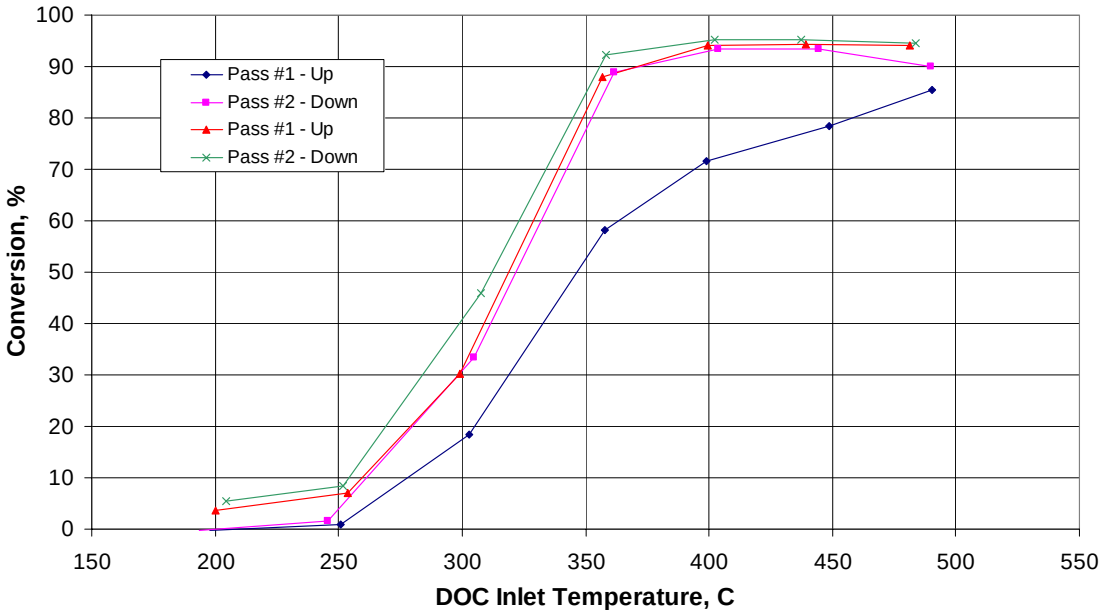

Figure A-5: CO light-off curves for four temperature sweeps from 200-500°C for field-deactivated DOC 4363-180.

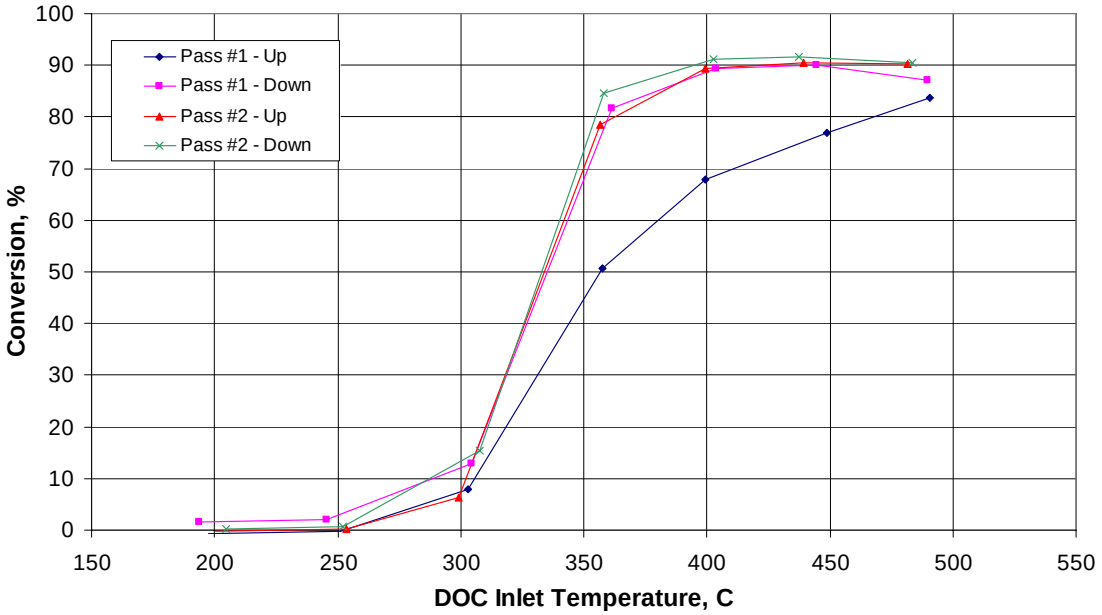

Figure A-6: C_2H_4 light-off curves for four temperature sweeps from 200-500°C for field-deactivated DOC 4363-180.

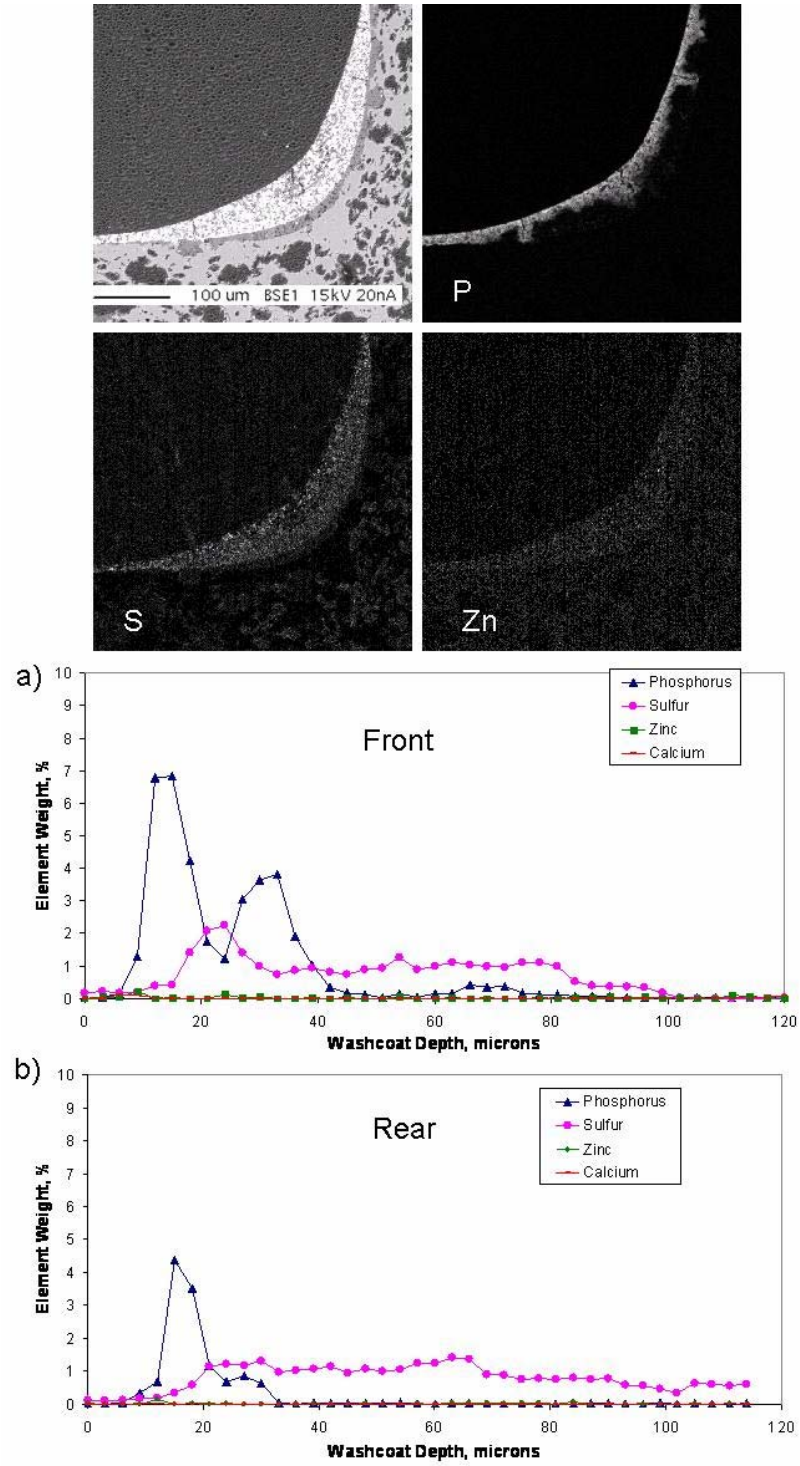

Figure A-7: Elemental maps and concentration profiles of oil-derived contaminants at the front and rear locations for the ZDDP-doped fuel injection poisoning DOC after BFR evaluations. a) Front b) Rear.

VITA

Scott Eaton was born in Augusta, ME on 6 September 1980. He graduated from Gardiner Area High School in May 1998. While there, he attended the State of Maine Young Scholars Program for talented high school mathematics and science students. Later, he graduated Magna Cum Laude from the University of Maine – Orono in May 2004 with a degree in Mechanical Engineering. While in attendance, Scott became a member of Pi Mu Epsilon, Pi Tau Sigma and Phi Sigma Phi. After graduation, he worked at the Naval Undersea Warfare Center – Division Newport as an engineering intern within the sonar array department. In the fall of 2004, he attended the University of Tennessee - Knoxville where he earned his Master of Science degree of Mechanical Engineering in August of 2006.

Scott is a member of the Society for Automotive Engineers and The American Society of Mechanical Engineers.